Alessio Giove

PREPARATION OF ION-IMPRINTED POLYMERS FOR THE HYDROMETALLURGICAL SEPARATION OF Co(II) AND Ni(II) IONS: THE EFFECT OF METAL-CHELATOR COMPLEXES ON SELECTIVITY

ACTA UNIVERSITATIS LAPPEENRANTAENSIS 1129

Alessio Giove

PREPARATION OF ION-IMPRINTED POLYMERS FOR THE HYDROMETALLURGICAL SEPARATION OF Co(II) AND Ni(II) IONS: THE EFFECT OF METAL-CHELATOR COMPLEXES ON SELECTIVITY

Dissertation for the degree of Doctor of Science (Technology) to be presented with due permission for public examination and criticism in the Auditorium 1318 of the Student Union House at Lappeenranta-Lahti University of Technology LUT, Lappeenranta, Finland on the 19th of April 2024, at noon.

The dissertation was written under a joint supervision agreement between Lappeenranta-Lahti University of Technology LUT, Finland and Université de Toulon, France and jointly supervised by supervisors from both Universities.

Acta Universitatis
Lappeenrantaensis 1129

Supervisors Docent Katri Laatikainen
LUT School of Engineering Sciences
Lappeenranta-Lahti University of Technology LUT
Finland

Associate Professor Catherine Branger
MAPIEM
Université de Toulon
France

Reviewers Professor Benjamin Carbonnier
Department of Macromolecular Science and Engineering
Université Paris Est Créteil
France

Dr. Antonio Martín-Esteban
Instituto Nacional de Investigación y Tecnología Agraria y Alimentaria - Consejo Superior de Investigaciones Científicas
Spain

Opponent Professor Ari Väisänen
Department of Chemistry
University of Jyväskylä
Finland

President Professor Ian Nicholls
Department of Chemistry & Biomedical Sciences
Linnaeus University
Sweden

ISBN 978-952-412-064-7
ISBN 978-952-412-065-4 (PDF)
ISSN 1456-4491 (Print)
ISSN 2814-5518 (Online)

Lappeenranta-Lahti University of Technology LUT
LUT University Press 2024

Abstract

Alessio Giove
Preparation of ion-imprinted polymers for the hydrometallurgical separation of Co(II) and Ni(II) ions: the effect of metal-chelator complexes on selectivity
Lappeenranta 2024
188 pages
Acta Universitatis Lappeenrantaensis 1129
Diss. Lappeenranta-Lahti University of Technology LUT
ISBN 978-952-412-064-7, ISBN 978-952-412-065-4 (PDF), ISSN 1456-4491 (Print), ISSN 2814-5518 (Online)

This doctoral project addressed the challenging separation of Co(II) and Ni(II) ions in hydrometallurgical processes. The experimental work focused on the synthesis of new chelating monomers, the study of their complexes with the target ions and their application to prepare ion imprinted polymers (IIPs). Three new chelating monomers, named PIM-MMA, bis-AMP-MMA, and AMP-MMA, were synthesized using pyridine ligands as precursors. PIM-MMA monomer was excluded from the complex formation study due to its high tendency to homopolymerization. Nevertheless, it was used to prepare Ni(II)-imprinted polymers at varying Ni(II)/PIM-MMA ratios. These materials showed enhanced Ni(II) adsorption capacity when compared to the corresponding non-imprinted polymer (NIP), and a light selectivity for Ni(II) ions, which was however limited. The formation of complexes with Co(II) and Ni(II) ions was studied with both bis-AMP-MMA and AMP-MMA monomers. Both monomers formed 1:2 complexes with Co(II) and Ni(II) ions. In the case of bis-AMP-MMA, these complexes had similar stability constants, while AMP-MMA complex with Ni(II) ions was more stable than the one formed with Co(II) ions. IIPs were prepared with both monomers optimizing the pre-polymerization mixture according to complex formation study results. Bis-AMP-MMA-based adsorbents were characterized by poor selectivity in the separation of Co(II) ions in presence of Ni(II) ions. Conversely, the Ni(II)-IIP based on AMP-MMA (AMP-Ni-IIP) exhibited high selectivity for Ni(II) ions in presence of Co(II) ions. These selectivity study results aligned with those of the complex formation study for both monomers and highlighted the importance of optimizing metal/chelator complexes to prepare highly selective IIPs. Additionally, the adsorption capacity of AMP-Ni-IIP in both neutral and acidic media (169.5 mg/g at pH 7 and 138.9 mg/g at pH 2), combined with its selectivity for Ni(II) ions, provided a valuable alternative for the selective separation of Ni(II) ions in hydrometallurgical processes.

Keywords: adsorption, selectivity, ion imprinted polymers, nickel, cobalt, hydrometallurgy

Acknowledgements

This work was carried out in the LUT School of Engineering Sciences at Lappeenranta-Lahti University of Technology LUT, Finland, and MAPIEM laboratory at University of Toulon, France, between 2019 and 2024. I want to express my gratitude to both institutions and to the Research council of Finland for their constant financial and scientific support.

I thank the reviewers of this doctoral thesis, Dr. Antonio Martín-Esteban and Prof. Benjamin Carbonnier, for dedicating their expertise and time to the improvement of this manuscript.

During my PhD I was very fortunate to be supervised by two incredible women and researchers. Every day you encouraged me to be a better person and researcher, you taught me working methodologies, provided your knowledge in the most complex situations and represented an important point of reference in the most difficult moments of this path. For this I want to sincerely thank Dr. Katri Laatikainen and Dr. Catherine Branger. You will always have a special place in my life and career.

A huge thanks goes to Prof. Eveliina Repo for her professional advice and for her unlimited kindness and humanity. You welcomed me into your group without ever making me lack your support and availability. You did everything you could to help me every time it was possible. Thank you so much for that.

I thank Youssef for being a true friend, for the time spent together inside and outside the university, for always being there in times of need, for helping me several times both with experiments and with scientific articles. This journey was more beautiful, compelling, and simple thanks to your constant presence. Thank you with all my heart.

I warmly thank Svetlana and Emile for the thousand pieces of advice, the many scientific discussions, their constant availability in times of need and the endless coffees and lunches spent together. I also want to sincerely thank Mehran, Vitalii, Mahdi, Amin, Tuomas, Reza, Salla, Atieh, Markku, Tobias, Kosi and all the other amazing people with whom I shared my journey at LUT (too many! Forgive me if I forgot mentioning someone). Your presence in my doctorate made the working days at university lighter and more interesting.

My gratitude also goes to Farah and Alexandre for bringing joy in the days at the office and laboratory in France. We shared many beautiful moments both inside and outside the university and you made me feel part of the group from the first moment. I thank you for always helping me with experiments but also with many problems of daily life. I wish anyone who moves to a new place to find people like you because you have made everything much easier for me. Together with you I met many beautiful people in the MAPIEM laboratory, Manar, Aurelie, Elliot, Alexandre Lutz, Linh, Nathan and the list could go on and on. I want to thank you all for making my experience in France unique.

I warmly thank Yolanda for being my adventure companion in discovering France. We visited many new places together, we shared lunches, dinners, sunny days and windy days (a little too windy at times). The moments we spent together made my time in France unforgettable and I will always carry with me many beautiful memories.

In these 5 years I have met many special people both at LUT and in the MAPIEM laboratory. Each of you has enriched my journey and I want to thank you from the bottom of my heart.

Ringrazio Eleni, Paolo, Federico Fico, Giovanni, Teddy, Andrea, Raimondo, Franco e tutti gli amici di Brindisi e degli anni spesi a Padova. Spesso non ci siamo visti per mesi ma ogni volta è stato come se il tempo non fosse mai passato. Grazie di cuore.

Un ringraziamento speciale va ad Elena. Questi anni all'estero non solo non hanno intaccato il nostro rapporto ma lo hanno reso speciale. Abbiamo condiviso tanti viaggi, avventure e bellissime giornate. Hai sempre avuto una parola di conforto e mi sei stata vicina nei momenti più difficili e per questo sono felice di aver condiviso con te anche alcuni tra i più belli. Grazie per esserci sempre o, almeno, ogni volta che serve davvero.

Ringrazio infine la mia famiglia per aver sempre creduto in me e non aver mai fatto pesare la mia assenza.

Grazie mamma per avermi dato la vita, spero tu sia orgogliosa del mio percorso.

Alessio Giove
March 2024
Lappeenranta, Finland

A mia madre

Ho sceso, dandoti il braccio, almeno un milione di scale
e ora che non ci sei è il vuoto ad ogni gradino.
Anche così è stato breve il nostro lungo viaggio.
Il mio dura tuttora, nè più mi occorrono
le coincidenze, le prenotazioni,
le trappole, gli scorni di chi crede
che la realtà sia quella che si vede.

Ho sceso milioni di scale dandoti il braccio
non già perché con quattr'occhi forse si vede di più.
Con te le ho scese perché sapevo che di noi due
le sole vere pupille, sebbene tanto offuscate,
erano le tue.

Contents

Scientific papers and oral communications

List of publications and author's contribution

Paper I: Y. El Ouardi, A. Giove, M. Laatikainen, C. Branger, K. Laatikainen, Benefit of ion imprinting technique in solid-phase extraction of heavy metals, special focus on the last decade. *Journal of Environmental Chemical Engineering*, Volume 9, Issue 6, **2021**, 106548, ISSN 2213-3437, https://doi.org/10.1016/j.jece.2021.106548.

A. Giove was responsible for writing the original draft and for data curation in Paper I. Dr. Y. El Ouardi, the principal author, investigator, and corresponding author of this paper, was responsible for writing, reviewing, and editing the original draft and for data curation. Dr. M. Laatikainen was responsible for writing the original draft. Dr. C. Branger was responsible for the supervision of the work, and for writing, reviewing, and editing the original draft. Dr. K. Laatikainen, the administrator of the project, was responsible for the supervision of the work, and for writing, reviewing, and editing the original draft.

Paper II: A. Giove, Y. El Ouardi, A. Sala, F. Ibrahim, S. Hietala, E. Sievänen, C. Branger, K. Laatikainen, Highly selective recovery of Ni(II) in neutral and acidic media using a novel Ni(II)-ion imprinted polymer. *Journal of Hazardous Materials*, Volume 444, Part B, **2023**, 130453, ISSN 0304-3894, https://doi.org/10.1016/j.jhazmat.2022.130453.

A. Giove, the principal author, investigator, and corresponding author of this paper, was responsible for the synthesis and characterization of monomer and polymers, the application of polymers, for data curation and for writing, review and editing the original draft. Dr. Y. El Ouardi was responsible for the application of polymers and for writing, review and editing the original draft. Dr. A. Sala was responsible for monomer synthesis and for writing, review and editing the original draft. Dr. F. Ibrahim was responsible for polymers characterization and for writing, review and editing the original draft. Dr. S. Hietala was responsible for polymer characterization and for writing, review and editing the original draft. Dr. E. Sievänen was responsible for monomer characterization. Dr. C. Branger was responsible for the supervision of the work, and for writing, reviewing, and editing the original draft. Dr. K. Laatikainen, the administrator of the project, was responsible for the supervision of the work, and for writing, reviewing, and editing the original draft.

Oral communication

A. Giove, Y. El Ouardi, A. Sala, F. Ibrahim, K. Laatikainen, C. Branger, Synthesis of new selective monomers for the design of original Ni(II) and Co(II) ion imprinted polymers. *X Franco-Italian Days of Chemistry*, **26th and 27th April 2022**, Palais des Congrès Neptune, Toulon (France).

Nomenclature

Latin alphabet

A	Area	m^2
C	Concentration	g/L
F	Molar fraction into a copolymer	
K	Constant	-
K_d	Distribution coefficient	-
k	Selectivity coefficient	-
k'	Relative selectivity coefficient	-
m	Mass	g
q	Adsorption capacity	mg/g
R^2	Correlation coefficient	-
V	Volume	L
x	Molar fraction in solution	-

Greek alphabet

β	stability constant	-
δ	chemical shift	ppm

Subscripts

0	initial
e	equilibrium
F	Freundlich
L	Langmuir
n	number 1…n
m	maximum
t	time 0…t

Abbreviations

4-VP	4-vinylpyridine
5-VHQ	5-vinyl-8-hydroxyquinoline
8-HQ	8-hydroxyquinoline
AA	Acrylic acid
AAPTS	3-(2-aminoethylamino) propyltrimethoxysilane
AC	Activated carbon
ACN	Acetonitrile
AIBN	Azobisisobutyronitrile
AM	Acrylamide
AMP	2-(aminomethylpyridine)
AQ	8-aminoquinoline

ATR	Attenuated total reflectance
BET	Brunauer-Emmett-Teller
BJH	Barrett-Joyner-Halenda
BPO	Benzoyl peroxide
Bis-AMP	Bis-2-(pyridylmethyl)amine
C_4H_5ClO	Methacryloyl chloride
$CDCl_3$	Deuterated chloroform
CH_2Cl_2	Dichloromethane
CMPS	Chloromethylated polystyrene
CN^-	Cyanide
$Cd(NO_3)_2 \cdot 4H_2O$	Cadmium nitrate tetrahydrate
$Co(ClO_4)_2 \cdot 6H_2O$	Cobalt perchlorate hexahydrate
$Co(NO_3)_2 \cdot 6H_2O$	Cobalt nitrate hexahydrate
$Cu(ClO_4)_2 \cdot 6H_2O$	Copper perchlorate hexahydrate
$Cu(NO_3)_2 \cdot 2.5H_2O$	Copper nitrate hemihydrate
Cyanex®	Bis-2,4,4-trimethylpentyl phosphinic acid
D2EHPA	Di-2-ethylhexylphosphoric acid
DBDA15C4	5,6,14,15-dibenzo-1,4-dioxa-8,12-diazacyclopentadecane-5,14-diene
DEM	2-(diethylamino) ethyl methacrylate
DMF	Dimethylformamide
DMSO	Dimethylsulfoxide
DMSO-d_6	Deuterated dimethyl sulfoxide
DPA	Dipicolinic acid
DPC	Diphenylcarbazide
DVB	Divinylbenzene
ECH	Epichlorohydrin
EGDMA	Ethylene glycol dimethylacrylate
FTIR	Fourier transform infrared
H_2SO_4	Sulfuric acid
HAQ	1-hydroxy-2-(prop-2′-enyl)-9,10-anthraquinone
HCl	Hydrochloric acid
HEMA	2-hydroxyethylmethacrylate
HEPES	N-(2-hydroxyethyl)piperazine-N-2-ethanesulfonic acid
HNO_3	Nitric acid
HPPA	Hydroxypropylpicolylamine
ICP-MS	Inductively coupled plasma-mass spectroscopy
IIPs	Ion-imprinted polymers
$LiCoO_2$	Lithium cobalt oxide
LSM	Least-squares minimization
MAA	Methacrylic acid
MAH	Methacryloylhistidine
$Mg(NO_3)_2 \cdot 6H_2O$	Magnesium nitrate hexahydrate
$MgSO_4$	Magnesium sulfate
MMA	Methyl methacrylate

$Mn(NO_3)_2 \cdot 4H_2O$ Manganese nitrate tetrahydrate
NaOH Caustic soda or Sodium hydroxide
$N(CH_2CH_3)_3$ Triethylamine
NdFeB Neodymium-iron-boron
$Ni(ClO_4)_2 \cdot 6H_2O$ Nickel perchlorate hexahydrate
Ni-MH Ni-metal-hydride
$Ni(NO_3)_2 \cdot 6H_2O$ Nickel nitrate hexahydrate
$Ni(OH)_2$ Nickel hydroxide
NMR Nuclear magnetic resonance
OPIM Octyl derivative of 2,2'-(pyridyl)imidazole
PETA Pentaerythrityl triacrylate
PETRA Pentaerythritol triacrylate
PIM 2,2'-(pyridyl)imidazole
REEs rare earths elements
ROS Reactive oxygen species
RSD Relative standard deviation
$S_2O_3^{2-}$ Thiosulfate
$SC(NH_2)_2$ Thiourea
SEM Scanning electron microscopy
Sm-Co-RE Samarium-cobalt rare earth
TEMED N,N,N',N'-tetramethylene diamine
TEOS Tetraethoxysilane
TMPTA Trimethylolpropane triacrylate
TRIM Trimethylolpropane trimethacrylate
UV-Vis UV-visible
Vbamp Vinylbenzyl derivative of 2-(aminomethyl)pyridine
VbiDA [N-(4-vinylbenzyl)imino]diacetic acid

1 Introduction

1.1 Research background

The separation of metal ions from complex mixtures is a highly relevant topic in both academic and industrial research. Due to their chemical and physical similarities and frequent co-occurrence in natural resources, the separation of nickel and cobalt is a major challenge in the metallurgical industry. Nickel is predominantly sourced from sulfide and laterite ores found primarily in Australia, Indonesia, South Africa, Russia, and Canada [1]. In contrast, ore deposits for the exclusive supply of cobalt are rare, with Morocco and Canada being the sole locations where they can be found. This leads to approximately 98% of industrially available cobalt being produced as a by-product of nickel or copper mining [2]. Hydrometallurgy has been established in recent decades as a more eco-sustainable alternative to the energy-demanding pyrometallurgical processes [3]. Hydrometallurgical processes are conducted in water-based solutions, reducing energy consumption, and minimizing the release of hazardous by-products into the environment [4]. Hydrometallurgical separation processes begin with the dissolution of the metal-containing feed to release the target metal in solution [5]. This first step, known as leaching, is a non-selective process and impurities such as metal ions, organic matter, and inorganic compounds are dissolved together with the target metal. To purify and concentrate the target metal in the solution, common metal separation techniques like solvent extraction [6], precipitation [7], cementation [8], ion exchange [9], or adsorption [10] are implemented. These techniques often lack selectivity, especially when dealing with metal species with similar chemical properties, as is the case of the separation of Co(II) and Ni(II) ions. To enhance selectivity, researchers frequently seek the development of new selective materials capable of interacting specifically with the target species. This was achieved, for example, by testing new extractants for solvent extraction [11] or new precipitating agents for chemical precipitation [12], and with the design of new resins for ion exchange or adsorption [13]. A convenient alternative to increasing the selectivity of adsorbent materials is represented by the ion imprinting technique [14]. Ion-imprinted polymers (IIPs) are porous adsorbents whose polymeric network is formed in the presence of a specific target ion, namely template ion [15]. The preparation of IIPs begins with the complexation of the template ion with a functional chelating monomer. The complex is then copolymerized and finally the template ions are released, forming ion-imprinted cavities. The shape and size of these binding cavities are complementary to those of the template ion, enhancing the selectivity of IIPs toward it. The selectivity of IIPs is affected by the stability and stoichiometry of the complex between the template ion and the chelating molecules [16]. The preparation of IIPs for the selective separation of Co(II) and Ni(II) is the core topic of this doctoral project. The literature about the properties of cobalt and nickel, their industrial recovery, and the methodologies for their selective separation, and about the preparation of IIPs and the optimization of the pre-polymerization conditions introduced in this section, are deeply explored in Chapter 2 of this manuscript.

1.2 Purpose of the study and research limits

This PhD project aims to prepare highly selective IIPs as a solution to the complex hydrometallurgical separation of Co(II) and Ni(II) ions. The stability sequence for first-row transition metals complexes generally follows the Irving-Williams series represented as Mn(II) < Fe(II) < Co(II) < Ni(II) < Cu(II) > Zn(II) [17]. Typically, Cu(II) complexes exhibit the highest stability but there are specific cases, such as with 1,10-phenanthroline ligand, where Ni(II) complexes are more stable [18]. In previous studies conducted by the project supervisors' team, it was demonstrated that, by adjusting the metal/chelator stoichiometry with an *in situ* complex formation study, it was possible to change the selectivity order of IIPs for transition metals [16]. The complex formation between ligands and metal ions can be studied *ex situ*, by physically isolating the complexes through their crystallization or precipitation, or *in situ*, with spectroscopic methods. The *ex situ* complex isolation methods show limitations such as time-demanding crystal growth and the presence of impurities trapped within the complex crystals [19,20]. To optimize the complex formation, and consequently the IIPs pre-polymerization conditions, a new *in situ* spectroscopic method was proposed as an alternative to the time-demanding *ex situ* complex isolation [21]. The primary objective of this doctoral work is to produce highly selective adsorbents through the synthesis of original monomers, the study of their complexes with Cu(II), Co(II), and Ni(II) ions, and their application in IIPs preparation. Given this, the main intermediate targets for the experimental work are listed below:

- Synthesis of original functional monomers based on 2,2'-(pyridyl)imidazole (PIM), bis-2-(pyridylmethyl)amine (bis-AMP) and 2-(aminomethylpyridine) (AMP) ligands.
- Investigation of the interactions between the functional monomers and metal ions including Co(II), Ni(II), and Cu(II) through an *in-situ* complex formation study. As result of this study, the optimum pre-polymerization conditions to enhance the selectivity of IIPs are determined.
- Preparation of IIPs for Co(II) and Ni(II) ions and full characterization of their structures.
- Extensive binding and selectivity study of the IIPs to investigate the effect of the new functional monomers and pre-polymerization conditions on metal adsorption and selectivity.

The investigation into complex formation concerning the new functional monomers was focused on their interactions with Cu(II), Co(II), and Ni(II) ions. The ions Co(II) and Ni(II) were chosen because their selective separation is a major challenge in the metallurgical industry and their recovery is a major concern, due to limited occurrence in nature and significant impact on human health. The investigation of the interactions with Cu(II) ion was grounded by the high stability of its complexes with various ligands, a factor which could significantly influence the selectivity of the novel adsorbents.

However, although the complex formation study was initially limited to these three metal ions, the investigation on IIPs selectivity was extended to other metal ions commonly encountered in hydrometallurgical separation processes, including Cd(II), Mg(II), and Mn(II) ions. The materials studied in this thesis were prepared on a laboratory scale with a bottom-up approach, with the synthesis of new monomers and the preparation of IIPs. Consequently, the adsorption experiments were carried out in batch systems, where a small quantity of adsorbent was sufficient to conduct an extensive series of adsorption experiments.

1.3 Structure of the manuscript

This doctoral manuscript is divided into seven chapters. Chapter 1 defines the research background, the purpose of the thesis and the research limits. Chapter 2 provides a literature review concerning the major properties of cobalt and nickel, their industrial recovery, and the methodologies for their selective separation. This chapter also focuses on the components and polymerization techniques applied to prepare IIPs, the optimization of the pre-polymerization conditions, and the description of the Co(II)-IIPs and Ni(II)-IIPs reported in literature. The experimental work and the results obtained during this doctoral project are described and discussed in Chapters 3, 4, 5, 6, and 7. Chapter 3 describes in detail the reagents, equipment, methods, and experimental procedures used to carry out the laboratory work. In chapters 4, 5, and 6 the results concerning each of the three novel monomers are described and discussed. This includes the synthesis and characterization of the new monomers, the preparation and characterization of IIPs, and their application in metal adsorption experiments. Finally, chapter 7 summarizes the conclusions related to the whole experimental work and outlines the future perspectives.

2 Literature study

Table of contents

2.1 Cobalt and nickel

2.1.1 General properties of cobalt and nickel

Properties of cobalt

Cobalt is a transition metal with atomic number 27 that can exist in several oxidation states including -1, 0, +1, +2, +3, +4, and +5 [22,23]. Metallic cobalt is a gray, ductile, brittle, and magnetic element which displays a low reactivity, remaining unoxidized in both dry and moist air under typical environmental temperatures [24]. The magnetic properties and thermal resistance allow the use of cobalt to produce ferromagnetic and high-temperature strength alloys [25,26]. Cobalt's variety of oxidation states make it a diffused coordination center. Organometallic complexes are in fact available for each of the oxidation states of cobalt, among which Co(II) and Co(III) are the most common [27]. Co(II) complexes typically have coordination number 6 or 4 and distorted octahedral or tetrahedral geometries, while Co(III) complexes almost exclusively have coordination number 6 and distorted or regular octahedral geometries [27].

Properties of nickel

Nickel is also a transition metal, very close to cobalt in the periodic table since its atomic number is 28. Nickel is a hard, malleable, and ductile silver-white metal which shows magnetic properties below 360 °C [28]. It is a metal characterized by high resistance to corrosion and to high temperatures. These two properties, combined with its capability to dissolve a large amount of alloying elements, lead to its widespread use in the production of metal alloys [29]. In addition to its metallic form, nickel can exist in several oxidation states, including -1, +1, +2, +3, and +4, which make this element an important coordination center in chemistry and biochemistry [30]. Pharmaceuticals, organic compounds, and polymers can be synthesized using homogeneous nickel catalysis, wherein the reactions primarily involve nickel intermediates in oxidation states of Ni(0), Ni(I), Ni(II), and/or Ni(III) [31]. Hartman et al. studied the complexation of a large series of aminopyridine ligands with Ni(II) (the oxidation state considered in this manuscript), which resulted in octahedral complexes with coordination number 6 in condensed phase, and lower coordination number, equal to either 4 or 5, in gaseous phase [32].

2.1.2 Applications

Application of cobalt

Historically, cobalt was used as a blue dye and its oldest application is estimated to be in the late bronze age, around the 16th century BC [33]. The application of cobalt minerals as pigments is still ongoing and there are several examples in the literature of cobalt-based pigments used to color blue or violet porcelain and ceramics [34–37]. The chemical properties of cobalt allowed it to be widely used in various other sectors of modern industry. Cobalt is a suitable element in the production of superalloys since it imparts

strength, heat resistance, and corrosion resistance to these high-performance alloys, which find application in jet engines and industrial gas turbines where reliability and performance under harsh conditions are essential [38]. Cobalt superalloys were also implemented for permanent surgical implants that required high yield strength and fatigue resistance, high elastic modulus, and that the implant could be safely imaged with magnetic resonance [39,40]. Cobalt was used as a catalyst for chemical reactions such as the hydrogenation of CO_2 [41,42] and the Fischer-Tropsch synthesis [43], which consists in the catalytic conversion of syngas into products like hydrocarbons, oxygenates, and water [44]. Cobalt was used in combination with samarium to produce samarium-cobalt rare earth (Sm-Co-RE) permanent magnetic materials [45]. These materials are considered a valid alternative to the more common neodymium-iron-boron (NdFeB) magnets thanks to their high resistance to corrosion, oxidation, and high temperature, which allows their use in extreme conditions [46]. Sm-Co-RE magnets find various applications including aerospace, microwave communications, magnetic machinery, and production of electric vehicle components [46,47]. Cobalt was also widely applied in the form of lithium cobalt oxide ($LiCoO_2$) in the production of cathodes for rechargeable lithium batteries, providing high stability and charge density to the batteries [48–51].

Application of nickel

The main industrial applications of nickel are the production of stainless steel (46% of Ni supply), followed by the production of nonferrous alloys and superalloys (34% of Ni supply), electroplating (14% of Ni supply) and other uses such as chemical catalysis and the production of battery cathodes (6% of Ni supply) [52]. Different types of stainless steels are available including austenitic steel, ferritic steel, martensitic steel, and duplex steel, and the average percentage of nickel within them range between 0.5-8% [52]. The presence of nickel in stainless steel positively affects both the corrosion resistance of the materials [53] and their toughness and ductility [54]. In addition to the production of stainless steel, nickel is used in combination with other metals to produce nonferrous alloys and superalloys. Examples of nonferrous alloys of nickel include the Ni-Cr alloy used for dental cast [55], the Ni-Ti alloy to produce shape-memory materials [56], and the Ni-Cu alloy applied as a corrosion-resistance catalyst [57]. Approximately 50% by weight of the materials utilized in aerospace engines, particularly in gas turbines, consist of nickel-based superalloys [58]. The wide application of nickel superalloy in such extreme conditions comes from their high heat resistance resulting in high melting temperature, retaining of mechanical and chemical properties at high temperatures, and resistance to thermal fatigue and thermal shock [58,59]. In addition to the formation of metal alloys, it is possible to transfer some properties of nickel onto another material through the electroplating technique [60]. Electroplating consists in electrochemical deposition of a thin layer of nickel on a substrate, giving it resistance to corrosion, higher durability, and a pleasant external appearance [61,62]. Nickel is used in the production of cathodes for Ni-Cd and Ni-metal-hydride (Ni-MH) batteries. Ni-Cd batteries, which contain nickel oxyhydroxide as cathode and metallic cadmium as anode, gained importance as a compact, reliable, life-long electrochemical system which can be reused for a high number of cycles and which have a large temperature operation range [63]. Ni-

MH batteries' electrodes are represented by a hydrogen storage alloy (MH) as anode and nickel hydroxide ($Ni(OH)_2$) as cathode [64]. The mechanism for a Ni–MH battery, described as the movement of hydroxide ions between the metal hydride MH electrode and the $Ni(OH)_2$ electrode, produces a long battery cycle life of more than 1000 cycles, higher power capability, and a dense electrode structure [65]. Nickel is also used as a coordination center for producing several organo-nickel catalysts which are involved in the polymerization of olefines such as ethylene [66–68], propylene [69,70], and 1-hexene [71–73].

2.1.3 **Impact on human health**

Impact of cobalt

Cobalt compounds mainly exist in two valence states, Co(II) (cobaltous) and Co(III) (cobaltic), with the former being more commercially and environmentally prevalent [24,74]. The sole recognized biological role of cobalt is as a component of vitamin B_{12}, while excessive exposure to other cobalt compounds has been associated with toxicity to the environment and the human body [75]. Humans are regularly exposed to various cobalt compounds in their daily lives, primarily encountering it through inhalation of ambient air and the ingestion of food and water containing cobalt compounds [75]. Toxic reactions resulting from cobalt exposure depend on its chemical form, with occupational and environmental exposures mainly involving metallic cobalt particles, and medical exposure, such as in surgical implants, involving cobalt nanoparticles and ions [76,77]. Responses to cobalt particle cause adverse tissue reactions [77] and can be categorized into metal reactivity and metal allergy. Metal reactivity is a normal immunity response to a large amount of metal debris, like adverse respiratory effects, while metal allergy, is an adaptive immunity response to a small amount of metal debris, such as contact dermatitis [75]. Systemic toxic reactions can occur when Co(II) ions enter the bloodstream and spread to different organs [76]. An increased presence of free Co(II) ions compared to bound cobalt increases the risk of toxic effects [78]. Molecular mechanisms of free Co(II) toxicity include the generation of reactive oxygen species, the interruption of mitochondrial function, disturbances in calcium and iron homeostasis, interference with thyroid iodine uptake, induction of genotoxic effects, and possible interference with DNA repair processes [74]. Finley et al. found that reversible hematological and endocrine symptoms are typically linked to lower blood cobalt concentrations (around 300 μg/L), while more severe effects such as neurologic and cardiac symptoms are observed at higher cobalt levels (>700 μg/L) [79].

Impact of nickel

Nickel serves biological functions in plants, bacteria, archaea, and unicellular eukaryotes, where it catalyzes biochemical reaction in several enzymes including urease [80], hydrogenase [81], CO dehydrogenase [82], acetyl-CoA synthase [82], methyl-coenzyme M reductase [83], superoxide dismutase [84], acireductone dioxygenase [80], glyoxalase I [80], and lactate racemase [85]. Even though evolved species do not possess nickel-

containing enzymes, nickel is considered a potentially essential element for animal and human life [86]. The exact role of nickel, making it an essential element, is not completely clarified, and is possibly linked to its use by mammal microbiota [87]. Acting as an immunotoxic and carcinogenic agent, the exposure to nickel at varying doses and durations can cause harmful health effects including contact dermatitis, cardiovascular disease, asthma, lung fibrosis, and respiratory tract cancer [88]. Human exposure to nickel primarily occurs through oral ingestion via water and food, where nickel can be present as a contaminant [89]. Inhalation exposure and handling of nickel-containing items also represent significant pathways for nickel-induced toxicity, impacting the respiratory tract, lungs, and immune system, and causing allergic contact dermatitis, respectively [89]. The exact molecular mechanisms of nickel-induced toxicity are still not fully understood, but mitochondrial dysfunctions and oxidative stress are considered central factors in the toxic effects of this metal [89]. Mitochondria serve as the primary sites for the generation of reactive oxygen species (ROS), which, when present in excess, can cause oxidative stress and damage to unsaturated fatty acids, proteins, and mitochondrial DNA [90]. Mitochondrial dysfunction can interfere with the electron transfer chain, amplifying the ROS generation, which in turn increases oxidative stress, forming a detrimental cycle [91].

2.2 Cobalt and nickel recovery methods

As described in Section 2.1, cobalt and nickel have both a high industrial value, due to their wide range of applications, and an important impact on human health. For this reason, their recovery from ores and industrial concentrates is of fundamental importance. The recovery of cobalt and nickel from ores or concentrates can be carried out with different metal separation processes. This section describes the advantages and limitations of the main cobalt and nickel separation processes, including pyrometallurgical separation, electrolytic separation, biometallurgical separation, and hydrometallurgical separation processes.

2.2.1 Pyrometallurgical separation process

Pyrometallurgy allows the separation of metals from their ores through high temperature processes [92]. The pyrometallurgical separation processes can be divided into raw material preparation, roasting, smelting, and refining steps [93]. Raw material preparation involves the transformation of the starting material, such as concentrate or ore, into a feedstock that possesses specific chemical composition and physical properties required for the subsequent operations [93]. This first step can involve physical operations like batching, mixing, drying, granulating, and pellet-making, and chemical transformations like incineration, calcination, and pyrolysis [93,94]. The raw material preparation is generally followed by the roasting process. In oxidative roasting, the ores are heated in the presence of a controlled amount of oxygen to a temperature lower than the melting point of the target metal, turning the sulfide minerals into metal oxides [95]. The following operation, smelting, consists of the reduction of metal oxides to metal at a

temperature of up to 1400 °C with a carbon-containing reducing agent such as coal, coke, shell charcoal, or anthracite [96]. The obtained products include the target metal and a waste material consisting of slag and the residual of reducing agent utilized for oxide reduction. The target metal, at this stage, retains impurities like sulfur and carbon residues, necessitating an additional purification step [93]. The last purification step, called refining, varies according to the type of impurity and the metal to be treated, and it can take place with physical, chemical, or electrochemical processes. In vacuum distillation, an example of physical refining, the metal is brought to high temperatures under reduced pressure so that the metal remains in the reactor in a condensed form and the impurities evaporate [97]. Chemical refining methods involve chemical reaction such as oxidation, sulfidation, chlorination, or alkalization to eliminate impurities based on their different chemical properties [93]. Electrowinning is a commonly applied electrochemical process for metal recovery [98]. In this process, the target metal ion solution is subjected to an electric current which causes the solid metal deposition on the cathode, while by-products are collected at the anode [98].

Pyrometallurgy is a highly efficient and rapid method for treating large volumes of raw material, showing good flexibility to accept heterogeneous and complex feeds [3]. The major limitations of this technique are related to its strong environmental impact. In fact, pyrometallurgical separations are highly energy demanding and produce polluting by-products such as sulfur and carbon dioxides and particulates [3].

2.2.2 **Electrolytic separation process**

Electrolytic separation processes use electric current to recover metals directly from ores and concentrates [99–101]. Conventional electrolytic techniques can be summarized as two-step processes. Firstly, the metal-containing raw materials are dissociated into anions (typically sulfide S^{2-}) and cations (metal ions) using a supporting electrolyte as a solvent. This is followed by the application of an electric potential difference between the electrodes, with the metal being deposited at the cathode and usually a gas being generated at the anode [101]. The selection of an appropriate electrolyte is crucial, as properties such as high ionic conductivity, rapid mass transport rates, chemical and thermal stability, and a high solubility for the feedstock are required [101,102].

The electrolytic separation process has advantages including adaptability to ores of different grades and lower energy cost and environmental impact when compared with conventional pyrometallurgical methods [100,103]. The main limitations of this method are related to the choice and application of the electrolyte. As reported by Allanore in his review on electrolytes for metal separation processes [102], there is a general lack of understanding and study of the physical chemistry, thermodynamic and electrochemical properties of electrolytes. Furthermore, in the case of separation of metals from molten sulfide salts, major challenges such as limited solubility of sulfur ions within the electrolyte, limited selectivity of sulfide reduction approaches, and the production of solid powders are encountered [99].

2.2.3 Biometallurgical separation process

Biometallurgy refers to the application of biotechnological processes involving interactions between microorganisms and metals or metal-bearing minerals [104]. The two main branches of biometallurgy are bioleaching and bioremediation [105]. Bioleaching, also referred to as biomining, involves the extraction and recovery of metals from ores and waste materials [106]. Bioremediation deals with the elimination or immobilization of harmful contaminants, including radionuclides and heavy metals, from polluted sites [107]. The role of microorganisms in the bioleaching of primary ores aim of oxidize the metal sulfides in the raw material to allow their separation in subsequent steps [106]. The type of microorganism used is directly linked to the metal to be oxidized. In the case of cobalt and nickel, acidophilic bacteria such as *Acidithiobacillus ferrooxidans* [108] and *Acidithiobacillus thiooxidans* [109] are commonly used. Once the metal is oxidized, it is then separated from the solution with common separation techniques such as solvent extraction [110], precipitation [111], ion exchange [112], or adsorption [113].

Bioleaching offers several benefits including high specificity, low energy requirements, the absence of toxic chemicals, and reduced secondary waste production [105,114,115]. The industrial application of bioleaching is limited by the challenging scalability of the process due to the availability and cost of microorganisms, the request for strictly controlled conditions, and a longer duration of the process when compared with traditional chemical leaching [5,104]. Synthetic biology is an emerging field that combines biology, engineering, and computer science to develop new biological systems and organisms with enhanced functionalities [116], and it can provide a toolbox for tailoring organisms for new applications including metal mining, where metal-selective and robust microorganism are required [117].

2.2.4 Hydrometallurgical separation process

Hydrometallurgy is a process of recovering metals from ores, concentrates, or industrial sludges which involves the use of aqueous solutions [118]. Guranathne et al. schematized the hydrometallurgical separation processes into three phases: metal dissolution (leaching step) to obtain the leach solution, purification, and concentration of the leach solution to produce the leach liquor and, finally, the solid metal recovery from the leach liquor (Figure 2.1) [5].

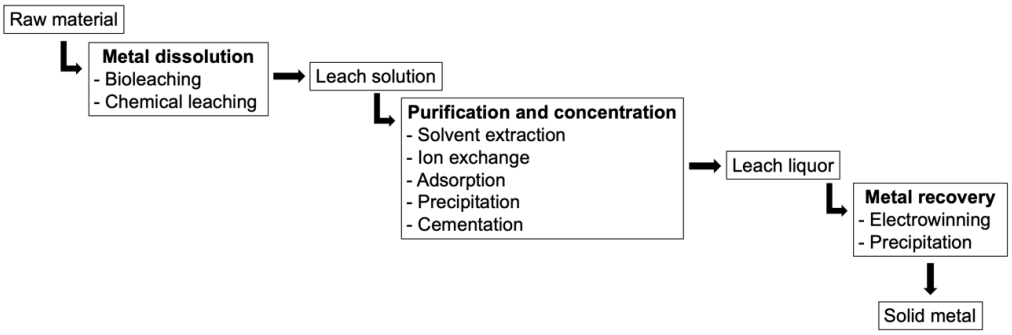

Figure 2.1. Schematization of hydrometallurgical separation processes. Adapted from reference [5].

After sorting and preparing the waste materials, the initial stage in hydrometallurgy is the dissolution of metals, which may occur with chemical leaching or bioleaching methods [119]. The bioleaching process has been described in sub-section 2.2.3. Chemical leaching involves the dissolution or complexation of metals by utilizing leaching agents such as acids, alkali, thiosulfate ($S_2O_3^{2-}$), thiourea ($SC(NH_2)_2$), cyanide (CN^-), and halides [5].

Acidic leaching facilitates the simultaneous dissolution of targeted metals as they are transformed into ionic states by the introduction of hydronium ions from the acidic solvent [120]. Inorganic acids including sulfuric [121], hydrochloric [122], nitric [123], and phosphoric [124] acids are commonly chosen for acidic leaching. Investigations into metal dissolution from waste materials have explored organic acids like citric [125], malic [126], succinic [127], and acetic [128] acids. However, when compared with inorganic acids, the organic acids yield lower metal dissolution rates [129,130]. For alkaline leaching, caustic soda (NaOH) and its derivatives [131–133] or ammoniacal compounds derivatives [134,135] are commonly used. Although it is industrially applied to a lesser extent than acid leaching, basic leaching can be more selective in the extraction of specific heavy metals [5,132]. The choice between acid or alkaline leaching must take into consideration various process parameters, such as the type of raw material, the environmental impact, and the corrosion resistance of the process equipment [136,137].

The use of the other leaching agents, including cyanide, thiosulfate, thiourea, and halides involves problems of environmental or economic sustainability. Due to their high gold recovery yield and cost-effectiveness, cyanide leaching agents have been used in gold mining for over a century [138]. However, the recognized toxicity of cyanide ions for both humans and the environment, combined with the high number of accidents that have occurred in recent decades relating to gold ore where cyanide leaching agents were used, has led to the development of alternatives with a lower environmental impact [139]. A thiosulfate leaching agent was studied as an alternative to cyanides for gold recovery [140]. Even though the metal recovery could be successfully performed with thiosulfate compounds, it resulted in slow gold dissolution and high consumption of expensive reactants, making the process economically unsustainable at an industrial level [141,142].

Thiourea was tested as another alternative to cyanides. Despite a lower environmental impact, thiourea has a higher cost, requires a high amount of reactants, and its application as a leaching agent causes sulfur precipitation and oxidation of solution into disulfide formamidine, resulting in surface passivation [143,144]. Halides, including chloride, bromide, and iodine were efficiently applied as metal leaching agents [145]. Among them, iodine is considered the most suitable leaching solvent due to its lower hazard level and lower volatility [146]. However, the widespread use of iodine on an industrial scale is limited by its high market cost [5].

The leach solution obtained after metal dissolution is then purified and concentrated with common metal separation techniques like solvent extraction, precipitation, cementation, ion exchange, or adsorption to produce the leach liquor. Finally, the solid metal is recovered from the leach liquor through precipitation or electrowinning [5].

Pyrometallurgical and hydrometallurgical techniques are the main approaches used to recover metals from ores and industrial wastes. As previously discussed, even though pyrometallurgy is a highly efficient and rapid method for treating large volumes of raw material, it shows major limitations such as high energy demand and production of polluting by-products [3]. These problems are partially overcome by hydrometallurgical processes, where there is a net decrease in energy consumption and the production of by-products is limited to the reagents used to dissolve and purify the raw materials [4]. Furthermore, the hydrometallurgical processes have the major advantage of being able to regulates the levels of impurities at different stages, providing a balance between metal purity and process cost [4,5].

2.3 Separation techniques for metal purification and concentration

As discussed in sub-section 2.2.4, the three main stages of the hydrometallurgical process are the leaching step, the purification and concentration of leach solution, and the metal recovery from the leach liquor. Techniques commonly used to purify and concentrate the leach solution are solvent extraction, precipitation, cementation, adsorption, and ion exchange. The precipitation method can also be used in the metal recovery step as an alternative to electrowinning. This section describes each of these separation techniques from the point of view of hydrometallurgical separations.

2.3.1 Solvent extraction

Solvent extraction is a chemical process used to separate a substance from a solution by transferring it into a second immiscible liquid phase containing an extractant [147]. Guimarães and Mansur separated calcium and magnesium from a concentrated nickel sulfate solution using, in two different steps, two extractants [148]. The first solvent extraction was performed with di-2-ethylhexylphosphoric acid (D2EHPA, Figure 2.2) at pH 3 and led to the removal of 98.6% of calcium. The second extraction was performed using bis-2,4,4-trimethylpentyl phosphinic acid (Cyanex® 272, Figure 2.2) at pH 5.7 as

extractant and 99% of magnesium was separated. In this step, less than 10% of the initial nickel was co-extracted with magnesium. The nickel-enriched leach liquor obtained after the solvent extraction of calcium and magnesium was finally suitable to recover nickel with electrowinning.

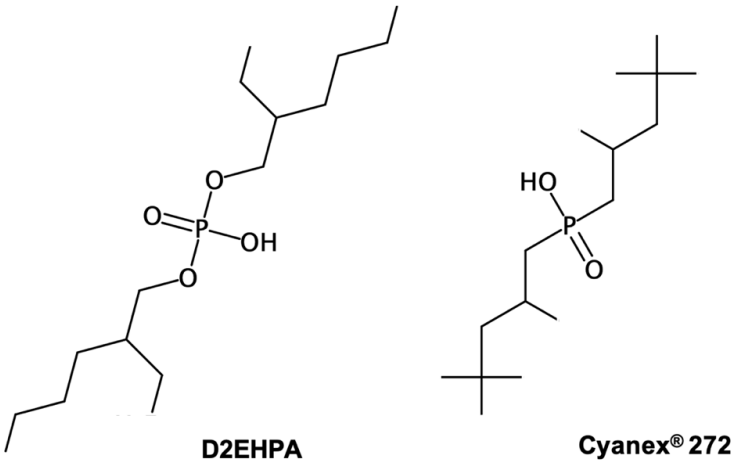

Figure 2.2. Structures of D2EHPA and Cyanex® 272 extractants.

Granata et al. developed a multi-step solvent extraction process to separate manganese and cobalt from nickel contained in a mixed battery waste solution [149]. The authors first tried to carry out the whole separation process with Cyanex® 272 as the sole extractant. However, a selective separation of cobalt and manganese was not possible as these two metals were co-extracted by Cyanex® 272. For this reason, manganese was first completely separated from nickel and cobalt with a multi-step solvent extraction with D2EHPA at pH 4. The separation of cobalt from nickel was then carried out with a separate solvent extraction process using Cyanex® 272 as the extractant at pH 5.5 and nickel-enriched leach liquor was obtained.

Solvent extraction is a versatile, convenient, and efficient method for the separation of metallic species from mixed metal aqueous media [150]. However, limitations relating to its environmental and health impact are an issue. The extractant is commonly diluted in toxic and volatile organic solvents such as kerosene [151,152], hexane [153], and heptane [154], and the processes are carried out at temperatures around 40–70 °C, resulting in fast loss of solvent, air pollution, and operator safety concerns [155].

2.3.2 **Precipitation**

Precipitation is a historically important metal separation method that is currently widely applied in hydrometallurgy [156]. Separation and recovery of metals with the precipitation method involves chemical reagents capable of forming insoluble compounds with either impurities or with the target ions present in solution [157].

Precipitation methods can be used both in the leach solution purification and concentration step and in the metal recovery step [158,159].

Metal ions dissolved in solution are typically precipitated as hydroxides, carbonates, or sulfides. For example, Chen et al. proposed a hydrometallurgical process to recover iron, nickel, and chromium from a stainless-steel industry sludge [160]. After acidic leaching, 99% of iron could be efficiently recovered by a two-stage solvent extraction with D2EHPA at pH 1.5. At the end of the separation process, the recovery of 99.5% of nickel and 75% of chromium was achieved by chemical precipitation with NaOH. Laokhen et al. applied precipitation as the first step in their hydrometallurgical separation process [161]. Nickel was precipitated by adjusting the solution pH to 13 with a solution of 2 M NaOH. The nickel precipitate was then separated and dissolved in 2 M sulfuric acid. Finally, 61% of nickel was recovered with the electrowinning method. Takano et al. separated nickel, cobalt, and rare earths elements (REEs) from spent nickel–metal-hydride batteries [162]. The precipitation method was applied as a final step to recover 87% of nickel and 90% cobalt as a nickel–cobalt mixed sulfide agent with less than 0.05% of REEs as impurity, using Na_2S as precipitating agent. Meshram et al. studied the recovery of lithium, cobalt, nickel, and manganese from the cathodic active material of spent lithium batteries [163]. The metals were leached with 1 M H_2SO_4 and 0.075 M $NaHSO_3$ as reducing agent. Cobalt with a purity of 95.91% (with 3.81% of nickel and 0.28% of manganese as impurities) was recovered from the leach liquor using oxalic acid as precipitating agent at pH 1.5. NaOH was then added to leach liquor enriched in manganese, nickel, and lithium, to reach a pH value of 7.5 and 92% of manganese was precipitated as carbonate with Na_2CO_3. The remaining solution was led to pH 9 through further addition of NaOH and saturated with Na_2CO_3 to precipitate 89% of nickel as carbonate. Lithium with a purity of 98% was finally recovered as carbonate salt at pH 14.

The precipitation method was applied as a multi-step process for the separation and recovery of different metals. However, this method requires detailed planning of the separation process, which in any case does not guarantee the absence of partial co-precipitation of two or more metals [163].

2.3.3 **Cementation**

Cementation, a special precipitation technique, is an important and widely used method for the hydrometallurgical separation processes of metal ions [164]. The cementation process involves a spontaneous reaction where a relatively inexpensive solid metal is used to recover a more valuable dissolved metal. It is a redox process in which the target metal ions are precipitated in their elemental metallic state on the surface of the sacrificial metal through spontaneous electrochemical reduction, while the sacrificial metal is solubilized in its oxidized state [165]. The cementation efficiency is closely related to the difference in redox potential (E) between the target metal ($E_{M^{x+}/M}$) and the sacrificial metal ($E_{S^{x+}/S}$). A sacrificial metal is suitable for target metal reduction when $E_{S^{x+}/S}$ is lower than $E_{M^{x+}/M}$ [166]. Makhloufi et al. studied the cementation of Ni(II) ions from acidic

sulfate solutions using a zinc electrode [167]. The variation of Ni(II) concentration during the cementation process was monitored with cyclic voltammetry. The process resulted in a diffusion-controlled first-order reaction whose rate was influenced by the variation of zinc electrode surface area over time. The cementation reaction caused a progressive corrosion of the zinc electrode. This corrosion initially resulted in an expanded surface area, contributing to an enhanced efficiency of the cementation process. However, a prolonged cementation and increased corrosion of the zinc electrode negatively affected the process efficiency, highlighting the need for precise control and optimization of the process. The efficiency of the cementation process can be improved by using one or more cementation activators. Cementation activators are substances which are introduced in the treated solution to enhance the kinetic of the metal deposition process [168]. Boyanov et al. studied the cementation of cobalt and nickel from a $ZnSO_4$ industrial solution using zinc dust as sacrificial metal and $CuSO_4 \cdot 5H_2O$ and $KSbC_4H_2O_6 \cdot 1.5H_2O$ as activators [8]. In the first step, the cementation after addition of $CuSO_4 \cdot 5H_2O$ was studied, resulting in nickel reduction to a greater extent than the one of cobalt, producing metallic nickel with a purity of 67-69%. The following addition of $KSbC_4H_2O_6 \cdot 1.5H_2O$ as second activator resulted in the recovery of 98% of metallic cobalt within an optimum time of 60-75 minutes, after which back-dissolution occurred. Choi et al. studied the cementation of cadmium, cobalt, nickel, and zinc ions in sulfate solution with aluminum as sacrificial metal and activated carbon (AC) as cementation activator [169]. The cementation of the target metals was first tested without the activator, which resulted in around 0% of metal recovery. After the addition of AC, the metal recovery values increased to 96%, 61%, 57%, and 45% for zinc, nickel, cobalt, and cadmium, respectively. The authors explained this result by identifying the role of AC as an electron bridge from aluminum (electron donor) to metal ions (electron acceptors). The major limitation of this process appeared to be the passivation of the solid metal surface by the $Al(OH)_3$ developed during the process, which prevented further metal ion removal from the sulfate solutions.

2.3.4 **Adsorption**

IUPAC defines adsorption as an increase in the concentration of a dissolved substance at the interface of a condensed and a liquid phase due to the operation of surface forces [170]. Adsorption can be a physical or chemical phenomenon and the difference lies in the type of interaction between adsorbate and adsorbent. Physical adsorption is based on weak interactions such as van der Waals forces, while chemical adsorption involves the formation of stronger chemical interactions such as covalent or ionic bonds [171,172]. In hydrometallurgy, adsorbates are metal ions while adsorbents are commonly natural or synthetic solid materials.

The most widely applied natural adsorbents are activated carbon [173–175], clay minerals [176,177], zeolites [178,179], and biomass [180–182]. The use of natural adsorbents brings significant advantages in terms of both environmental and economic sustainability as they are typically available in large quantities, are of low cost, and their disposal is facilitated by their biodegradability [183,184]. However, these materials have various applicative limitations including low reusability in harsh conditions, lack of selectivity,

low thermal stability, and slow adsorption kinetic [185,186]. To overcome these disadvantages, several synthetic adsorbents such as silica-based materials or polymeric resins were designed.

Although silica is a naturally occurring mineral, silica-based adsorbents are synthetic materials. They are mainly produced by the sol-gel process through hydrolyzation and condensation of an organoalkoxysilane precursor [187]. Silica-based materials for the adsorption of Ni(II) or Co(II) were applied in several forms and compositions, including silica gel [188–190], mesoporous and nanoporous silica [191,192], and silica-based nanotubes [193]. Salmani et al. synthesized a mesoporous silica adsorbent for Co(II) adsorption [192]. The material was characterized by SEM, showing a high porosity honeycomb-like structure and was able to separate up to 89% of Co(II) from a starting concentration of 5 mg/L in 8 h. Faghihian et al. modified a silica aerogel with amino propyltriethoxysilane and tested the new material for Cu(II) and Ni(II) adsorption [190]. The material proved to be a good adsorbent for both Ni(II) and Cu(II) with maximum adsorption capacities at pH 6 equal to 27.7 mg/g and 47.6 mg/g, respectively. Silica-based adsorbents commonly have a high surface area, which results in a high adsorption capacity. Moreover, these materials have high thermal and corrosion resistance, cost-effective synthesis, and functional groups which can be easily modified [194,195]. Despite these good features, their industrial application is limited by the polluting by-product released and the difficult scale-up and control of the sol-gel synthesis methods [194].

Polymeric resins for metal adsorption were prepared by direct copolymerization of commercial monomers, such as the poly(styrene-*co*-divinylbenzene) Amberlite™ XAD 4 [196] and Amberlite™ XAD 16 [197] resins. Due to their hydrophobicity, these resins suffered a limited binding capacity for polar analytes and needed a conditioning step with a wetting solvent before their application as adsorbents [198]. The impregnation of commercial resins with ligands allowed to overcome this problem and to increase the selectivity of the sorbents [199]. However, a significant limitation of the impregnated resins was the partial leaching of the ligands during the adsorption process [198]. This issue, which caused a limited reusability of the resins, was addressed by the immobilization of ligands onto the resin structures through the formation of chemical bonds [200,201]. Classes of ligands commonly used for the preparation of polymeric resins applied for the adsorption of Co(II) and Ni(II) ions include amines [202,203], carboxylic acids [204], thiolates [205], and imidazole derivatives [206,207]. Examples of functionalized resins, such as Amberlite™ XAD 2 modified by *o*-aminophenol, [208] poly(vinylpyridine) modified by dithizone [205], and chloromethylated polystyrene (CMPS) modified by 1-vinylimidazole [207] are illustrated in Figure 2.3.

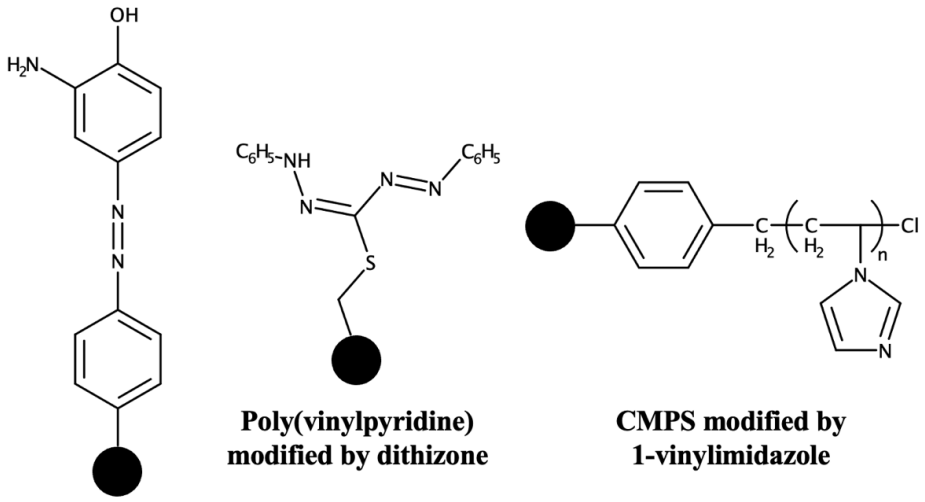

Figure 2.3. Structures of polymeric resins used for metal adsorption. The black circles represent the poly(styrene-*co*-divinylbenzene) backbone in Amberlite™ XAD 2 modified by *o*-aminophenol [208], the poly(vinylpyridine) backbone in poly(vinylpyridine) modified by dithizone [205], and the polystyrene backbone in chloromethylated polystyrene (CMPS) modified by 1-vinylimidazole [207].

Li et al. synthesized a polyamine chelating resin for Ni(II) and Co(II) adsorption [203]. The maximum adsorption capacities in single component systems were equal to 0.98 mmol/g for Ni(II) and 0.74 mmol/g for Co(II). In binary systems, containing both Ni(II) and Co(II) ions, the resin showed a slightly higher selectivity for Ni(II). However, the co-adsorption of both Ni(II) and Co(II) ions occurred. This led to the reduction of the adsorption capacity for both ions when compared to single component solutions. Chen et al. introduced 1-vinylimidazole onto the surface of chlorinated polystyrene to prepare a novel chelating adsorbent [207]. The polymeric resin was tested in Cd(II), Pb(II), Cu(II) and Ni(II) ions adsorption experiments. The adsorption capacity at pH 5 was equal to 2.82, 1.77, 1.22, and 0.83 mmol/g for Cd(II), Ni(II), Pb(II), and Cu(II), respectively. In addition to a high adsorption capacity, the material showed good reusability up to 10 adsorption/desorption cycles and a fast desorption rate. When selectivity was tested in multi-component solutions, the resin showed higher affinity for Cd(II) over Ni(II), Cu(II) and Pb(II) ions. However, the co-adsorption of the other competitive ions occurred.

The separation of heavy metals by adsorption offers several benefits, including fast kinetics, simple equipment requirement, low energy consumption, and the possibility to address a wide range of contaminants [209,210]. However, these materials show limitations such as high production and regeneration costs, loss of material during the regeneration cycles, and limited selectivity [209,211].

2.3.5 **Ion exchange**

Ion exchange is a reversible chemical process involving the replacement of specific ions contained in a solution with those present in a solid phase material, named ion exchanger. The replacement of ions occurs via direct contact between the treated solution and the ion exchanger. The ion exchanger can be regenerated by eluting the exchanged ions with an appropriate solvent, thereby restoring it to its initial condition. Commercially available cation exchange resins are usually formed by a porous crosslinked poly(styrene-*co*-divinylbenzene) network to which functional groups, acting as ion exchange sites, are anchored [212]. The functional groups of cation exchange resins are commonly sulfonic, carboxylic, or phosphonic acids [212]. Examples of cation exchange resins containing each of these functional groups, including the sulfonic acid resin Amberlite™ IRC 120 [213], the iminodiacetic acid resin Lewatit® TP 207 [214], and the aminophosphonic acid resin Lewatit® TP 260 [215] are illustrated in Figure 2.4.

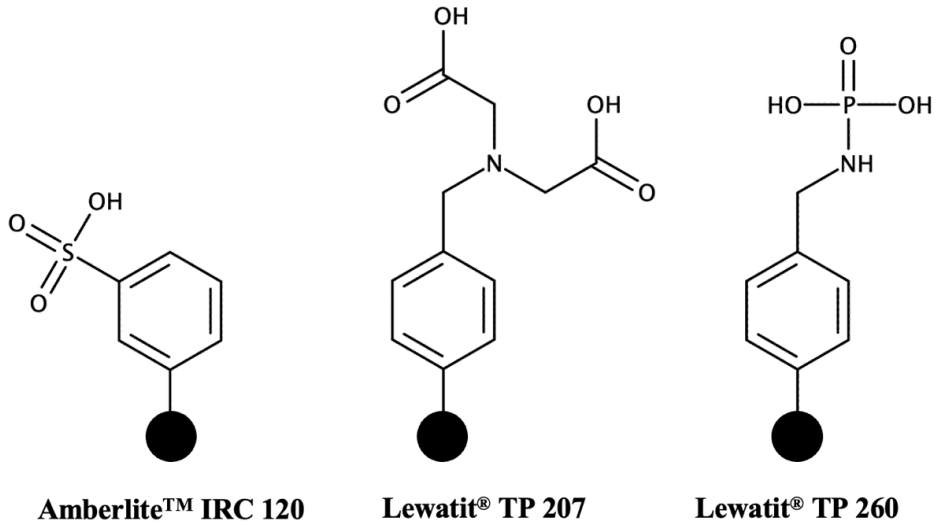

Figure 2.4. Structures of the cation exchange resins Amberlite™ IRC 120 [213], Lewatit® TP 207 [214], and Lewatit® TP 260 [215]. The black circle represents the poly(styrene-*co*-divinylbenzene) backbone of the resins.

The nature of the resin strongly affects the selectivity toward a specific ion. Jurrius et al. separated copper and zinc with concentrations of 20 mg/L and 30 mg/L from a 20 g/L cobalt solution using two different ion-exchange resins [216]. The separation of copper was carried out with the iminodiacetic acid-based resin Lewatit® TP 207. This first step was followed by the separation of zinc with the aminophosphonic acid-based resin Lewatit® TP 260. The concentration of both copper and zinc in the cobalt solution was reduced to a value below 1 mg/L. Taute et al. developed an ion exchange process to remove zinc in concentration of 30 mg/L from a 70 g/L nickel metal refinery solution

[217]. Two different ion exchangers were tested, the resin Lewatit® VP OC 1026 (functional group D2EHPA, Figure 2.2) and the resin Purolite S950 (functional group aminophosphonic acid). The best separation was obtained with the ion exchanger Lewatit® VP OC 1026, which allowed the separation of zinc up to 40% of its initial concentration. According to the results, D2EHPA used as a functional group (Lewatit VP OC 1026) was more selective to zinc over nickel than aminophosphonic acid (Purolite S950).

The main advantages of ion exchange resins include their ability to remove metals at parts per billion (ppb) levels, the possibility to manage large volumes of effluent [218], and the versatility for both continuous and batch flow [219]. The major limitations of this technique are the instability to acids or ionizing radiations [220], the sensitiveness to pH variations [219], and its ineffectiveness when dealing with metal solutions containing impurities such as organic matter or particulate, because the exchange matrix is prone to get fouled by impurities [221].

2.4 Selective separation of cobalt and nickel

As described in the previous section, when dealing with the separation of metal species with similar chemical properties, as in the case of Co(II) and Ni(II) ions, common separation techniques often lack selectivity. Different approaches to enhancing selectivity were proposed in literature. This section provides a description of the methodologies used to increase the selectivity in the separation of Co(II) ions from Ni(II) ions and vice versa.

2.4.1 Selective solvent extraction

To discuss the selectivity of solvent extractants it is fundamental to introduce two parameters, the pH_{50} and the $\Delta(pH_{50})$ [222]. The value of pH_{50} corresponds to the pH value to reach 50% of target metal extraction. The value of $\Delta(pH_{50})$ is defined as the difference in pH_{50} values for two metals extracted in the same conditions [222]. The higher the $\Delta(pH_{50})$, the more selective is the separation of two metals by solvent extraction. The industrial separation of cobalt and nickel by solvent extraction began in the 1970s at Matthey Rustenburg Refiners in South Africa, using D2EHPA as selective extractant [223]. The selectivity of this process was strongly influenced by the extraction temperature. When the solvent extraction was carried out at 20 °C, the $\Delta(pH_{50})$ value for cobalt and nickel extraction was limited to ~ 1 pH unit (Figure 2.5), resulting in the co-extraction of the two metals. The selective separation of cobalt and nickel was achieved by increasing the temperature to 50 °C. At this temperature the $\Delta(pH_{50})$ for cobalt and nickel extraction was equal to ~ 2 pH unit (Figure 2.5), allowing their selective extraction.

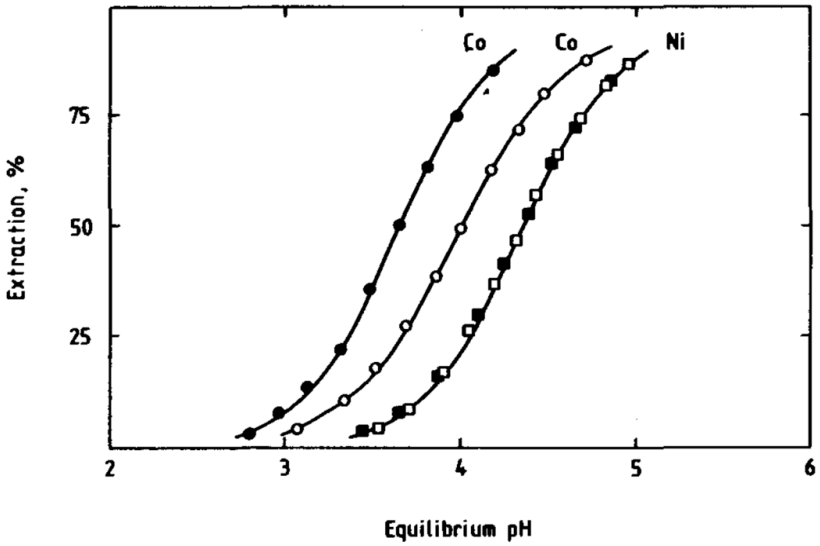

Figure 2.5. Extraction of cobalt and nickel by 0.45 M D2EHPA in xylene at 20 °C (empty symbols) and 50 °C (full symbols). Reprinted without modification from reference [223].

The selectivity of D2EHPA as extractant for cobalt and nickel separation derived from the different hydrophobicity of its complexes with the two metals [224]. The complex between cobalt and D2EHPA is hydrophobic and thus has higher affinity for the organic phase. Conversely, the complex between nickel and D2EHPA can contain up to two water molecules, which make it more hydrophilic and increase its affinity for the aqueous phase [224]. The selectivity of cobalt and nickel solvent extraction was significantly enhanced with the introduction of the dialkyl phosphinic acid reagent Cyanex® 272 [11]. This innovative reagent enabled the selective extraction of cobalt from solutions with a Ni/Co ratio exceeding 100 [11]. Following its introduction to the market, Cyanex® 272 was applied in several hydrometallurgical processes involving cobalt and nickel separation [225–230]. Beyond its remarkable selectivity in cobalt extraction, the success of Cyanex® 272, which is estimated to be involved in around 40% of Western hemisphere cobalt recovery, can also be attributed to its chemical stability and high resistance to oxidative degradation [231].

2.4.2 **Selective precipitation**

As described in sub-section 2.3.2, precipitation methods through the addition of a precipitating agent were used for the separation and/or recovery of cobalt and nickel, mainly as metal hydroxides or sulfides. Cobalt and nickel hydroxides have very close solubility products, equal to $1 \cdot 10^{-15}$ and $2 \cdot 10^{-15}$, respectively, which result in their co-precipitation [232]. Oustadakis et al. studied the precipitation of cobalt and nickel as hydroxides from a sulfate leach liquor containing 0.16 g/L of Co(II), 3.77 g/L of Ni(II), 0.76 g/L of Mn(II) and 21 g/L of Mg(II) at pH 4.5 [233]. The optimum precipitation

conditions were obtained at pH 9 with the addition of 0.2 g of MgO as nucleation agent. In this conditions, poor selectivity was obtained as 99.93% of the initial nickel, 99.04% of the initial cobalt and 92.21% of the initial manganese were precipitated. The resulting mixed precipitate material contained 25% of nickel, 1.5% of cobalt, 3% of manganese, and 26% of magnesium (deriving from unreacted MgO). The difference in cobalt and nickel sulfides solubility products, equal to $3 \cdot 10^{-26}$ and $1.4 \cdot 10^{-24}$, respectively, is slightly higher than one of the corresponding hydroxides, but still too low to ensure the selective separation of the two metals [232]. Xie et al. studied the recovery of nickel, copper and cobalt from sulfide tailings containing these three metals and iron [234]. The metals contained in the sulfide tailings were leached by a mixed nitric-sulfuric acids solution. This step was followed by the recovery of 95% of the leached iron by precipitation at 90-95 °C and pH 1.9 with Na-jarosite, a family of iron-hydroxysulfate minerals. The remaining solution, enriched in nickel, copper, and cobalt, was treated with a 10% solution of Na_2S at pH 7.5. This operation resulted in the recovery of 95% of the leached nickel, 99% of the leached copper, and 98% of the leached cobalt as a mixture of their sulfide precipitates [221]. A sharp improvement in selectivity was achieved by Chen et al., who proposed a selective-precipitation method with organic precipitating agents to recover nickel, cobalt, manganese, and lithium from waste cathodes solution [12]. As a first step, 98% of the initial nickel was recovered using dimethylglyoxime as precipitating agent at pH 6. Dimethylglyoxime selectively reacted with nickel to form Ni-dimethylglyoxime precipitate, resulting in the almost quantitative precipitation of nickel, which contained only a minor amount of other metals as impurities. A second precipitation was then carried out introducing ammonium oxalate at pH 6, which resulted in the precipitation of 97% of the initial cobalt and a minor extent of manganese. Manganese was then separated by solvent extraction with D2EHPA at pH 5 which led to the recovery of 97% of the initial amount. Finally, 89% of the initial lithium was recovered through precipitation with 0.5 M Na_3PO_4. The selectivity in precipitation method was thus improved by using a nickel-selective precipitating agent [12].

2.4.3 Selective adsorbents and ion exchangers

Adsorbents and ion exchangers have great potential to eliminate trace amounts of metal cations, below 1 mg/L, which is crucial to meet the high-purity electrolytes requirement in cobalt and nickel electrowinning [235,236].

In sub-sections 2.3.4 and 2.3.5, a clear distinction was made between adsorbents and ion exchangers with the aim of providing a clearer picture of their operating principle. However, the retention mechanism of a material, either adsorption or ion exchange, can vary depending on the experimental conditions and target metal ion [237,238]. For example, the bis-2-(pyridylmethyl)amine (bis-AMP) containing Dowex™ M4195 chelating resin was studied for the retention of several ions, among which UO_2(IV), Co(II), and Ni(II) [238]. The retention of UO_2(IV) was found to occur via the ion exchange mechanism, while the retention of the other ions studied occurred via metal-chelating adsorption. Dowex™ M4195 was used at the Chambishi Metals refinery (Zambia) for the treatment of sulfide concentrates leach liquor to obtain copper and cobalt

cathode products [235]. The resin was applied to reduce the nickel concentration below 160 mg/L in a starting solution containing ~900 mg/L of nickel and 40 g/L of cobalt. The separation reduced the percentage of nickel as impurity within the cobalt cathode product to a level below 0.1%. However, a major limitation of Dowex™ M4195 resin was the strong copper retention, which required highly concentrated H_2SO_4 or ammonia for its elution. This problem was solved by the modification of bis-AMP with hydroxypropyl functionality to produce the hydroxypropylpicolylamine (HPPA) Dowex™ XUS 43605 resin, which allowed the elution of copper in milder conditions [13]. Dowex™ M4195 and Dowex™ XUS 43605 resin structures are shown in Figure 2.6.

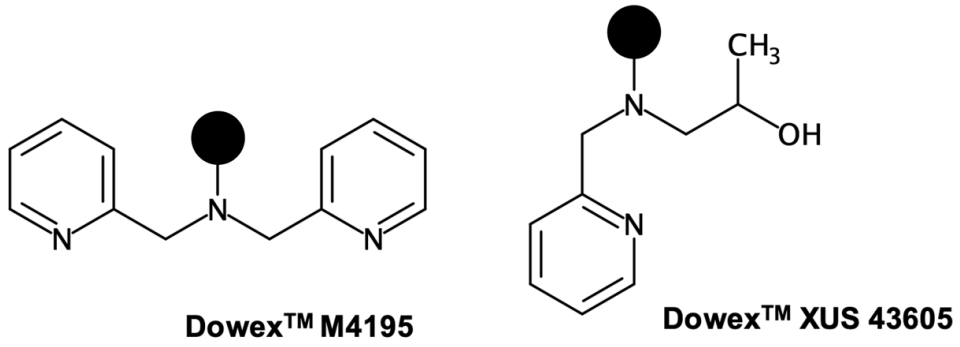

Figure 2.6. Dowex™ M4195 and Dowex™ XUS 43605 structures. The black circle represents the poly(styrene-*co*-divinylbenzene) backbone of the resins.

As discussed, the selective separation of cobalt and nickel with adsorbents and ion exchangers was mainly obtained through the design and synthesis of materials with new functionalities. However, when dealing with hydrometallurgical solutions, the competitive adsorption of other metal species during cobalt and nickel separation typically occurred. This issue required sequential separation processes and accurate stepwise leaching procedures, and highlighted the lack of selectivity of these materials.

2.5 Ion-imprinted polymers

The ion imprinting technique is an efficient and convenient tool for enhancing the selectivity of adsorbent materials. This technique was first introduced by Nishide et al. who synthetized poly(vinylpyridine) resins with different metal ions as a template [239]. The ion-imprinted resins showed an increased selectivity toward the template ion when compared to the same resin synthetized without a metal template. In the following decades the ion-imprinting technique was widely applied for the separation of several valuable and/or hazardous ions, including rare earth elements [240], radionuclides [241], heavy metals [242], and noble metals [243]. The synthesis of metal selective IIPs is the core topic of this doctoral manuscript, and a more in-depth description of this class of materials is provided in this section.

2.5.1 Preparation of ion-imprinted polymers

Prasada Rao et al. defined ion-imprinted polymers (IIPs) as nano-porous polymeric materials which, after leaching of the template ion introduced during their preparation, can selectively rebind, sense or transport the target analyte in the presence of closely related inorganic ions [15]. The peculiar selectivity of IIPs derives from their method of preparation, which can be schematized in three steps (Figure 2.7) [14].

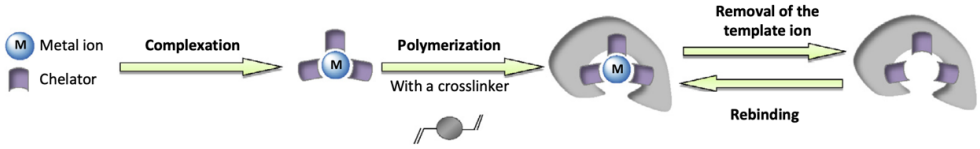

Figure 2.7. Synthesis of ion-imprinted polymers. Adapted from reference [14].

First a complex is formed between a chelator (either a ligand or a chelating monomer) and a template ion. The complex is then immobilized using a crosslinker, forming a stable polymeric network. Finally, the ion used as a template is removed by a leaching agent, generating three-dimensional binding sites. The binding sites obtained with this procedure are complementary to the ion used as a template and are expected to be selective toward it.

2.5.2 Components in IIPs synthesis

The components necessary for the synthesis of IIPs are a chelator, a template ion, a crosslinker, a solvent, and an initiator. The choice of each of these components strongly affects the performance and morphology of the final product. It is therefore essential to understand the impact of each of them.

Chelator and template ion

The chelator possesses one or more donor atoms (e.g., oxygen, nitrogen, sulfur, or phosphorus) owning lone electron pairs which interact with the target ion through coordinate covalent bonds (Figure 2.8). The stoichiometry and stability of the complex determine how specific the IIP cavities will be toward the target ion, thereby strongly influencing its selectivity [16]. The study of complex formation between chelator and template ions is discussed in detail in sub-section 2.5.3.

The chelators used in the literature to synthetize IIPs can be divided into three categories: commercial monomers, ligands physically trapped in the IIPs, and ligands modified by the introduction of a polymerizable group (chelating monomers). Commercial monomers for IIPs production include acrylic acid (AA) [244], methacrylic acid (MAA) [245], 1-vinylimidazole [246,247], 4-vinylpyridine (4-VP) [248], and acrylamide [249]. The presence of a polymerizable group within their structure combined with their relatively

low cost make their application a fast and convenient way to prepare IIPs. The introduction of the trapping technique [250] and the search for highly selective chelators led to an extensive application of ligands in IIPs preparation. The trapping technique allows the incorporation of a ligand that does not have a polymerizable group within the IIP structure. The ligand-template ion complex is mixed with a monomer which is then copolymerized with a crosslinker. In this way, once the polymerization is complete, the ligand is physically trapped within the polymeric network. Many examples of ligands trapped within IIPs are available in the literature, including the widely applied diphenylcarbazide (DPC) [251–254], 5,7-dichloroquinolin-8-ol [250,255,256], phenobarbital [257], 8-hydroxyquinoline (8-HQ) [258], dimethylglyoxime [259], and dithizone [260]. Although trapping has significantly increased the number of chelators that can be used in the preparation of IIPs, it shows the major disadvantage that the IIPs produced with this technique can release the ligand during diverse application steps. This was demonstrated and described by Moussa et al. in their work by preparing an IIP with a ternary complex of neodymium, 4-VP and 5,7-dichloroquinoline-8-ol as template ion, monomer, and ligand, respectively [255]. A release of the 5,7-dichloroquinoline-8-ol ligand up to 51% during the IIP leaching, sedimentation, and washing steps was evidenced via HPLC-UV analysis. The modification of the ligands through the introduction of a polymerizable group in their structure allows us to overcome this problem. Several commercial ligands have been modified and used for IIPs preparation, such as 8-HQ [261], iminodiacetic acid [19,262], and crown ethers [263–265]. The modification of the ligand structure with polymerizable groups (such as vinyl, acrylate, methacrylate, or acrylamide groups) allows its stable introduction within the IIPs due to the formation of covalent bonds with the crosslinker. Although the modification of the commercial ligands is advantageous for the stability of the IIPs during their application, this process requires a further synthesis compared to the normal preparation of IIPs and therefore involves an additional demand of time and money. Some examples of chelators for each of these three categories are shown in Figure 2.8.

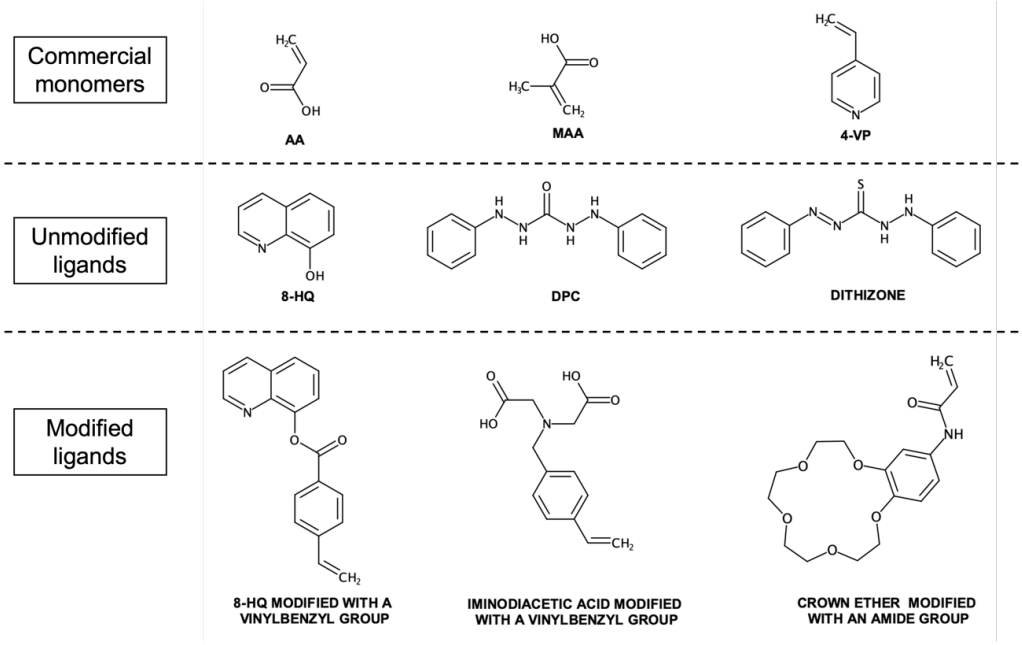

Figure 2.8. Some examples of commercial monomers, unmodified ligands and modified ligands (8-HQ [261], iminodiacetic acid [262], and crown ether [263]) used for IIPs preparation.

Initiator and crosslinker

The synthesis of IIPs commonly occurs via free radical polymerization. The initiator has the task of producing the first radicals to start the propagation of the polymeric chain. The initiator used in almost all the synthesis of IIPs is azobisisobutyronitrile (AIBN) [242]. Benzoyl peroxide (BPO) [248,266] and N,N,N',N'-tetramethylene diamine (TEMED) [267,268] represent two alternative initiators applied for IIPs preparation.

In the synthesis of IIPs, crosslinkers are used as co-monomers and their main role is to stabilize the binding cavities within the three-dimensional polymeric network [14]. The ratio between monomer and crosslinker also significantly influences the porosity of the final product [269]. The most applied crosslinker in the synthesis of IIPs via radical polymerization is the ethylene glycol dimethylacrylate (EGDMA) [16,270–275], followed by divinylbenzene (DVB) [276–279] as a widely diffused alternative. Other crosslinkers used to a lesser extent in the radical polymerization of IIPs include trimethylpropane triacrylate (TMPTA) [254,280], 3-(acryloyloxy)-2-hydroxypropyl methacrylate [281], pentaerythritol triacrylate (PETRA) [282], and trimethylolpropane trimethacrylate (TRIM) [280,283]. When IIPs are synthetized via sol-gel process or polycondensation, the most used crosslinkers are tetraethoxysilane (TEOS) [284–287] and epichlorohydrin (ECH) [288–291], respectively. Figure 2.9 illustrates the structures of the most common crosslinkers used for IIPs preparation.

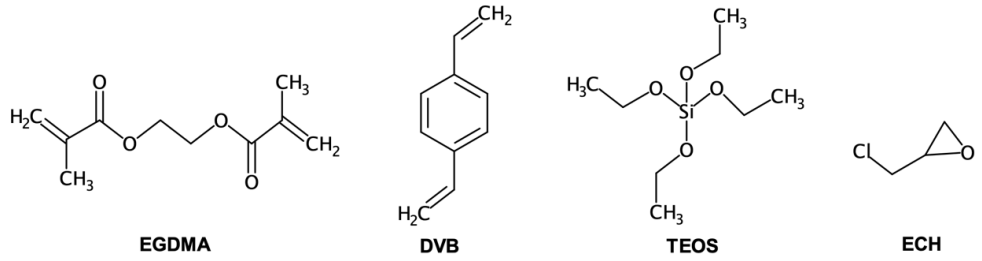

Figure 2.9. Commonly used crosslinkers for IIPs preparation.

Solvent

In the preparation of IIPs, the two main roles of the solvent are to solubilize all the components of the pre-polymerization mixture and to generate pores in the polymer structure. To underline the importance of the solvent in the generation of pores, in the field of IIPs it is often referred to as porogen [292]. Even though there are some examples of IIPs synthesis in water [268,293,294], the porogen is commonly an organic solvent and its polarity plays a crucial role for its choice. Polar protic solvents such as ethanol and methanol (relative polarity respect to water equal to 0.654 and 0.762, respectively) strongly interact with the metal-ligand complex, reducing its stability. It is therefore convenient to apply aprotic solvents such as acetone [295–297], dimethylformamide (DMF) [298,299], dimethylsulfoxide (DMSO) [271,300,301], and acetonitrile (ACN) [302–304] (relative polarity respect to water equal to 0.355, 0.386, 0.444, and 0.460, respectively). Non-polar solvents such as toluene [305] and chloroform [254] (relative polarity respect to water equal to 0.099 and 0.259, respectively) have weak interaction with the metal-ligand complex, favoring its stability. Despite this, being unable to solubilize all the components of the pre-polymerization mixture they are often used in mixtures with polar solvents [254,306].

2.5.3 Chelator-template ion: complex formation study

The selectivity of IIPs derives from the complementarity of the binding sites in terms of size, shape, dimension, and charge with those of the target ion [14]. The level of complementarity between the chelating binding site and the target ion depends on specificity and strength of the complex they form in the pre-polymerization mixture. Based on the ratio between the chelator and template ion [16] and on the solvent in which the reactants are solubilized [307], complexes with different stoichiometries can be formed. As illustrated at the beginning of this section (sub-section 2.5.1), in the preparation of IIPs, the complex is immobilized with a crosslinker and, once the metal has been removed by a leaching agent, a cavity complementary to the metal is generated. The complex structure adjusted in the pre-polymerization media determines the complex structure within the IIP, with relevant effects on adsorption capacity and selectivity [16]. In 1:1 metal-chelator stoichiometry complexes, the metal interacts with only one chelator molecule and the resulting cavity within the IIP structure is likely to present low

selectivity toward the target metal. Conversely, if the complex immobilized by the crosslinker has a 1:2 or 1:3 metal-chelator stoichiometry, the resulting cavity will have a more specific geometry, being more complementary to the target metal, and the resulting IIP might be more selective. For this reason, the study of the formation of complexes between chelator and metal ion and the optimization of the stoichiometry in the pre-polymerization mixture are of crucial importance to producing highly selective IIPs. The formation of the complexes can be realized *ex situ*, by physically isolating the complex, or *in situ*, in pre-polymerization conditions.

Ex situ complex formation study

The production of IIPs with *ex situ* complex formation involves the separate synthesis of the complex between chelator and metal ion. Once synthesized, the complex is isolated and then added as a second step to the pre-polymerization mixture. Similarly, the *ex situ* complex formation study requires that, before the complex is analyzed with the technique that best suits its chemical properties, it is physically isolated. Complexes for IIPs synthesis are commonly isolated through their crystallization or precipitation [19,20,308]. Birlik et al. synthetized a Cr(III)-IIP using methacryloylhistidine (MAH) as chelator and $Cr(NO_3)_3 \cdot 9H_2O$ as Cr(III) source [20]. The Cr(III)-MAH complex was prepared *ex situ* and isolated by precipitation. For this purpose, MAH was first dissolved in ethanol, then Cr(III) was added and slowly dissolved through stirring at room temperature, and finally the solvent evaporated. The Cr(III)-MAH complex crystals were then purified through recrystallization in ethanol/acetonitrile mixture. The complex crystal were used in the synthesis of a Cr(III)-IIP which showed a higher selectivity toward Cr(III) with Co(II), Ni(II), Cr(IV) as competitive ions. Saraji et al. produced a Ni(II)-IIP using 4-VP as monomer, EGDMA as crosslinker, AIBN as initiator, and dithizone as Ni(II) chelator [308]. Ni(II)-dithizone complex was isolated *ex situ* by precipitation following the dissolution of dithizone in NH_4OH and addition of a $Ni(NO_3)_2 \cdot 6H_2O$ solution under vigorous stirring. The precipitate was then washed with water and dried before being used for the preparation of the Ni(II)-IIP. The Ni(II)-IIP obtained was selective toward Ni(II) ions in solutions containing Co(II), Cu(II), and Cd(II) as competitive ions. Bhaskarapillai et al. synthetized a Co(II)-IIP for the treatment of radioactive waste containing cobaltous ions using [N-(4-vinylbenzyl)imino]diacetic acid (VbIDA) as functional monomer [19]. To prepare the Co(II)-VbIDA complex, Vbida was dissolved in a NaOH solution at pH 9 and a water solution of $Co(NO_3)_2 \cdot 6H_2O$ was added dropwise under constant stirring until the formation of a precipitate. The precipitate was filtered, freeze-dried to remove the water, and recrystallized with dry methanol twice. Elemental analysis of the complex crystals showed the presence of a significant amount of sodium impurities that were impossible to remove, thus the authors applied the Co(II)-VbIDA complex as such to produce the Co(II)-IIP. The Co(II)-IIP was tested for the recovery of radioactive ions within a solution containing an excess of iron, reducing the cobalt activity by up to 55%. As described, the *ex situ* complex isolation method was successfully applied in the synthesis of IIPs, but showed limitations such as time-demanding crystal growth and the presence of impurities which are physically trapped within the complex crystals and are therefore hard to remove [19,20].

In situ complex formation study

In situ complex formation is the most commonly used method to prepare IIPs. In this approach, the chelator and template ion are directly introduced with a previously defined ratio within the pre-polymerization mixture. UV-Vis spectroscopy is commonly used to check the formation of complexes between metal and chelator [16,271,309–311]. If only one complex is formed, the molar ratio method and Job's plot of data can be applied to determine its stoichiometry. Fasihi et al. successfully applied the molar ratio method to optimize the pre-polymerization mixture of an IIP containing a 1:1 complex formed by 1-hydroxy-2-(prop-2′-enyl)-9,10-anthraquinone (HAQ) with UO_2(II) ions [311]. The method consisted of collecting the UV-Vis spectra of different solutions where the concentration of HAQ was kept constant and the one of UO_2(II) was varied. The complex they formed resulted in the appearance of a single inflection point in the absorbance-molar ratio plot, and the stoichiometric ratio between HAQ and UO_2(II) equal to 1:1 was the one used to optimize the pre-polymerization mixture. On the other hand, when a metal and a chelator form multiple complexes with different stoichiometry, these will result in the overlapping of more absorption bands, which must be deconvoluted and analyzed with more advanced methodologies. Various alternatives for the elaboration of the multiple-complexes UV-Vis absorption spectra have been applied in IIPs synthesis, including the non-linear fitting of spectroscopic data [309,312], the Job's continuous variation method [313–316], and the least-squares minimization (LSM) method [307].

A ligand titration coupled to a non-linear fitting of the spectroscopic data was used by Shamsipur et al. to determine the stoichiometry and stability of two complexes formed by the chelator 5,6,14,15-dibenzo-1,4-dioxa-8,12-diazacyclopentadecane-5,14-diene (DBDA15C4) with Cu(II) [312]. In the same way as for the molar ratio method, a series of solutions containing Cu(II) at constant concentration and an increasing concentration of DBDA15C4 were analyzed by UV-Vis spectroscopy. The absorbance-molar ratio plot relating these spectra showed the presence of two inflection points at the stoichiometric metal-chelator ratios equal to 1:1 and 1:2. This first analysis confirmed the formation and the stoichiometry of the two complexes. The UV-Vis spectra were then processed with a non-linear fit, which allowed the authors to estimate the stability constant of the two complexes.

Job's continuous variation method was applied to elucidate the distribution of binary and ternary complexes used in IIPs synthesis [313–316]. This method provides that the signal deriving from a ML_n complex through the equilibrium (Eq. 2.1):

$$M + nL \rightleftharpoons ML_n \tag{2.1}$$

Where M, L, and n are the metal ion, ligand, and their stoichiometric ratio, respectively, when the sum of M and L concentrations ($[M] + [L]$) is kept constant, will reach a maximum at (Eq. 2.2) [316]:

$$\frac{[M]}{[M]+[L]} = \frac{1}{n+1} \tag{2.2}$$

Daniel et al. applied the continuous variation method to elucidate the formation of a ternary complex between Pd(II), 8-aminoquinoline (AQ) and 4-VP [314]. To fit the method, the ternary complex was converted into a pseudo-binary complex by keeping the concentrations of 4-VP or AQ in large excess with respect to the one of Pd(II). The signal deriving from the complex reached its maximum when the ratios $\frac{[Pd(II)]}{[Pd(II)]+[AQ]}$ and $\frac{[Pd(II)]}{[Pd(II)]+[4-VP]}$ were equal to 0.36 and 0.37, proving the presence of a 1:2:2 Pd(II):AQ:4-VP ternary complex.

The LSM is a mathematical technique used to optimize the parameters to fit a set of data points in a model, and was applied for processing UV-Vis spectral data through a commercial program such as HypSpec [317]. Laatikainen et al. applied the LSM method to investigate the effect of the complex stoichiometry on IIPs selectivity by adjusting the metal-chelator ratio before polymerization [16]. The vinylbenzyl derivative of 2-(aminomethyl)pyridine (Vbamp) was chosen as functional monomer for the chelation of Ni(II) ions. The *in situ* complex formation study was carried out by collecting the UV-vis spectra of solutions at a different Ni(II)/Vbamp ratio under the polymerization conditions. The distribution of species in solution at equilibrium was obtained from spectral data by applying a LSM scheme through the commercial program HypSpec. This study allowed the authors to choose which complex (1:1, 1:2, or 1:3) to introduce into the pre-polymerization mixture simply by choosing the correct ratio between Ni(II) and Vbamp. The adjustment of the pre-polymerization mixture, as a result, allowed us to obtain an IIP which was highly selective for Ni(II) in the presence of high amounts of Zn(II) as competitive ion, even in acidic conditions.

Ex situ versus in situ complex formation study

Laatikainen et al. performed a comparative study between *ex situ* and *in situ* complex formation for the preparation of Ni(II)-IIPs [21]. In the first case, the complex was isolated *ex situ* by precipitation and was introduced in the pre-polymerization mixture. In the second case, the optimal ratio for the formation of the metal-ligand complex was determined *in situ* using the LSM method, and the complex was then directly prepared in the pre-polymerization mixture. Vbamp was used as chelator, while $Ni(NO_3)_2 \cdot 6H_2O$ and $Ni(ClO_4)_2 \cdot 6H_2O$ were used as Ni(II) sources for the *in situ* and *ex situ* complex formation, respectively. The *ex situ* complex isolation was performed by mixing $Ni(ClO_4)_2 \cdot 6H_2O$ and Vbamp in a 1:1 water-ethanol mixture which resulted, after one day, in the precipitation of the Ni(II):Vbamp 1:3 complex. For the *in situ* complex formation study, the spectra of 14 solutions containing Ni(II) and Vbamp with a constant total concentration (as sum of the two components) but with different Ni(II)/Vbamp ratios were collected in the same conditions (solvent and temperature) as that of the Ni(II)-IIP synthesis. The LSM was applied by processing the UV-Vis spectra with HypSpec program to extrapolate the complexes' distribution at equilibrium and, consequently, to determine the stoichiometric ratios to isolate the Ni(II)-Vbamp complexes. Furthermore, the stability constants, extinction coefficients, and concentrations for the absorbing species at equilibrium were estimated. The Ni(II)-IIPs prepared with the two different

methods showed similar surface areas, Ni(II) binding capacity and selectivity for Ni(II) ions. This study demonstrated that the more complicated and time-demanding *ex situ* complex isolation could be effectively substituted by a quicker and easier *in situ* complex study [322].

2.5.4 **IIPs polymerization techniques**

The majority of the IIPs reported in the literature were synthesized by free radical polymerization [242]. The most applied polymerization techniques for IIPs synthesis include bulk, precipitation, and suspension polymerizations. As an alternative to classical radical polymerizations, several research groups have produced IIPs by implementing the sol-gel process. This sub-section describes the main properties associated with each of these polymerization techniques.

Bulk polymerization

The bulk polymerization method, extensively applied in IIPs preparation [318–322], is a straightforward and convenient approach for their synthesis [322]. Bulk polymerization of IIPs requires the presence of a small volume of solvent, enough to solubilize the initiator, the monomers, and the template in a single phase and to favor pore formation. Polymers obtained with this method results in a monolithic block which needs to be crushed, ground, and sieved to obtain particles of the right size for the metal separation application [323]. The process of grinding and sieving is time-consuming and results in irregular particles, offering only limited control over their size and shape [314]. Moreover, the crushing, grounding, and sieving operations can destroy part of the imprinted sites, reducing the efficiency of the IIP [324]. A further limitation is represented by the small amount of solvent involved in the process, which causes poor heat dissipation during the propagation phase of the polymerization and may result in the creation of hotspots and thermal degradation in the final product [325]. These problems can be overcome by the preparation of IIPs with polymerization methods that produce microspheres or bead-shaped materials in solution, such as precipitation polymerization or suspension polymerization[314].

Precipitation polymerization

Several recent examples of IIPs produced by precipitation polymerization are available in the literature [247,270,326–329]. Precipitation polymerization begins as a homogeneous radical polymerization, as all the components of the pre-polymerization mixture are solubilised in a single phase [330]. The selected solvent must be such as to solubilize the monomers but not the polymer's particles, which are formed during the process. Once the reaction begins and the first polymer nuclei are formed, they precipitate, and their growth takes place by further absorption and polymerization of monomer [331]. The main advantage of this technique is the control of the size of the obtained polymer beads, which can be micrometric or nanometric [332], while important

limitations are a complicated selection of the proper solvent, a long reaction time, and the use of a high amount of solvent [333].

Suspension polymerization

In a typical suspension polymerization set-up, an organic solvent containing water-insoluble monomers and an oil-soluble initiator are dispersed within a continuous aqueous phase by applying intense stirring and small quantities of suspending agents as stabilizer [334]. The dispersed monomer droplets undergo a gradual transformation from a highly mobile liquid state to a sticky syrup-like dispersion and, finally, to solid polymer particles [334]. This technique allows the production of polydispersed IIP beads, the average size of which can be controlled by varying the stirring rate, with dimensions ranging from units to hundreds of micrometers [274,335,336]. The stabilizer represents a major concern for this method, as it can be trapped in the final product and result as a contaminant [337]. As an alternative to the ordinary suspension (organic phase suspended in water), Branger et al. prepared IIPs using an inverse suspension, dispersing a polar organic phase containing all the reactants for the polymerization in mineral oil used as a continuous phase [16,262]. The use of the inverse suspension allowed the avoidance of both the use of stabilizers and the risk of transfer to the aqueous phase of the metal ions used as template [262].

Sol-gel process

The name of the sol-gel process derives from the gradual transformation of a colloidal solution, named sol, into a gelatinous biphasic system referred to as gel [187]. A typical sol-gel process can be described with the following steps [338]. The sol-mixture is formed via the hydrolyzation of an organo-alkoxysilane precursor. This initial phase is followed by the polycondensation of the colloidal particles with the formation of a crosslinked polymer network. The water released as a by-product of the polycondensation remains trapped within the polymer network, leading to the formation of a hydro-gel system. Finally, the remaining solvent is evaporated to obtain a solid porous material. To produce IIPs with the sol-gel process it is sufficient to introduce the ion template into the sol-mixture during the gelation process [339–341]. The major advantages of sol-gel processes are that the synthesis is carried out at low temperature, and the shape of the end-product can be configured in different forms like powder, thin films, fibers, and monoliths [342]. An important limitation, on the other hand, is represented by the shrinkage and cracking of the end-product during the gel drying process [343,344].

2.5.5 **IIPs adsorption performance evaluation**

The adsorption capacity and the selectivity of an IIP are two crucial parameters to outline its performance. This sub-section provides the tools for the estimation of the adsorption capacity and selectivity properties of IIPs.

Adsorption capacity

The adsorption capacity at equilibrium q_e in batch experiments, expressed by the Eq. 2.3, represents the amount of target ion adsorbed per unit mass of adsorbent.

$$q_e = \frac{(C_0-C_e)}{m} \times V \quad (2.3)$$

where C_0 and C_e are the initial metal ion concentration in solution before adsorption and the concentration at equilibrium, respectively, m is the mass of the adsorbent, and V is the volume of the solution.

The maximum adsorption capacity of a material can be determined by carrying out adsorption experiments at constant temperature (isotherm), pH and ionic strength at a different initial concentration of target ion. The experimental isotherm data obtained in this way can be fitted by several isotherm models, including Langmuir [345], Freundlich [346], Langmuir-Freundlich [347], Temkin [348], and Scatchard [349]. Langmuir and Freundlich models are the most applied to describe the IIPs metals' adsorption in literature [242].

In the case of a single adsorbate, Langmuir's model [345] assumes that the surface containing the binding sites is homogenous, all the binding sites have equivalent adsorption energy, and there is no interaction between adsorbate molecules on adjacent sites. Langmuir's model is expressed by Eq. 2.4.

$$q_e = \frac{q_m K_L C_e}{1+K_L C_e} \quad (2.4)$$

where q_m is the maximum adsorption capacity and K_L is the Langmuir constant.

Freundlich's model [346] is an empirical model that effectively describes adsorption on heterogeneous surfaces. Freundlich's model is expressed by Eq. 2.5.

$$q_e = K_F C_e^{1/n} \quad (2.5)$$

where K_F is the Freundlich constant related to the adsorption capacity and n is related to the adsorption strength.

Selectivity

The selectivity of an IIP can be evaluated through the selectivity coefficient k, (Eq. 2.6), which is an indicator of the preference of the IIP toward the target ion when present in solution together with a competitive ion.

$$k = \frac{K_{d,target\ ion}}{K_{d,competitive\ ion}} \quad (2.6)$$

Where $K_{d,target\ ion}$ and $K_{d,competitive\ ion}$ are the distribution coefficients of the target ion and competitive ion, respectively. The K_d values can be calculated with Eq. 2.7.

$$K_d = \frac{q_e}{c_e} \tag{2.7}$$

Values of $k > 1$ indicate that the IIP selectively adsorbs the target ion over the competitive ion.

The relative selectivity coefficient (Eq. 2.8), calculated as the ratio between the k values of IIP and NIP, measures the effect of ion imprinting on the adsorbent selectivity.

$$k' = \frac{k_{IIP}}{k_{NIP}} \tag{2.8}$$

Values of $k' > 1$ imply that the selectivity for the target ion of the IIP is higher than that of the corresponding non-imprinted material under the same conditions.

A more in-depth description of the values of the selectivity coefficients and adsorption capacities of Co(II)-IIPs and Ni(II)-IIPs present in the literature is provided in sub-section 2.5.6.

2.5.6 **IIPs for Co(II) and Ni(II) separation**

The application of IIPs for the separation of Co(II) and Ni(II) from other competitive ions was deeply studied in the literature. As discussed in sub-section 2.5.1, the typical procedure for IIPs preparation involves the formation of a metal-chelator complex followed by the copolymerization with a crosslinking agent. The metal-chelator affinity and the preparation method strongly influence the IIPs' performance in terms of adsorption capacity and selectivity toward the target ion. This sub-section provides a literature overview of the separation of Co(II) and Ni(II) ions with IIPs, with focus on the methodologies and reagents involved in their preparation.

IIPs for the separation of Co(II) ions

The effect of two commercial functional monomers, MAA and 4-VP, on IIPs adsorption performance was studied by Yusof et al., who prepared two Co(II)-IIPs via bulk polymerization procedure [350]. Dipicolinic acid (DPA) was used in both cases as a complexing agent for Co(II) ions and the ternary complex between Co(II), DPA, and either MAA or 4-VP was crosslinked by EGDMA. The Co(II)-IIP prepared with MAA as functional monomer showed higher adsorption capacity and selectivity toward Co(II) ions when compared with the one prepared with 4-VP. The best performance, obtained with the MAA-containing Co(II)-IIP, resulted in a maximum Co(II) adsorption capacity equal to 15.4 mg/g, and selectivity coefficients with Ni(II), Fe(III) and Mg(II) as competitive ions equal to 18.5, 13.8, and 30.1, respectively. The monomer 4-VP was also used by Jagirani together with 2-hydroxyethylmethacrylate (HEMA) as Co(II)

complexing agents to prepare a Co(II)-IIP via precipitation polymerization [351]. This material showed a high Co(II) adsorption capacity, which reached the value of 243.9 mg/g at pH 6. However, the selectivity coefficients with Co(II) as target ion and Pb(II), Cu(II), Cr(II), Zn(II), Cd(II), and Ni(II) as competitive ions, were limited to the values range of 2.1-2.8.

A higher selectivity toward Co(II) ions was achieved by Beyki et al. [329] and Khoddami et al. [285] who prepared different types of magnetic-IIPs. Beyki et al. prepared a core-shell bio-based magnetic Co(II)-IIP combining γ-Fe_2O_3 with 8-HQ grafted chitosan in the presence of EPH as a crosslinker [329]. The 8-HQ grafting onto chitosan structure was confirmed by FTIR spectroscopy, while the core-shell structure of the final nanocomposite material was elucidated by TEM. The imprinted material maximum adsorption capacity for Co(II) ions at pH 8 was equal to 100 mg/g. The selectivity was studied with Ni(II), Cd(II) and Pb(II) as competitive ions and selectivity coefficients values were equal to 42, 11, and 2, respectively. The adsorption mechanism was partially clarified by FTIR spectroscopy. The addition of Co(II) ions caused the shift of Fe-O, C=C, and C-O peaks to lower wavenumbers, suggesting that both 8-HQ and the functional groups of magnetic chitosan were involved in Co(II) adsorption. A magnetic Co(II)-IIP was also prepared by Khoddami et al. combining the surface imprinting method with the sol-gel process [285]. The Co(II)-IIP was prepared including titana-coated magnetite nanoparticles (Fe_3O_4/TiO_2) in a solution containing Co(II), 3-(2-aminoethylamino) propyltrimethoxysilane (AAPTS), and TEOS used as template, ligand, and crosslinker, respectively. The particles were recovered by applying an external magnetic force to the solution. The Co(II)-IIP was tested for Co(II) adsorption, resulting in maximum adsorption capacity at pH 8 equal to 35.21 mg/g. The material showed remarkable selectivity for Co(II) when coupled with Ni(II), Pb(II), and Cd(II) as competitive ion, with selectivity coefficient values equal to 79.7, 41.2, and 56.5, respectively. These values are among the highest for Co(II)-IIPs reported in literature (Table 2.1).

Table 2.1. Maximum adsorption capacity q_{max} and selectivity coefficient values *k* of several Co(II)-IIPs reported in the literature.

Chelator	**pH**	**q_{max} (mg/g)**	***k* (divalent ions M(II))**							**Ref.**
			Ni	**Cd**	**Cu**	**Mn**	**Mg**	**Pb**	**Zn**	
4-VP and HEMA	6.0	243.9	2.8	2.2	2.1	/	/	2.3	2.1	[351]
Triglycine	5.0	181.7	3.8	/	10.8	/	/	/	8.4	[352]
Glycylglycine	8.4	175.0	4.2	/	/	/	54.3	/	/	[353]
2-pyridinecarboxaldehyde	7.5	132.8	1.2	/	/	/	/	/	/	[354]
8-HQ grafted onto chitosan	8.0	100.0	42.0	11.0	/	/	/	2.0	/	[329]

3-(2-aminoethylamino) propyltrimethoxysilane	8.0	35.2	79.7	56.5	/	/	/	41.2	/	[285]
bis(2-methacryloxyethyl) phosphate and glycylglycine	8.0	33.4	3.6	/	5.2	/	7.4	/	10.4	[355]
1-vinylimidazole	7.0	23.1	/	50.3	20.0	/	/	7.6	11.0	[247]
DPA	/	15.4	18.5	/	/	/	30.1	/	/	[350]

IIPs for the separation of Ni(II) ions

The commercial monomer 4-VP was selected as a complexing agent by Kumar et al. to prepare Ni(II)-IIPs via the precipitation polymerization method [277]. Several Ni(II)-IIPs were prepared using in each of them 4-VP as ligand and testing the effect of different functional monomers and crosslinkers. Acrylamide (AM), HEMA, and MAA were tested as functional monomers while DVB, pentaerythrityl triacrylate (PETA), TMPTA, and EGDMA were used as a crosslinkers. The Ni(II)-IIP synthetized with MAA and EGDMA as functional monomer and crosslinker, respectively, showed higher adsorption capacity, thus the experimental work was continued on the Ni(II)-IIP synthetized with these two reactants. The maximum adsorption capacity of Ni(II)-IIP was obtained at pH 6 and reached the value of 125 mg/g. This value was among the highest reported in the literature for Ni(II) adsorption by IIPs (Table 2.2). The selectivity was studied against several ions, among which Co(II), Cu(II), Pb(II), and, Zn(II), with selectivity coefficient values up to 4.2, 4.4, 5.0, and 6.1, respectively. The authors explained the selectivity of the Ni(II)-IIP by comparing the radius for Ni(II) with those of the competitive ions. The radius of each competitive ion was larger than the one of Ni(II) and, therefore, they could not easily fit into the Ni(II)-complementary binding cavities of the imprinted material. Ashouri et al. prepared a Ni(II)-IIP via bulk polymerization using 2-vinylpyridine, diphenylcarbazone, EGDMA and ACN as functional monomer, ligand, crosslinker, and solvent, respectively [356]. The optimal pH value for Ni(II) adsorption was 6.0 and the maximum adsorption capacity was equal to 3.26 mg/g. The selectivity coefficient values for the Ni(II)-IIP were equal to 3.3, 102.3, 95.9. 85.1, 175.9, and 53.4 with Co(II), Cu(II), Mn(II), Pb(II), and Zn(II). The complete separation of Ni(II) and Co(II) ions was therefore not possible, while the selectivity against the other competitive ions studied was found to be very high. The Ni(II)–IIP was also applied to the determination of trace amount of Ni(II) in synthetic and tap water samples. The analytical method had a good Ni(II) limit of detection, equal to 0.38 μg/L.

Otero-Romaní et al. prepared several Ni(II)-IIP via precipitation polymerization using either 4-VP or 2-(diethylamino) ethyl methacrylate (DEM) as functional monomer, DVB as crosslinker, AIBN as initiator, and acetonitrile/toluene (3:1) mixture as porogen [357]. The Ni(II)-IIPs were prepared either with or without the ligand 8-HQ as Ni(II) complexing agent. The polymer particles of each material were packed into empty SPE

cartridges and applied for Ni(II) adsorption from seawater samples. The best Ni(II) recovery performance were obtained for the Ni(II)-IIP synthetized with DEM as monomer and in presence of 8-HQ as complexing agent with an adsorption capacity equal to 1.35 mg/g. The ligand 8-HQ was physically trapped into the DEM-DVB polymer matrix providing the imprinting cavities for Ni(II) ions. The optimum pH for Ni(II) adsorption with the 8-HQ containing IIPs was equal to 8.5 ± 0.5. The authors attributed this result to the amphoteric nature of 8-HQ. This ligand, which forms oximium (8-hydroxyquinolinium) ion by protonation of nitrogen in acid solutions and oxinate ion in basic solutions, can interact with Ni(II) ions only in basic solutions, where the hydroxyl group is not protonated. The same research group prepared, in a separate work, a Ni(II)-IIP using the vinylated version of 8-HQ, 5-vinyl-8-hydroxyquinoline (5-VHQ), to allow its immobilization into the polymeric network [358]. The monomers DEM and DVB were selected as functional monomer and crosslinker, respectively, as well as in the previous work. The Ni(II) adsorption performance of the 5-VHQ containing Ni(II)-IIP were compared with those of the Ni(II)-IIP containing 8-HQ, the non-vinylated form of the ligand. The use of 5-VHQ as Ni(II) complexing agent resulted in an increased Ni(II) adsorption capacity, which was equal to 1.98 mg/g at pH 9. The use of 8-HQ in its vinylated form 5-VHQ was also beneficial for the Ni(II)-IIP selectivity, which was tested with the ions of several elements including Al, As, Cd, Co, Cr, Cu, Fe, Mn, Pb, Sn, Ti, V, and Zn. The selectivity coefficient with Al(III) as competitive ions was extremely high, with a value equal to 500.4. The selectivity for Ni(II) in the presence of all the other competitive ions was still remarkable, but with selectivity coefficient values the range reduced to 11.8-39.2. The authors attributed the improved performance of the Ni(II)-IIP containing 5-VHQ to the more rigid imprinting cavities which could be obtained linking the chelator to the polymer chain, when compared with the physical trapping of 8-HQ into the polymer matrix.

A modified Ni(II) chelator was synthetized by Laatikainen et al., who prepared a highly selective Ni(II)-IIP using as functional monomer 2-(aminomethyl)pyridine (AMP) ligand functionalized with a vinylbenzyl group [16]. The maximum adsorption capacity was obtained at pH 7 and was up to 11.74 mg/g, while the highest selectivity coefficient value with Zn(II) as competitive ion was obtained at pH 4 and was equal to 262. The importance of correct selection of the stoichiometry between template ions and functional monomers to obtain high selectivity was highlighted in this work. The selectivity coefficient value of the Ni(II)-IIP was also influenced by the pH of the solution. When the solution pH was reduced from pH 7 to pH 4, the adsorption of Ni(II) ions by the Ni(II)-IIP was halved, while the adsorption of Zn(II) ions decreased tenfold. Consequently, the selectivity coefficient for Ni(II) adsorption at pH 4 sharply increased when compared to pH 7.

Table 2.2. Maximum adsorption capacity q_{max} and selectivity coefficient *k* values of several Ni(II)-IIPs reported in the literature.

Chelator	**pH**	**q_{max} (mg/g)**	***k* (divalent ions M(II))**							**Ref.**
			Co	**Cd**	**Cu**	**Mn**	**Mg**	**Pb**	**Zn**	

4-VP	6.0	125.0	4.2	/	4.4	/	/	5.0	6.1	[277]
4-vinyl benzoic acid	6.5	88.6	91.6	/	111.1	/	/	/	78.6	[359]
DPC	7.0	86.3	/	/	/	/	5.3	/	/	[254]
DPC	9.0	40.2	14.1	18.8	5.3	/	22.3	26.8	31.9	[360]
2-(Allylmercapto) nicotinic acid	6.0	38.8	4.2	16.9	32.7	/	219.6	/	33.6	[361]
2-acrylamido-2-methyl-1-propanesulfonic acid	7.0	20.3	4.1	/	3.6	/	/	5.9	5.8	[362]
3-aminopropyltrimethoxysilane	8.0	12.6	32.8	/	46.0	/	/	/	43.8	[363]
Vbamp	7.0	11.7	/	/	/	/	/	/	42.0	[16]
N-methacryloyl-histidine methyl ester	6.5	5.5	/	/	4.2	/	/	/	3.6	[268]
Diphenylcarbazone	6.0	3.3	102.3		95.9	85.1		175.9	53.4	[356]
5-VHQ	9.0	2.0	39.2	16.3	22.0	28.7	/	20.5	27.1	[358]

2.6 **Design of new chelating monomers**

As discussed in the previous section, several commercial ligands and monomers were used as chelators to prepare Co(II)-IIPs and Ni(II)-IIPs, and a further step toward a higher efficiency can be made by producing new chelators which can more specifically interact with the target ion. One effective method of producing new chelators is to modify commercial ligands by introducing a polymerizable function into their structure. In this way, the chelator can be stably introduced into the polymer network, avoiding its undesired release from the adsorbent. The commercial ligands 2-(2-pyridyl)imidazole (PIM), bis-AMP, and AMP (Figure 2.10) were selected as starting material to produce three new chelating monomers and a justification for their choice is provided in this section.

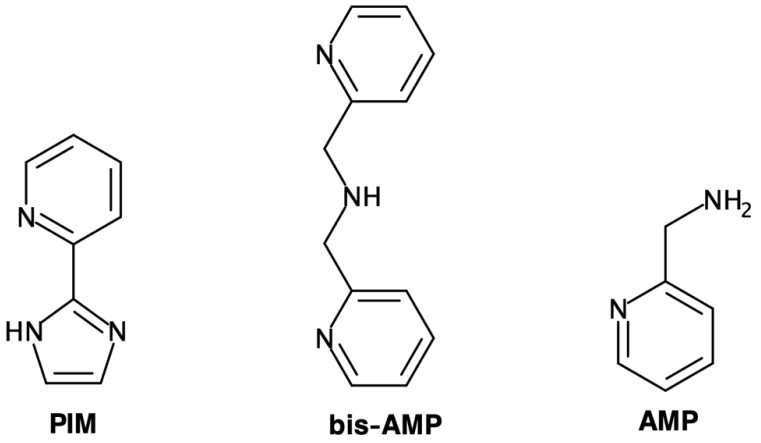

Figure 2.10. Structures of the ligands PIM, bis-AMP, and AMP.

2.6.1 **PIM as a precursor for a new monomer**

The PIM ligand was selected by Okewole et al. as precursor for the synthesis of three novel Ni(II) extractants [364]. The authors motivated the choice of PIM due to the presence of both the imidazole and pyridyl groups within its structure. These groups enable PIM to form stable complexes with metal ions and to maintain low protonation levels in acidic conditions, respectively. Moreover, the 1-position of the imidazole group in PIM allowed for the functionalization of this ligand with large alkyl groups. The authors functionalized PIM with heptyl, octyl, and decyl groups and the best results for Ni(II) extraction were obtained with the octyl derivative extractant (OPIM). The extractant showed good selectivity for Ni(II) in sulfate and sulfate/chloride media in the pH range 0.5-3.5. In particular, the extraction of metal ions such as Fe(III), Mn(II), Mg(II), and Ca(II) did not occur, while in the case of Co(II) as competitive ion, a $\Delta(pH_{50})$ of 1.6 was observed, making the separation of these two ions selective. The same research group extended this study to a solid phase system, where a chloromethylated resin was functionalized with PIM and applied for the separation of Ni(II) ions in synthetic sulfate solutions [365]. The selectivity for Ni(II) over Cu(II), Co(II), and Fe(III) was obtained via selective decomplexation since the Ni(II)-PIM complex was found to be more stable than the complexes with the other competitive ions. The selectivity toward Ni(II) was thus achieved first using less concentrated sulfuric acid solutions, which were leaching the competitive ions but not Ni(II). A similar result was obtained by Ndayambaje et al. who modified polyacrylonitrile nanofibers with PIM ligand and applied the new material in Ni(II) adsorption experiments [206]. The PIM nanofibers showed a Ni(II) adsorption capacity up to 47 mg/g and the equilibrium was attained in just 1 min. The selectivity for Ni(II) in the presence of Co(II) as competitive ion was obtained via elution with EDTA in a column system. The strong complexation of Ni(II) ion in the presence of competitive ions such as Cu(II), Co(II) and Fe(II) [365], combined with the possibility to functionalize the imidazolyl group and the low protonation of the pyridyl group in acidic media, made

PIM an optimal candidate for producing a new extractant for the separation of Ni(II) ions in acidic solutions [364]. These results motivated the choice of PIM as precursor for a novel chelating monomer in this project. It is in fact reasonable to expect that a new PIM-based monomer can form highly stable complexes with the Ni(II) ion to prepare selective IIPs for nickel(II).

2.6.2 **bis-AMP as a precursor for a new monomer**

The bis-AMP ligand is known to form complexes with several metal ions. Romary et al. studied the complexation of bis-AMP with Cu(II), Ni(II), Co(II), Zn(II), Cd(II), Mn(II), and Ag(I) ions in a 0.1 M KNO_3 solution [366]. With each of the analyzed metal ions, bis-AMP could form complexes with stoichiometry 1:1 and 1:2 with the stability order Cu(II)>Ni(II)>Co(II)>Zn(II)>Cd(II)>Mn(II)>Ag(I). The stability constants of these complexes were relatively low, and the authors attributed this result to the high steric limitations of bis-AMP ligand deriving from the mutually fixed position of the pyridine groups. The bis-AMP ligand is also known to be an effective metal adsorbent in acidic media due to the low pKa values for its three nitrogen donors, which are equal to 0.5–1.6 for pKa_1, 2.1–2.7 pKa_2, and 3.4–4.1 for pKa_3 [367]. As described in sub-section 2.4.3, the ligand bis-AMP was used in the preparation of commercial chelating resins (Figure 2.6) currently applied in the industrial separations of Co(II) and Ni(II) ions. The resin Dowex^{TM} M4195, which contains the ligand bis-AMP within its structure, was applied for the treatment of sulfide concentrates to produce copper and cobalt cathode products [235]. This resin was able to reduce the concentration of nickel within the final product below 0.1%. However, it suffered as a major limitation a strong retention of Cu(II) ions, which could only be eluted with highly concentrated sulfuric acid or ammonia. This result was in good agreement with the work of Romary et al., where the complexes of bis-AMP with Cu(II) ions resulted in being more stable than those with Co(II) and Ni(II) [366].The low basicity of bis-AMP ligand combined with its well-known Co(II) and Ni(II) ions complexation properties and the current industrial application of this molecule make it a promising and industrially interesting candidate as precursor for the synthesis of a novel chelating monomer for the separation of Co(II) and Ni(II) ions in acidic media. The application of this monomer to prepare Co(II)-IIPs and/or Ni(II)-IIPs can provide a further increase in selectivity with the formation of selective binding cavities.

2.6.3 **AMP as a precursor for a new monomer**

Laatikainen et al. studied the AMP ligand as a Ni(II) chelator in two distinct experimental conditions [307]. The first study was carried out in aqueous solutions containing high zinc concentration, to reproduce the experimental condition commonly found in hydrometallurgy. The second study was conducted in a methanol/2-methoxyethanol mixture, to replicate a condition which could be relevant for IIPs preparation. In both cases, the AMP ligand formed octahedral complexes with stoichiometry 1:1, 1:2, and 1:3 with Ni(II) ions, as observed in a previous complexation study conducted in aqueous solutions [368]. The difference with the complexation in pure water lay in a shifting of

complexation equilibrium toward higher stoichiometry complexes, and in a reduction of the stability constant values in the organic solvent mixture. The effect of AMP within a chelating resin structure was studied comparing the commercial resins WP-1 and CuWRAM [369]. WP-1 is a mesoporous silica-based resin functionalized with a poly(ethyleneimine) layer [370], while CuWRAM is its analog, which was further functionalized with AMP (Figure 2.11) [371].

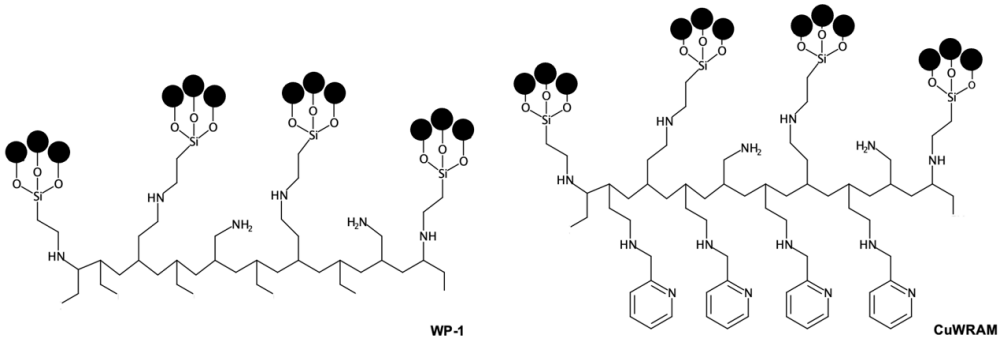

Figure 2.11. Structures of WP-1 and CuWRAM [370,371]. The black circles represent the silica-based backbone of the resins.

The proton titration of the sorbents showed that the addition of AMP in CuWRAM reduced the global basicity of the resin. This allowed CuWRAM resin to be more efficient in metal adsorption at lower pH values due to a reduced protonation in acidic conditions. The stability of complexes with Ni(II) and the efficiency in acidic environments of AMP-containing resins motivated the choice of this ligand as precursor for the synthesis of a new chelating monomer [16]. This monomer, named Vbamp, was synthetized by introducing a vinylbenzyl group into AMP structure, and was applied for Ni(II)-IIPs preparation. The aim of this study was to clarify the effect of the complex stoichiometry on IIPs performance. The authors found that the relative amounts of complexes with different stoichiometry was influenced by several factors, including the Ni/Vbamp ratio, the anion in the Ni(II) salt, and temperature. The polymer showed remarkable Ni(II) selectivity when coupled with Zn(II) as competitive ion, and the best results were obtained when the complex at Ni(II)/Vbamp stoichiometry 1:2 was the major Ni(II)-containing species in the pre-polymerization mixture. The new monomer synthesized in this doctoral thesis differs from Vbamp as it involves the functionalization of AMP with a methacrylic group rather than a vinylbenzyl group. The methacrylic group, in addition to a polymerizable vinyl function introduced in Vbamp, also provides a carbonyl group whose oxygen could act as additional electron donor atom. This modification turned AMP from a bidentate ligand into a potential tridentate monomer. This structural difference is expected to enhance the performance of the new Ni(II)-IIP produced with the novel AMP monomer when compared with those of the Vbamp-based Ni(II)-IIPs.

2.7 Conclusion

The literature study provided in this chapter highlighted how common metal separation techniques often suffer from a lack of selectivity when dealing with the separation of Co(II) and Ni(II) ions. To overcome this problem, different methodologies were applied to improve the selectivity of common separation techniques such as precipitation, solvent extraction, or adsorption. Among these methodologies, the ion imprinting technique allows the preparation of adsorbent materials with complementary cavities to a target ion, increasing the selectivity toward it. The efficiency of IIPs in metal ions separation, mainly outlined in terms of adsorption capacity and selectivity, is strongly affected by the strength and stability of the complex formed between the chelator and the target ion. For this reason, the synthesis of new chelating monomers and the study of their complexes with the target ions is a crucial step for their highly selective separation. In this doctoral project, three new chelating monomers were synthetized by modifying PIM, bis-AMP, and AMP ligands, and were applied for the preparation of IIPs. The experimental work and results obtained for each of the new monomers are described and discussed in the following chapter of this manuscript. Chapter 3 presents a comprehensive description of the reagents, equipment, methods, and experimental procedures used to perform the laboratory work. The general workflow for each material includes the synthesis of a new functional monomer, its chemical characterization, and its application to prepare IIPs and the study of the metal binding properties of the new materials. The results concerning the new monomer and adsorbents prepared with PIM ligand as precursor are described and discussed in Chapter 4. Similarly, those related to bis-AMP and AMP ligands are illustrated and discussed in Chapters 5 and 6, respectively. In conclusion, Chapter 7, the final chapter of this manuscript, offers an overview about the main results obtained in this doctoral thesis and outlines the future perspective concerning the preparation and application of IIPs.

3 Materials and methods

Table of contents

3.1 Chemical products

3.1.1 Solvents

The solvents dichloromethane (99.8%, anhydrous, CH_2Cl_2), deuterated dimethyl sulfoxide (deuteration degree ≥ 98.8%, DMSO-d_6) and deuterated chloroform (deuteration degree ≥ 98.8%, $CDCl_3$) were purchased from Sigma-Aldrich (Steinheim, Germany). The solvent dimethyl sulfoxide (99.9%, DMSO) was purchased from Merck (Darmstadt, Germany). Each solvent was used without further purification. Ultrapure water was obtained with a Milli-Q purification system (Millipore).

3.1.2 Reactants

The reagents listed below were used without further purification. The chemicals 2-(2-pyridyl)imidazole (97%, PIM), bis(2-pyridylmethyl)amine (97%, bis-AMP), 2-(aminomethyl)pyridine (99%, AMP), triethylamine (99%, $N(CH_2CH_3)_3$), nickel nitrate hexahydrate (99.9%, $Ni(NO_3)_2{\cdot}6H_2O$), nickel perchlorate hexahydrate (98%, $Ni(ClO_4)_2{\cdot}6H_2O$), cobalt perchlorate hexahydrate (quality level 100, $Co(ClO_4)_2{\cdot}6H_2O$), copper perchlorate hexahydrate (98%, $Cu(ClO_4)_2{\cdot}6H_2O$), cadmium nitrate tetrahydrate (98%, $Cd(NO_3)_2{\cdot}4H_2O$), magnesium nitrate hexahydrate (99%, $Mg(NO_3)_2{\cdot}6H_2O$), 2,2-azobis(2-methylpropionitrile) (98%, AIBN), mineral oil (heavy), sodium hydroxide (≥ 98%, NaOH), sulfuric acid (≥ 98%, H_2SO_4) and magnesium sulfate (99.5%, anhydrous, $MgSO_4$) were purchased from Sigma-Aldrich (Steinheim, Germany). Manganese nitrate tetrahydrate (≥ 98.5%, $Mn(NO_3)_2{\cdot}4H_2O$), cobalt nitrate hexahydrate (≥ 98%, $Co(NO_3)_2{\cdot}6H_2O$) and copper nitrate hemihydrate (98%, $Cu(NO_3)_2{\cdot}2.5H_2O$) were purchased from Merck (Darmstadt, Germany), VWR (Fontenay-Sous-Bois, France) and Alfa Aesar (Kandel, Germany), respectively. N-(2-hydroxyethyl)piperazine-N-2-ethanesulfonic acid (≥ 99%, HEPES) and hydrochloric acid (37%, HCl) were purchased from Fisher Scientific (Loughborough, U.K.). Nitric acid (67-69%, HNO_3) and hydrochloric acid (34-37%, HCl) used for ICP-MS analysis were purchased from Romil (Espoo, Finland).

The monomer methacryloyl chloride (97%, C_4H_5ClO), purchased from Alfa Aesar, was distilled under reduced pressure at 40°C to remove the polymerization inhibitor. The monomers ethylene glycol dimethacrylate (98%, EGDMA) and methyl methacrylate (99%, MMA), purchased from Acros Organics (Geel, Belgium) and Sigma-Aldrich, respectively, were washed three times with a 10% NaOH, twice with ultrapure water and dried with $MgSO_4$ to remove the polymerisation inhibitors.

3.2 Equipment

3.2.1 Nuclear magnetic resonance (NMR) spectroscopy

Liquid-state ^{1}H and ^{13}C NMR spectra were collected with a Bruker Advance 400-MHz spectrometer operating at 400 MHz. Solid-state ^{13}C CPMAS NMR spectra were collected with a Bruker Advance III spectrometer operating at 500 MHz using a double resonance CPMAS probehead. Chemical shifts (δ) are given in ppm. The multiplicity of signals in the ^{1}H NMR spectra are named as follows: singlet (s), doublet (d), triplet (t), and multiplet (m).

3.2.2 UV-visible (UV-Vis) spectroscopy

The UV-Vis absorption spectra were collected with an Agilent 8453 UV-Vis spectrophotometer equipped with a thermostatic cuvette holder. The spectra were collected at 80°C in the wavelength range 300-900 nm, with a resolution of 1 nm. The samples were placed in a glass cuvette with a length path of 1 cm.

3.2.3 Fourier transform infrared (FTIR) spectroscopy

The FTIR spectra were collected with a PerkinElmer FTIR Frontier spectrometer equipped with the attenuated total reflectance (ATR) sampling accessory. The spectra were collected in the range of 4000-400 cm^{-1} as result of an average of 8 scans with a resolution of 4 cm^{-1}.

3.2.4 Inductively coupled plasma-mass spectroscopy (ICP-MS)

The metal ions concentration in the adsorption experiments was measured using an Agilent 7900 ICP-MS. The samples were diluted with ultrapure water containing 1% of HCl and 1% of HNO_3 in 10 mL metal-free tubes (Sarstedt). Each metal concentration was obtained as the average of three measurements of the same sample. The metal concentration measurements with a relative standard deviation (RSD) $\leq$ 5% were considered as reliable data for the adsorption experiments.

3.2.5 Optical microscope

The average particles diameter of polymers was measured with an Olympus SZX9 optical microscope as the average of 20 or 40 polymer particles.

3.2.6 Scanning electron microscopy (SEM)

The surface morphology figures of polymers were captured using either a Hitachi SU3500 scanning electron microscope or a Gemini® Supra 40 VP scanning electron microscope. When the polymers conductivity was low, the materials were metallized with gold.

3.2.7 Nitrogen adsorption-desorption measurements

The nitrogen adsorption-desorption measurements were carried out at -196.15 °C on a Micromeritics Gemini V analyser. The samples were pre-conditioned at 80°C under vacuum to eliminate the adsorbed gases and humidity. The specific surface area and pore size distribution of polymers were determined with Brunauer-Emmett-Teller (BET) and Barrett-Joyner-Halenda (BJH) methods.

3.3 Synthesis of functional monomers

The synthesis of each of the three new monomers described in this doctoral manuscript was performed in a three-neck round-bottom flask immersed in an ice bath. The flask contained a magnetic stirrer and its necks were connected to a condenser, an argon purge system, and a dropping funnel (Figure 3.1).

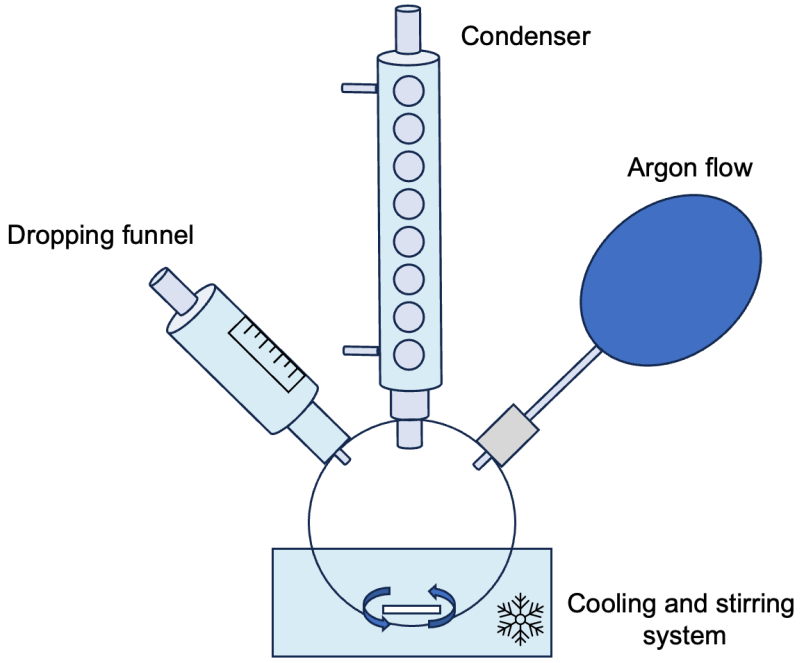

Figure 3.1. Schematization of the monomers synthesis set-up.

3.3.1 Synthesis of PIM-MMA

The synthesis of the PIM-based functional monomer, PIM-MMA, was carried out as follows. Two different solutions, named solution A and solution B, were prepared under argon atmosphere. To prepare the solution A, 30 mL of anhydrous dichloromethane were saturated in an ultrasound bath with $NaNO_2$. The solid phase was separated, and the remaining saturated solution was introduced in a three-neck round-bottom flask, mixed with 1.34 g (9.24 mmol) of PIM and 1.30 mL (9.24 mmol) of trimethylamine and cooled in an ice bath with NaCl. Solution B was prepared by dissolving 0.89 mL (9.24 mmol) of methacryloyl chloride in 10 mL of anhydrous dichloromethane. Solution B was then poured dropwise into the three-neck round-bottom flask containing solution A and stirred for 24 hours under argon atmosphere. The reaction product was washed three times with ultrapure water and then dried with $MgSO_4$. Finally, dichloromethane was removed with a rotary evaporator and PIM-MMA was obtained with a yield of 47%. The reaction product was finally analyzed with ^{1}H-NMR spectroscopy.

3.3.2 Synthesis of bis-AMP-MMA and AMP-MMA

The synthesis of the bis-AMP-based and AMP-based functional monomers, bis-AMP-MMA and AMP-MMA followed the same procedure. Two different solutions, named solution A and solution B, were prepared under argon atmosphere. Solution A was prepared by dissolving 0.89 mL (9.24 mmol) of methacryloyl chloride in 30 mL of anhydrous dichloromethane contained in a three-neck round-bottom flask cooled in an ice bath with NaCl. Solution B was prepared by dissolving 9.24 mmol of ligand (either 1.84 g of bis-AMP or 1.00 g of AMP) and 1.30 mL (9.24 mmol) of trimethylamine in 10 mL of anhydrous dichloromethane. Solution B was then poured dropwise in three-neck round-bottom flask containing solution A and stirred for 24 hours. The reaction product was washed three times with water and dried with $MgSO_4$. Finally, the dichloromethane was removed with a rotary evaporator to obtain the functional monomer. The monomers bis-AMP-MMA and AMP-MMA were obtained with a yield of 51% and 49%, respectively. The reaction products were analyzed with ^{1}H-NMR and ^{13}C-NMR spectroscopies.

3.4 Functional monomers polymerization test

Polymerization tests were carried out using the monomers bis-AMP-MMA and AMP-MMA through their inverse suspension copolymerization with MMA. The reactor for the polymerization tests consisted of a three-neck round-bottom flask equipped with a head mixer set at 700 rpm for the whole experiment.

3.4.1 bis-AMP-MMA polymerization test

The polymerization test on bis-AMP-MMA was carried out as follows. As a first step, 30 mL of mineral oil was introduced in the reactor and heated at 80 °C under argon

atmosphere. In a separate flask, 186 mg (0.695 mmol) of bis-AMP-MMA, 626 mg (6.26 mmol) of MMA and 4 mg (0.024 mmol) of AIBN were dissolved in 0.7 mL of DMSO-d_6 to form the pre-polymerization mixture. The monomers solution was stirred for 1 h under argon atmosphere and then quickly added to the pre-heated reactor to start the polymerization. The whole reaction lasted 48 h and two intermediate samplings were performed after 6 and 24 h. Both the intermediate sampling and the final reaction product were finally analyzed with ^{1}H-NMR spectroscopy.

3.4.2 **AMP-MMA polymerization test**

The polymerization test on AMP-MMA slightly differed from what is described for bis-AMP-MMA (sub-section 3.5.1). As a first step, 30 mL of mineral oil was introduced in the reactor and heated at 80 °C under argon atmosphere. In a separate flask, 122 mg (0.695 mmol) of AMP-MMA, 626 mg (6.255 mmol) of MMA and 4 mg (0.024 mmol) of AIBN were dissolved in 3 mL of DMSO-d_6 to form the pre-polymerization mixture. The mixture was then quickly added to the pre-heated reactor to start the polymerization. The whole reaction lasted 24 h and two intermediate samplings were performed after 4 and 6 h. Each of the two intermediate samplings and the final reaction product were finally analyzed with ^{1}H-NMR spectroscopy.

3.5 **Complex formation study**

The complex formation study was carried out on bis-AMP-MMA and AMP-MMA monomers coupled, in separated experiments, with Cu(II), Co(II), and Ni(II) ions. The effect of counter ion was tested by introducing in solution each metal as either its nitrate or perchlorate salt. The samples were prepared as DMSO solutions in 3 mL glass cuvettes and were analyzed within the wavelength range of 300-900 nm. The complex formation study on monomer/metal pair encompassed a total of 15 UV-Vis spectra, acquired at 80 °C. Each set of spectra contained 13 spectra generated at distinct monomer/template ratios, while maintaining their combined concentrations at 0.1 M. Additionally, each dataset was supplemented with the spectra for the monomer and the metal ion, both at a concentration of 0.1 M. The spectra related to bis-AMP-MMA and AMP-MMA complex formation study are shown in Figures 3.1 and 3.2, respectively.

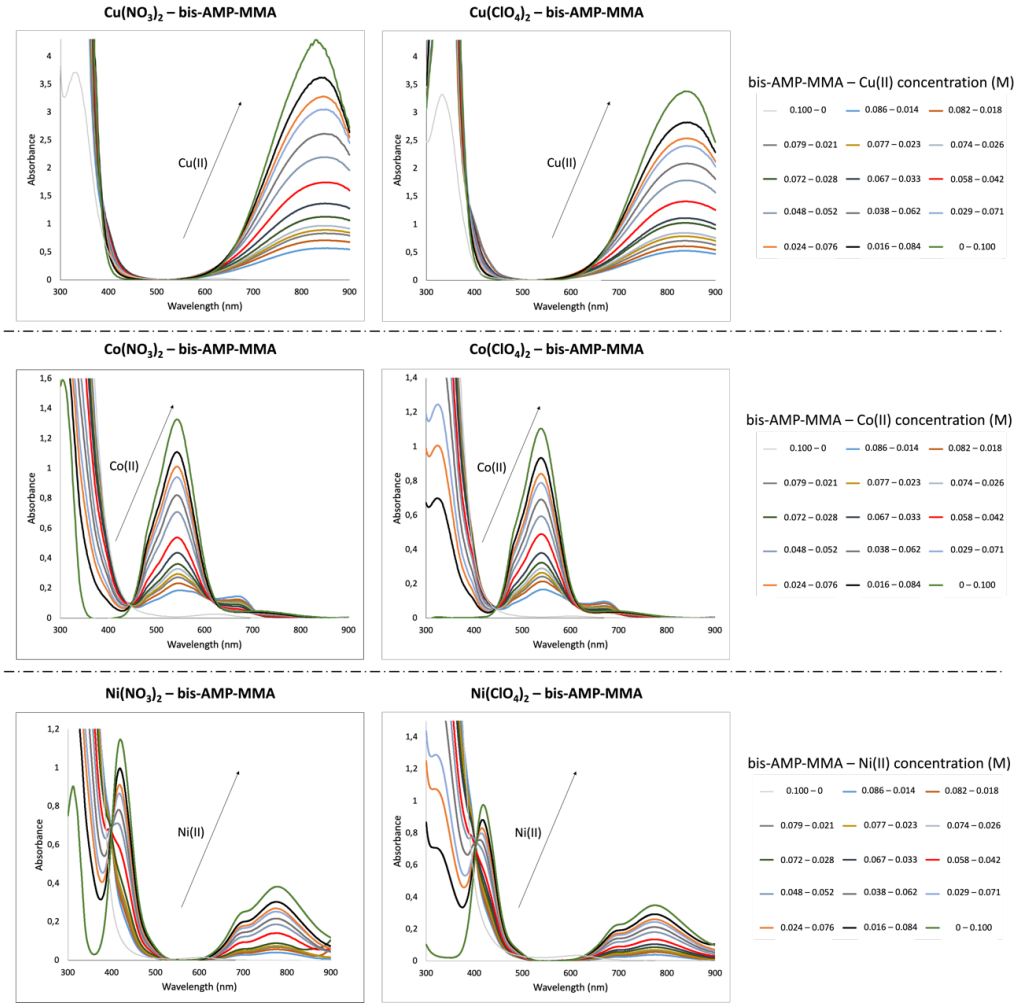

Figure 3.1. UV-Vis spectra of solutions containing bis-AMP-MMA coupled with Cu(II), Co(II) or Ni(II) nitrate or perchlorate salts at different monomer/metal ratios collected in DMSO at 80 °C.

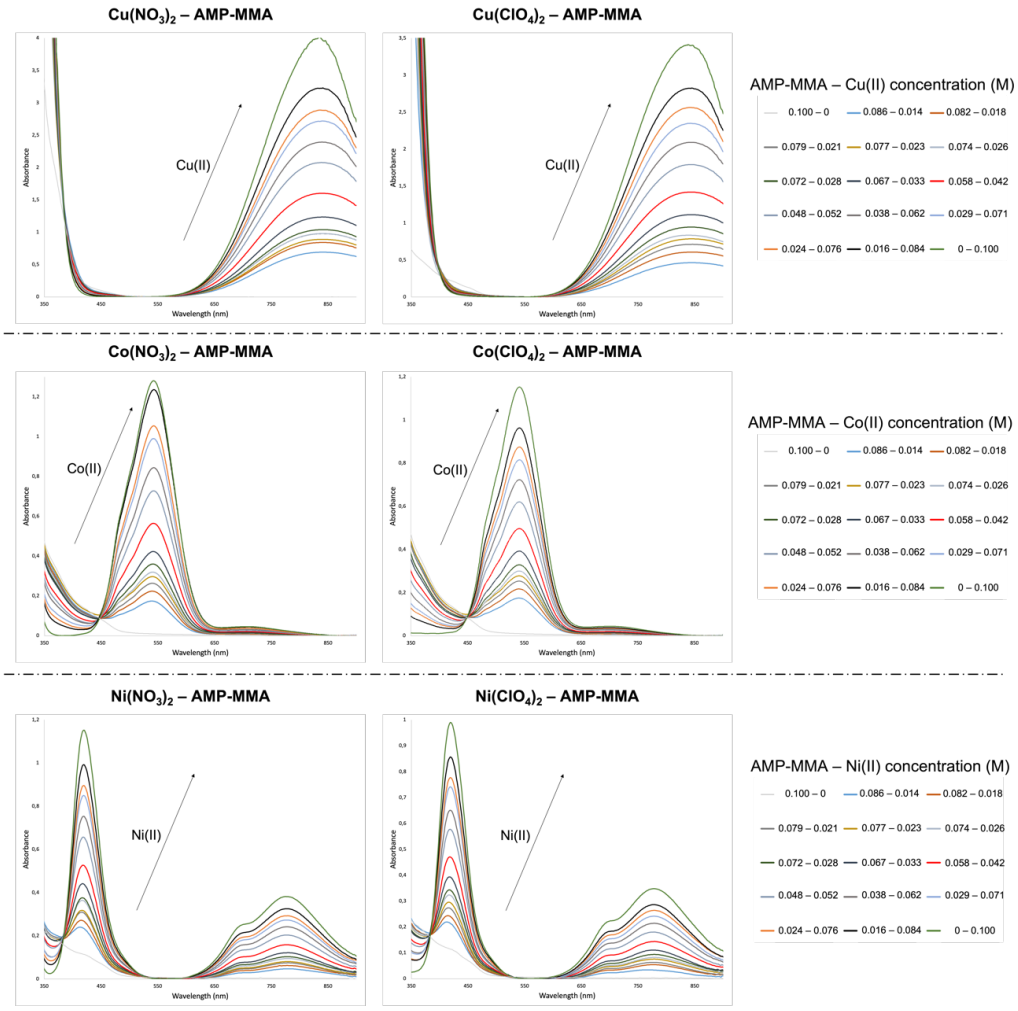

Figure 3.2. UV-Vis spectra of solutions containing AMP-MMA coupled with Cu(II), Co(II) or Ni(II) nitrate or perchlorate salts at different monomer/metal ratios collected in DMSO at 80 °C.

The UV-Vis spectra were finally processed with HypSpec, a program based on the LS minimization scheme, to extrapolate the complexes distribution and to determine their stability constants at equilibrium [317]. Stability constant estimation using HypSpec involves an iterative trial-and-error process. The program begins with an initial guess for stability constants, progressively refining the values through continuous data elaboration until the system converges to the final estimates. Stability constant values with various transition metals were already available in the literature for ligands used as precursors in the synthesis of bis-AMP-MMA and AMP-MMA [307,366]. These values were thus set as initial guesses for the program. This facilitated HypSpec to converge to the final stability constant values with a reduced number of iterations, making the entire trial-and-error process faster and more efficient. A more detailed description of the calculations

concerning the extrapolation of the complexes distribution and the estimation of stability constants values with HypSpec was previously provided in the literature [21,307].

3.6 Preparation and characterization of polymeric adsorbents

Each functional monomer was copolymerized with EGDMA via inverse suspension polymerization to obtain the related IIPs and NIPs. Additionally, Poly(EGDMA) was synthesized and served as a reference material for the chemical characterization of both IIPs and NIPs. The polymerization reactor consisted of a 250 mL three-neck flask, partially immersed in a heating system, equipped with a condenser, a head mixer, and an argon purging system.

3.6.1 Preparation of PIM-MMA Ni(II)-IIPs and NIP

Two distinct PIM-MMA-Ni(II)-IIPs were prepared by varying the Ni(II)/PIM-MMA ratio in the pre-polymerization mixture. These two IIPs are denoted as PIM-Ni-IIP-1:2 and PIM-Ni-IIP-1:3, with Ni(II)/PIM-MMA ratios of 1:2 and 1:3, respectively. As the first step, 120 mL of mineral oil (continuous phase) was introduced into the reactor and heated to 80 °C under an argon atmosphere. In a separate flask, the Ni(II)/PIM-MMA complex was prepared by dissolving either 404 mg (1.39 mmol, in the case of PIM-Ni-IIP-1:2) or 269 mg (0.93 mmol, in the case of PIM-Ni-IIP-1:3) of $Ni(NO_3)_2 \cdot 6H_2O$ and 593 mg (2.78 mmol) of PIM-MMA in 12 mL of DMSO. This solution was stirred for 1 hour under argon, and then 9 mL of EGDMA (50.1 mmol) and 150 mg (0.90 mmol) of AIBN were added to form the pre-polymerization mixture (dispersed phase). The dispersed phase was quickly introduced into the reactor, and the polymerization was carried out for 7 hours at 80 °C with a stirring rate of 700 rpm. The reaction product, consisting of polymer particles, was vacuum-filtered, washed with chloroform, and purified with a 1:1 acetone-chloroform mixture in a Soxhlet extractor for 24 hours. The polymer beads were washed 5 times with 40 mL of 1 M H_2SO_4 and MilliQ water over a 24-hour period. Finally, the polymer particles were dried under vacuum at 50 °C, resulting in 6.0 g of dry PIM-Ni-IIP-1:2 and 6.2 g of dry PIM-Ni-IIP-1:3. The corresponding NIP, PIM-NIP, was obtained and purified following each step described for the preparation of the Ni(II)-IIPs, including the leaching step. The only difference was the absence of $Ni(NO_3)_2 \cdot 6H_2O$ in the pre-polymerization mixture. The obtained product consisted of 5.8 g of dry polymer particles.

3.6.2 Preparation of bis-AMP-MMA IIPs and NIP

A Co(II)-IIP (bis-AMP-Co-IIP) and a Ni(II)-IIP (bis-AMP-Ni-IIP) were prepared using bis-AMP-MMA as the functional monomer. The preparation of both IIPs followed the same procedure, with the sole exception of the template ion used: $Co(NO_3)_2 \cdot 6H_2O$ for bis-AMP-Co-IIP and $Ni(NO_3)_2 \cdot 6H_2O$ for bis-AMP-Ni-IIP. The procedure began by introducing 127 mL of mineral oil (continuous phase) into the reactor and heating it to 80 °C under an argon atmosphere. In a separate flask, the template/bis-AMP-MMA complex

was prepared by dissolving 404 mg (1.39 mmol) of the template ion salt ($Co(NO_3)_2 \cdot 6H_2O$ for bis-AMP-Co-IIP and $Ni(NO_3)_2 \cdot 6H_2O$ for bis-AMP-Ni-IIP) and 743 mg (2.78 mmol) of bis-AMP-MMA in 3 mL of DMSO. This solution was stirred for 1 hour under argon, and then 4.5 mL of EGDMA (25.05 mmol) and 15 mg (0.09 mmol) of AIBN were added to form the pre-polymerization mixture (dispersed phase). The dispersed phase was quickly introduced into the reactor, and the polymerization was carried out for 6 hours at 80 °C with a stirring rate of 400 rpm. The resulting reaction product, resulting in polymer particles, was vacuum-filtered, washed with chloroform, and purified with a 1:1 acetone-chloroform mixture in a Soxhlet extractor for 24 hours. The polymer particles were washed 5 times with 40 mL of 3 M NH_4OH and MilliQ water over a 24-hours period. Finally, the polymer particles were dried under vacuum at 50 °C, resulting in 2.8 g of dry bis-AMP-Co-IIP and 2.7 g of dry bis-AMP-Ni-IIP. The corresponding NIP (bis-AMP-NIP) was obtained and purified following each step described for the synthesis of the two IIPs, including the leaching step. The only exception was the absence of the template ion salt in the pre-polymerization mixture. The obtained product consisted of 2.6 g of dry polymer particles.

3.6.3 **Preparation of AMP-MMA Ni(II)-IIP and NIP and poly(EGDMA)**

The Ni(II)-IIP of AMP-MMA monomer (AMP-Ni-IIP) was synthetized as follows. First, 120 mL of mineral oil (continuous phase) were introduced in the reactor and heated at 80 °C under argon atmosphere. In a separate flask, the Ni(II)/AMP-MMA complex was prepared by dissolving 404 mg (1.39 mmol) of $Ni(NO_3)_2 \cdot 6H_2O$ and 490 mg (2.78 mmol) of AMP-MMA in 12 mL of DMSO. This solution was first stirred for 1 h under argon atmosphere and then 4.5 mL of EGDMA (25.05 mmol) and 15 mg (0.09 mmol) of AIBN were added to form the pre-polymerization mixture (dispersed phase). The dispersed phase was quickly introduced in the reactor and the polymerization was carried out for 4 h at 80 °C with a stirring rate of 700 rpm. The reaction product, consisting of polymer particles, was vacuum filtered, washed with chloroform and purified with a 1:1 acetone-chloroform mixture in a Soxhlet extractor for 24 h. The polymer particles were washed 5 times with 40 mL of 0.1 M HCl and MilliQ water over a 24-hour period. Finally, the polymer particles were dried under vacuum at 25 °C resulting in 3.2 g of dry polymer.

The corresponding NIP (AMP-NIP) was obtained and purified following each step described for the preparation of AMP-Ni-IIP, including the leaching step. The only difference was the absence of $Ni(NO_3)_2 \cdot 6H_2O$ in the pre-polymerization mixture. The obtained product consisted of 3.3 g of dry polymer particles.

Poly(EGDMA) was prepared following the same procedure applied for AMP-NIP, apart from the absence of AMP-MMA in the pre-polymerization mixture, obtaining 2.8 g of dry polymer.

3.6.4 Polymer characterization

The chemical composition of IIPs, NIPs and poly(EGDMA) was assessed with FTIR and solid state ^{13}C CPMAS NMR spectroscopies. The morphology of IIPs and NIPs was studied with optical microscope, SEM, and nitrogen adsorption-desorption experiments.

3.7 Adsorption experiments

The metal ion adsorption experiments were performed as follows. A fixed amount of adsorbent and 10 mL of target ion solution were introduced in a 15 mL Corning© tube. The amount of adsorbent was equal to 20 mg for the adsorption experiments with PIM-MMA IIPs and NIP and 10 mg for those with bis-AMP-MMA and AMP-MMA IIPs and NIPs. Each metal ion was introduced in solution as nitrate salt. The 15 mL Corning© tube was shaken at 120 rpm for 20 h at room temperature. After this, the obtained dispersion was centrifuged at 5000 rpm for 5 min and filtered with a 0.45 μm surfactant-free cellulose acetate filter. The filtered solution was finally diluted with ultrapure water containing 1% of HCl and 1% of HNO_3 in 10 ml metal-free tubes and analyzed with ICP-MS. The adsorption capacity values were calculated using Eq. 2.3.

3.7.1 Effect of pH

The effect of pH on the adsorption capacity for each polymer was determined performing adsorption experiments on the target ion solutions prepared with different pH values. The target ion solution pH was adjusted with concentrated NaOH or HCl solutions.

3.7.2 Effect of contact time on adsorption

The effect of contact time on adsorption was investigated by performing adsorption experiments at different contact time, ranging from 5 min to 24 h. The metal solutions pH value was equal to 6.0 for the experiments carried out with PIM-MMA polymers and 6.5 for those with bis-AMP-MMA polymers. The pH value was adjusted with concentrated NaOH.

3.7.3 Adsorption isotherms

The adsorption isotherms were obtained by performing adsorption experiments at different target ion concentrations, ranging from 0.02 to 1 g/L. The pH value was adjusted with HCl (for pH 2) and NaOH (for pH 6 and 6.5) or controlled with HEPES buffer (for pH 7). The data related to the adsorption isotherms were fitted using both the Langmuir (Eq. 2.4) and Freundlich (Eq. 2.5) models.

3.7.4 Selectivity

The selectivity of each adsorbent was studied by performing adsorption experiments on binary solutions containing the target ion (either Ni(II) or Co(II)) and a competitive ion including either Ni(II) or Co(II), Cu(II), Cd(II), Mn(II), and Mg(II). The target ion concentration was equal to 0.01 g/L in each selectivity experiment. Different target ion/competitive ion ratios were investigated, including the values 1:1, 1:10 and 1:100. The pH values were adjusted with HCl (for pH 2) and NaOH (for pH 6 and 6.5) or controlled with HEPES buffer (for pH 7). The selectivity coefficient values k and the relative selectivity coefficient values k' were calculated with Eq. 2.6 and Eq. 2.8, respectively.

3.7.5 Polymer reusability

The reusability of the IIPs was studied for up to 5 adsorption-desorption cycles using HNO_3 (1 or 3 M), HCl (1 or 3 M) or NH_4OH (1 or 3 M) as leaching agents. Each regeneration cycle consisted of an adsorption experiment followed by a 30 min wash with 10 mL of leaching agent in 15 mL Corning© tubes at 120 rpm. The polymer particles were then rinsed with MilliQ water and dried in a vacuum oven at 60 °C for 24 h before being applied in the following adsorption-desorption cycle.

The adsorption efficiency ($adsorption\ efficiency_n\%$) was calculated after each adsorption-desorption cycle with Eq. 3.1:

$$Adsorption\ efficiency_n\% = \frac{q_{e,n}}{q_{e,1}} \quad (3.1)$$

where $q_{e,n}$ is the adsorption capacity of the cycle n (with n equal to 1, 2, 3, 4 or 5) and $q_{e,1}$ is the adsorption capacity of the first cycle.

4 Synthesis and characterization of novel Ni(II)-IIPs based on modified 2,2'-(pyridyl)imidazole

Table of contents

4.1 Introduction

As presented in Chapter 2, due to its Ni(II) binding properties, 2,2'-(pyridyl)imidazole (PIM) found diverse applications in the separation of Ni(II) from other metal ions including Fe(III), Mn(II), Mg(II), Ca(II), and Co(II). The reactivity of the nitrogen in the 1-position of the imidazole group in PIM (Figure 4.1) offers possibilities for its modification to synthetize new chelating agents or to functionalize resin beads. In the first case, PIM was modified with an octyl group to create OPIM, a chelating agent applied in the solvent extraction of Ni(II) ions [364]. In the second case, PIM ligand was anchored to Merrifield resin beads, which are composed of chloromethylated poly(styrene-*co*-DVB) [365]. In this chapter, a different modification of the 1-position of the imidazole group of the PIM ligand is proposed, with the aim of turning PIM ligand into a chelating monomer, PIM-MMA. For this purpose, a methacrylic group was introduced into the structure of PIM ligand to provide a polymerizable vinyl function.

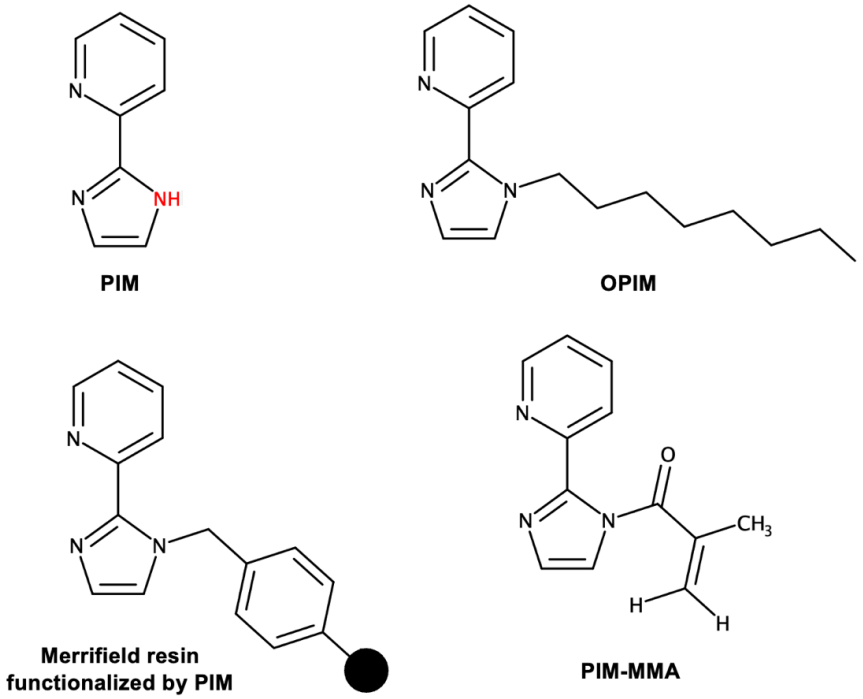

Figure 4.1. Structures of PIM, OPIM [364], Merrifield resin modified by PIM [365] and PIM-MMA. The nitrogen in the 1-position of the imidazole group of PIM is highlighted in red. The black circle in Merrifield resin modified by PIM represents the poly(styrene-*co*-DVB) backbone of the resin.

The preparation of a new PIM-based monomer aims to facilitate its stable incorporation into new polymeric adsorbents and effectively utilize the Ni(II) binding properties of PIM ligand. This chapter describes the synthesis of PIM-MMA and its application in the preparation of Ni(II)-IIPs. The application of the ion imprinting technique is expected to

enhance the selectivity of the new adsorbent materials toward Ni(II) ions, facilitating their selective separation.

4.2 Synthesis of PIM-MMA

The synthesis of the PIM-derivative monomer, PIM-MMA, was carried out by reacting the PIM ligand with methacryloyl chloride to introduce a methacrylic group within its structure (Figure 4.2).

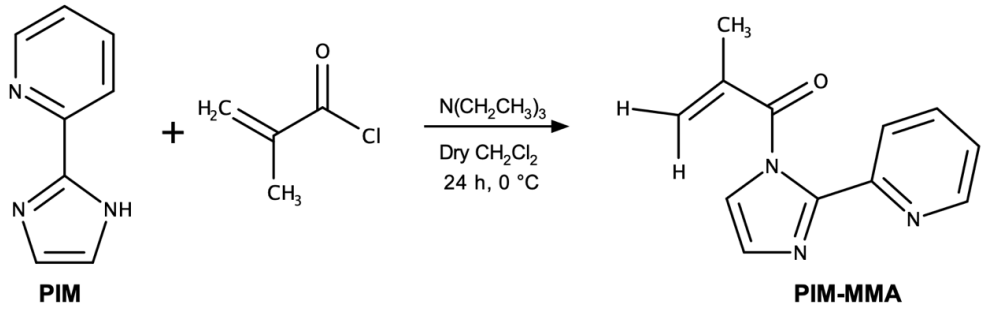

Figure 4.2. Synthesis of PIM-MMA chelating monomer.

The synthesis of PIM-MMA was first carried out without any special caution. This first attempt resulted in the presence of a high rate of the homopolymer of PIM-MMA in the final product. This was confirmed by the ^{1}H-NMR spectrum of the reaction product (Figure 4.3). In this spectrum, the peaks of the PIM-MMA homopolymer backbone could be observed at 3.7-3.8 ppm, 1.9-2.0 ppm and 1.2-1.4 ppm, commonly associated with the polymerization of the methacrylic group [372]. Additionally, a slight broadening of the peaks of PIM protons and a default of vinyl protons of the MMA moiety was observed.

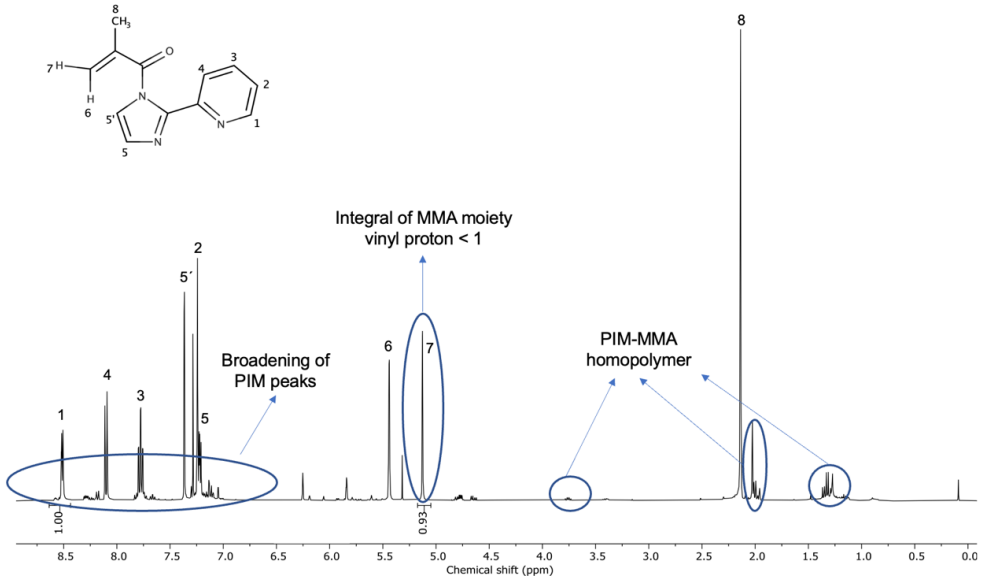

Figure 4.3. ^{1}H-NMR spectrum in $CDCl_3$ of PIM-MMA synthetized without inhibitor of polymerization.

The formation of PIM-MMA homopolymer could be significantly reduced by the introduction of sodium nitrite ($NaNO_2$) as an inhibitor of polymerization. This enabled the reduction of PIM-MMA homopolymer in the reaction product to a molar amount of less than 5%. This reaction product containing a small amount of homopolymer was used without other purifications in the following experiments. The ^{1}H-NMR spectrum of PIM-MMA synthetized in the presence of $NaNO_2$ is shown in Figure 4.4. The vinyl protons peaks at 5.43 and 5.12 ppm (Table A.1) confirmed the modification of PIM-MMA structure through the addition of the methacrylic group.

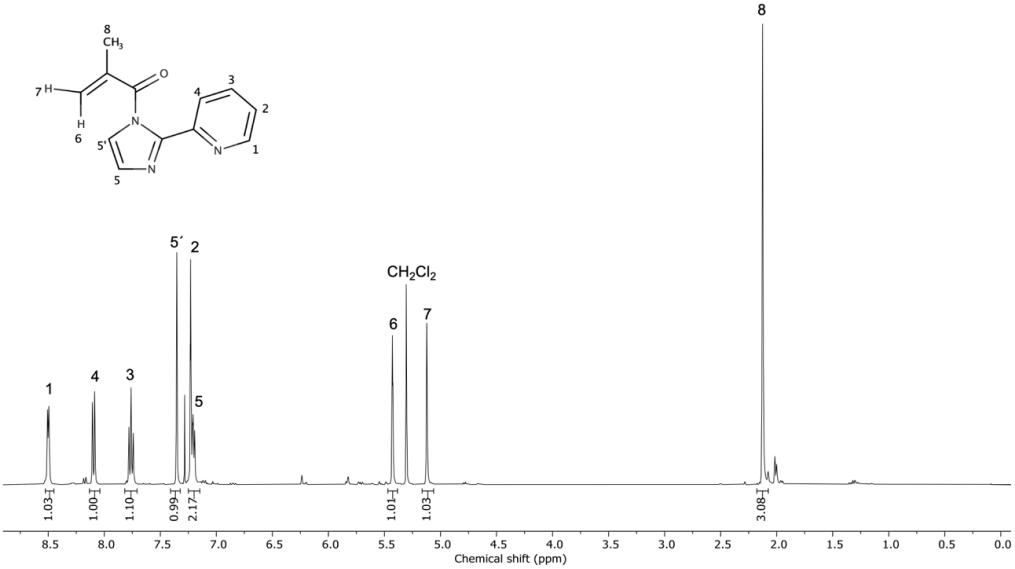

Figure 4.4. ^{1}H-NMR spectrum of PIM-MMA in $CDCl_3$ synthetized in presence of $NaNO_2$ as polymerization inhibitor.

Conducting an *in-situ* complex formation study between a chelating monomer and a metal ion under the same conditions applied for the preparation of IIPs is a quick and convenient method to control the complex structure in the pre-polymerization mixture (sub-section 2.5.3). Even though the introduction of $NaNO_2$ as polymerization inhibitor effectively slowed down the homopolymerization of PIM-MMA, this reaction was not completely avoided. Consequently, to prevent any polymerization of PIM-MMA within the UV-Vis cuvette, the complex formation study was not conducted on PIM-MMA.

4.3 Preparation of PIM-MMA polymers

All the polymers described in this thesis were prepared by inverse suspension polymerization, with mineral oil as the non-polar continuous phase. This polymerization method was applied as an alternative to the normal suspension polymerization (where water is the continuous phase) to prepare bead-shaped materials [262]. The choice of an inverse suspension was made to prevent the transfer of metal ions to the aqueous phase [274,335,336]. The crosslinker and porogen selected to prepare the IIPs were EGDMA and DMSO, respectively. A comparative study of IIPs prepared with different crosslinkers including EGDMA, DVB, PETA, and TMPTA revealed that involving EGDMA as crosslinker resulted in IIPs with more stable imprinting cavities and higher adsorption capacity [277]. DMSO was selected as a non-toxic, polar aprotic solvent, capable of solubilizing all the selected components for IIPs preparation with a boiling point (equal to 189 °C) higher than the polymerization temperature (80 °C).

Since it was not possible to study the formation of complexes between PIM-MMA and Ni(II), the synthesis of PIM-MMA IIPs was carried out by introducing the metal ion and the functional monomer according to the desired stoichiometries of the complexes. Thus, Ni(II) and PIM-MMA were introduced, in two separate experiments, with ratios of 1:2 and 1:3 into the pre-polymerization mixture. The IIPs prepared with a Ni(II)/PIM-MMA ratio of 1:2 and 1:3 were named PIM-Ni-IIP-1:2 and PIM-Ni-IIP-1:3, respectively. EGDMA, used as crosslinker, was introduced in the polymerization mixture with a PIM-MMA/EGDMA ratio equal to 1:18. The synthesis route for the preparation of PIM-Ni-IIP-1:2 and PIM-Ni-IIP-1:3 is shown in Figure 4.5. The corresponding NIP, PIM-NIP, was prepared to be used as a reference material in adsorption experiments.

The preparation of PIM-Ni-IIP-1:2, and PIM-Ni-IIP-1:3 included a leaching step, which involved 5 washes with 1 M H_2SO_4 to release the Ni(II) ions and generate ion-imprinted cavities. In order to compare the NIP with preparation conditions as close as possible to that of the IIPs, it was also submitted to this acidic treatment. As a matter of fact, in a recent work, Cao et al. studied the effect of acidic leaching on NIP particles prepared with EGDMA as crosslinker [373]. They proved that it was essential to apply the same post-treatment to the NIP after its synthesis in order to have a similar impact on the porous structure of the polymer.

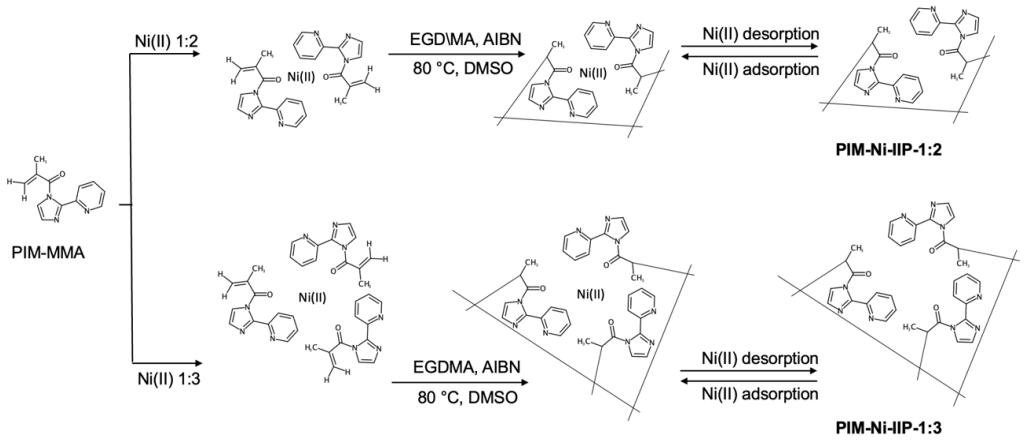

Figure 4.5. Synthesis route for the preparation of PIM-MMA IIPs.

The polymer particles of PIM-NIP, PIM-Ni-IIP-1:2 and PIM-Ni-IIP-1:3 are shown in Figure 4.6. The polymer particles of each material were characterized by different shades of yellow-orange. This is likely to derive from the presence of PIM-MMA monomer within their structures, as the color of pure poly(EGDMA) is white. The chemical composition and morphology of these polymer particles is described in the following sections (Section 4.4 and Section 4.5).

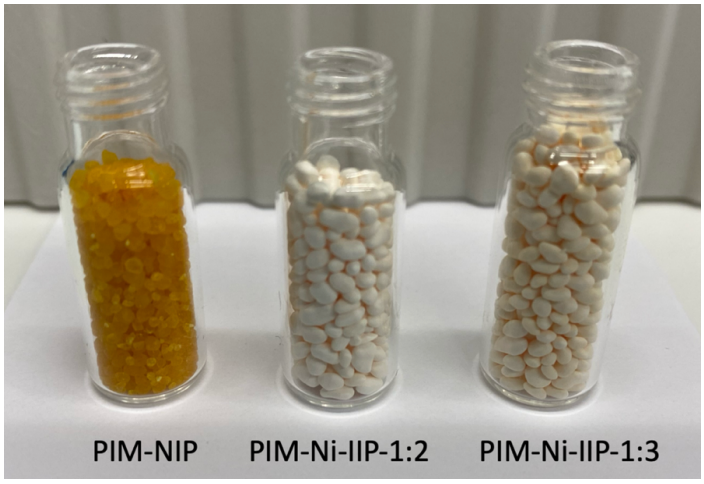

Figure 4.6. PIM-NIP, PIM-Ni-IIP-1:2, and PIM-Ni-IIP-1:3 polymer particles prepared via inverse suspension polymerization. The photographs were taken after the particles were subjected to the leaching step.

The homopolymer of the crosslinker EGDMA, poly(EGDMA), was synthetized in a similar way, to be used as a reference material for the chemical characterization of the IIPs and NIPs prepared in this doctoral thesis. By comparing the chemical composition of poly(EGDMA) with those of the IIPs and NIPs, it was possible to confirm the incorporation of the functional monomers within these materials.

4.4 Characterization of the chemical structure of PIM-MMA polymers

The chemical structure of the three PIM-MMA polymers was studied by FTIR (Figure 4.7) and ^{13}C CP-MAS NMR (Figure 4.8) spectroscopies. The presence of PIM-MMA within PIM-NIP, PIM-Ni-IIP-1:2 and PIM-Ni-IIP-1:3 polymer particles was verified by comparing their spectra with that of poly(EGDMA).

From the FTIR spectra (Figure 4.7), it was possible to detect in each material the presence of typical poly(EGDMA) absorption bands, including the stretching of C=O and C-O at 1725 and 1144 cm^{-1}, respectively, and the -OCH_2 deformation vibration band at 1460 cm^{-1} [292]. The incorporation of PIM-MMA into PIM-NIP, PIM-Ni-IIP-1:2, and PIM-Ni-IIP-1:3 was confirmed by the presence of C-N aromatic amine stretching bands at 1298 and 1320 cm^{-1}. FTIR spectra were collected for both materials before and after the leaching process, and no changes in their chemical composition were observed.

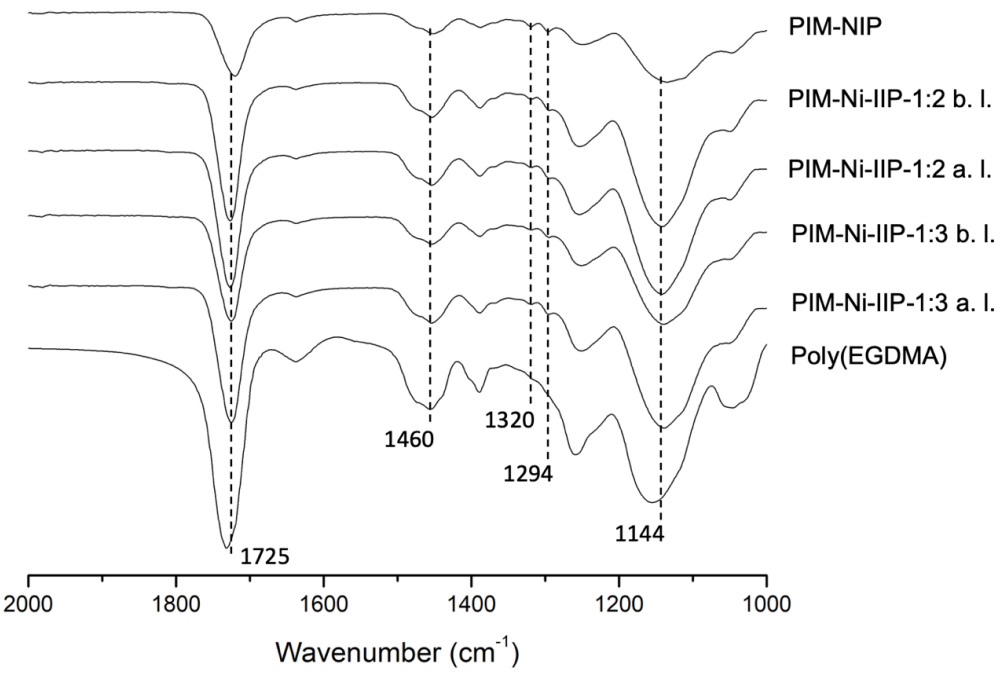

Figure. 4.7. FTIR spectra of PIM-NIP, PIM-Ni-IIP-1:2, and PIM-Ni-IIP-1:3 before leaching (b. l.) and after leaching (a. l.) and poly(EGDMA).

The presence of PIM-MMA within PIM-NIP, PIM-Ni-IIP-1:2, and PIM-Ni-IIP-1:3 was also confirmed by the ^{13}C CPMAS NMR spectra of these polymers (Figure 4.8). The presence of poly(EGDMA) in each material resulted in the carbonyl carbon (C=O) peak at 177.1 ppm, the pendant vinyl carbon ($C=CH_2$) peak at 137.1 ppm, the ester carbon (-COO-) peak at 62.9 ppm, the quaternary carbon (>C<) peak at 45.8 ppm, the methylene carbon ($-CH_2-$) peak at 24.5 ppm, and the methyl carbon ($-CH_3$) peak at 18.4 ppm [374,375]. With a PIM-MMA/EGDMA ratio of 1:18 in PIM-NIP, PIM-Ni-IIP-1:2, and PIM-Ni-IIP-1:3, the bands related to PIM-MMA were relatively weak and only a single aromatic carbon peak at 124.5 ppm was distinctly detectable in these polymers. However, this result was consistent with those obtained with FTIR spectroscopy and provided an additional validation about the correct integration of PIM-MMA within PIM-NIP, PIM-Ni-IIP-1:2, and PIM-Ni-IIP-1:3 polymer particles.

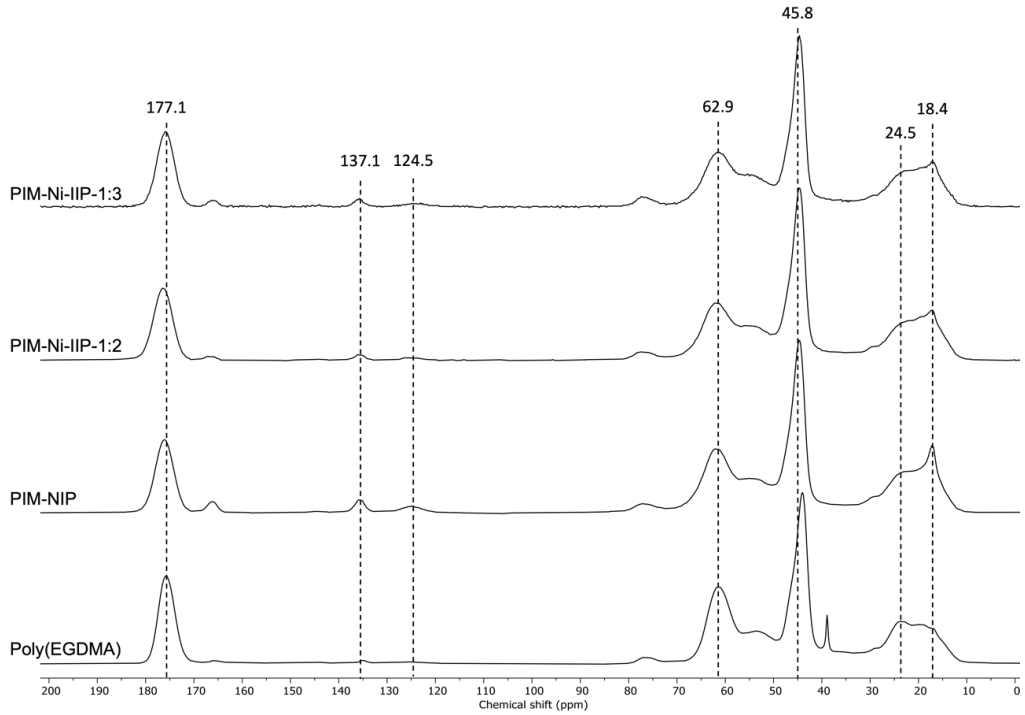

Figure 4.8. ^{13}C CPMAS NMR spectra of PIM-NIP, PIM-Ni-IIP-1:2, PIM-Ni-IIP-1:3, and poly(EGDMA).

4.5 Morphology of PIM-MMA polymers

The chemical characterization of PIM-NIP, PIM-Ni-IIP-1:2, and PIM-Ni-IIP-1:3 was followed by the study of their morphology through the determination of the average particle diameter with an optical microscope, the surface and internal morphologies with SEM, and the specific surface area, pore size and pore volume with nitrogen adsorption/desorption experiments.

4.5.1 Optical microscope analysis

The average particle diameter of PIM-NIP, PIM-Ni-IIP-1:2, and PIM-Ni-IIP-1:3 was determined by analyzing the optical microscope images of each material (Figure 4.9).

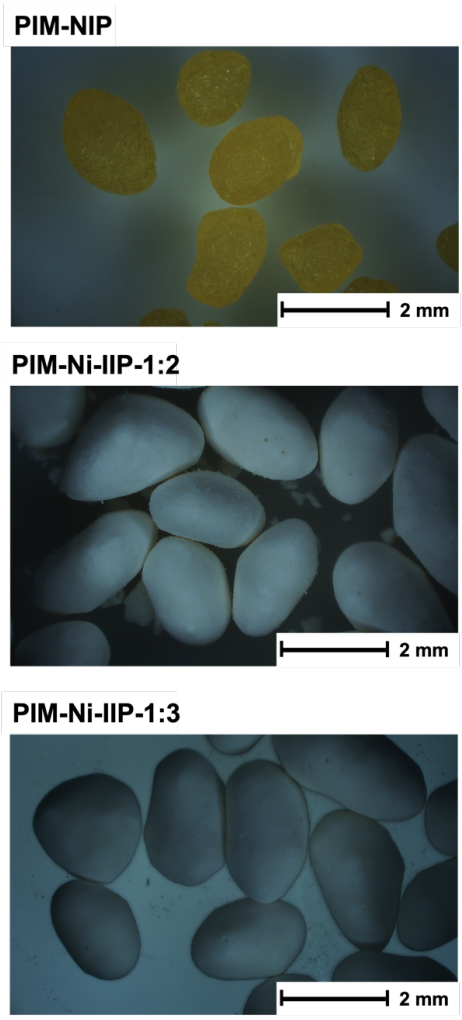

Figure 4.9. PIM-NIP, PIM-Ni-IIP-1:2, and PIM-Ni-IIP-1:3 images taken with a numerical optical microscope after Ni(II) ions leaching procedure.

The average particle diameter was determined by averaging the measurements of 40 polymer particles from each sample. Since the particles had an elongated shape rather than being a perfect sphere, as evidenced in Figure 4.9, each diameter was calculated as the average distance between their vertical and horizontal ends. The polymer particles in the IIPs had similar dimensions, with average diameters of 2.16 ± 0.49 mm for PIM-Ni-IIP-1:2 and 2.12 ± 0.56 mm for PIM-Ni-IIP-1:3. In contrast, PIM-NIP particles were smaller, with an average diameter of 1.54 ± 0.39 mm.

4.5.2 SEM pictures of whole and crushed polymer particles

The surface morphology and internal structure of PIM-NIP, PIM-Ni-IIP-1:2, and PIM-Ni-IIP-1:3 were studied with SEM pictures of their whole and crushed particles (Figure 4.10).

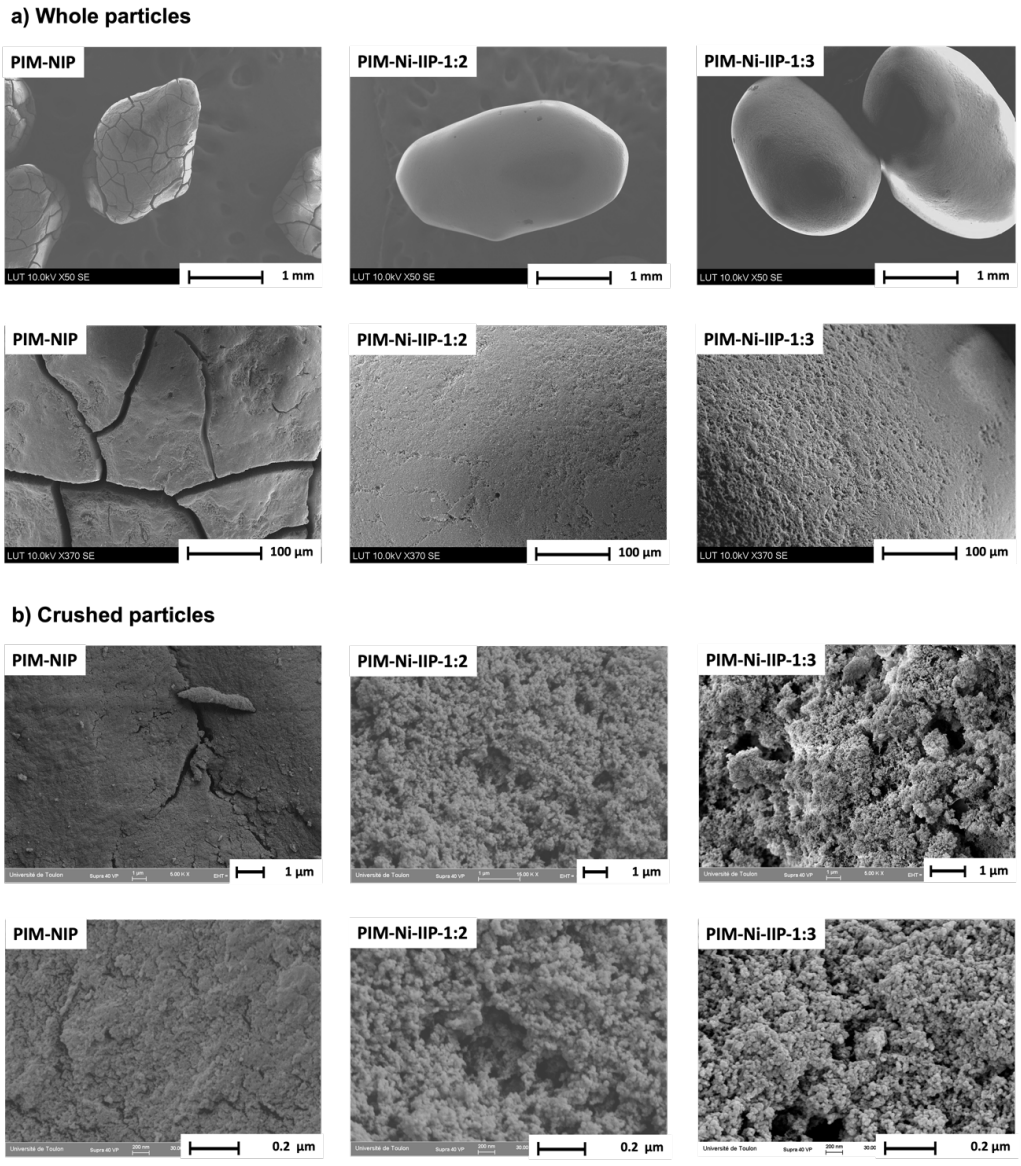

Figure 4.10. SEM pictures of outer surface of (a) whole polymer particles, and (b) internal section of crushed polymer particles of PIM-NIP, PIM-Ni-IIP-1:2, and PIM-Ni-IIP-1:3 captured after the leaching step.

The SEM images of whole polymer particles (Figure 4.10a) revealed a distinct contrast between the outer surfaces of PIM-NIP and PIM-IIPs particles. The surface of PIM-NIP exhibited cracks among blocks of smooth material. In contrast, the surfaces of both IIPs appeared more homogeneous and superficial cracks were not observed. When comparing the surface characteristics of the two IIPs, PIM-Ni-IIP-1:3 exhibits a slightly greater roughness than PIM-Ni-IIP-1:2. The internal morphology was investigated through SEM images of the internal section of crushed polymer particles (Figure 4.10b). The internal structures of PIM-NIP and the two PIM-IIPs differed significantly. While the internal structure of PIM-NIP particles was compact, those of the two IIPs exhibited a greater roughness.

4.5.3 Nitrogen adsorption-desorption experiments

Nitrogen adsorption-desorption experiments were conducted for the three PIM-MMA polymers, and the corresponding isotherms are depicted in Figure 4.11.

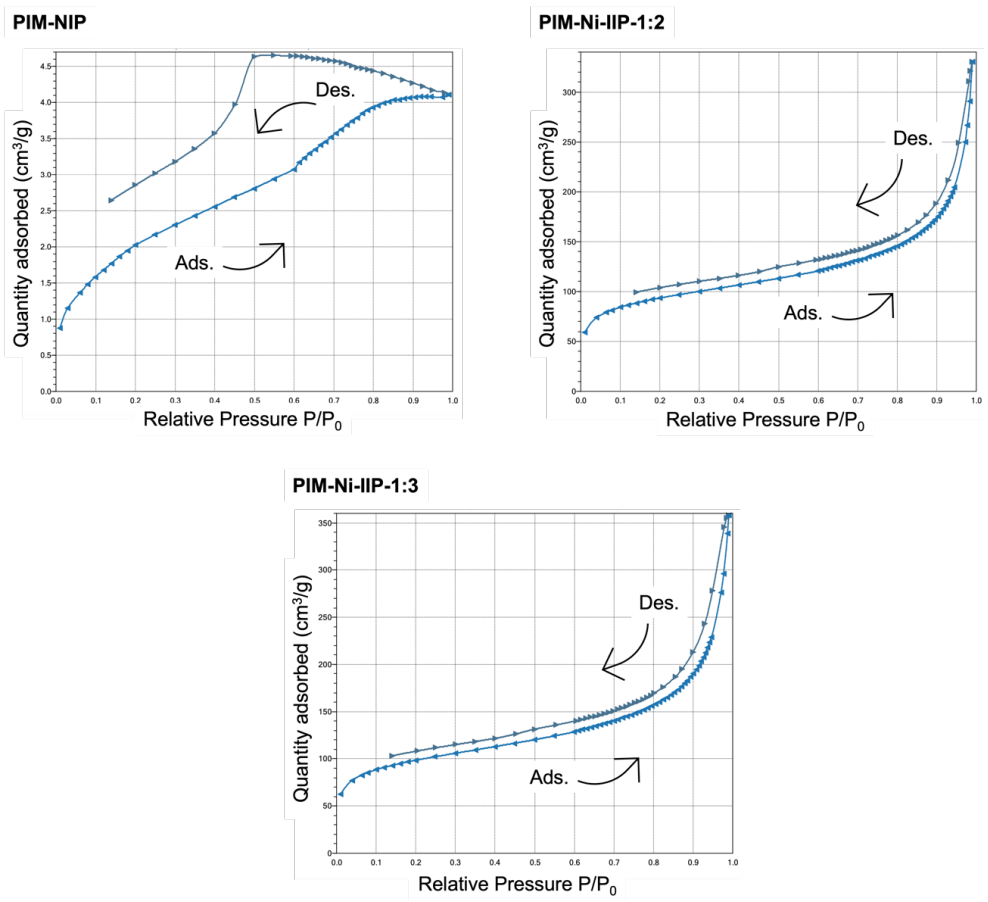

Figure 4.11. Nitrogen adsorption-desorption isotherms of PIM-NIP, PIM-Ni-IIP-1:2, and PIM-Ni-IIP-1:3.

The nitrogen adsorption-desorption isotherm for PIM-NIP exhibited, according to IUPAC classification (Figures A.1 and A.2), a Type IV isotherm with hysteresis loop H2, indicating a not well-defined distribution of pore size and shape. In contrast, both IIPs displayed Type II isotherms (Figure A.1) with hysteresis loop H3 (Figure A.2), suggesting the presence of slit-shaped pores. The presence of a discontinuity within the relative pressure range of 0.4-0.5 in the desorption curves for each material indicates the possible occurrence of cavitation.

The BJH [376] and BET [377] methods were used to determine the average pore diameters, total pore volumes, and specific surface areas for each material (Table 4.1).

Table 4.1. Average pore diameters, total pore volumes, and specific surfaces of PIM-NIP, PIM-Ni-IIP-1:2, and PIM-Ni-IIP-1:3 determined with BJH and BET methods.

Material	**Average pore diameter (nm)**	**Total pore volumes (cm^3/g)**	**Specific surface area (m^2/g)**
PIM-NIP	3.3	0.006	7.8
PIM-Ni-IIP-1:2	5.9	0.511	344.2
PIM-Ni-IIP-1:3	6.2	0.554	357.1

The average pore diameters, measuring 3.3 nm for PIM-NIP, 5.9 nm for PIM-Ni-IIP-1:2, and 6.2 nm for PIM-Ni-IIP-1:3, allowed for the classification of these materials as mesoporous polymers. The total pore volumes and specific surface areas of the IIPs were notably higher in comparison to PIM-NIP. A lower total pore volume and specific surface area for PIM-NIP when compared to both IIPs could be expected from the observations made with SEM (Figure 4.10). SEM images revealed that both IIPs displayed porous surfaces and highly porous internal structures, while PIM-NIP polymer particles exhibited smooth surfaces and compact internal structures.

4.6 Ni(II) adsorption experiments

After completing the characterization of PIM-Ni-IIP-1:2 and PIM-Ni-IIP-1:3, these materials, along with PIM-NIP as a reference, were tested in Ni(II) adsorption experiments. These experiments encompassed the effect of pH, the time dependence of Ni(II) adsorption, the determination of Ni(II) adsorption isotherms, and the assessments of polymer selectivity and reusability.

4.6.1 Effect of pH

Assessing how the pH impacts the adsorption capacity of an adsorbent is critical when determining the optimal pH range for its application. In the case of Ni(II) adsorbents,

literature commonly reports that pH values below 4 result in a significant or complete reduction in Ni(II) adsorption capacity [277,359,363,378]. This occurs due to the protonation of the adsorbent in acidic environments, resulting in electrostatic repulsion with the positively charged metal ion. Simultaneously, the hydronium ions, present in a high concentration in acidic media, competes with Ni(II) ions for the binding sites of the adsorbent, reducing its adsorption.

The effect of pH on Ni(II) adsorption capacity of PIM-Ni-IIP-1:2, PIM-Ni-IIP-1:3, and PIM-NIP was examined within the pH range 3-7 (Figure 4.12).

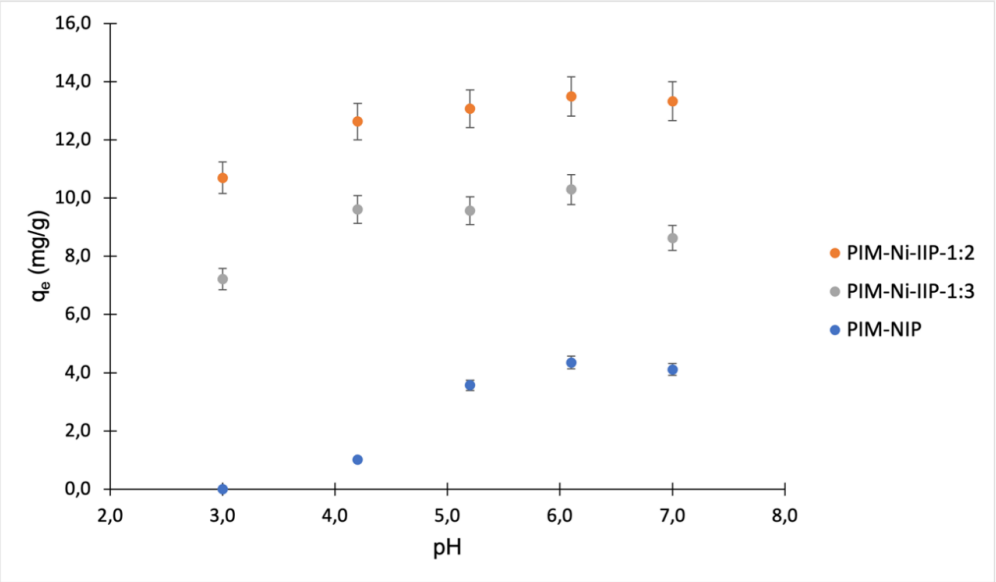

Figure 4.12. Effect of pH on Ni(II) adsorption capacity of PIM-Ni-IIP-1:2, PIM-Ni-IIP-1:3, and PIM-NIP. The initial Ni(II) ions concentration was equal to 500 mg/L. The pH value was adjusted with concentrated HCl and NaOH.

For all three polymers, the most favorable adsorption performances were observed within the pH range of 5-7, with the highest capacity achieved at pH 6. As the pH decreased below this range, PIM-Ni-IIP-1:2 and PIM-Ni-IIP-1:3 showed a slight reduction in adsorption capacity, while PIM-NIP exhibited a sharp decline. In detail, shifting from pH 6 to pH 4 resulted in a Ni(II) adsorption capacity decrease of only 6% and 7% for PIM-Ni-IIP-1:2 and PIM-Ni-IIP-1:3, respectively, while PIM-NIP suffered a substantial 77% reduction. At pH 3, the adsorption capacity of PIM-NIP approached zero and was considered negligible due to falling below the margin of experimental error. The lower reduction in the adsorption capacity of the PIM-Ni-IIP-1:2 and PIM-Ni-IIP-1:3 compared to PIM-NIP could be attributed to the positive effect of the ion-imprinting technique. When comparing the performances of the two IIPs, PIM-Ni-IIP-1:2, which was prepared with a Ni(II)-PIM-MMA ratio of 1:2, exhibited higher adsorption capacity compared to PIM-Ni-IIP-1:3, prepared with a Ni(II)-PIM-MMA ratio of 1:3. As the most favorable

adsorption results were achieved at pH 6, this pH value was selected to perform the following adsorption experiments.

4.6.2 **Time dependence of Ni(II) adsorption**

The relationship between adsorption capacity and the contact time between adsorbent materials and the Ni(II) solution was investigated through adsorption experiments of varying durations. Figure 4.13 presents the outcomes of these experiments for PIM-NIP, PIM-Ni-IIP-1:2, and PIM-Ni-IIP-1:3.

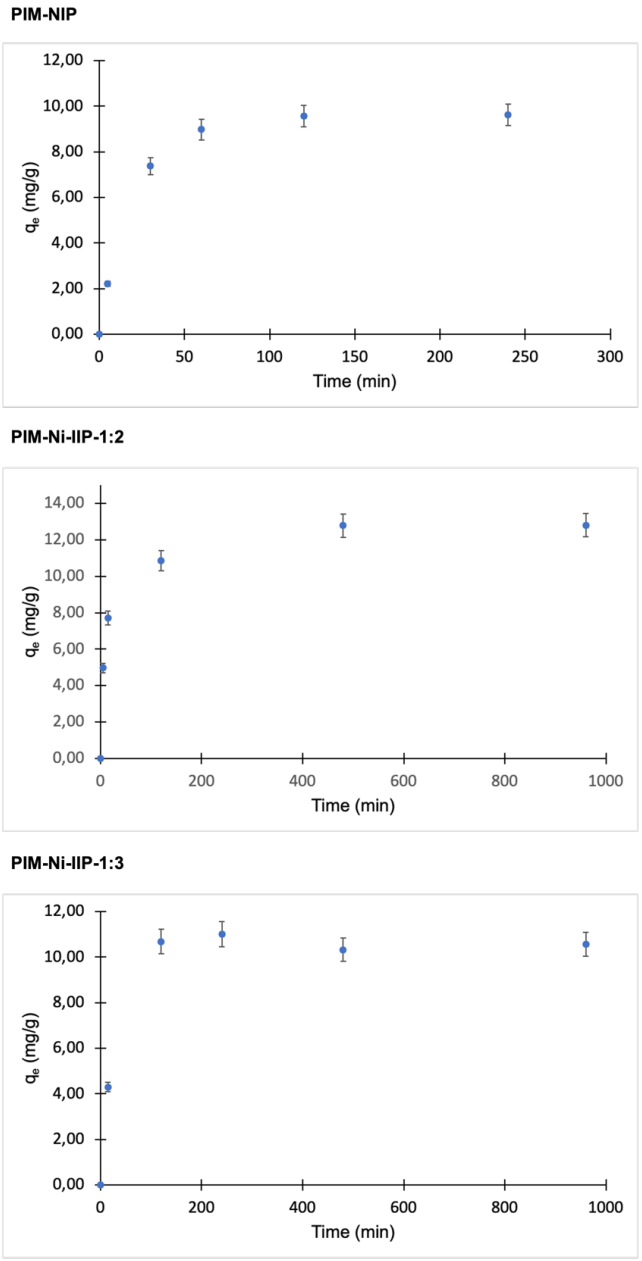

Figure 4.13. Impact of contact time on the Ni(II) adsorption capacity of PIM-NIP, PIM-Ni-IIP-1:2, and PIM-Ni-IIP-1:3. The initial concentration of Ni(II) ions was 500 mg/L, and the solutions pH was adjusted to 6 with NaOH.

The Ni(II) adsorption capacity of PIM-NIP increased during the first hour, after which it remained relatively constant. In the case of the two IIPs, the adsorption capacity of PIM-

Ni-IIP-1:3 reached a plateau within two hours, while a constant adsorption capacity value was observed for PIM-Ni-IIP-1:2 in the time interval ranging from 2 to 8 hours. To ensure efficient Ni(II) adsorption, a contact time of at least 20 hours was selected for the subsequent experiments.

4.6.3 Ni(II) adsorption isotherms

Ni(II) adsorption experiments were conducted for each adsorbent to determine their respective maximum adsorption capacities. These experiments were carried out at pH 6 at room temperature, using Ni(II) solutions with increasing concentrations. The resulting adsorption data for each adsorbent is shown in Figure 4.14.

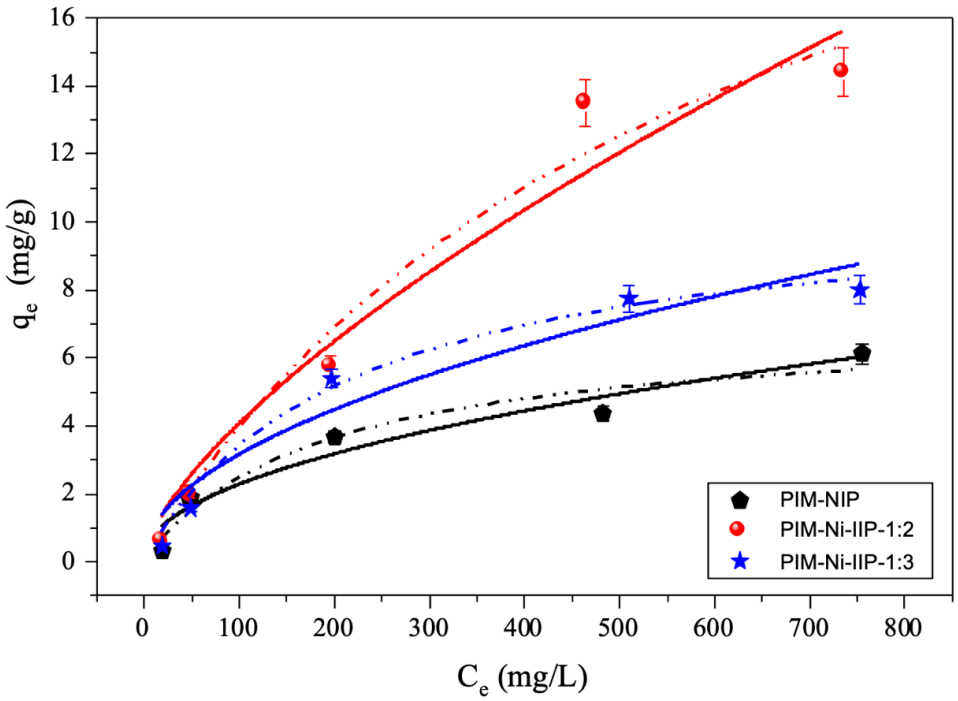

Figure 4.14. Ni(II) adsorption by PIM-NIP, PIM-Ni-IIP-1:2, and PIM-Ni-IIP-1:3. The adsorption data was interpolated with Langmuir (dashed lines) and Freundlich (continuous lines) models. The range of initial Ni(II) ions concentration was 20-750 mg/L and the pH was adjusted to 6 with NaOH.

The adsorption capacity of each material exhibited a significant increase in the Ni(II) concentration range of 20-200 mg/L. As the Ni(II) concentration approached 500 mg/L, the Ni(II) adsorption capacity of PIM-NIP and PIM-Ni-IIP-1:3 slightly increased, while a substantial variation was observed for PIN-Ni-IIP-1:2. Finally, when the Ni(II) concentration was around 800 mg/L, a minor variation in the adsorption capacity of each material was observed. The maximum adsorption capacity for each set of experiments

was determined by fitting the adsorption data with the Langmuir (Eq. 2.4) and Freundlich (Eq. 2.5) models (Table 4.2).

Table 4.2. Langmuir and Freundlich model parameters for Ni(II) adsorption with PIM-NIP, PIM-Ni-IIP-1:2, and PIM-Ni-IIP-1:3 at pH 6.

Model	**Parameter**	**Adsorbent**		
		PIM-NIP	**PIM-Ni-IIP-1:2**	**PIM-Ni-IIP-1:3**
Langmuir	$q_{e,max}$ (mg/g)	7.03	27.91	10.73
	K_L	0.005	0.002	0.005
	R^2	0.930	0.968	0.985
Freundlich	1/n	0.488	0.680	0.511
	K_F	0.236	0.174	0.295
	R^2	0.929	0.944	0.918

The effective interpolation of adsorption data by the Langmuir model suggests a material with homogenous binding sites with equivalent adsorption energy and no interaction between adsorbate molecules on adjacent sites [345]. Conversely, isotherm data effectively interpolated by the Freundlich model is indicative of a material where the adsorption occurs on heterogeneous surfaces [346]. In the case of the isotherm data of PIM-NIP, both models yielded similar correlation coefficients R^2, making it challenging to precisely distinguish whether the binding sites are homogeneous or heterogeneous. The isotherm adsorption data for both IIPs were most accurately interpolated by the Langmuir model, indicating a higher homogeneity of the adsorption sites.

PIM-Ni-IIP-1:2 exhibited the highest maximum adsorption capacity, followed by PIM-Ni-IIP-1:3 and PIM-NIP, with values of 27.91, 10.73, and 7.03 mg/g, respectively. This result was consistent with the observations previously made during the investigation of the effects of pH on Ni(II) adsorption capacity. The enhanced Ni(II) adsorption capacity of both IIPs in comparison to PIM-NIP is likely to derive from the presence of Ni(II)-imprinted cavities within these materials. When comparing the maximum adsorption capacity of PIM-Ni-IIP-1:2 to existing literature data for other Ni(II)-imprinted materials (Table 2.2), it falls within the middle range of values. For this reason, to consider this adsorbent as a viable alternative to the materials described in the literature, it is fundamental for it to exhibit a high selectivity for Ni(II) ions.

4.6.4 **Selectivity**

The ion imprinting technique was initially developed to enhance the selectivity of adsorbents for a specific target ion [239]. Selectivity is therefore a key property in ion-imprinted materials, and its value can be expressed using the selectivity coefficient k (Eq. 2.6). The adsorbent selectivity toward Ni(II) ions was investigated at pH 6 using bi-components solutions containing Ni(II) paired with one divalent metal ion M(II) among Co(II), Cd(II), Mn(II), and Mg(II). These metals were chosen as they are commonly encountered as competitive ions in the hydrometallurgical separation processes. The selectivity coefficient k and relative selectivity coefficient k' (Eq. 2.8) values for each M(II)/Ni(II) pair at different M(II)/Ni(II) ratios are reported in Table 4.3.

Table 4.3. Selectivity coefficient and relative selectivity coefficient values for PIM-NIP, PIM-Ni-IIP-1:2, and PIM-Ni-IIP-1:3 at pH 6 with Co(II), Cd(II), Mn(II) or Mg(II), as competitive ions.

M(II)	$\frac{\mathbf{M(II)}}{\mathbf{Ni(II)}}$	**PIM-NIP**	**PIM-Ni-IIP-1:2**		**PIM-Ni-IIP-1:3**	
		$\boldsymbol{k}$	$\boldsymbol{k}$	$\boldsymbol{k'}$	$\boldsymbol{k}$	$\boldsymbol{k'}$
Co(II)	1	1.35	1.34	1.00	0.62	0.46
	9	0.84	1.23	1.50	0.85	1.01
Cd(II)	1	1.15	1.70	1.50	0.45	0.39
	9	2.68	2.84	1.10	0.70	0.26
Mn(II)	1	1.41	11.28	8.00	1.30	0.92
	9	0.81	1.37	1.70	1.19	1.50
Mg(II)	1	0.44	1.31	3.00	0.70	1.59
	9	1.19	1.44	1.20	0.75	0.63

The k values associated with PIM-NIP provided insights into the adsorbent selectivity before the imprinting technique was applied. Among the studied competitive ions, when the M(II)/Ni(II) ratio was set to 1, only the adsorption of Mg(II) yielded a k value below 1 (specifically, 0.44), whereas Co(II), Cd(II), and Mn(II) as competitive ions resulted in k values above 1. This suggests that, among the examined ions, only the adsorption of Mg(II) was favored over that of Ni(II) by PIM-NIP. For PIM-Ni-IIP-1:2, the k values for each M(II)-Ni(II) pair consistently exceeded 1. Additionally, the relative selectivity coefficient k' indicated an improved selectivity compared to PIM-NIP. These two results showed the beneficial impact of the imprinting technique on selectivity for this material. The same trend was not observed for PIM-Ni-IIP-1:3, where the selectivity for Ni(II) ions

was poor. This could derive from the presence of uncomplexed PIM-MMA, which in the synthesis of this polymer was introduced in excess respect to the synthesis of PIM-Ni-IIP-1:2, resulting in non-specific binding sites. However, since it was not possible to conduct a study on complex formation with this monomer, this conclusion remains a hypothesis.

Among the three materials discussed in this chapter, PIM-Ni-IIP-1:2 exhibited the highest selectivity for Ni(II) ions. Its *k* values with Co(II), Cd(II), Mn(II), and Mg(II) as competitive ions was as high as 1.34, 2.84, 11.28, and 1.44, respectively. When the M(II)/Ni(II) molar ratio was set to 9, there was only a slight variation in the *k* values of PIM-Ni-IIP-1:2 when Co(II), Cd(II), or Mg(II) were introduced as competitive ions. Conversely, a significant decrease in selectivity was observed with Mn(II) as a competitive ion. To determine if a *k* value is high enough to ensure the selective separation of a target ion from a competitive ion, it is required to define the initial concentrations of both ions and the desired level of purity for the target ion. As an example, in a binary solution where both ions have the same concentration, an adsorbent with a *k* value equal to 9 ensures the recovery of the target ion with a purity of 90%, where the 10% of impurity is ideally constituted by the competitive ion. This separation can be considered sufficiently selective or not according to the purity required by the application where the target metal will be involved. Consequently, it is not possible to establish an absolute threshold for what constitutes a sufficiently high selectivity coefficient. In the case of PIM-Ni-IIP-1:2, despite the selectivity study suggesting a slight preference of this material for Ni(II) ions, the *k* values, apart from the case of Mn(II) as a competitive ion, were limited to values below or slightly higher than 2. Even though a target of purity was not strictly defined, these values cannot be considered high enough to conduct the selective separation of Ni(II) ions.

4.6.5 **Reusability of PIM-Ni-IIP-1:2**

In both this chapter and the following ones, the material with the best absorption capacity and selectivity for the target ion was subjected to a reusability study. In this chapter, the reusability study was conducted on PIM-Ni-IIP-1:2 through 5 adsorption-desorption cycles (Figure 4.15). After each adsorption experiment, the desorption of Ni(II) ions was performed using NH_4OH 3 M as the Ni(II) leaching agent. The material reusability was assessed by calculating the residual adsorption capacity after each adsorption cycle in relation to the first cycle (Eq. 3.1).

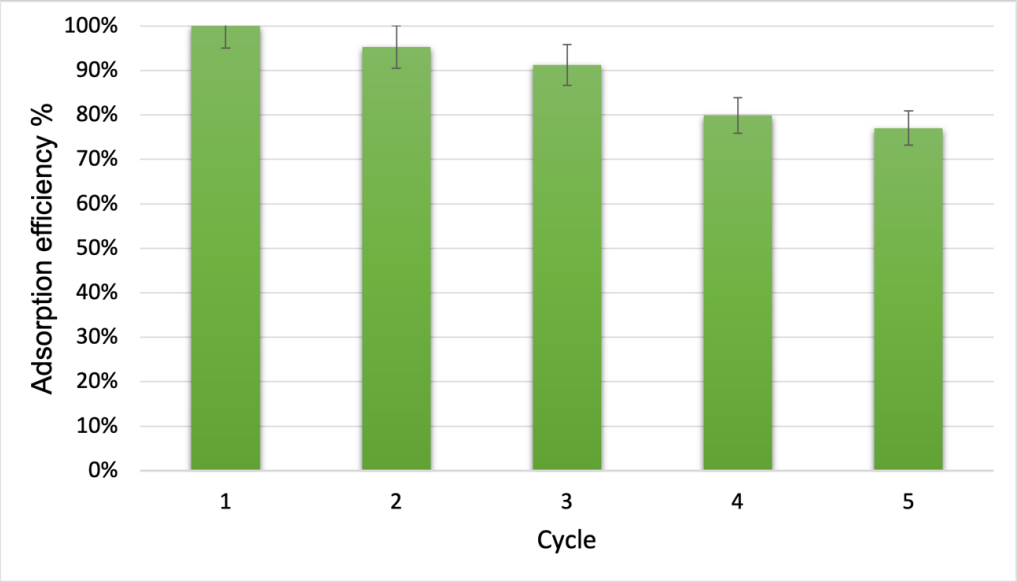

Figure 4.15. PIM-Ni-IIP-1:2 adsorption efficiency in 5 adsorption-desorption cycles with NH_4OH 3M as leaching agent. The initial Ni(II) ions concentration was equal to 500 mg/L and the solution pH was 6.

This test demonstrated that PIM-Ni-IIP-1:2 could be effectively reused in Ni(II) adsorption experiments, with an approximately 5% reduction in adsorption efficiency after the first adsorption-desorption cycle, increasing to around 23% in the fifth cycle.

4.7 Conclusion

In this chapter, the synthesis of a novel chelating monomer, PIM-MMA, based on 2-(2-pyridyl)imidazole (PIM) and its application in the preparation of Ni(II)-IIPs, were described. The synthesis of PIM-MMA, confirmed via ^{1}H-NMR spectroscopy, required the presence of a polymerization inhibitor to avoid its homopolymerization. The tendency of PIM-MMA to undergo homopolymerization prevented the possibility of conducting an *in-situ* complex formation study as it would polymerize within the UV-Vis cuvette.

Two different IIPs, named PIM-Ni-IIP-1:2 and PIM-Ni-IIP-1:3, were prepared introducing in the pre-polymerization media Ni(II) and PIM-MMA with 1:2 and 1:3 ratios, respectively. However, since the complex formation study on PIM-MMA could not be conducted, there was no conclusive evidence regarding the presence of 1:2 or 1:3 complexes within the polymerization media of these materials. The related non-imprinted polymer, PIM-NIP, was synthesized under the same experimental conditions, omitting the presence of Ni(II) in the pre-polymerization medium. The presence of PIM-MMA within each of the three materials was verified by FTIR and ^{13}C CP-MAS NMR spectroscopies. The morphology of the polymer particles was studied by SEM and nitrogen adsorption-desorption experiments. PIM-NIP polymer particles exhibited low

porosity and specific surface area. In contrast, both IIPs displayed considerably higher porosity and specific surface area.

The materials were finally applied in Ni(II) adsorption experiments, encompassing investigations into the impact of pH, contact time dependency, adsorption isotherms, selectivity, and reusability. PIM-Ni-IIP-1:2 consistently exhibited a higher adsorption capacity in comparison to PIM-Ni-IIP-1:3 and PIM-NIP with a maximum adsorption capacity at pH 6 equal to 27.91 mg/g. Moreover, PIM-Ni-IIP-1:2 demonstrated a higher selectivity for Ni(II) ions with *k* values as high as 1.34, 2.84, 11.28, and 1.44 with Co(II), Cd(II), Mn(II), and Mg(II) as competitive ions, respectively. However, the selectivity for Ni(II) was not sufficiently high to enable its selective separation, and the synthesis of more selective chelators was still required.

5 Synthesis and characterization of novel IIPs based on modified bis(2-pyridylmethyl)amine

Table of contents

5.1 Introduction

Bis-AMP ligand forms complexes with 1:1 and 1:2 stoichiometries with various metal ions, among which the most stable are those with Cu(II), Ni(II) and Co(II) ions [366]. The metal binding properties of bis-AMP in acidic media made it a versatile precursor to prepare chelating resins, such as the commercial resin Dowex™ M4195 [367]. In this resin, the bis-AMP ligand was anchored to poly(styrene-*co*-DVB) through its secondary amine group (Figure 5.1). Despite its effective application in the industrial separation of Ni(II) ions from Co(II) ions, this resin was limited by the strong retention of Cu(II) ions when present in solution [235]. To enhance the selectivity of bis-AMP ligand, in this chapter its modification with a methacrylic group to turn it into a chelating monomer, named bis-AMP-MMA (Figure 5.1), was proposed.

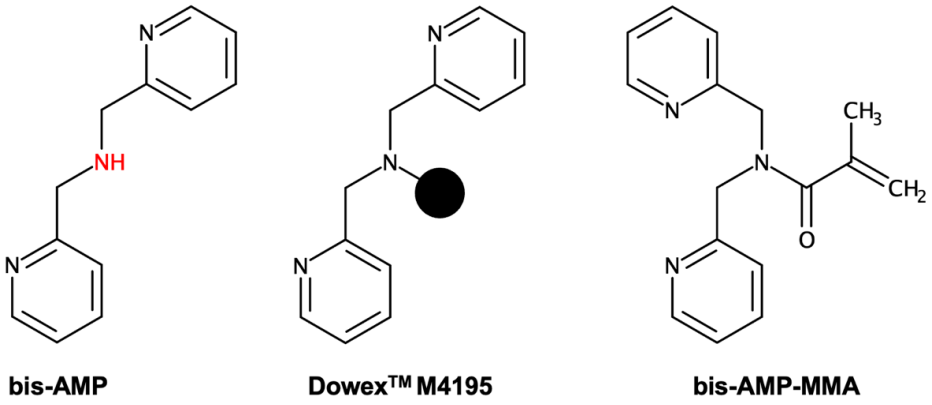

Figure 5.1. Structures of bis-AMP, Dowex™ M4195, and bis-AMP-MMA. The secondary amine group of bis-AMP is highlighted in red. The black circle in Dowex™ M4195 represents the poly(styrene-*co*-DVB) backbone of the resin.

The aim of the modification of bis-AMP by introducing a polymerizable function was to synthetize a novel chelating monomer which could be used to prepare selective adsorbents with the ion imprinting technique. The formation of complexes between bis-AMP-MMA and Cu(II), Co(II) and Ni(II) ions was studied to optimize the pre-polymerization conditions for the preparation of Co(II)-IIPs and Ni(II)-IIPs. The application of the ion imprinting technique was expected to enhance the selectivity of the bis-AMP-based materials through the formation of selective binding cavities.

5.2 Synthesis of bis-AMP-MMA

The monomer bis-AMP-MMA was synthetized by reacting the bis-AMP ligand with methacryloyl chloride. Through this process, a methacrylic group was introduced into bis-AMP structure, as illustrated in Figure 5.2.

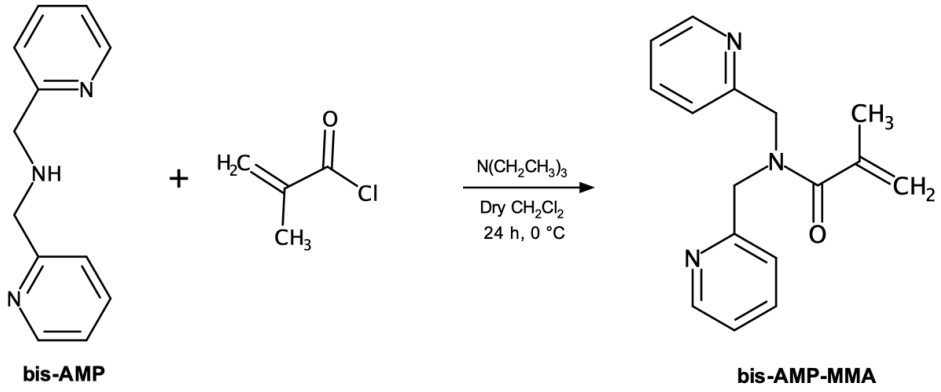

Figure 5.2. Synthesis of bis-AMP-MMA monomer.

The introduction of the methacrylic group within the bis-AMP structure was confirmed by the vinyl protons peak at 5.18 ppm (Table A.2) in the ^{1}H NMR spectrum (Figure 5.3.a), and by the vinyl carbons peaks at 140.4 ppm and 115.5 ppm (Table A.3) in the ^{13}C NMR spectrum (Figure 5.3.b).

a) ^{1}H NMR spectrum

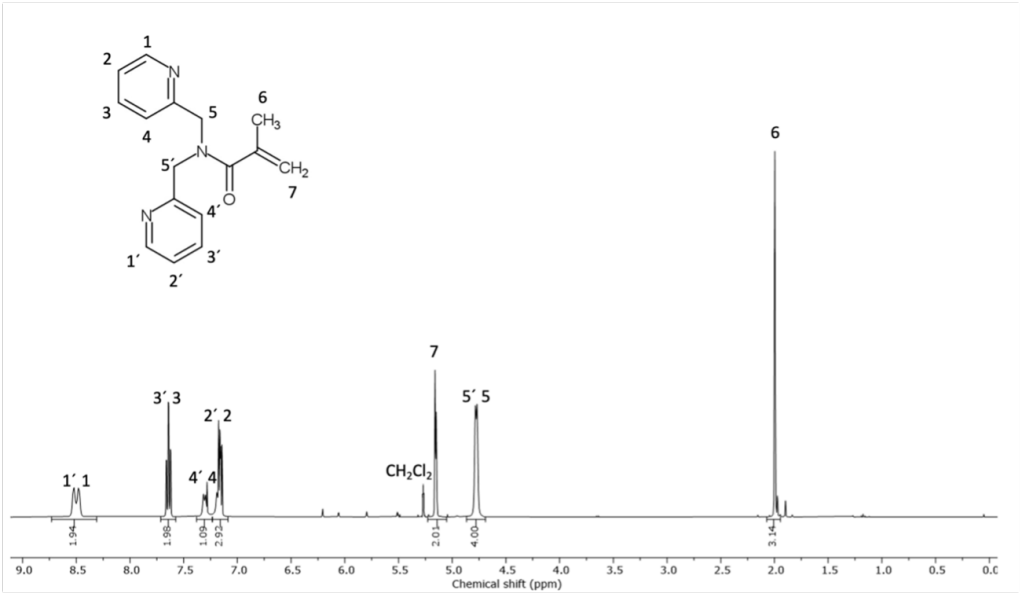

b) ^{13}C NMR spectrum

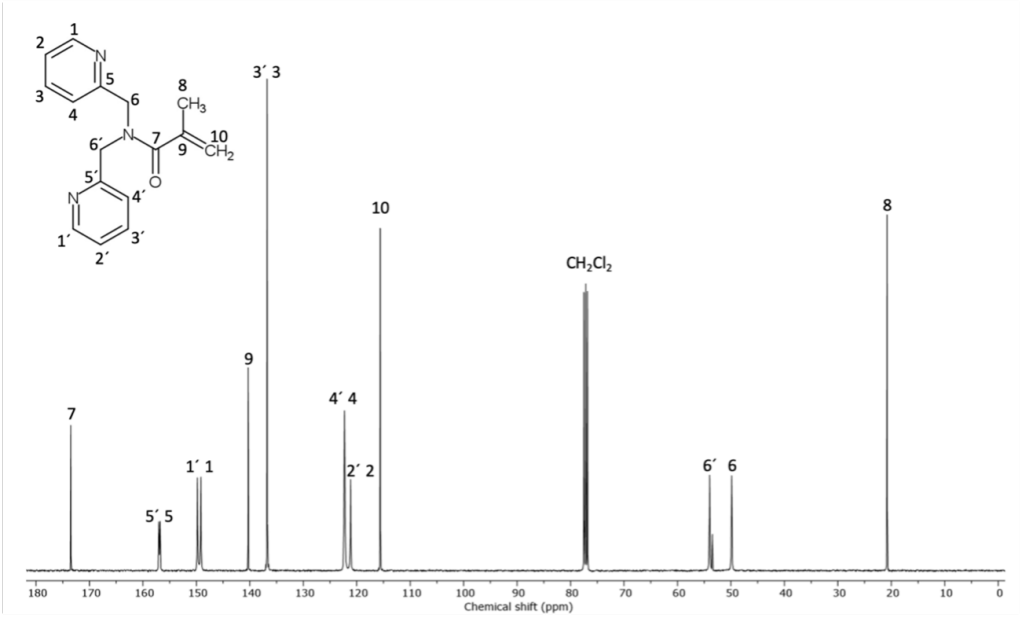

Figure 5.3. ^{1}H NMR spectrum (a) and ^{13}C NMR spectrum (b) of bis-AMP-MMA in $CDCl_3$.

The study on the bis-AMP-MMA monomer was completed by evaluating its reactivity in a copolymerization reaction with MMA and with the study of the formation of complexes with Cu(II), Co(II), and Ni(II) ions.

5.3 Polymerization test

The synthesis of bis-AMP-MMA was followed by its copolymerization with MMA to evaluate its applicability in polymer preparation. MMA was chosen as the comonomer for this polymerization test due to the similarity in its structure to EGDMA [379], the crosslinker used for IIPs preparation. The selection of MMA was driven by the need to prepare a linear and soluble copolymer whose composition can be characterized by liquid ^{1}H-NMR. The bis-AMP-MMA/MMA ratio was equal to 1:9, both monomers were dissolved in DMSO-d_6, and the polymerization mixture, put under argon atmosphere, was suspended in mineral oil pre-heated to 80 °C. These polymerization conditions were selected to closely resemble those applied for IIPs preparation. The whole test lasted 48 h, with intermediate sampling after 6 h and 24 h. The intermediate sampling and the final reaction product were analyzed with ^{1}H-NMR spectroscopy (Figure A.3) to determine the conversion percentage of each monomer into polymer and the fraction of bis-AMP-MMA within the copolymer ($F_{bis-AMP-MMA}$) at different reaction times (Table 5.1). A detailed description of the calculations to determine the conversion percentage of both monomers and $F_{bis-AMP-MMA}$ is provided in Annex.A.3.

Table 5.1. Monomers conversion percentage and $F_{bis-AMP-MMA,t}$ at different reaction times.

Reaction time	bis-AMP-MMA conversion	MMA conversion	$F_{bis-AMP-MMA,t}$
6 h	14.0%	90.4%	1.7%
24 h	16.0%	92.7%	1.9%
48 h	16.0%	92.9%	1.9%

From the initial 1:9 bis-AMP-MMA/MMA ratio, a $F_{bis-AMP-MMA}$ into the final copolymer of around 10% could be expected. However, after 6 h of reaction, only 14% of the initial bis-AMP-MMA was converted into monomer, together with 90.4% of the initial MMA, resulting in a $F_{bis-AMP-MMA}$ of 1.7% (Table 5.1). This value was very low, and a plausible reason for the limited reactivity of bis-AMP-MMA could arise from its high steric hindrance. When the reaction time was increased to 24 h and 48 h, only minor variations in the monomers conversion values and $F_{bis-AMP-MMA}$ were observed (Table 5.1). Consequently, a reaction time of 6 hours was chosen for the preparation of bis-AMP-MMA IIPs and NIP.

5.4 Complex formation study

As discussed in sub-section 2.5.3, the selectivity of IIPs is influenced by the complementarity of their binding sites in terms of size, shape, and charge with those of the target ion. The correspondence of binding sites with the target ion depends on the specificity and stability of the template/chelator complex in the pre-polymerization mixture. The ratio between the chelator and template ion can result in the formation of complexes with varying stoichiometries and stability. The binding cavities of IIPs prepared by polymerizing complexes with a 1:1 metal/chelator stoichiometry are more likely to present a lower selectivity than those prepared with 1:2 or 1:3 complexes. This is because the cavity formed around higher stoichiometry complexes is supposed to have a more specific geometry, with a higher complementarity to the template ion. Therefore, investigating the metal/chelator complex formation and optimizing the stoichiometry in the pre-polymerization mixture are critical steps in the preparation of highly selective IIPs.

The structure and species distribution of bis-AMP-MMA complexes with Cu(II), Co(II) and Ni(II) ions (generally indicated as M(II)) were investigated to control the stoichiometry of the complexes introduced in the IIPs. The distribution of the complex species was determined by analyzing the UV-Vis absorption spectra recorded in DMSO at 80 °C (Figure 3.1), which were the solvent and temperature selected for the polymerization. The M(II)/bis-AMP-MMA ratio was varied from 0.1 to 5.3 using both nitrates and perchlorates salts as metal sources. The UV-Vis spectra for each M(II)/bis-AMP-MMA couple were processed with the HypSpec program to determine the complex distribution curves (Figure 5.4) and stability constants of complexes at equilibrium, as previously described in the literature [21,307,317].

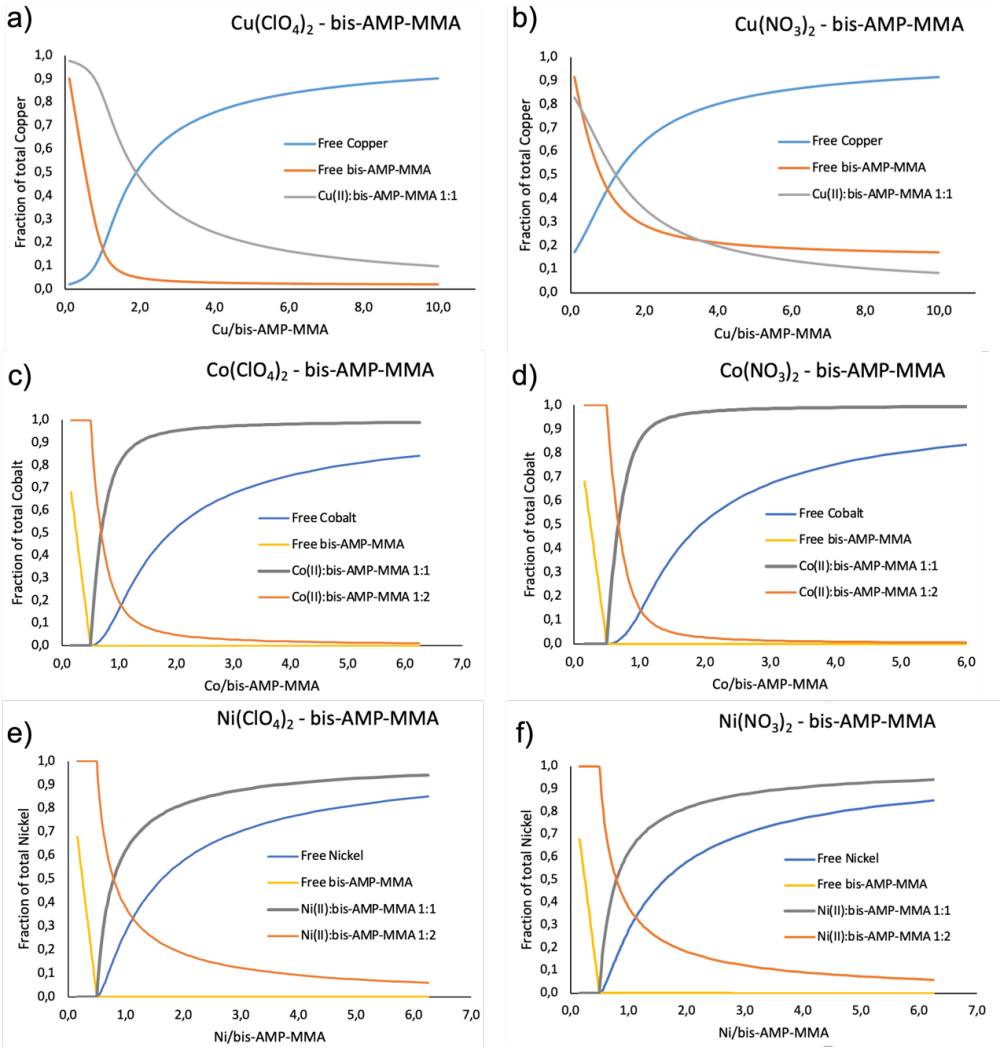

Figure 5.4. Species distribution curves for bis-AMP-MMA coupled with Cu(II), Co(II) or Ni(II) nitrate or perchlorate salts in DMSO at 80°C determined from UV-Vis spectra at different M(II)/bis-AMP-MMA ratios with HypSpec program.

The molar fraction of each absorbing species in the solution, determined from the species distribution curves of Figure 5.4, are reported in Table 5.2 for the M(II)/bis-AMP-MMA ratios of 1.00, 0.50, and 0.33. The molar fractions of M(II)/bis-AMP-MMA complexes ($x_{1:1}$, $x_{1:2}$) and uncomplexed M(II) ($x_{M(II)}$) are related to the total concentration of M(II), while the molar fraction of uncomplexed bis-AMP-MMA ($x_{bis-AMP-MMA}$) is related to initial concentration.

Table 5.2. Species distribution at 80 °C for DMSO solutions containing M(II) and bis-AMP-MMA with M(II)/bis-AMP-MMA ratios equal to 1.00, 0.50, and 0.33.

M(II) salt	M(II)/bis-AMP-MMA ratio	$x_{1:1}$	$x_{1:2}$	$x_{1:3}$	$x_{M(II)}$	$x_{bis-AMP-MMA}$
$Cu(NO_3)_2$	1.00	0.56	/	/	0.44	0.44
	0.50	0.71	/	/	0.29	0.64
	0.33	0.76	/	/	0.24	0.75
$Cu(ClO_4)_2$	1.00	0.83	/	/	0.17	0.17
	0.50	0.95	/	/	0.05	0.52
	0.33	0.97	/	/	0.03	0.68
$Co(NO_3)_2$	1.00	0.74	0.13	/	0.13	/
	0.50	0.01	0.99	/	/	< 0.01
	0.33	/	1.00	/	/	0.35
$Co(ClO_4)_2$	1.00	0.68	0.16	/	0.16	/
	0.50	0.01	0.99	/	/	< 0.01
	0.33	/	1.00	/	/	0.35
$Ni(NO_3)_2$	1.00	0.45	0.27	/	0.28	/
	0.50	0.01	0.99	/	/	< 0.01
	0.33	/	1.00	/	/	0.32
$Ni(ClO_4)_2$	1.00	0.45	0.26	/	0.29	/
	0.50	0.06	0.93	/	< 0.01	/
	0.33	/	1.00	/	/	0.34

The step-wise stability constants ($\beta_{1:1}$ and $\beta_{1:2}$) for M(II)/bis-AMP-MMA complexes, determined with the HypSpec program, are reported in Table 5.3.

Table 5.3. Stability constants values of M(II)/bis-AMP-MMA complexes in DMSO at 80°C determined with the HypSpec program.

M(II)	M(II)/bis-AMP-MMA 1:1 complex		M(II)/bis-AMP-MMA 1:2 complex	
	log $\beta_{1:1}$		log $\beta_{1:2}$	
Cu(II)	$Cu(NO_3)_2$	$Cu(ClO_4)_2$	$Cu(NO_3)_2$	$Cu(ClO_4)_2$

	1.70 ± 0.11	2.70 ± 0.14	Not detected	
Co(II)	$Co(NO_3)_2$	$Co(ClO_4)_2$	$Co(NO_3)_2$	$Co(ClO_4)_2$
	7.72 ± 0.08	7.50 ± 0.09	13.93 ± 0.17	13.76 ± 0.16
Ni(II)	$Ni(NO_3)_2$	$Ni(ClO_4)_2$	$Ni(NO_3)_2$	$Ni(ClO_4)_2$
	7.22 ± 0.04	7.11 ± 0.23	14.01 ± 0.07	13.80 ± 0.32

From the results presented in Figure 5.4 and Tables 5.2 and 5.3, it was possible to draw several conclusions regarding the formation of complexes between bis-AMP-MMA and Cu(II), Co(II), and Ni(II) ions.

When bis-AMP-MMA was combined with Cu(II), only the 1:1 complex was formed (Figures 5.4.a and 5.4.b). However, this complex could not be isolated in any of the solutions analyzed at different Cu(II)/bis-AMP-MMA ratios. In fact, the 1:1 complex consistently coexisted with uncomplexed Cu(II) ions and bis-AMP-MMA (Table 5.2 and Figures 5.4.a and 5.4.b). The stability constant of the 1:1 complex obtained with Cu(II) introduced as perchlorate salt was one logarithmic order higher than the corresponding nitrate. The log $\beta_{1:1}$ values were equal to 2.70 and 1.70 for perchlorate and nitrate salts, respectively (Table 5.3). The presence of a different counterion can affect the stability of complexes, as previously observed in the literature [307]. The reason for this phenomenon was not completely elucidated, but hypothetically it may derive from the formation of different outer-sphere complexes between the metal ion and the different counter anions.

In the case of Co(II) ions, two distinct complexes with 1:1 and 1:2 stoichiometries were formed (Figures 5.4.c and 5.4.d). The influence of the counter ion had a negligible effect, with slightly higher stability constant values for both 1:1 and 1:2 complexes when Co(II) was introduced as nitrate (Table 5.3). The 1:1 complex could not be isolated in solution as it coexisted with uncomplexed Co(II) and 1:2 complex (Table 5.2 and Figures 5.4.c and 5.4.d). On the other hand, when the Co(II)/bis-AMP-MMA ratio was set at 0.50, it was possible to isolate the Co(II)/bis-AMP-MMA complex in solution with a 1:2 stoichiometry (Table 5.2 and Figures 5.4.c and 5.4.d). At this specific ratio, 99% of the initial Co(II) existed in the solution as the 1:2 complex, along with 1% of the 1:1 complex and less than 1% of free monomer.

The results obtained from the complex formation study between bis-AMP-MMA and Ni(II) ions were very similar to those obtained for Co(II) ions. Ni(II)/bis-AMP-MMA complexes with stoichiometry 1:1 and 1:2 were detected in solution (Figures 5.4.e and 5.4.f) and only the 1:2 complex could be isolated (Table 5.2). The complexes formed with the nitrate salt of Ni(II) were slightly more stable than the corresponding perchlorates (Table 5.3). When the Ni(II)/bis-AMP-MMA ratio was set at 0.50, it was possible to isolate the Ni(II)/bis-AMP-MMA complex with a 1:2 stoichiometry in the solution (Table

5.2 and Figures 5.4.e and 5.4.f). At this ratio, 99% of the initial Ni(II) was involved in the formation of the 1:2 complex and 1% in the formation of the 1:1 complex.

Through the complex formation study, it was evidenced that complexes between bis-AMP-MMA and Co(II) or Ni(II) ions can be successfully isolated by controlling the composition of the polymerization mixture. In this context, a complex was considered to be "isolated" when it was the only species dissolved in solution or, alternatively, if the molar fraction of the other dissolved species was less than 1%. For both Co(II) and Ni(II) ions, 0.5 M(II)/bis-AMP-MMA ratio allowed the isolation of complexes with a 1:2 stoichiometry in solution. Consequently, both Co(II)/bis-AMP-MMA and Ni(II)/bis-AMP-MMA couples were chosen for the preparation of ion-imprinted polymers (IIPs), with pre-polymerization mixtures optimized with a M(II)/bis-AMP-MMA ratio of 0.5. Despite this, the analogous stability of bis-AMP-MMA complexes with Co(II) and Ni(II) ions may negatively impact the selectivity of bis-AMP-MMA-based adsorbents in the separation of these two metals.

5.5 Preparation of bis-AMP-MMA polymers

Both the Co(II)-IIP, bis-AMP-Co-IIP, and the Ni(II)-IIP, bis-AMP-Ni-IIP, were prepared via inverse suspension with a template/monomer ratio equal to 0.5, as determined with the complex formation study. EGDMA was used as a crosslinker and was introduced in the polymerization mixture with a bis-AMP-MMA/EGDMA ratio equal to 1:9. The synthesis route to prepare both the IIPs of bis-AMP-MMA is illustrated in Figure 5.5.

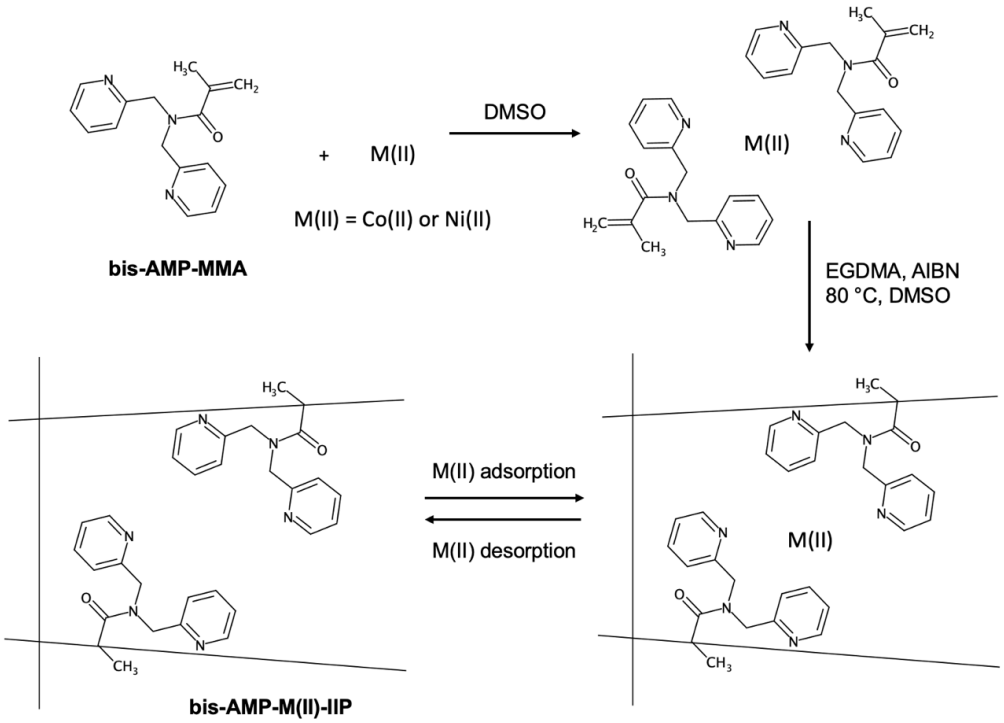

Figure 5.5. Synthesis route for the preparation of bis-AMP-MMA IIPs.

The synthesis of the corresponding NIP, bis-AMP-NIP, was conducted using the same experimental conditions as those described for bis-AMP-Co-IIP and bis-AMP-Ni-IIP, except for the absence of metal ions in the pre-polymerization mixture.

The preparation of bis-AMP-MMA polymers was first carried out with the head mixer set at 700 rpm. This condition led to the formation of powder-like polymer particles (Figure 5.6.a). To increase particle size, the polymerization was repeated by reducing the head-mixer rate to 400 rpm. This adjustment resulted in a notably larger particle size for bis-AMP-NIP, while IIPs polymer particles were still obtained as powder (Figure 5.6.b). A more detailed description of the morphology of these polymer particles is provided in the following section (Section 5.6).

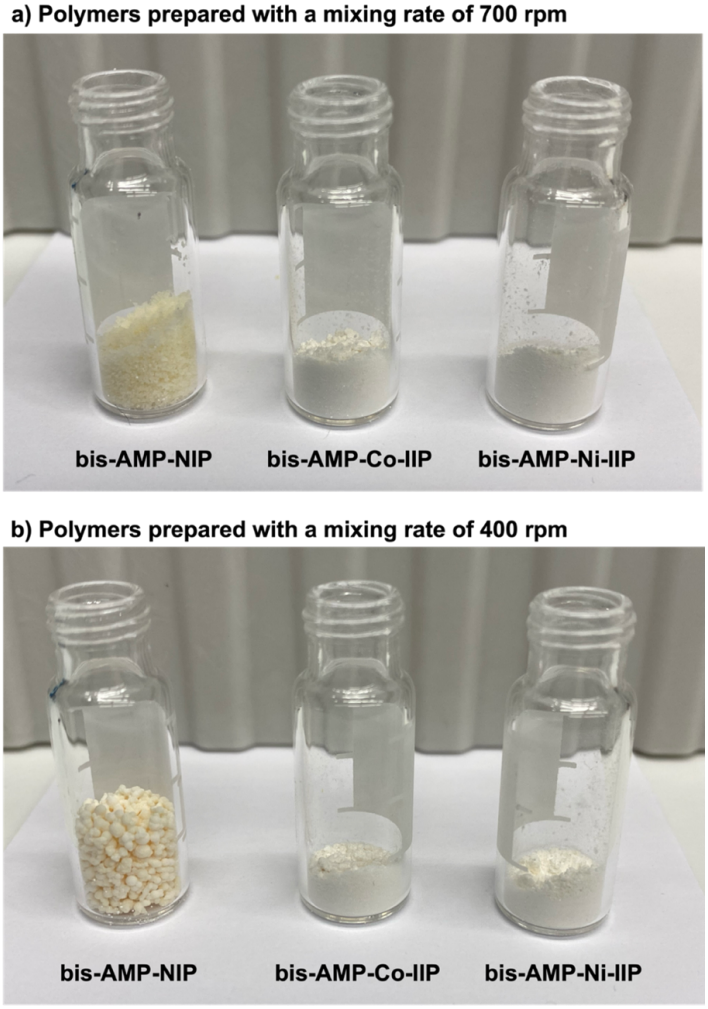

Figure 5.6. Polymer particles of bis-AMP-NIP, bis-AMP-Co-IIP, and bis-AMP-Ni-IIP obtained via inverse suspension polymerization with a mixing rate of 700 rpm (a) and 400 rpm (b).

Despite the small particle size, the IIPs prepared with a mixing rate of 400 rpm, together with bis-AMP-NIP, were still characterized and applied in metal adsorption experiments.

5.6 Characterization of the chemical structure of bis-AMP-MMA polymers

The chemical structure of the three bis-AMP-MMA polymers was determined by FTIR (Figure 5.7) and ^{13}C CP-MAS NMR (Figure 5.8) spectroscopies. The presence of bis-AMP-MMA within bis-AMP-NIP, bis-AMP-Co-IIP, and bis-AMP-Ni-IIP polymer particles was verified by comparing their spectra with the one of poly(EGDMA).

The presence of poly(EGDMA) in the FTIR spectrum of each material was identified by its characteristic absorption bands (Figure 5.7). These included the C=O stretching band at 1725 cm^{-1}, the C-O stretching band at 1144 cm^{-1}, and the -OCH_2 deformation vibration band at 1460 cm^{-1} [292]. In the bis-AMP-MMA polymers, distinct C=C and C=N pyridine stretching bands at 1571 cm^{-1} and 1591 cm^{-1}, as well as C-N aromatic amine stretching bands at 1295 cm^{-1} and 1319 cm^{-1}, were present. These bands were not visible in the spectrum of poly(EGDMA), used as a reference material. The preparation of bis-AMP-Co-IIP and bis-AMP-Ni-IIP included a leaching step, which involved 5 washes with 3 M NH_4OH to release the template ions and generate ion-imprinted cavities. This eluent was chosen as it was already successfully used for the elution of strongly retained metals from the bis-AMP containing resin Dowex™ M4195 [235], as previously described in Chapter 2 . FTIR spectra were collected for both materials before and after the leaching process, and no changes in their chemical composition were observed. This result showed a good chemical resistance of both materials.

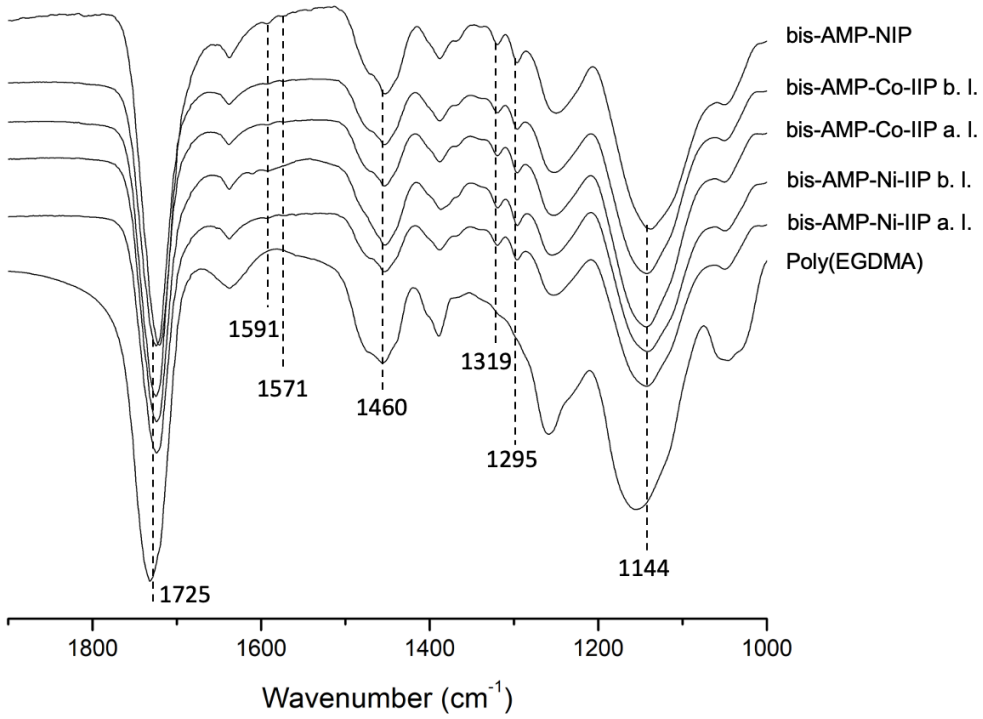

Figure. 5.7. FTIR spectra of bis-AMP-NIP, bis-AMP-MMA IIPs before leaching (b. l.) and after leaching (a. l.), and poly(EGDMA).

The presence of bis-AMP-MMA within bis-AMP-NIP, bis-AMP-Co-IIP, and bis-AMP-Ni-IIP was also confirmed by the ^{13}C CPMAS NMR spectra (Figure 5.8) of these polymers. Poly(EGDMA) was the major component in each material, and its

characteristic signals were present in each spectrum. These signals included the carbonyl carbon (C=O) peak at 177.1 ppm, the pending vinyl carbon ($C=CH_2$) peak at 137.1 ppm, the ester carbon (-COO-) peak at 62.9 ppm, the quaternary carbon (>C<) peak at 45.8 ppm, the methylene carbon ($-CH_2-$) peak at 24.5 ppm, and the methyl carbon ($-CH_3$) peak at 18.4 ppm [374,375]. The presence of bis-AMP-MMA within bis-AMP-NIP, bis-AMP-Co-IIP, and bis-AMP-Ni-IIP was confirmed by the pyridine peaks in the aromatic carbon zone, including two weak peaks at 157.9 ppm and 149.3 ppm, along with a more intense peak at 124.5 ppm, which were not observed in the poly(EGDMA) spectrum. This result was consistent with the observation conducted with FTIR spectroscopy and provided an additional validation about the correct integration of bis-AMP-MMA within bis-AMP-NIP, bis-AMP-Co-IIP, and bis-AMP-Ni-IIP polymer particles.

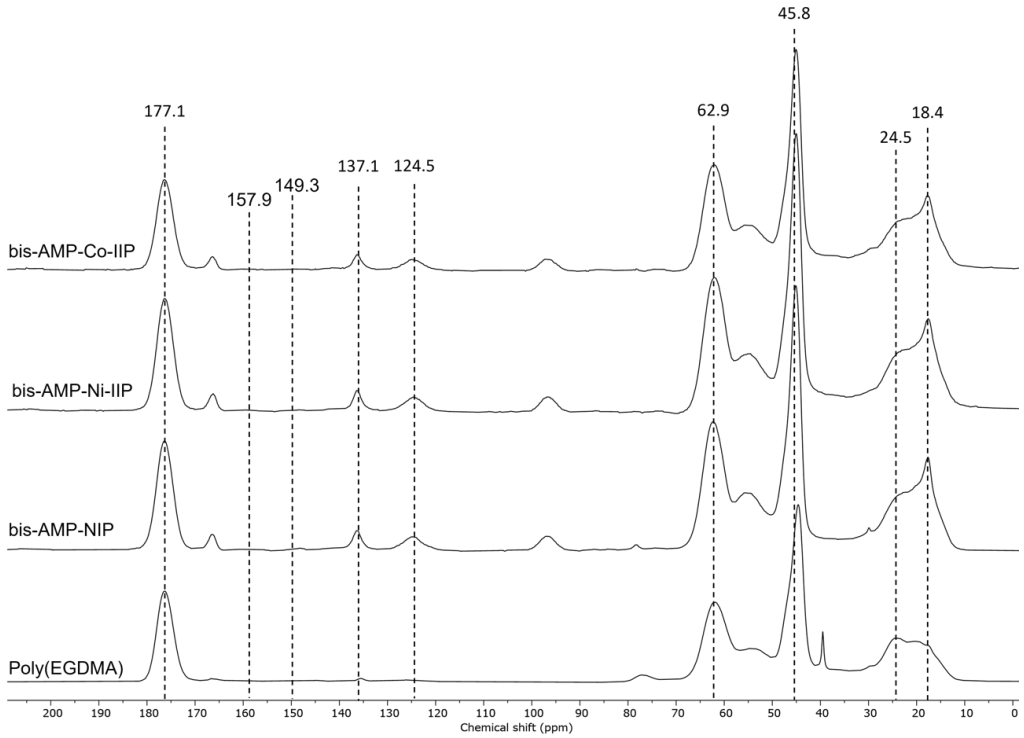

Figure 5.8. ^{13}C CPMAS NMR spectra of bis-AMP-Co-IIP, bis-AMP-Ni-IIP, bis-AMP-NIP and Poly(EGDMA).

5.7 Morphology of bis-AMP-MMA polymers

The chemical characterization of bis-AMP-MMA polymer particles was followed by the study of their surface morphology with optical microscope and SEM. Additionally, the specific surface area, pore size, and pore volume were determined through nitrogen adsorption/desorption experiments.

5.7.1 Optical microscope and SEM analysis

Due to the small size of bis-AMP-Co-IIP and bis-AMP-Ni-IIP particles, only the bis-AMP-NIP particles could be studied using a numerical optical microscope (Figure 5.9). The bis-AMP-NIP particles appeared as irregular clusters of multiple spherical particles with varying sizes, approximately in the millimeter range.

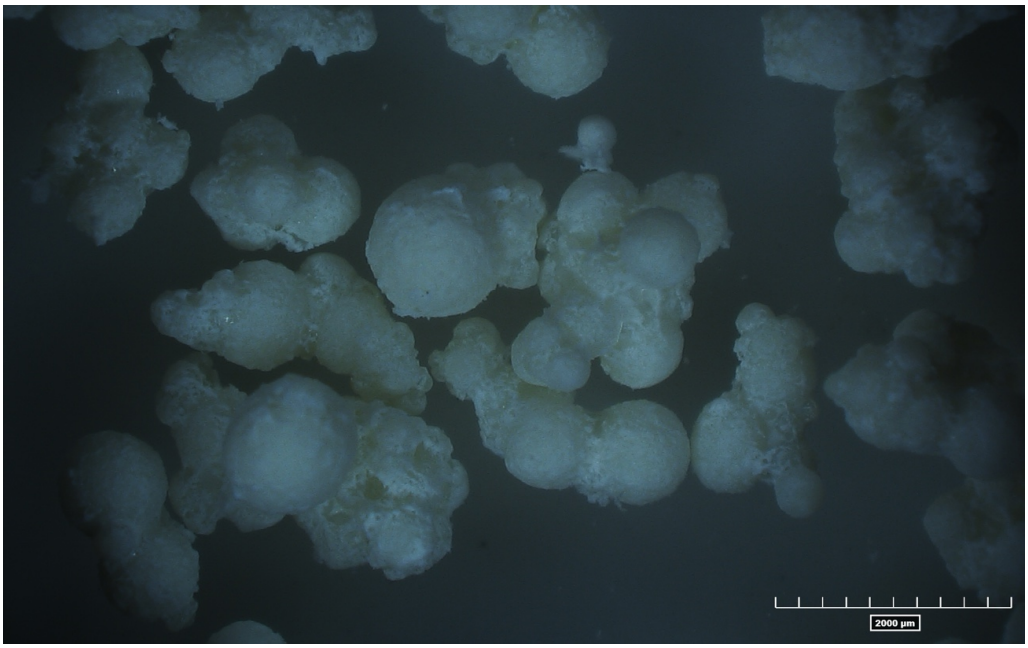

Figure 5.9. Polymer particles of bis-AMP-NIP taken with a numerical optical microscope.

The higher resolution of SEM compared to that of the optical microscope facilitated the examination of polymer particles from both the IIPs. The SEM images of whole particles of bis-AMP-NIP, bis-AMP-Co-IIP, and bis-AMP-Ni-IIP are presented in Figure 5.10.

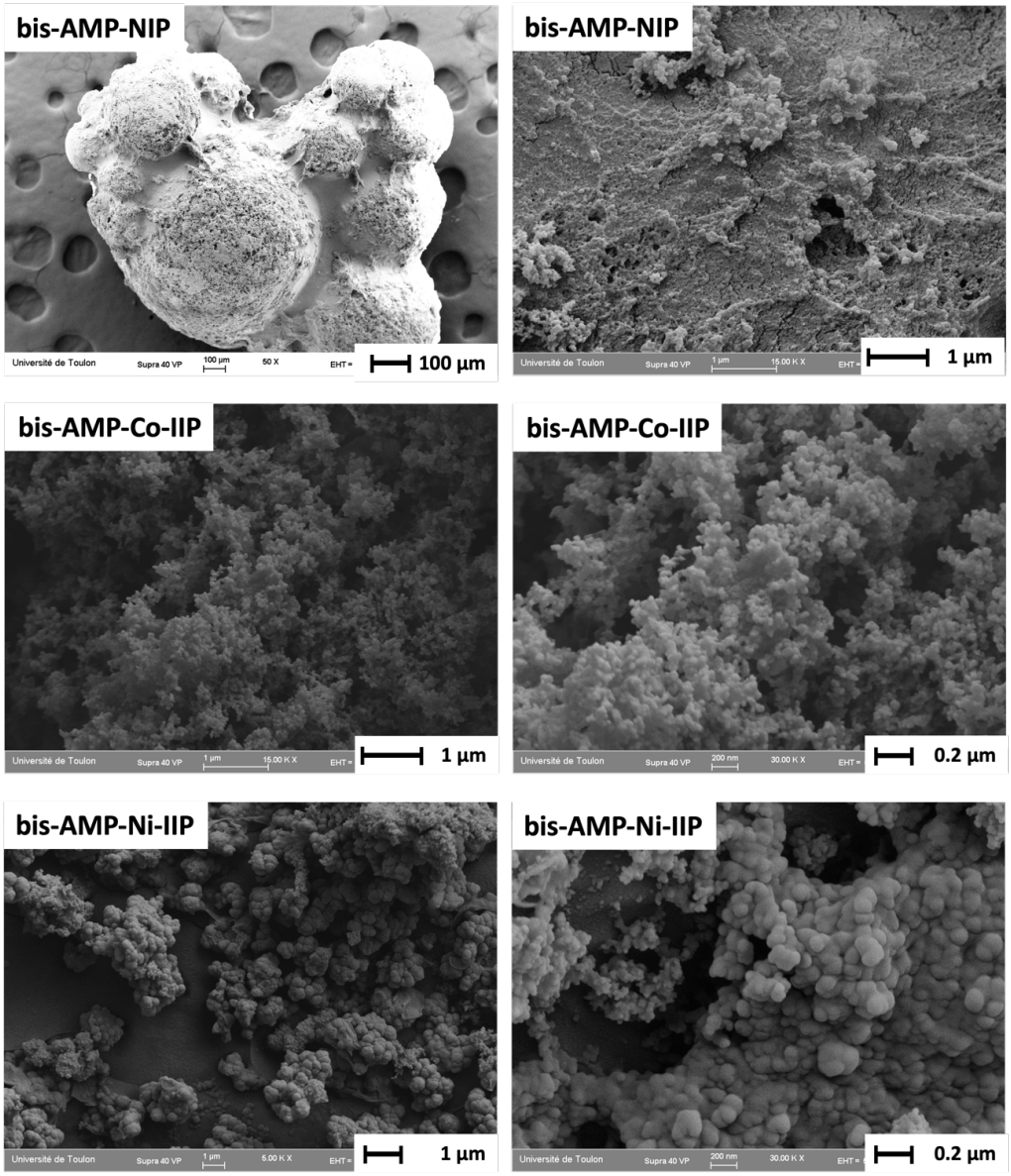

Figure 5.10. SEM pictures of whole polymer particles of bis-AMP-NIP, bis-AMP-Co-IIP, and bis-AMP-Ni-IIP.

Consistently with the optical microscope analysis, SEM images of bis-AMP-NIP displayed irregular particles formed through the random aggregation of multiple spheres. The surface of bis-AMP-NIP particles featured high roughness. Both bis-AMP-Co-IIP and bis-AMP-Ni-IIP appeared as clusters of numerous particles whose size did not exceed

a few tens of nanometers. The sharply different morphology of bis-AMP-NIP from those of the two IIPs might have a strong impact of the adsorption capacities of these materials.

5.7.2 Nitrogen adsorption-desorption experiments

Nitrogen adsorption-desorption experiments were conducted for the three bis-AMP-MMA polymers, and the corresponding isotherms are illustrated in Figure 5.11.

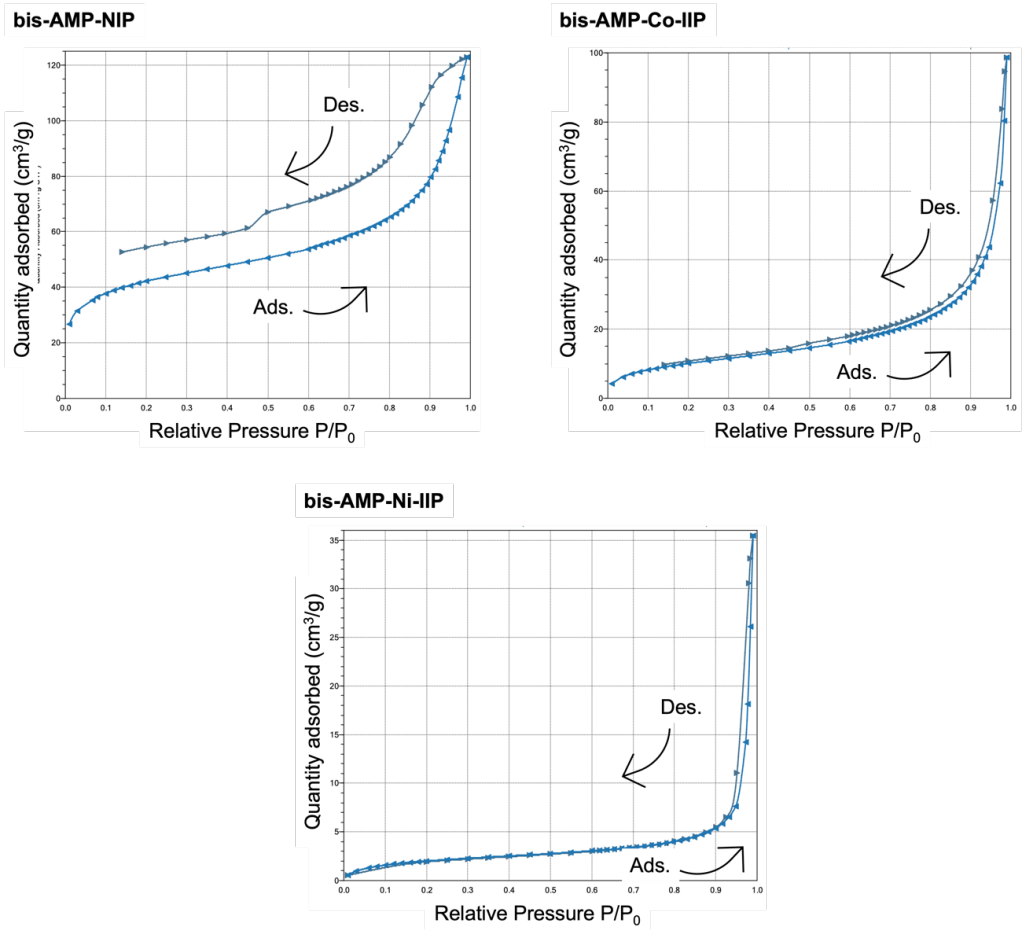

Figure 5.11. Nitrogen adsorption-desorption isotherms of bis-AMP-NIP, bis-AMP-Co-IIP, and bis-AMP-Ni-IIP.

The nitrogen adsorption-desorption isotherms for all three materials displayed, according to IUPAC classification (Figure A.1), a Type II isotherm shape. The isotherm of bis-AMP-NIP exhibited a hysteresis loop H4 (Figure A.2), suggesting the presence of narrow slit-like pores. In contrast, the isotherms for both the IIPs had a hysteresis loop H3 (Figure

A.2), which suggests the presence of aggregates of plate-like particles and the formation of slit-shaped pores.

The BJH and BET methods were used to determine the average pore diameters, total pore volumes, and specific surface areas for each material (Table 5.4).

Table 5.4. Average pore diameters, total pore volumes, and specific surfaces of bis-AMP-NIP, bis-AMP-Co-IIP, and bis-AMP-Ni-IIP determined with BJH and BET methods.

Material	Average pore diameter (nm)	Total pore volumes (cm^3/g)	Specific surface area (m^2/g)
bis-AMP-NIP	4.9	0.190	153.9
bis-AMP-Co-IIP	16.3	0.152	37.4
bis-AMP-Ni-IIP	0.3	0.055	7.7

According to the average pore diameter values (Table 5.4), bis-AMP-NIP and bis-AMP-Co-IIP could be classified as mesoporous materials, while bis-AMP-Ni-IIP was classified as microporous material. The total pore volumes and specific surfaces area were sharply different among the three materials. The polymer particles of bis-AMP-NIP showed the highest values with total pore volumes and specific surface area equal to 0.190 cm^3/g and 153.9 m^2/g, respectively. Among the two IIPs, bis-AMP-Ni-IIP exhibited the lowest total pore volume and specific surface area, with values of 0.055 cm^3/g and 7.7 m^2/g, respectively. The relatively low total pore volume and specific surface area in both IIPs might have a negative impact on their adsorption capacity when compared to bis-AMP-NIP.

5.8 Co(II) adsorption experiments

The characterization of bis-AMP-MMA polymers was followed by Co(II) adsorption experiments with bis-AMP-NIP and bis-AMP-Co-IIP. These experiments encompassed the effect of pH, the impact of the time dependence of Co(II) adsorption, the determination of Co(II) adsorption isotherms, and the assessments of polymer selectivity and reusability.

5.8.1 Effect of pH

The first adsorption experiments were conducted to assess the effect of pH on Co(II) adsorption to determine the optimal pH range for their application. The effect of pH on Co(II) adsorption capacity of bis-AMP-NIP and bis-AMP-Co-IIP was investigated within the pH range 3.5-8 (Figure 5.12).

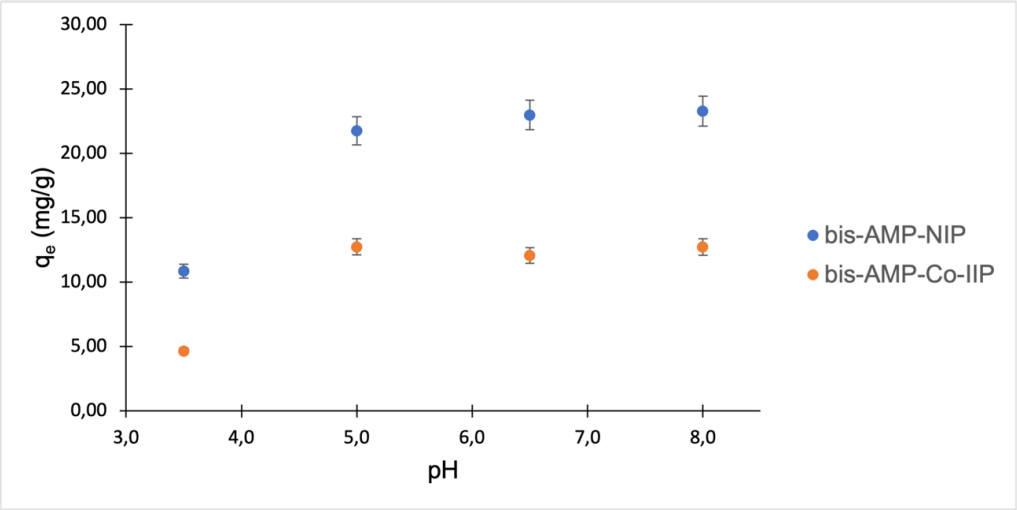

Figure 5.12. Effect of pH on Co(II) adsorption capacity of bis-AMP-NIP and bis-AMP-Co-IIP. The initial Co(II) ions concentration was equal to 1 g/L. The pH value was adjusted with concentrated HCl and NaOH.

The most favorable adsorption performance for both bis-AMP-NIP and bis-AMP-Co-IIP were observed within the pH range of 5-8. The trend in adsorption capacities with pH was consistent for both materials, with a decrease in performance at pH 3.5. As illustrated in Figure 5.12 the adsorption capacity of bis-AMP-Co-IIP was consistently lower than that of bis-AMP-NIP across the entire pH range under investigation. This difference might be attributed to the substantial difference in specific surface area between the two materials, which measured 37.4 m^2/g for bis-AMP-Co-IIP and 153.9 m^2/g for bis-AMP-NIP (Table 5.4). Given the stable performance in the pH range of 5-8, pH 6.5 was selected for conducting the following adsorption experiments.

5.8.2 Time dependence of Co(II) adsorption

Before proceeding with the selectivity study, the impact of time on Co(II) adsorption capacity was investigated through adsorption experiments of varying durations. Figure 5.13 illustrates the results of these experiments for bis-AMP-NIP and bis-AMP-Co-IIP.

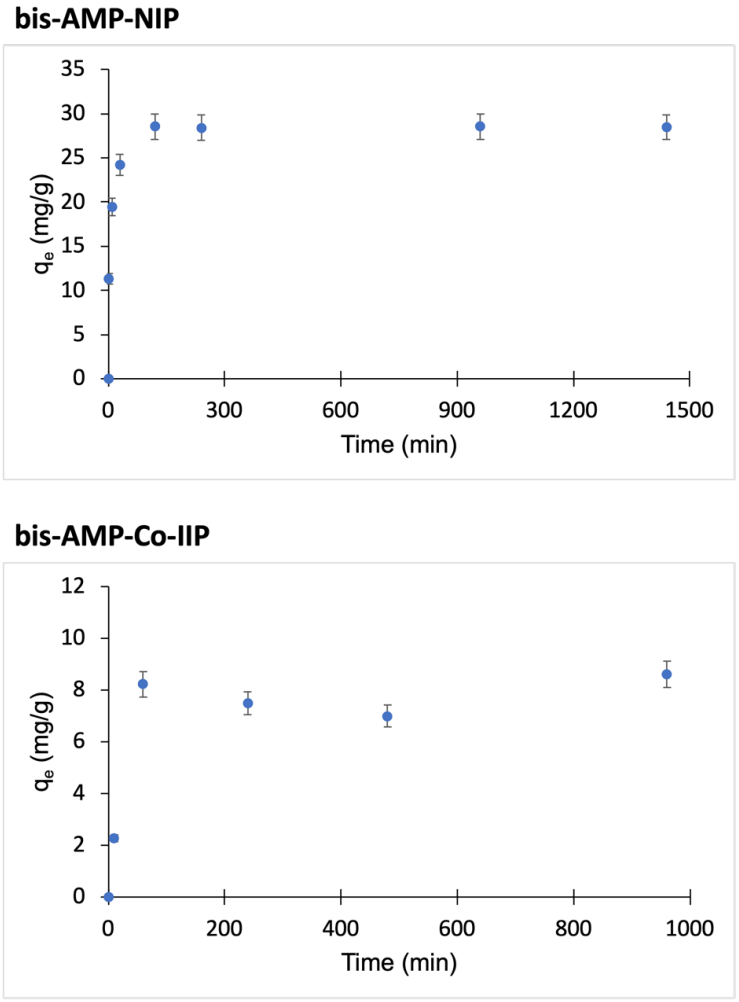

Figure 5.13. Impact of contact time on the Co(II) adsorption capacity of bis-AMP-NIP and bis-AMP-Co-IIP. The initial concentration of Co(II) ions was 500 mg/L, and the solutions pH was adjusted to 6.5 with NaOH.

The adsorption capacity of Co(II) ions by bis-AMP-NIP increased during the initial two hours and then reached a plateau. For bis-AMP-Co-IIP, the most significant increase in adsorption capacity occurred within the first hour, and the value remained quite steady afterward, within the margin of experimental error. The following adsorption experiments were carried out with a contact time exceeding two hours to ensure an efficient Co(II) adsorption with both materials.

5.8.3 Co(II) adsorption isotherms

Co(II) adsorption experiments were conducted for bis-AMP-NIP and bis-AMP-Co-IIP to determine their respective maximum adsorption capacities. These experiments were carried out at room temperature, using Co(II) solutions with increasing concentrations at pH 6.5. The resulting adsorption data is shown in Figure 5.14.

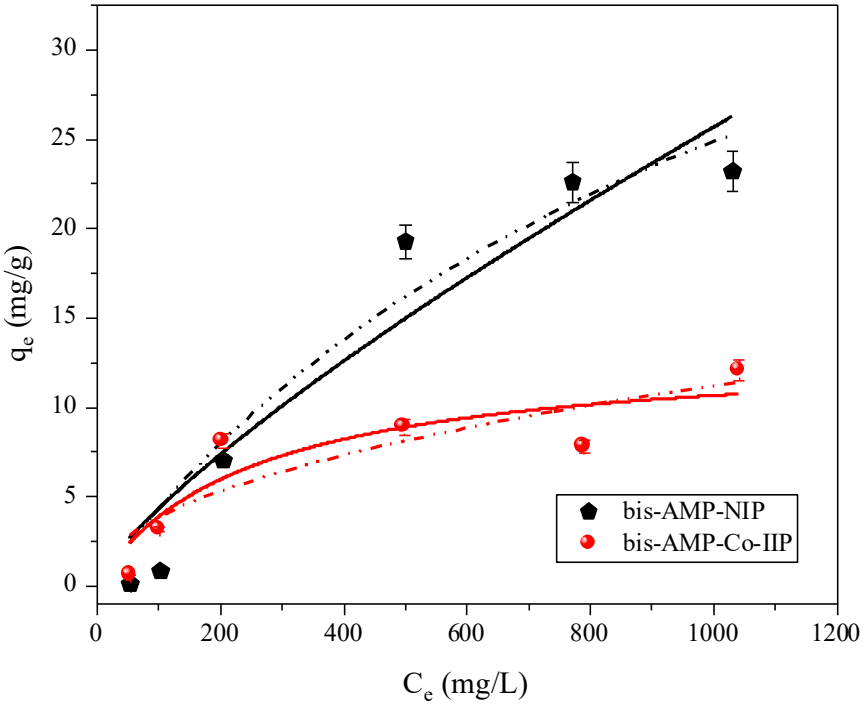

Figure 5.14. Co(II) adsorption by bis-AMP-NIP and bis-AMP-Co-IIP. The adsorption data was interpolated with Langmuir (dashed lines) and Freundlich (continuous lines) models. The range of initial Co(II) ions concentration was 20-1050 mg/L and the pH was adjusted to 6.5 with NaOH.

The adsorption capacity of bis-AMP-NIP exhibited a sharp increase in the Co(II) concentration range of 20-450 mg/L, after which a minor variation was observed. In the case of bis-AMP-Co-IIP, the most significant increase in Co(II) adsorption capacity occurred within the Co(II) concentration range of 20-200 mg/L. At higher Co(II) concentrations the adsorption capacity was relatively steady. The maximum adsorption capacity for each material was determined by fitting the adsorption data with the Langmuir (Eq. 2.4) and Freundlich (Eq. 2.5) models (Table 5.5).

Table 5.5. Langmuir and Freundlich models' parameters for Co(II) adsorption with bis-AMP-NIP and bis-AMP-Co-IIP at pH 6.5.

Model	Parameter	Adsorbent

		bis-AMP-NIP	bis-AMP-Co-IIP
Langmuir	$q_{e,max}$ (mg/g)	54.0	13.3
	K_L	0.008	0.004
	R^2	0.926	0.781
Freundlich	1/n	0.783	0.471
	K_F	0.114	0.430
	R^2	0.893	0.721

For both materials, Langmuir's model offered a better correlation of the adsorption data in comparison to Freundlich's model (Table 5.5). This suggested the presence of homogeneous binding sites with uniform adsorption energy and no interaction between adsorbate molecules on adjacent sites. However, the correlation coefficient (R^2) value for Langmuir's model when bis-AMP-Co-IIP was used as the adsorbent was limited to 0.781, indicating that this model did not provide an efficient interpolation for the adsorption data. In accordance with the results obtained in the study of the effect of pH and impact of time, bis-AMP-NIP showed a higher maximum adsorption capacity than bis-AMP-Co-IIP, with values equal to 54.0 mg/g and 13.3 mg/g, respectively. From these results, a positive effect of the imprinting technique on the adsorption capacity of bis-AMP-Co-IIP compared to bis-AMP-NIP was not evident. This might be attributed to the more challenging introduction of the 1:2 complex into bis-AMP-Co-IIP, in contrast to the incorporation of uncomplexed bis-AMP-MMA into bis-AMP-NIP. This could potentially lead to a higher number of binding sites into bis-AMP-NIP polymer particles. The Co(II) adsorption capacity of bis-AMP-NIP, when compared with one of other Co(II) adsorbents described in the literature (Table 2.1), falls within the middle range of values. To complete the evaluation of the adsorption performance of these two materials, the experiments continued with a study of their selectivity.

5.8.4 **Selectivity**

The selectivity of bis-AMP-NIP and bis-AMP-Co-IIP toward Co(II) ions was investigated at pH 6.5 using bi-component solutions containing Co(II) paired with one divalent metal ion M(II) among Ni(II), Cd(II), Mn(II), and Mg(II). The selectivity coefficient k (Eq. 2.6) and relative selectivity coefficient k' (Eq. 2.8) values for each M(II)/Co(II) pair at different M(II)/Co(II) ratios are reported in Table 5.6.

Table 5.6. Selectivity coefficient and relative selectivity coefficient values for Co(II) adsorption with bis-AMP-NIP and bis-AMP-Co-IIP at pH 6.5 with Ni(II), Cd(II), Mn(II), or Mg(II) as competitive ions.

M(II)		bis-AMP-NIP	bis-AMP-Co-IIP

	$\frac{\mathbf{M(II)}}{\mathbf{Co(II)}}$	k	k	k'
Ni(II)	1	1.50	1.27	0.85
	9	2.09	0.93	0.45
Cd(II)	1	1.31	1.37	1.05
	9	1.25	1.62	1.29
Mn(II)	1	1.13	0.87	0.77
	9	1.37	2.78	2.03
Mg(II)	1	1.17	0.26	0.22
	9	0.34	0.73	2.17

The *k* values for bis-AMP-NIP (Table 5.6) offered insights into the adsorbent selectivity before the application of the imprinting technique. When the M(II)/Co(II) ratio was set to 1, the adsorption of Co(II) resulted in *k* values above 1 for all the examined competitive ions. This observation indicated that bis-AMP-NIP exhibited a preference for Co(II) adsorption over other metal ions when introduced at equal concentrations into the solution. At the same M(II)/Co(II) ratio, bis-AMP-Co-IIP showed selectivity for Co(II) when paired with Ni(II) and Cd(II) ions as competitive metals. Conversely, bis-AMP-Co-IIP displayed a preference for adsorbing Mn(II) and Mg(II) over Co(II).

When the M(II)/Co(II) molar ratio was set to 9, there was only a slight variation in the *k* values of bis-AMP-NIP with Ni(II), Cd(II), and Mn(II) as a competitive ion and the adsorption of Co(II) was still preferred over their adsorption. On the other hand, when an excess of Mg(II) was present in the solution, the selectivity of bis-AMP-NIP for Co(II) over this metal was lost. In the case of bis-AMP-Co-IIP, when the M(II)/Co(II) ratio was set to 9, this material lost its selectivity for Co(II) adsorption in the presence of Ni(II) ions, while the *k* values with Cd(II), Mn(II), and Mg(II) as competitive ions slightly increased. The *k'* values were in most cases close to or lower than 1, indicating that the imprinting technique was not effective on bis-AMP-Co-IIP. This result might arise from the difficult incorporation of the 1:2 Co(II)/bis-AMP-MMA complex within this material. Despite the selectivity of bis-AMP-NIP being generally higher than the one of bis-AMP-Co-IIP, its selectivity coefficients were still very low. Consequently, the selective separation of Co(II) ions with both materials was not possible. The lack of selectivity of bis-AMP-MMA-containing materials in separating Co(II) ions from Ni(II) ions could be expected from the results of the complex formation study (Section 5.4). This study revealed that bis-AMP-MMA forms 1:1 and 1:2 complexes with both Co(II) and Ni(II) ions with very similar stability constant values (Table 5.3). This similarity offered a

plausible explanation for the absence of selectivity in Co(II) and Ni(II) separation using bis-AMP-MMA materials.

Due to the lack of selectivity in the complexation of Co(II) and Ni(II) ions with bis-AMP-MMA (Section 5.4) and the extremely low specific surface area of bis-AMP-Ni-IIP (Table 5.4), the adsorption experiments with bis-AMP-Ni-IIP as Ni(II) adsorbent were not performed. However, the adsorption experiments on bis-AMP-MMA materials were concluded by examining the reusability of bis-AMP-NIP, which, despite its lack of selectivity, displayed good Co(II) adsorption capacity.

5.8.5 **Reusability of bis-AMP-NIP**

In this section, the reusability study was conducted on bis-AMP-NIP, who showed the best Co(II) adsorption performance among bis-AMP-MMA-based materials. The regeneration of this adsorbent was studied through 5 Co(II) adsorption-desorption cycles (Figure 5.15). The adsorption experiments were followed by the desorption of Co(II) ions with 3 M NH_4OH as the Co(II) leaching agent. The material reusability was assessed by calculating the residual adsorption capacity after each adsorption cycle in relation to the first cycle (Eq. 3.1).

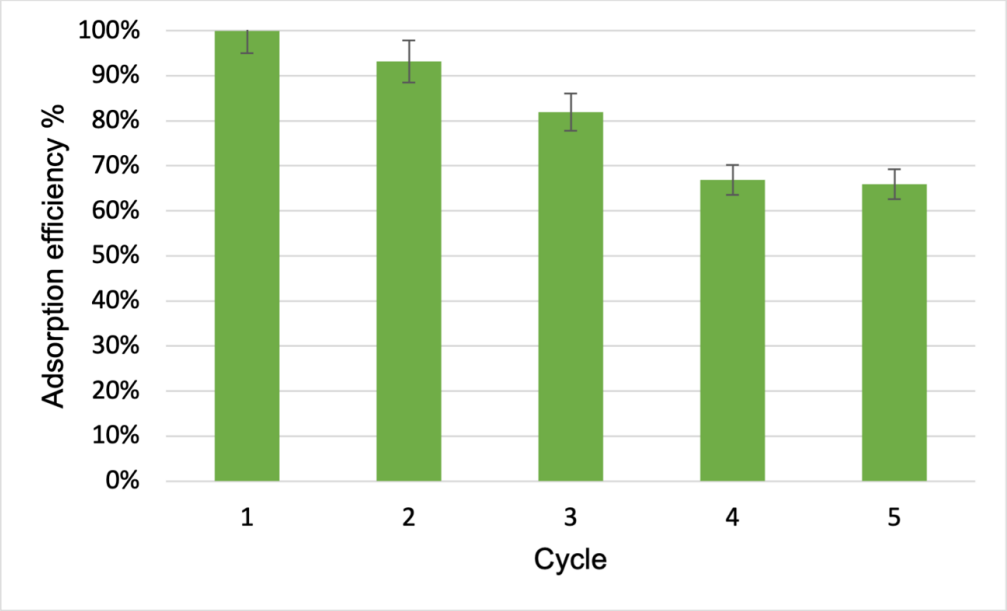

Figure 5.15. Adsorption efficiency of bis-AMP-NIP in 5 adsorption-desorption cycles with 3 M NH_4OH as leaching agent. The initial Co(II) ions concentration was equal to 1 g/L and the solution pH was 6.5.

The adsorption capacity of bis-AMP-NIP decreased by 7% after the first adsorption-desorption cycle, with a gradual decline in efficiency that led to a 33% drop in performance by the fourth cycle. The performance reduction was stabilized in the fifth

cycle, with a reduction of 35%. This study demonstrated that bis-AMP-NIP can be efficiently reused for three adsorption-desorption cycles before facing a significant performance drop in the fourth cycle.

5.9 Conclusion

This chapter described the synthesis of a novel chelating monomer, bis-AMP-MMA, based on bis(2-pyridylmethyl)amine (bis-AMP) and its application in the preparation of IIPs. The synthesis of bis-AMP-MMA, verified with ^{1}H-NMR and ^{13}C-NMR spectroscopies, was followed by the assessment of its reactivity in polymerization reaction and by a complex formation study. The complex formation study was conducted with Cu(II), Co(II) and Ni(II) ions, resulting in the formation of a 1:1 complex with Cu(II) and 1:1 and 1:2 complexes with both Co(II) and Ni(II) ions. The 1:1 complex formed with Cu(II) ions could not be isolated in solution. The complexes with a 1:2 stoichiometry formed with Co(II) or Ni(II) ions could be isolated in solution when the M(II)/bis-AMP-MMA ratio was set to 0.5.

Based on these results, a Co(II)-IIP, bis-AMP-Co-IIP, and a Ni(II)-IIP, bis-AMP-Ni-IIP, were prepared optimizing the pre-polymerization media with a 0.5 M(II)/bis-AMP-MMA ratio. The corresponding NIP, bis-AMP-NIP, was also prepared under the same conditions but without the metal template. The chemical composition of the three materials was determined by FTIR and ^{13}C CP-MAS NMR spectroscopies. Morphology studies were carried out using optical microscopy, SEM, and nitrogen adsorption-desorption experiments. The IIPs consisted of powder materials composed of agglomerates of nanoparticles, while bis-AMP-NIP particles were irregular aggregates of microspheres with high roughness. The specific surface areas differed significantly with values of 153.9 m^2/g for bis-AMP-NIP, 37.4 m^2/g for bis-AMP-Co-IIP, and 7.7 m^2/g for bis-AMP-Ni-IIP.

Co(II) adsorption experiments were carried out with bis-AMP-NIP and bis-AMP-Co-IIP, including investigations into pH impact, time dependence of Co(II) adsorption, adsorption isotherms, selectivity, and reusability. Both materials exhibited optimal adsorption performance in the pH range of 5-8. At pH 6.5, the maximum Co(II) adsorption capacities were 54.0 mg/g for bis-AMP-NIP and 13.3 mg/g for bis-AMP-Co-IIP. The higher adsorption capacity of bis-AMP-NIP might be attributed to its larger specific surface area. However, both materials showed limited selectivity for Co(II) ions when Ni(II), Cd(II), Mn(II), and Mg(II) ions were present in solution. The selectivity results concerning bis-AMP-NIP are in agreement with the complex formation study, where the complexes of bis-AMP-MMA with Co(II) and Ni(II) ions were characterized by similar values of stability constants. Additionally, the poor imprinting effect observed for bis-AMP-Co-IIP might arise from the difficult introduction of the 1:2 complex into this material. Considering the limited incorporation of bis-AMP-MMA into the copolymer with MMA, a similar behavior was also hypothesized also for its copolymerization with EGDMA during the preparation of IIPs and NIP. The

incorporation of uncomplexed bis-AMP-MMA into bis-AMP-NIP was thus expected to be very low. In the case of Co(II)/bis-AMP-MMA, the situation could even be worse, as the monomer was involved in the formation of the Co(II)/bis-AMP-MMA 1:2 complex, where the bis-AMP-MMA molecules were locked around Co(II) ions.

Taking into account the scarce selectivity in the complexation of Co(II) and Ni(II) ions with bis-AMP-MMA and the limited specific surface area of bis-AMP-Ni-IIP, the adsorption experiments were not carried out with this material. Due to the poor selectivity of bis-AMP-MMA-based adsorbents, the synthesis of a novel chelating monomer and the preparation of selective adsorbents was still required.

6 Synthesis and characterization of a novel Ni(II)-IIP based on modified 2-(aminomethylpyridine)

Table of contents

6.1 Introduction

AMP ligand is known to form stable octahedral complexes with Ni(II) ions with stoichiometries 1:1, 1:2, and 1:3 [307]. Additionally, when AMP ligand was introduced within the structure of a chelating resin, as in the case of CuWRAM, its presence reduced the global basicity of the resin, enhancing the Ni(II) adsorption performance in acidic media [369]. These studies were followed by the modification of AMP ligand with a vinylbenzyl group through its primary amine group (Figure 6.1) to produce Vbamp, a chelating monomer applied for Ni(II)-IIPs preparation [16]. This material showed remarkable selectivity for Ni(II) ions in the presence of an excess of Zn(II) ions. The monomer introduced in this chapter, AMP-MMA, was also obtained from a modification of the primary amine group of AMP ligand, as for Vbamp. However, the structure of AMP-MMA differs from that of Vbamp due to the functionalization of AMP with a methacrylic group instead of a vinylbenzyl group (Figure 6.1).

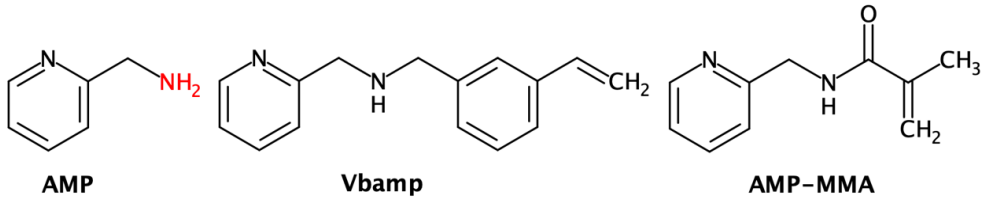

Figure 6.1. Structures of AMP, Vbamp [16], and AMP-MMA. The primary amine group of AMP is highlighted in red.

The methacrylic group in AMP-MMA, along with the polymerizable vinyl function, adds a carbonyl group within the AMP structure. The carbonyl oxygen serves as an additional electron-donor atom, turning the bidentate AMP ligand into a potential tridentate chelating monomer. Based on the structural difference between AMP-MMA and Vbamp, enhanced Ni(II) adsorption performance of the new Ni(II)-IIP prepared with AMP-MMA could be expected.

An additional motivation to prepare a novel monomer based on AMP ligand stemmed from the results concerning bis-AMP-MMA, detailed in Chapter 5. This monomer exhibited a low tendency to polymerize, and a plausible explanation could lie in its high steric hindrance (Section 5.3). The substitution of bis-AMP ligand by its mono-pyridine analog, AMP, could represent a solution to overcome this problem. From this structural difference (one single pyridine group instead of two), it was legitimate to expect that a monomer with lower steric hindrance could enhance the monomer-to-polymer conversion rate. The search for a higher conversion was crucial to increasing the incorporation of the monomer and of its complex within the IIP structure. For all these reasons, the AMP ligand was considered as an optimal candidate for synthesizing a novel chelating monomer to be applied for IIPs preparation.

6.2 Synthesis of AMP-MMA

The AMP ligand was modified by reaction with methacryloyl chloride, introducing into its structure a methacrylic group (Figure 6.2).

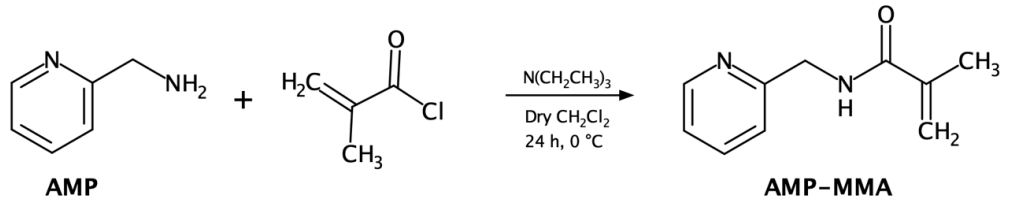

Figure 6.2: Synthesis of AMP-MMA monomer.

The introduction of the methacrylic group within the AMP structure was confirmed by the vinyl proton peaks at 5.38 and 5.82 ppm (Table A.4) in the ^{1}H NMR spectrum (Figure 6.3.a) and by the vinyl carbons peaks at 139.7 and 120.0 ppm (Table A.5) in the ^{13}C NMR spectrum (Figure 6.3.b).

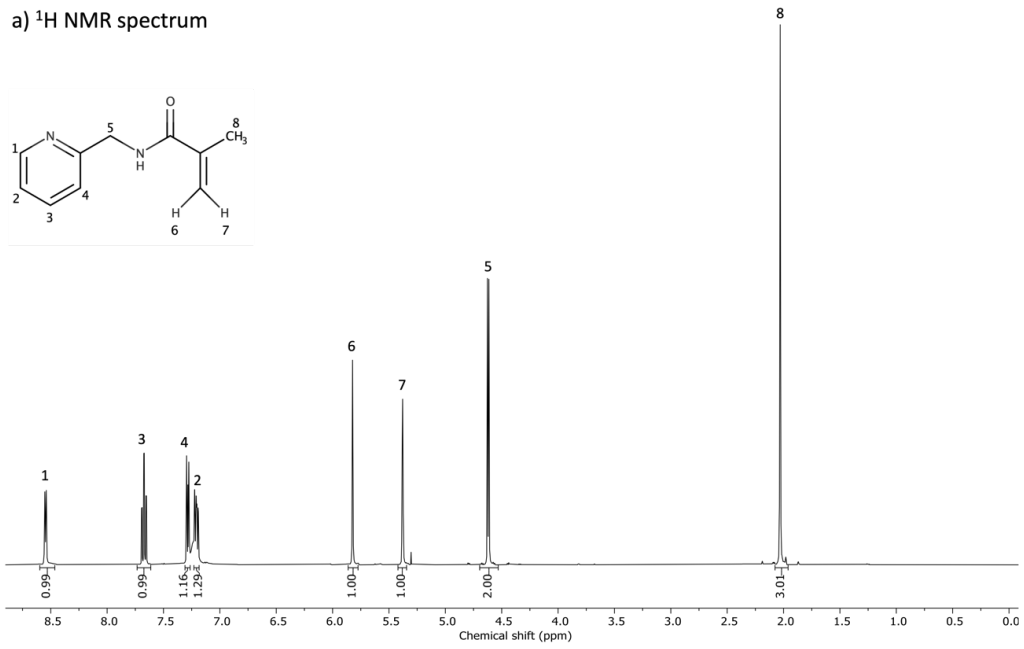

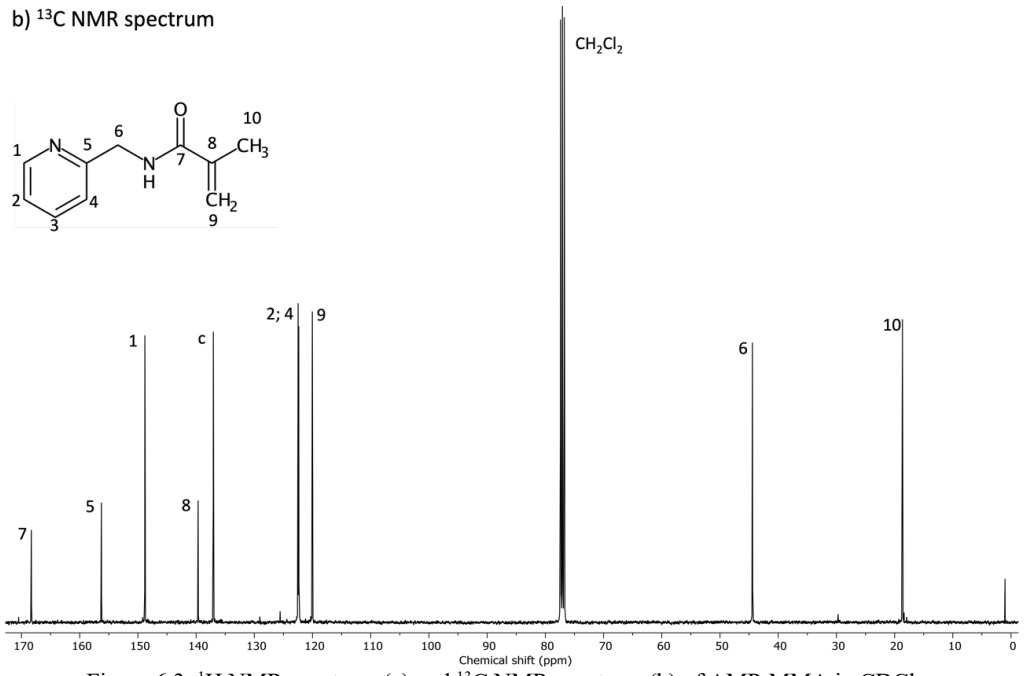

Figure 6.3. ^{1}H NMR spectrum (a) and ^{13}C NMR spectrum (b) of AMP-MMA in $CDCl_3$.

6.3 Polymerization test

The reactivity of AMP-MMA was assessed in a polymerization reaction with MMA as comonomer. This test was carried out using a similar procedure to that described for bis-AMP-MMA (Section 5.3). The AMP-MMA/MMA ratio was set to 1:9, the monomers were dissolved in DMSO-d_6, put under argon atmosphere, and the polymerization mixture was suspended in mineral oil pre-heated to 80 °C. These conditions were chosen to resemble those applied for IIPs preparation. The whole test lasted 24 h, with intermediate sampling after 4 h and 6 h. The intermediate sampling and the final reaction product were analyzed with ^{1}H-NMR spectroscopy (Figure A.5) to determine the conversion % of each monomer into polymer and the fraction of AMP-MMA within the copolymer ($F_{AMP-MMA}$) at different reaction times (Table 6.1). A detailed description of the calculations to determine the conversion % of both monomers and $F_{AMP-MMA}$ is provided in Annex A.4.

Table 6.1. Monomers conversion percentage and $F_{AMP-MMA,t}$ at different reaction times.

Reaction time	AMP-MMA conversion	MMA conversion	$F_{AMP-MMA,t}$
4 h	84%	93.2%	9.1%
6 h	90%	94.9%	9.5%
24 h	92%	95.7%	9.6%

The value of $F_{AMP-MMA}$ into the copolymer with MMA after 6 h of reaction was equal to 9.1%. This value was close to the approximately 10% expected from the initial 1:9 AMP-MMA/MMA ratio. The incorporation of AMP-MMA within the copolymer with MMA was significantly higher than that observed for bis-AMP-MMA (Section 5.3), where the $F_{bis-AMP-MMA}$ was lower than 2%. The higher reactivity of AMP-MMA compared to its bipyridine analogous is likely to derive from the lower steric hindrance of this monomer. From this difference, a higher number of binding sites with enhanced adsorption performance could be expected for AMP-MMA adsorbents.

When the reaction time was increased to 6 h and 24 h, only minor variation in the $F_{AMP-MMA}$ was observed (Table 6.1). Consequently, a reaction time of 4 h was chosen for the preparation of AMP-MMA IIP and NIP.

6.4 Complex formation study

The complex formation study of AMP-MMA followed a similar procedure to what was described for bis-AMP-MMA in Section 5.4. The structure and species distribution of AMP-MMA complexes with Cu(II), Co(II) and Ni(II) ions (generally indicated as M(II)) were investigated to optimize the pre-polymerization mixture for IIPs preparation. The distribution of the complex species was determined by analyzing the UV-Vis absorption

spectra recorded in DMSO at 80 °C (Figure 3.2), which were the solvent and temperature selected for the polymerization. The M(II)/AMP-MMA ratio was varied from 0.1 to 5.3 using both nitrates and perchlorates salts as metal sources. The UV-Vis spectra for each M(II)/AMP-MMA couple were processed with the HypSpec program to determine the complex distribution curves (Figure 6.4) and stability constants of complexes at equilibrium, as previously described in the literature [21,307,317].

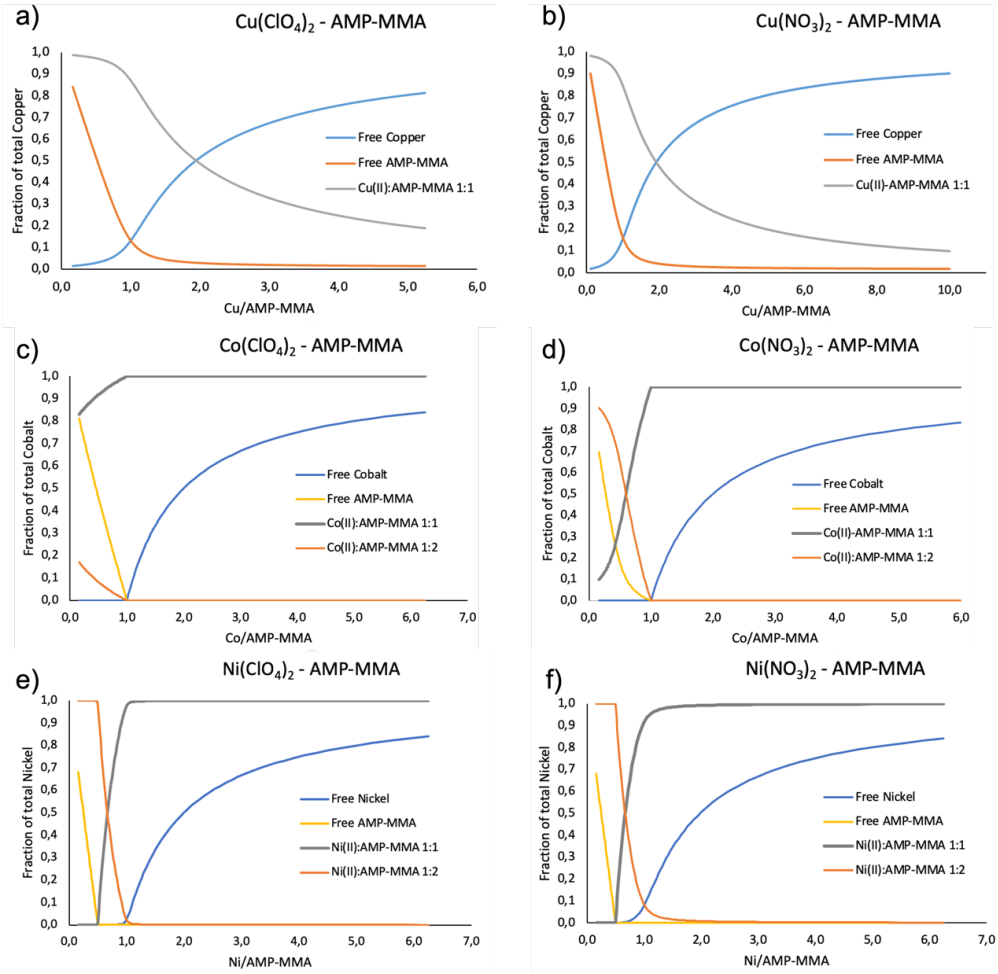

Figure 6.4. Species distribution curves for AMP-MMA coupled with Cu(II), Co(II) or Ni(II) nitrate or perchlorate salts in DMSO at 80°C determined from UV-Vis spectra at different M(II)/bis-AMP-MMA ratios with the HypSpec program.

The molar fraction of each absorbing species in the solution, determined from the species distribution curves in Figure 6.4, are reported in Table 6.2 for the M(II)/AMP-MMA ratios of 1.00, 0.50, and 0.33. The molar fractions of M(II)/AMP-MMA complexes ($x_{1:1}$, $x_{1:2}$) and uncomplexed M(II) ($x_{M(II)}$) are related to the total concentration of M(II), while

the molar fraction of uncomplexed AMP-MMA ($x_{AMP-MMA}$) is related to its initial concentration.

Table 6.2. Species distribution at 80 °C for DMSO solutions containing M(II) and AMP-MMA with M(II)/AMP-MMA ratios equal to 1.00, 0.50, and 0.33.

M(II) salt	$\frac{\mathbf{M(II)}}{\mathbf{Ni(II)}}$	$x_{1:1}$	$x_{1:2}$	$x_{1:3}$	$x_{M(II)}$	$x_{AMP-MMA}$
$Cu(NO_3)_2$	1.00	0.86	/	/	0.14	0.13
	0.50	0.97	/	/	0.03	0.51
	0.33	0.98	/	/	0.02	0.67
$Cu(ClO_4)_2$	1.00	0.84	/	/	0.16	0.16
	0.50	0.96	/	/	0.04	0.51
	0.33	0.97	/	/	0.03	0.67
$Co(NO_3)_2$	1.00	1.00	/	/	/	/
	0.50	0.36	0.64	/	/	0.18
	0.33	0.18	0.82	/	/	0.38
$Co(ClO_4)_2$	1.00	1.00	/	/	/	/
	0.50	0.92	0.08	/	/	0.46
	0.33	0.88	0.12	/	/	0.62
$Ni(NO_3)_2$	1.00	0.84	0.08	/	0.08	/
	0.50	0.01	0.99	/	/	/
	0.33	/	1.00	/	/	0.32
$Ni(ClO_4)_2$	1.00	0.96	0.02	/	0.02	0.01
	0.50	0.09	0.91	/	/	/
	0.33	/	1.00	/	/	0.32

The step-wise stability constants ($\beta_{1:1}$ and $\beta_{1:2}$) for M(II)/AMP-MMA complexes in DMSO at 80 °C determined with the HypSpec program are summarized in Table 6.3.

Table 6.3. Stability constants of M(II)/AMP-MMA complexes in DMSO at 80 °C determined with HypSpec program.

M(II)	M(II)/AMP-MMA 1 :1 complex		M(II)/AMP-MMA 1 :2 complex	
	log $\beta_{1:1}$		log $\beta_{1:2}$	
Cu(II)	$Cu(NO_3)_2$	$Cu(ClO_4)_2$	$Cu(NO_3)_2$	$Cu(ClO_4)_2$
	2.80 ± 0.17	3.00 ± 0.12	Not detected	
Co(II)	$Co(NO_3)_2$	$Co(ClO_4)_2$	$Co(NO_3)_2$	$Co(ClO_4)_2$
	10.67 ± 0.14	9.60 ± 0.62	12.79 ± 0.14	10.00 ± 0.61
Ni(II)	$Ni(NO_3)_2$	$Ni(ClO_4)_2$	$Ni(NO_3)_2$	$Ni(ClO_4)_2$
	8.49 ± 0.16	8.80 ± 0.96	14.92 ± 0.33	14.34 ± 1.56

From the results presented in Figure 6.4 and Tables 6.2 and 6.3, it was possible to draw several conclusions regarding the formation of complexes between AMP-MMA and Cu(II), Co(II), and Ni(II) ions.

When AMP-MMA was paired with Cu(II) ions, only the 1:1 complex was formed (Figure 6.4.a and 6.4.b). The introduction of Cu(II) as nitrate or perchlorate salts had a minimal effect on the stability constants of the 1:1 complex, with log $\beta_{1:1}$ value equal to 2.80 and 3.00, respectively (Table 6.3). At each Cu(II)/AMP-MMA ratio, the 1:1 complex was present in solution together with a residue of uncomplexed Cu(II) and AMP-MMA (Figure 6.4), so this complex could not be isolated.

The combination of AMP-MMA with Co(II) yielded to the formation of two different complexes in solutions with stoichiometry 1:1 and 1:2, as illustrated in Figures 6.4.c and 6.4.d. The type of the counter ion, in this case, had a more significant effect. The stability constants related to the nitrate salts were in fact higher by a factor of 10 for the 1:1 complex and a factor of more than 100 for the 1:2 complex (Table 6.3). The 1:1 complex could be isolated with a Co(II)/AMP-MMA ratio equal to 1.00 (Table 6.2). On the other hand, the 1:2 complex could not be isolated as it always coexisted in solution together with the 1:1 complex and uncomplexed AMP-MMA.

Finally, by coupling AMP-MMA with Ni(II) ions, complexes with 1:1 and 1:2 stoichiometries were formed (Figure 6.4.e and 6.4.f) and the one with 1:2 stoichiometry could be isolated in solution (Table 6.2). The effect of the counter ion on the stability of Ni(II) complexes was not negligible. In the case of Ni(II) introduced as nitrate salt, the stability constant of the 1:1 complex was slightly lower than that of the corresponding perchlorate, with log $\beta_{1:1}$ value equal to 8.49 and 8.80, respectively (Table 6.3). The opposite trend was observed for the 1:2 complexes, as the stability constant of the complex obtained with Ni(II) nitrate was slightly higher than the corresponding perchlorate, with log $\beta_{1:2}$ value equal to 14.92 and 14.34, respectively (Table 6.3). The higher separation in stability constants of 1:1 and 1:2 complexes when Ni(II) was

introduced as nitrate salt, equal to 6.4 logarithmic units, allowed for the isolation of the 1:2 complex at a Ni(II)/AMP-MMA ratio equal to 0.5 (Table 6.2). At this ratio, 99% of the initial Ni(II) was involved in the formation of the 1:2 complex, while only the remaining 1% existed as 1:1 complex.

Through the complex formation study, two distinct complexes between AMP-MMA and either Co(II) or Ni(II) ions were successfully isolated in solution. In the case of Co(II), when the Co(II)/AMP-MMA ratio was 1, a 1:1 stoichiometry complex was isolated in solution. On the other hand, in the case of Ni(II), a 1:2 stoichiometry complex was isolated in solution when the Ni(II)/AMP-MMA ratio was 0.5. As detailed in Chapter 2, a more specific geometry of the binding cavities and thus a higher selectivity of the IIP can be expected when the complex formed in the pre-polymerization mixture has a 1:2 or 1:3 stoichiometry. Consequently, Ni(II) was chosen as a template ion to prepare a Ni(II)-IIP with AMP-MMA.

6.5 Preparation of AMP-MMA polymers

The complex formation study on AMP-MMA was followed by the preparation of a Ni(II)-IIP, AMP-Ni-IIP, via inverse suspension polymerization. The pre-polymerization mixture was optimized by introducing the template ion Ni(II) and the monomer AMP-MMA with a ratio of 0.5, as determined with the complex formation study (Section 6.4). The crosslinker EGDMA was introduced in the polymerization mixture with an AMP-MMA/EGDMA ratio equal to 1:9. The synthesis route for the preparation of AMP-Ni-IIP is illustrated in Figure 6.5.

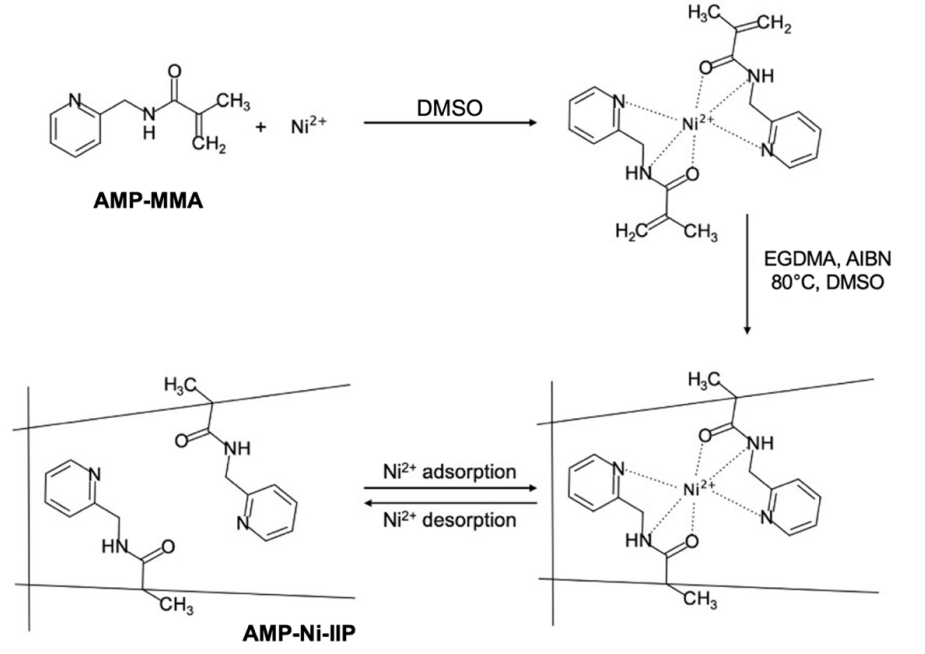

Figure 6.5. Synthesis route for the preparation of AMP-Ni-IIP.

The corresponding non-imprinted polymer, AMP-NIP, was prepared under the same experimental conditions, apart from the absence of Ni(II) ions in the pre-polymerization mixture. The polymer particles of both materials (Figure 6.6) were studied to determine their chemical structure (Section 6.6) and morphology (Section 6.7) and applied in Ni(II) adsorption experiments (Section 6.8).

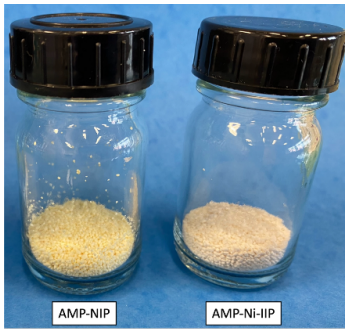

Figure 6.6. Polymer particles of AMP-NIP and AMP-Ni-IIP after leaching step obtained via inverse suspension polymerization.

6.6 Characterization of the chemical structure of AMP-MMA polymers

The chemical structure of both AMP-MMA polymers was studied by FTIR (Figure 6.7) and ^{13}C CPMAS NMR (Figure 6.8) spectroscopies. To verify the incorporation of AMP-MMA into their structures, the spectra of the two polymers were compared with the one of poly(EGDMA).

The presence of poly(EGDMA) resulted in the appearance of its characteristic absorption bands in the FTIR spectrum of each material (Figure 6.7). These included the stretching C=O stretching band at 1725 cm^{-1}, the C-O stretching band at 1144 cm^{-1}, and the -OCH_2 deformation vibration band at 1460 cm^{-1} [292]. The correct incorporation of AMP-MMA into AMP-NIP and AMP-Ni-IIP was confirmed by the presence of typical pyridine and amine bands in their FTIR spectra. In detail, it was possible to detect C=C and C=N pyridine stretching bands at 1575 cm^{-1} and 1593 cm^{-1}, and the C-N aromatic amine stretching bands at 1298 cm^{-1} and 1320 cm^{-1}. These bands were not visible in the spectrum of poly(EGDMA), used as a reference material. The preparation of AMP-Ni-IIP included a leaching step, which involved 5 washes with 0.1 M HCl to release the Ni(II) ions and generate ion-imprinted cavities. FTIR spectra were collected for this material before and after the leaching process, and no changes in its chemical composition were observed.

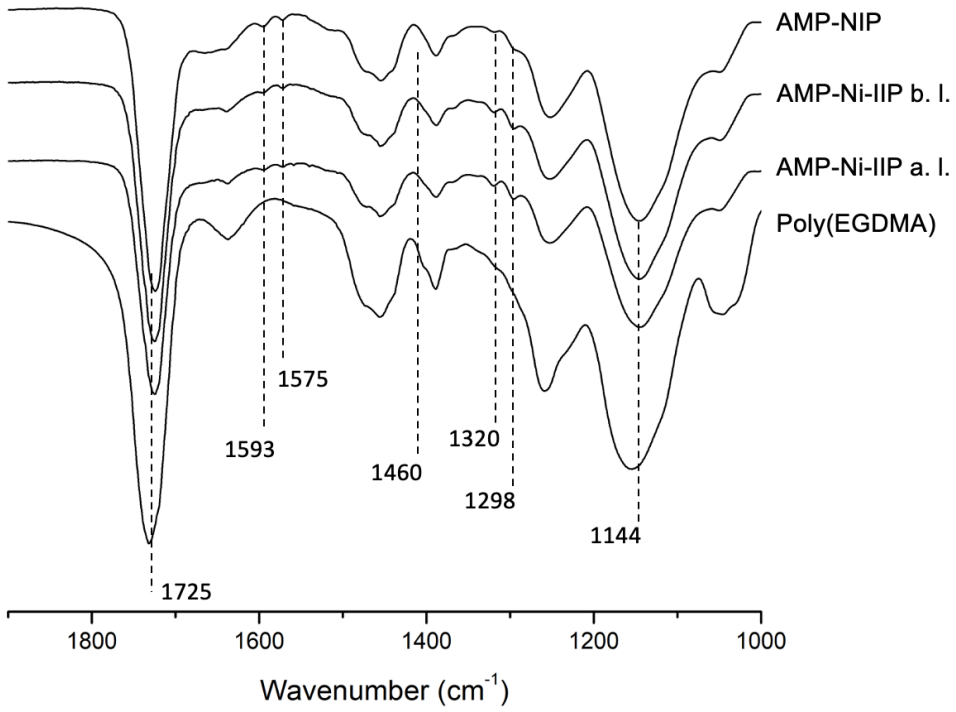

Figure. 6.7. FTIR spectra of AMP-NIP, AMP-Ni-IIP before leaching (b. l.) and after leaching (a. l.) and poly(EGDMA).

The results obtained with FTIR spectroscopy were confirmed by the ^{13}C CPMAS NMR spectra (Figure 6.8) of AMP-MMA polymers. The characteristic signals of poly(EGDMA), the major component in each material, were the most intense in each spectrum. These signals included the carbonyl carbon (C=O) peak at 177.1 ppm, the pending vinyl carbon ($C=CH_2$) peak at 137.1 ppm, the ester carbon (-COO-) peak at 62.9 ppm, the quaternary carbon (>C<) peak at 45.8 ppm, the methylene carbon ($-CH_2-$) peak at 24.5 ppm, and the methyl carbon ($-CH_3$) peak at 18.4 ppm [374,375]. The presence of AMP-MMA within AMP-NIP and AMP-Ni-IIP was confirmed by the pyridine peaks in the aromatic carbon zone, including two weak bands at 157.9 ppm and 149.3 ppm, and a more intense band at 124.5 ppm. These bands were not observed in the spectrum of poly(EGDMA). This result was consistent with the observation conducted with FTIR spectroscopy and provided an additional validation about the correct integration of AMP-MMA within AMP-NIP and AMP-Ni-IIP polymer particles.

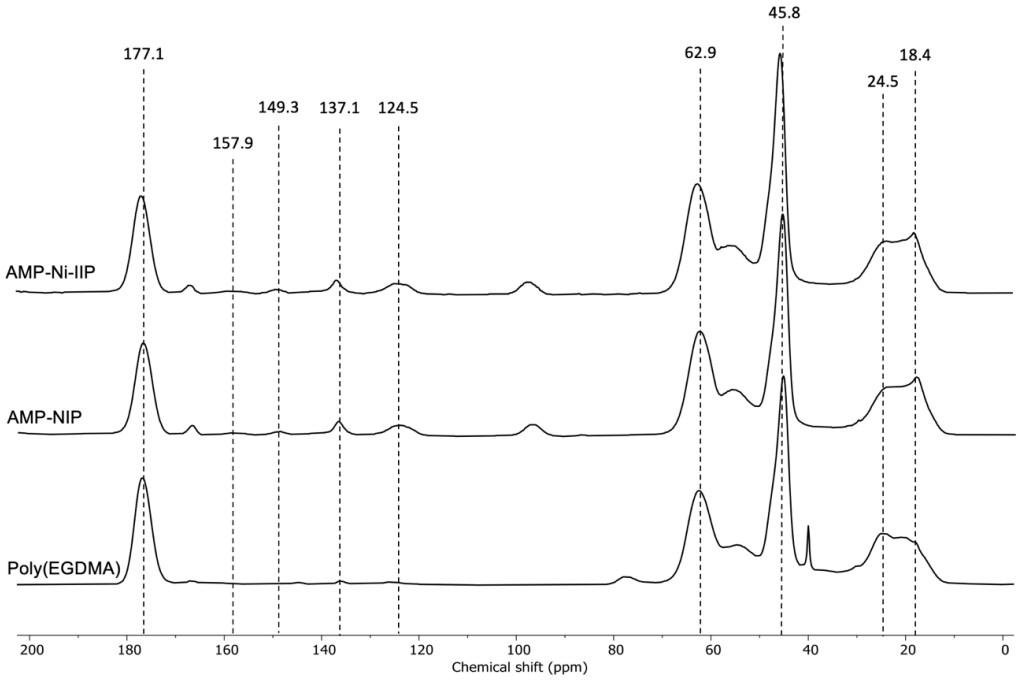

Figure 6.8. ^{13}C CPMAS NMR spectra of poly(EGDMA), AMP-NIP, and AMP-Ni-IIP.

6.7 Morphology of AMP-MMA polymers

The chemical characterization of AMP-MMA polymers was followed by the determination of their particles size with optical microscopy and surface morphology with

SEM. Additionally, the specific surface area, pore size, and pore volume were determined through nitrogen adsorption/desorption experiments.

6.7.1 **Optical microscope and SEM analysis**

The average particles size of AMP-NIP and AMP-Ni-IIP polymers was determined with a numerical optical microscope by averaging the diameter of 20 particles per each material. The average particle diameters for AMP-NIP and AMP-Ni-IIP were equal to 1.34 ± 0.60 mm and 0.92 ± 0.22 mm, respectively.

The surface morphology was studied with SEM images of whole particles for both polymers (Figure 6.9). The surface of AMP-NIP particles was characterized by the alternation of continuous smooth zone and superficial cracks. On the other hand, the surface of AMP-Ni-IIP was quite regular all over the polymer bead and showed a high rugosity.

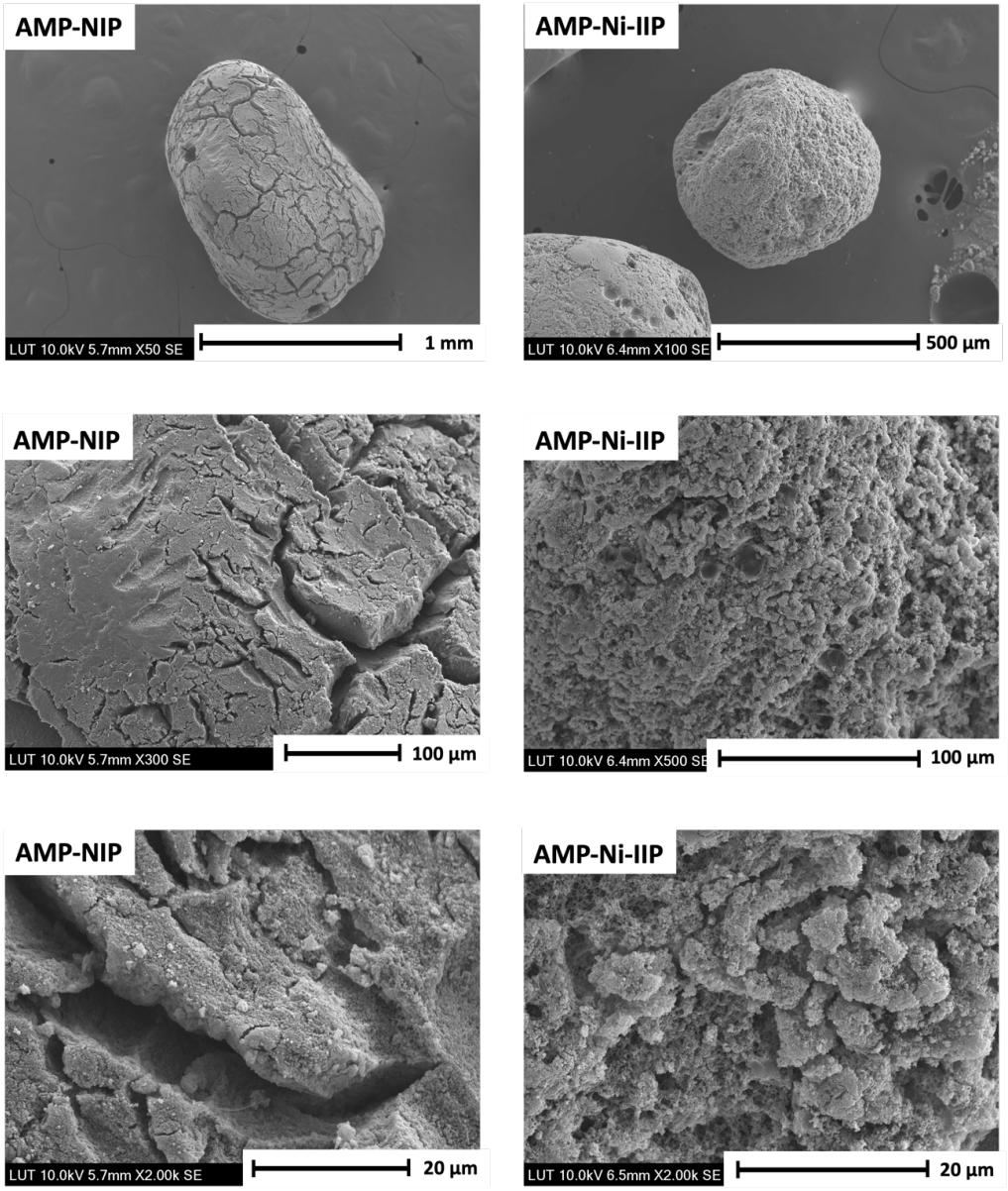

Figure 6.9. SEM pictures of whole polymer particles of AMP-NIP and AMP-Ni-IIP.

6.7.2 **Nitrogen adsorption-desorption experiments**

Nitrogen adsorption-desorption experiments were carried out for both the AMP-MMA polymers, and the corresponding isotherms are illustrated in Figure 6.10.

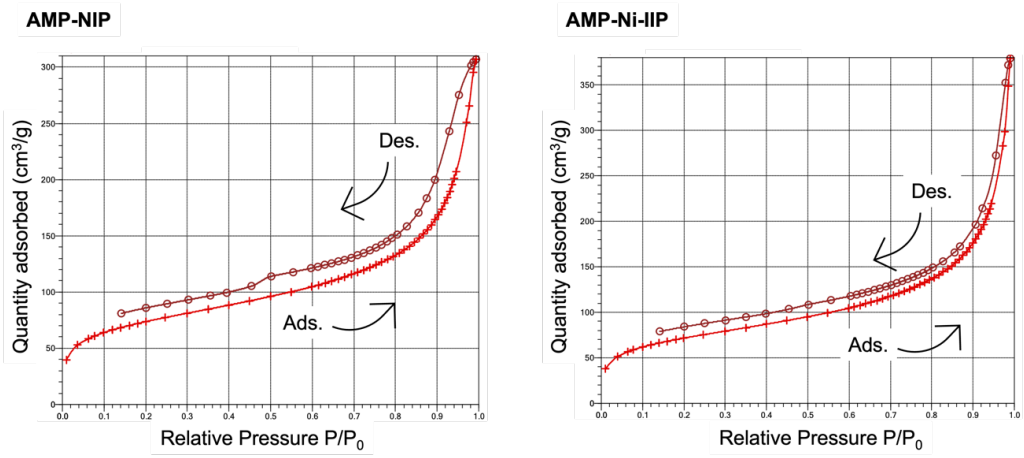

Figure 6.10. Nitrogen adsorption-desorption isotherms of AMP-NIP and AMP-Ni-IIP.

The nitrogen adsorption-desorption isotherms for both materials (Figure 6.10) displayed, according to IUPAC classification (Figures A.1 and A.2), a Type IV isotherm shape with hysteresis loop H4, suggesting the presence of mesopores (pore diameter from 2 to 50 nm). The average pore diameters, total pore volumes, and specific surface areas (Table 6.4) for both materials were determined with the BJH and BET methods.

Table 6.4. Average pore diameters, total pore volumes, and specific surfaces of AMP-NIP and AMP-Ni-IIP determined with BJH and BET methods.

Material	**Average pore diameter (nm)**	**Total pore volumes (cm^3/g)**	**Specific surface area (m^2/g)**
AMP-NIP	7.0	0.47	267.8
AMP-Ni-IIP	9.0	0.59	261.5

The prediction of mesoporous materials was confirmed by the average pore diameter values, which were equal to 7.0 nm and 9.0 nm for AMP-NIP and AMP-Ni-IIP, respectively. The two polymers had similar specific surface areas, with values equal to 267.8 m^2/g and 261.5 m^2/g for AMP-NIP and AMP-Ni-IIP, respectively. Despite this, AMP-Ni-IIP exhibited a higher total pore volume value, equal to 0.59 cm^3/g.

6.8 Ni(II) adsorption experiments

The characterization of AMP-MMA polymers was followed by their application in Ni(II) adsorption experiments, including the effect of pH, the determination of Ni(II) adsorption isotherms, and the assessments of polymer selectivity and reusability.

6.8.1 Effect of pH

The first objective of the adsorption experiments was to assess the effect of pH on Ni(II) adsorption capacity of AMP-NIP and AMP-Ni-IIP to determine the optimal pH range for their application. Three sets of adsorption experiments at different initial concentrations of Ni(II) ions were carried out, and the effect of pH was investigated within the pH range 1.4-7.6 (Figure 6.11).

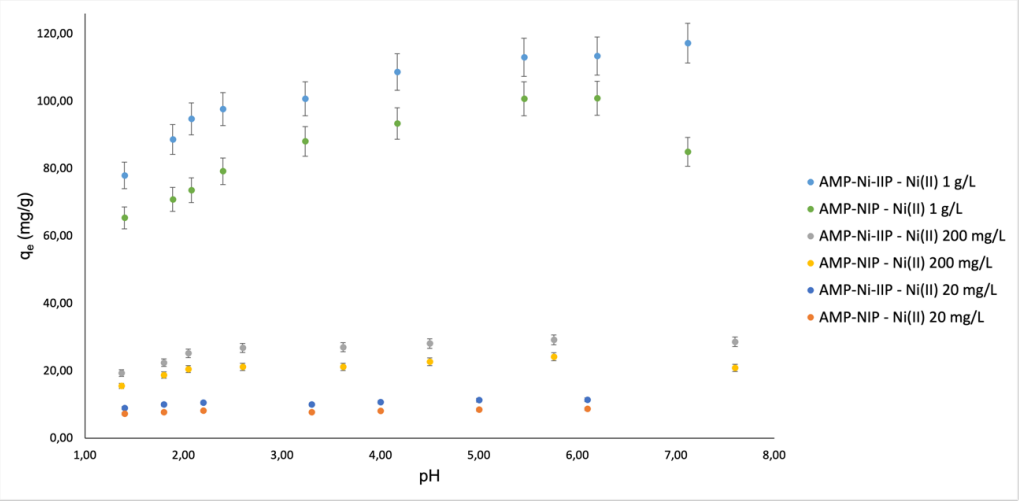

Figure 6.11. Effect of pH on Ni(II) adsorption capacity of AMP-NIP and AMP-Ni-IIP at three different initial Ni(II) concentrations (20 mg/L, 200 mg/L, and 1 g/L). The pH value was adjusted with concentrated HCl and NaOH.

The adsorption capacity of AMP-NIP and AMP-Ni-IIP followed a similar trend with the pH variation in each set of adsorption data obtained at different initial concentrations of Ni(II) ions (Figure 6.11). The adsorption capacity of both materials showed minimal variation at pH values above 4. Conversely, below this pH, a more significant decrease in adsorption efficiency was observed. As discussed in the introduction of this chapter, the AMP ligand is known to be characterized by a low basicity, which led to a low protonation degree in acidic media for the resin containing it [369]. From a monomer based on this ligand, it was therefore reasonable to expect a similar behavior in an acidic environment. When comparing the two materials, the adsorption capacity of AMP-Ni-IIP was always higher than the one of AMP-NIP determined under the same experimental conditions. This result highlighted a positive effect of the imprinting technique. The average value of the imprinting factor, equal to 1.25 ± 0.07, was in a similar range to that described in literature for others Ni(II)-IIPs [294,359]. Considering the good adsorption performance in both neutral and strongly acidic solutions, the following adsorption experiments were carried out at both pH 7 and pH 2.

6.8.2 Ni(II) adsorption isotherms

The maximum Ni(II) adsorption capacity of AMP-NIP and AMP-Ni-IIP were determined at both pH 7 and pH 2. The experiments were carried out at room temperature, using Ni(II) solutions with increasing initial concentrations. The adsorption results are shown in Figure 6.12.

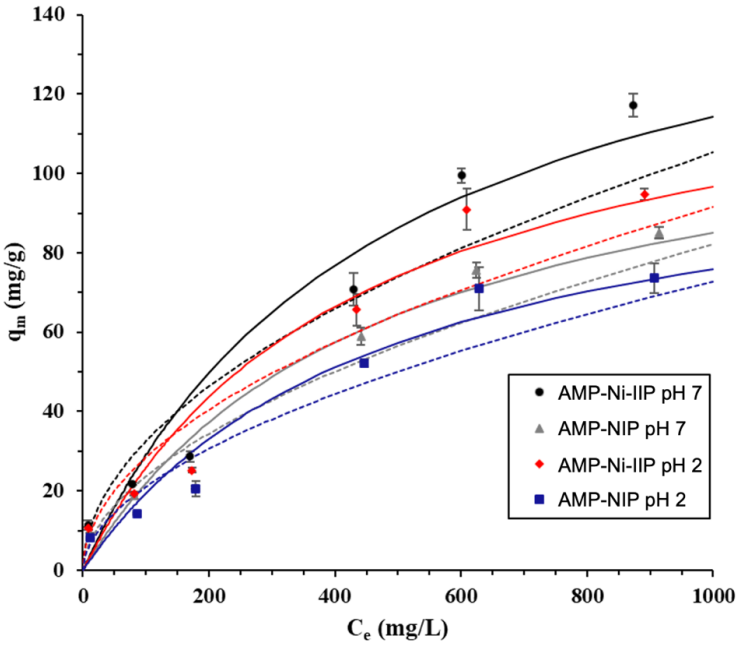

Figure 6.12. Ni(II) adsorption by AMP-NIP and AMP-Ni-IIP. The adsorption data was interpolated with Langmuir (continuous lines) and Freundlich (dashed lines) models. The range of initial Ni(II) ions concentration was 20-1000 mg/L. The pH was adjusted to 7 with HEPES buffer and 2 with NaOH.

The adsorption capacities of both materials at different initial concentration of Ni(II) ions followed a similar trend (Figure 6.12). For both materials, at pH 7, the adsorption capacity steadily increased across the entire concentration range. In contrast, at pH 2, the adsorption capacity stabilized at a Ni(II) concentration of around 600-650 mg/L. The maximum adsorption capacity for each material at different pH values was determined by fitting the adsorption data with the Langmuir (Eq. 2.4) and Freundlich (Eq. 2.5) models (Table 6.5).

Table 6.5. Langmuir and Freundlich parameters for Ni(II) adsorption with AMP-NIP and AMP-Ni-IIP at pH 7 and pH 2.

Model	Parameter	Adsorbent - pH

		AMP-NIP – pH 7	AMP-Ni-IIP – pH 7	AMP-NIP – pH 2	AMP-Ni-IIP – pH 2
Langmuir	$q_{e,max}$ (mg/g)	125.0	169.5	112.4	138.9
	K_L	2.13×10^{-3}	2.07×10^{-3}	2.09×10^{-3}	2.29×10^{-3}
	R^2	0.954	0.948	0.954	0.945
Freundlich	1/n	0.5405	0.510	0.539	0.5076
	K_F	1.964	3.105	1.758	2.745
	R^2	0.932	0.902	0.919	0.901

For both materials, at both pH values, Langmuir's model offered a better correlation of the adsorption data in comparison to Freundlich's model (Table 6.5). This suggested the presence of homogeneous binding sites with uniform adsorption energy and no interaction between adsorbate molecules on adjacent sites. In accordance with the results obtained in the study of the effect of pH, AMP-Ni-IIP showed a higher maximum adsorption capacity when compared to AMP-NIP. At pH 7, the maximum Ni(II) adsorption capacity was equal to 169.5 mg/g for AMP-Ni-IIP and 125.0 mg/g for AMP-NIP. As expected, at pH 2 the maximum adsorption capacity of both materials decreased, but the reduction was quite limited and remarkable adsorption performances were still observed. In detail, at pH 2, the maximum Ni(II) adsorption capacity was equal to 138.9 mg/g and 112.4 mg/g for AMP-Ni-IIP and AMP-NIP, respectively. These values were significantly higher than those observed for Vbamp-based Ni(II)-IIP (11.7 mg/g at pH 7) [16]. This result can be attributed to the presence of an extra carbonyl group in AMP-MMA, whose oxygen can act as a third chelating atom.

When compared with the adsorption capacity in neutral solutions of the other Ni(II)-imprinted materials described in the literature (Table 2.2), one of the AMP-Ni-IIP stands among the highest values. Additionally, AMP-Ni-IIP showed remarkable performance also in strong acidic solutions where the other Ni(II) adsorbents commonly suffer a sharper decline [277,359,380]. Considering the significant performances of AMP-Ni-IIP in both neutral and acidic media, an extended selectivity study was carried out for this material in both these experimental conditions.

6.8.3 **Selectivity**

The selectivity of AMP-NIP and AMP-Ni-IIP for Ni(II) ions was studied in bi-component solutions where Ni(II) was paired with one divalent metal ion M(II) among Co(II), Cu(II), Cd(II), Mn(II), and Mg(II). The selectivity study was carried out at both pH 7 and pH 2 to assess the effect of pH on selectivity. The selectivity coefficient *k* (Eq. 2.6) and relative

selectivity coefficient k' (Eq. 2.8) values for each M(II)/Co(II) pair at different M(II)/Co(II) ratios are reported in Table 6.6.

Table 6.6. Selectivity coefficient and relative selectivity coefficient values for Ni(II) adsorption with AMP-NIP and AMP-Ni-IIP at pH 7 and pH 2 with Co(II), Cu(II), Cd(II), Mn(II), or Mg(II) as competitive ions.

M(II)	$\frac{\mathbf{M(II)}}{\mathbf{Ni(II)}}$	**pH 7**			**pH 2**		
		k_{IIP}	k_{NIP}	k'	k_{IIP}	k_{NIP}	k'
Co(II)	1	3.8	1.8	2.1	3.0	2.4	1.3
	10	5.7	4.7	1.2	4.1	4.1	1.0
	100	25.2	11.4	2.2	23.2	9.5	2.4
Cu(II)	1	1.9	1.4	1.3	1.3	1.2	1.0
	10	4.0	3.0	1.3	3.7	2.2	1.7
	100	15.0	10.5	1.4	14.8	8.8	1.7
Cd(II)	1	6.8	2.6	2.7	6.4	3.1	2.1
	10	9.3	5.2	1.8	8.9	4.4	2.0
	100	38.6	15.7	2.5	32.1	16.5	2.0
Mn(II)	1	5.9	3.1	1.9	5.0	2.2	2.3
	10	8.1	5.7	1.4	7.8	3.9	2.0
	100	32.9	17.2	1.9	27.3	15.3	1.8
Mg(II)	1	2.7	1.3	2.1	2.2	1.6	1.4
	10	5.4	1.9	2.8	5.2	4.0	1.3
	100	23.1	12.7	1.8	21.6	11.4	1.9

The selectivity study results provided in Table 6.6 led to several conclusions regarding both AMP-NIP, as non-imprinted adsorbent, and AMP-Ni-IIP as material prepared with the imprinting technique.

When the M(II)/Ni(II) ratio was set to 1, the selectivity coefficients, k, of AMP-NIP were always superior to 1. This implied that the AMP-MMA monomer incorporated within this adsorbent preferred the interactions with the Ni(II) ion over the other competitive ions.

This result was consistent with the complex formation study for this monomer (Section 6.4), where the most stable complexes were those formed with Ni(II) ions.

The imprinting method had a positive effect on selectivity as the k values of AMP-Ni-IIP were always higher than those related to AMP-NIP, thus the relative selectivity coefficients, k', were always superior to 1. This result could be explained from the comparison of the ionic radii of Ni(II) with those of the competitive metals. The competitive ions Co(II), Cu(II), Cd(II), Mn(II), and Mg(II) toward which selectivity was studied all had a wider ionic radius than that of Ni(II) [381]. From the formation of binding sites around a stable complex between AMP-MMA and Ni(II), it was therefore reasonable to expect that the geometry and size of these cavities hardly allowed the entry of ions with a larger diameter.

When the M(II)/Ni(II) ratio was set to 10 and 100, the k values of both materials increased, showing that the selective adsorption of Ni(II) ions was possible even at a high concentration of competitive ions. The highest k values were obtained using AMP-Ni-IIP with a M(II)/Ni(II) ratio equal to 100 at pH 7. At these conditions, the k values were equal to 25.2, 15.0, 38.6, 32.9 and 23.1 with Co(II), Cu(II), Cd(II), Mn(II), and Mg(II) as competitive ions, respectively.

At pH 2, the k values of both materials were slightly lower than those observed at pH 7. A possible explanation for this result could arise from the presence of a high concentration of hydronium ions in acidic media, which competed with the target metal to form a complex with AMP-MMA.

When compared with the selectivity of other Ni(II)-imprinted materials reported in literature (Table 2.2), the k values of AMP-Ni-IIP stand in the middle-high range. These results, combined with the good adsorption capacity of AMP-Ni-IIP, make this chelating resin a valuable alternative for the selective adsorption of Ni(II) ions in acidic and neutral solutions.

6.8.4 **Reusability of AMP-Ni-IIP**

The set of Ni(II) adsorption experiments was completed with the study of the reusability of AMP-Ni-IIP up to 5 adsorption/desorption cycles (Figure 6.13). The adsorption experiments were followed by the desorption of Ni(II) ions, in separated experiments, using HNO_3, H_2SO_4 and NH_4OH at concentrations of 1 M and 3 M as leaching agents. As discussed in Chapter 2, these three eluents are among the most efficiently applied in hydrometallurgical industry, and the aim of this comparison was to evaluate their effect on the adsorption performance of AMP-Ni-IIP. The material reusability was assessed by calculating the residual adsorption capacity after each adsorption cycle in relation to the first cycle (Eq. 3.1).

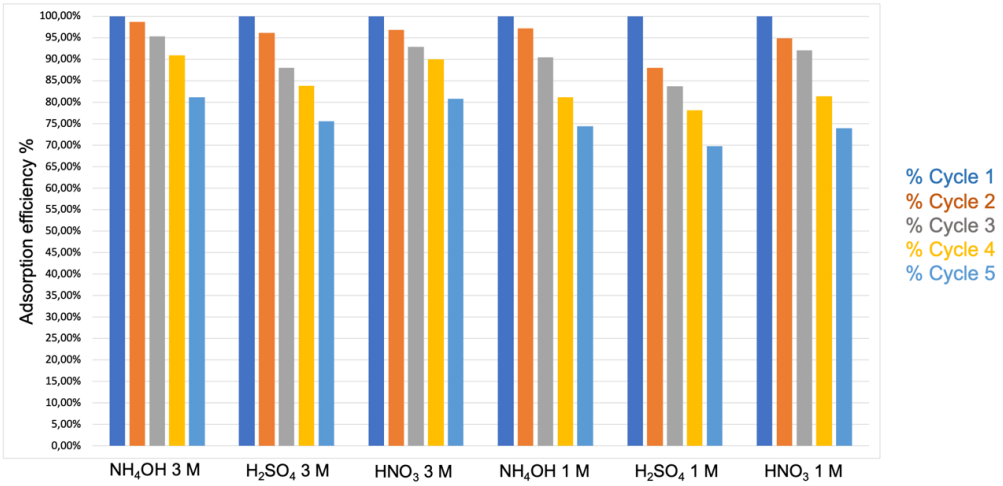

Figure 6.13. AMP-Ni-IIP adsorption efficiency up to 5 adsorption/desorption cycles with NH_4OH, H_2SO_4, and HNO_3 3 M and 1 M as leaching agents.

For each of the three leaching agents, their use with a 3 M concentration resulted in a more efficient regeneration of AMP-Ni-IIP. The application of H_2SO_4 as Ni(II) eluent led to a more significant reduction in the adsorption efficiency of AMP-Ni-IIP compared to the other two leaching agents. The regeneration with H_2SO_4 caused an efficiency reduction up to 12% after the first adsorption/desorption cycle and 30% in the fifth cycle. The regeneration with 3M NH_4OH or HNO_3 resulted in an efficiency reduction of 1% and 19% after the first and fifth cycle for NH_4OH and of 3% and 19% after the first and fifth cycle for HNO_3. The similar performance and the different chemical nature of these two eluents provided two valid alternatives to be applied based on the preference of a basic (NH_4OH) or acid (HNO_3) leaching agent.

6.9 Conclusion

This chapter described the synthesis of a novel chelating monomer, AMP-MMA, based on 2-(aminomethyl)pyridine (AMP) and its application in the preparation of a Ni(II)-IIP. The synthesis of AMP-MMA, verified with ^{1}H-NMR and ^{13}C-NMR spectroscopies, was followed by the assessment of its reactivity in polymerization reaction and by a complex formation study. The complex formation study was conducted with Cu(II), Co(II), and Ni(II) ions, resulting in the formation of a 1:1 complex with Cu(II) and 1:1 and 1:2 complexes with both Co(II) and Ni(II) ions. The 1:2 complex formed with Ni(II) ions was the most stable and could be isolated in solution when the Ni(II)/AMP-MMA ratio was equal to 0.5.

This Ni(II)/AMP-MMA ratio was applied to optimize the pre-polymerization mixture to prepare a novel Ni(II)-IIP, named AMP-Ni-IIP. The corresponding NIP, AMP-NIP, was also prepared under the same conditions but without the metal template. The chemical

composition of both materials was determined by FTIR and ^{13}C CP-MAS NMR spectroscopies. Morphology studies were carried out using optical microscopy, SEM, and nitrogen adsorption-desorption experiments. The materials consisted of polymer particles whose diameter was in the range of 1 mm. The specific surface areas were quite similar, with values of 267.8 m^2/g for AMP-NIP and 261.5 m^2/g for AMP-Ni-IIP, while AMP-Ni-IIP exhibited a higher total volume of pores, equal to 0.59 cm^3/g, which could positively impact its adsorption capacity.

Ni(II) adsorption experiments were carried out with both materials including investigations into the effect of pH, adsorption isotherms, selectivity, and reusability. Both materials exhibited optimal adsorption performance in the neutral solutions. However, only a slight reduction in adsorption capacity was observed when the pH was ≥ 2. For this reason, the maximum adsorption capacity and the selectivity were studied both at pH 7 and pH 2. Under each experimental condition, AMP-Ni-IIP showed better adsorption performance than AMP-NIP, highlighting a positive effect of the imprinting technique. The maximum Ni(II) adsorption capacity of AMP-Ni-IIP was equal to 169.5 mg/g at pH 7 and 138.9 mg/g at pH 2. The enhanced Ni(II) adsorption capacity compared to Vbamp-based Ni(II)-IIP can be attributed to the presence of an extra carbonyl group whose oxygen can act as a third chelating atom. In addition to a high Ni(II) adsorption capacity, AMP-Ni-IIP demonstrated a good selectivity for Ni(II) ions, with selectivity coefficient values up to 25.2, 15.0, 38.6, 32.9, and 23.1 with Co(II), Cu(II), Cd(II), Mn(II), and Mg(II) as competitive ions, respectively. This result was consistent with that observed in the complex formation study, where the stability of AMP-MMA complexes with Ni(II) was greater than those with Co(II) and Cu(II).

Considering the remarkable maximum adsorption capacity at both pH 2 and pH 7, among the highest values reported in literature for Ni(II)-imprinted materials, and the high selectivity for Ni(II) ions, AMP-Ni-IIP can be considered as a valuable alternative for the selective adsorption of Ni(II) ions from both neutral and acidic media.

7 General conclusions and perspectives

The objective of this doctoral thesis was to prepare highly selective adsorbent materials for the separation of Co(II) and Ni(II) ions. As described in the bibliographic study of this manuscript, the separation of Co(II) and Ni(II) ions poses a significant challenge in the hydrometallurgical industry due to the similarity in the physicochemical properties of these two metals. Highly selective adsorbents can be prepared with the ion imprinting technique. Polymeric materials prepared with this technique are referred to as ion-imprinted polymers (IIPs). The selectivity of IIPs is closely tied to the stability of the complex formed between a chelating agent incorporated into the polymer, whether a ligand or a chelating monomer, and the target ion. The target ion acts as a template during the polymerization process and, after its leaching, selective binding cavities are formed. The stability of the metal/chelator complexes is strongly dependent on the nature of the chelating agent. Therefore, the synthesis of new chelating monomers and the study of the complexes formed with the target ion are crucial steps in the preparation of highly selective IIPs. The experimental work carried out in this doctoral project involved the synthesis of three new chelating monomers and their application for the preparation of IIPs. The new monomers, named PIM-MMA, bis-AMP-MMA and AMP-MMA, were synthesized using 2,2'-(pyridyl)imidazole (PIM), bis-2-(pyridylmethyl)amine (bis-AMP) and 2-(aminomethylpyridine) (AMP) ligands as precursors, respectively. These ligands were selected due to their known ability to form stable complexes with one or both the target ions of this project, as previously described in the literature. The most important results and conclusions concerning the preparation of IIPs with each of these monomers and a correlation between the formation of metal/chelator complexes and selectivity of IIPs are provided below.

The monomer PIM-MMA showed a high tendency to homopolymerize during its synthesis. Although this phenomenon was slowed down by the introduction of polymerization inhibitor during its synthesis, it was not completely prevented. Consequently, the complex formation study could not be carried out on this monomer as it would polymerize within the UV-Vis cuvette. Nevertheless, PIM-MMA was used for the preparation of two Ni(II)-IIPs by combining Ni(II) and PIM-MMA at varying ratios in the pre-polymerization mixture. The IIP prepared with a Ni(II)/PIM-MMA ratio equal to 1:2 was named PIM-Ni-IIP-1:2, while the one prepared with a 1:3 ratio was named PIM-Ni-IIP-1:3. A non-imprinted polymer, PIM-NIP, was also prepared following a similar procedure as for the two IIPs, but without the inclusion of Ni(II) ions in the pre-polymerization mixture. All three materials were applied in Ni(II) adsorption experiments and their best adsorption performance were observed at pH 6. Under each experimental condition, both IIPs exhibited a higher Ni(II) adsorption capacity compared to PIM-NIP, indicating a positive effect of the imprinting technique on these materials. The highest value of maximum Ni(II) adsorption capacity, obtained with PIM-Ni-IIP-1:2, was equal to 27.91 mg/g at pH 6. Additionally, PIM-Ni-IIP-1:2 exhibited a higher selectivity for Ni(II) ions when compared to PIM-Ni-IIP-1:3 and PIM-NIP. Despite this, its selectivity coefficients with Co(II), Cd(II), Mn(II), and Mg(II) as competitive ions were limited to

1.34, 2.84, 11.28, and 1.44, respectively. These selectivity coefficients could not be considered high enough for the selective separation of Ni(II) ions. Consequently, the quest for highly selective adsorbents continued with the synthesis of a new chelating monomer.

In contrast to the high tendency for homopolymerization displayed by PIM-MMA, bis-AMP-MMA displayed a low reactivity, which probably originated from the significant steric hindrance of this monomer. This led to limited molar fraction of bis-AMP-MMA (< 2%) within the copolymer formed with MMA, used as a model comonomer in the polymerization test. The characterization of bis-AMP-MMA progressed by studying its complexes with Cu(II), Co(II), and Ni(II) ions (generally indicated as M(II)). This study revealed the formation of a complex with a 1:1 stoichiometry with Cu(II), and two complexes with 1:1 and 1:2 stoichiometries with both Co(II) and Ni(II) ions. Among these complexes, only those with a 1:2 stoichiometry formed with Co(II) or Ni(II) ions could be successfully isolated in solution. The isolation of the 1:2 complex was attained by combining either Co(II) or Ni(II) and bis-AMP-MMA at an M(II)/bis-AMP-MMA ratio of 0.5. Based on these results, a Co(II)-IIP, bis-AMP-Co-IIP, and a Ni(II)-IIP, bis-AMP-Ni-IIP were prepared by optimizing the pre-polymerization media with a 0.5 M(II)/bis-AMP-MMA ratio. Co(II) adsorption experiments were carried out with bis-AMP-Co-IIP and bis-AMP-NIP. The optimal adsorption performance for both materials were observed in the pH range of 5-8. The maximum Co(II) adsorption capacity was measured at pH 6.5 and was equal to 54.0 mg/g for bis-AMP-NIP and 13.3 mg/g for bis-AMP-Co-IIP. The higher adsorption capacity of bis-AMP-NIP likely arose from its specific surface area, which was four times larger than the one of bis-AMP-Co-IIP (153.9 m^2/g for bis-AMP-NIP and 37.4 m^2/g for bis-AMP-Co-IIP). Both materials exhibited limited selectivity for Co(II) ions in the presence of Ni(II), Cd(II), Mn(II), and Mg(II) as competitive ions. The selectivity study results concerning the separation of Co(II) ions from Ni(II) ions were in good agreement with the complex formation study. The stability constants of bis-AMP-MMA complexes with Co(II) and Ni(II) ions were similar. Consequently, a limited selectivity in the separation of these two metals with adsorbents based on this monomer could be expected. Concerning bis-AMP-Ni-IIP, due to the absence of selectivity in the complexation of Co(II) and Ni(II) ions with bis-AMP-MMA and to the very limited specific surface area of this IIP (7.7 m^2/g), adsorption experiments were not carried out with this material. The experimental work continued with the synthesis and characterization of the last monomer prepared in this doctoral project.

The structure of AMP-MMA closely resembled that of bis-AMP-MMA, except for the presence of a single pyridinic group instead of two. This structural difference, resulting in lower steric hindrance, led to increased reactivity in the polymerization reaction for AMP-MMA compared to bis-AMP-MMA. Consequently, the molar fraction of AMP-MMA within the copolymer with MMA ranged from 9.1% to 9.6%, which is significantly higher than 1.7%-1.9% range of bis-AMP-MMA. This result suggested the presence of a higher number of binding sites in the copolymer prepared with AMP-MMA compared to the one with bis-AMP-MMA. The investigation into AMP-MMA complexes with Cu(II), Co(II) and Ni(II) ions revealed the formation of a 1:1 complex with Cu(II) ions and 1:1

and 1:2 complexes with both Co(II) and Ni(II) ions. The 1:2 complex formed with Ni(II) ions was the most stable and could be isolated in solution when the Ni(II)/AMP-MMA ratio was set to 0.5. This Ni(II)/AMP-MMA ratio was thus applied to optimize the pre-polymerization mixture for the preparation of a Ni(II)-IIP, named AMP-Ni-IIP. Ni(II) adsorption experiments were conducted with both AMP-Ni-IIP and the corresponding NIP (AMP-NIP). The best Ni(II) adsorption performance was obtained in neutral solutions, with a minor decrease of the adsorption capacity at pH 4 and a more significant reduction only occurring below pH 2. For this reason, the maximum adsorption capacity and selectivity of AMP-MMA adsorbents were studied at both pH 7 and pH 2. Under each experimental condition, AMP-Ni-IIP exhibited a higher adsorption capacity compared to AMP-NIP, indicating a positive effect of the imprinting technique. The maximum Ni(II) adsorption capacity of AMP-Ni-IIP was 169.5 mg/g at pH 7 and 138.9 mg/g at pH 2, among the highest values for Ni(II)-imprinted materials reported in the literature. Additionally, AMP-Ni-IIP exhibited higher selectivity for Ni(II) ions compared to AMP-NIP. The selectivity coefficients of AMP-Ni-IIP with Co(II), Cu(II), Cd(II), Mn(II), and Mg(II) as competitive ions were up to 25.2, 15.0, 38.6, 32.9, and 23.1, respectively. The selectivity study results were consistent with the findings in the complex formation study. The stability of AMP-MMA complexes with Ni(II) was higher than those with Co(II) and Cu(II) ions. Consequently, a higher selectivity of AMP-MMA adsorbents for Ni(II) ions could be expected. The selectivity of AMP-Ni-IIP for Ni(II) ions, combined with its high adsorption capacity in both neutral and acidic solutions, make this adsorbent a valuable alternative for the selective adsorption of Ni(II) ions.

In conclusion, the strong correlation between the formation of metal/chelator complexes and the selectivity of IIPs was confirmed. Although the study of PIM-MMA complexes was not possible, the results related to bis-AMP-MMA and AMP-MMA monomers supported this thesis. In the case of bis-AMP-MMA, the investigation into its complexes with Co(II) and Ni(II) ions revealed the formation of complexes with similar stability constants. This finding was reflected in the selectivity study, where a scarce selectivity in the absorption of Co(II) in the presence of an equal concentration of Ni(II) was observed. Conversely, in the case of AMP-MMA, the complex formation study with Co(II) and Ni(II) ions indicated a higher stability in the complexes formed with the latter. This result was corroborated by the selectivity study on AMP-Ni-IIP, where the absorption of Ni(II) ions was significantly favored over that of Co(II) ions.

Considering the results in terms of adsorption capacity and selectivity achieved in this doctoral project, the extensions of the experimental work can involve either the scale-up of the preparation of IIPs or, alternatively, their application to produce sensors. The efficiency of the IIPs prepared in this project was examined in batch systems, where a small quantity of adsorbent material was sufficient for an extensive series of adsorption experiments. The industrial application of adsorbent materials commonly involves dynamic systems and continuous-flow processes which require a larger-scale production of the adsorbents. For this reason, the scale-up of the production of the IIPs prepared in this project and their application in dynamic systems and continuous-flow processes can provide an interesting industrial point of view regarding their efficiency. As mentioned

above, the IIPs prepared in this doctoral project were specifically designed for their utilization in metal adsorption experiments. Their design was thus focused on preparing polymer particles with suitable size for the ion exchange or adsorption of metal ions dissolved in solution. However, it is noteworthy that the application of IIPs as sensors in the field of analytical chemistry is gaining increasing interest. The development of sensors based on the original monomers and IIPs described in this project thus represents a significant path for future developments.

References

[1] Nickel Institute, About nickel, (2023). https://nickelinstitute.org/en/about-nickel-and-its-applications/ (accessed September 27, 2023).

[2] Cobalt institute, Cobalt Mining, (2023). https://www.cobaltinstitute.org/about-cobalt/cobalt-life-cycle/cobalt-mining/ (accessed September 27, 2023).

[3] F. Faraji, R. Golmohammadzadeh, C.A. Pickles, Potential and current practices of recycling waste printed circuit boards: A review of the recent progress in pyrometallurgy, J Environ Manage. 316 (2022) 115242. https://doi.org/10.1016/j.jenvman.2022.115242.

[4] M. Kaya, S. Hussaini, S. Kursunoglu, Critical review on secondary zinc resources and their recycling technologies, Hydrometallurgy. 195 (2020) 105362. https://doi.org/10.1016/j.hydromet.2020.105362.

[5] V. Gunarathne, A.U. Rajapaksha, M. Vithanage, D.S. Alessi, R. Selvasembian, Mu. Naushad, S. You, P. Oleszczuk, Y.S. Ok, Hydrometallurgical processes for heavy metals recovery from industrial sludges, Crit Rev Environ Sci Technol. 52 (2022) 1022–1062. https://doi.org/10.1080/10643389.2020.1847949.

[6] L. Zhang, L. Ji, L. Li, D. Shi, T. Xu, X. Peng, X. Song, Recovery of Co, Ni, and Li from solutions by solvent extraction with β-diketone system, Hydrometallurgy. 204 (2021) 105718. https://doi.org/10.1016/j.hydromet.2021.105718.

[7] Y.-J. Shih, C.-P. Lin, Y.-H. Huang, Application of Fered-Fenton and chemical precipitation process for the treatment of electroless nickel plating wastewater, Sep Purif Technol. 104 (2013) 100–105. https://doi.org/10.1016/j.seppur.2012.11.025.

[8] B.S. Boyanov, V. V. Konareva, N.K. Kolev, Purification of zinc sulfate solutions from cobalt and nickel through activated cementation, Hydrometallurgy. 73 (2004) 163–168. https://doi.org/10.1016/j.hydromet.2003.09.002.

[9] J.J. Eksteen, E.A. Oraby, V. Nguyen, Leaching and ion exchange based recovery of nickel and cobalt from a low grade, serpentine-rich sulfide ore using an alkaline glycine lixiviant system, Miner Eng. 145 (2020) 106073. https://doi.org/10.1016/j.mineng.2019.106073.

[10] M.H. Dehghani, K. Yetilmezsoy, M. Salari, Z. Heidarinejad, M. Yousefi, M. Sillanpää, Adsorptive removal of cobalt(II) from aqueous solutions using multi-walled carbon nanotubes and γ-alumina as novel adsorbents: Modelling and optimization based on response surface methodology and artificial neural network, J Mol Liq. 299 (2020) 112154. https://doi.org/10.1016/j.molliq.2019.112154.

[11] D.S. Flett, Solvent extraction in hydrometallurgy: the role of organophosphorus extractants, J Organomet Chem. 690 (2005) 2426–2438. https://doi.org/10.1016/j.jorganchem.2004.11.037.

[12] X. Chen, T. Zhou, J. Kong, H. Fang, Y. Chen, Separation and recovery of metal values from leach liquor of waste lithium nickel cobalt manganese oxide based cathodes, Sep Purif Technol. 141 (2015) 76–83. https://doi.org/10.1016/j.seppur.2014.11.039.

[13] C.R. Marston, Recovery of nickel using integrated continuous ion exchange and electo-winning process, WO2014025568A1, 2013.

[14] C. Branger, W. Meouche, A. Margaillan, Recent advances on ion-imprinted polymers, React Funct Polym. 73 (2013) 859–875. https://doi.org/10.1016/j.reactfunctpolym.2013.03.021.

[15] T.P. Rao, R. Kala, S. Daniel, Metal ion-imprinted polymers—Novel materials for selective recognition of inorganics, Anal Chim Acta. 578 (2006) 105–116. https://doi.org/https://doi.org/10.1016/j.aca.2006.06.065.

[16] K. Laatikainen, D. Udomsap, H. Siren, H. Brisset, T. Sainio, C. Branger, Effect of template ion-ligand complex stoichiometry on selectivity of ion-imprinted polymers, Talanta. 134 (2015) 538–545. https://doi.org/10.1016/j.talanta.2014.11.050.

[17] H. Irving, R.J.P. Williams, The stability of transition-metal complexes, Journal of the Chemical Society (Resumed). (1953) 3192. https://doi.org/10.1039/jr9530003192.

[18] C. V. Banks, R.I. Bystroff, Stability Orders in Transition Metal-1,10-Phenanthroline Complexes, J Am Chem Soc. 81 (1959) 6153–6158. https://doi.org/10.1021/ja01532a013.

[19] A. Bhaskarapillai, N. V. Sevilimedu, B. Sellergren, Synthesis and Characterization of Imprinted Polymers for Radioactive Waste Reduction, Ind Eng Chem Res. 48 (2009) 3730–3737. https://doi.org/10.1021/ie801640b.

[20] E. Birlik, A. Ersöz, E. Açıkkalp, A. Denizli, R. Say, Cr(III)-imprinted polymeric beads: Sorption and preconcentration studies, J Hazard Mater. 140 (2007) 110–116. https://doi.org/10.1016/j.jhazmat.2006.06.141.

[21] K. Laatikainen, C. Branger, B. Coulomb, V. Lenoble, T. Sainio, In situ complexation versus complex isolation in synthesis of ion imprinted polymers, React Funct Polym. 122 (2018) 1–8. https://doi.org/10.1016/j.reactfunctpolym.2017.10.022.

[22] L. Zhang, Y. Liu, L. Deng, Three-Coordinate Cobalt(IV) and Cobalt(V) Imido Complexes with N-Heterocyclic Carbene Ligation: Synthesis, Structure, and Their Distinct Reactivity in C–H Bond Amination, J Am Chem Soc. 136 (2014) 15525–15528. https://doi.org/10.1021/ja509731z.

[23] D.A. Kurtz, J. Zhang, A. Sookezian, J. Kallick, M.G. Hill, B.M. Hunter, A Cobalt Phosphine Complex in Five Oxidation States, Inorg Chem. 60 (2021) 17445–17449. https://doi.org/10.1021/acs.inorgchem.1c03020.

[24] D.G. Barceloux, D. Barceloux, Cobalt, J Toxicol Clin Toxicol. 37 (1999) 201–216. https://doi.org/10.1081/CLT-100102420.

[25] F. Gaucherand, E. Beaugnon, Magnetic texturing in ferromagnetic cobalt alloys, Physica B Condens Matter. 346–347 (2004) 262–266. https://doi.org/10.1016/j.physb.2004.01.062.

[26] J. Sato, T. Omori, K. Oikawa, I. Ohnuma, R. Kainuma, K. Ishida, Cobalt-Base High-Temperature Alloys, Science (1979). 312 (2006) 90–91. https://doi.org/10.1126/science.1121738.

[27] A.G. Blackman, Cobalt: Inorganic & Coordination Chemistry, in: Encyclopedia of Inorganic Chemistry, John Wiley & Sons, Ltd, Chichester, UK, 2006. https://doi.org/10.1002/0470862106.ia046.

[28] J.H. Tundermann, J.K. Tien, T.E. Howson, Updated by Staff, Nickel and Nickel Alloys, in: Kirk-Othmer Encyclopedia of Chemical Technology, John Wiley & Sons, Inc., Hoboken, NJ, USA, 2013. https://doi.org/10.1002/0471238961.1409031120211404.a01.pub3.

[29] H.S. Klapper, N.S. Zadorozne, R.B. Rebak, Localized Corrosion Characteristics of Nickel Alloys: A Review, Acta Metallurgica Sinica (English Letters). 30 (2017) 296–305. https://doi.org/10.1007/s40195-017-0553-z.

[30] H. Wang, S.M. Butorin, A.T. Young, J. Guo, Nickel Oxidation States and Spin States of Bioinorganic Complexes from Nickel L-edge X-ray Absorption and Resonant Inelastic X-ray Scattering, The Journal of Physical Chemistry C. 117 (2013) 24767–24772. https://doi.org/10.1021/jp402404b.

[31] N.M. Camasso, M.S. Sanford, Design, synthesis, and carbon-heteroatom coupling reactions of organometallic nickel(IV) complexes, Science (1979). 347 (2015) 1218–1220. https://doi.org/10.1126/science.aaa4526.

[32] J.R. Hartman, R.W. Vachet, J.H. Callahan, Gas, solution, and solid state coordination environments for the nickel(II) complexes of a series of aminopyridine ligands of varying coordination number, Inorganica Chim Acta. 297 (2000) 79–87. https://doi.org/10.1016/S0020-1693(99)00288-1.

[33] R. Giannini, I.C. Freestone, A.J. Shortland, European cobalt sources identified in the production of Chinese famille rose porcelain, J Archaeol Sci. 80 (2017) 27–36. https://doi.org/10.1016/j.jas.2017.01.011.

[34] A. Zucchiatti, A. Bouquillon, I. Katona, A. D'Alessandro, The 'della Robbia blue': A case study for the use of cobalt pigments in ceramics during the italian renaissance, Archaeometry. 48 (2006) 131–152. https://doi.org/10.1111/j.1475-4754.2006.00247.x.

[35] M. Llusar, A. Forés, J.A. Badenes, J. Calbo, M.A. Tena, G. Monrós, Colour analysis of some cobalt-based blue pigments, J Eur Ceram Soc. 21 (2001) 1121–1130. https://doi.org/10.1016/S0955-2219(00)00295-8.

[36] M.-C. Corbeil, J.-P. Charland, E.A. Moffatt, The Characterization of Cobalt Violet Pigments, Studies in Conservation. 47 (2002) 237–249. https://doi.org/10.1179/sic.2002.47.4.237.

[37] F. Du, B. Su, Further study of sources of the imported cobalt-blue pigment used on Jingdezhen porcelain from late 13 to early 15 centuries, Science in China Series E: Technological Sciences. 51 (2008) 249–259. https://doi.org/10.1007/s11431-008-0013-0.

[38] A. Tajne, T.V.K. Gupta, H. Ramani, Y. Joshi, A critical review on the machinability aspects of nickel and cobalt based superalloys in turning operation used for aerospace applications, Advances in Materials and Processing Technologies. (2023) 1–34. https://doi.org/10.1080/2374068X.2023.2185850.

[39] H.A. Zaman, S. Sharif, M.H. Idris, A. Kamarudin, Metallic Biomaterials for Medical Implant Applications: A Review, Applied Mechanics and Materials. 735 (2015) 19–25. https://doi.org/10.4028/www.scientific.net/AMM.735.19.

[40] C.O. Clerc, M.R. Jedwab, D.W. Mayer, P.J. Thompson, J.S. Stinson, Assessment of wrought ASTM F1058 cobalt alloy properties for permanent surgical implants, J Biomed Mater Res. 38 (1997) 229–234. https://doi.org/https://doi.org/10.1002/(SICI)1097-4636(199723)38:3%3C229::AID-JBM7%3E3.0.CO;2-R.

[41] S.L.-F. Chan, T.L. Lam, C. Yang, S.-C. Yan, N.M. Cheng, A robust and efficient cobalt molecular catalyst for CO_2 reduction, Chemical Communications. 51 (2015) 7799–7801. https://doi.org/10.1039/C5CC00566C.

[42] M.S. Jeletic, M.T. Mock, A.M. Appel, J.C. Linehan, A Cobalt-Based Catalyst for the Hydrogenation of CO_2 under Ambient Conditions, J Am Chem Soc. 135 (2013) 11533–11536. https://doi.org/10.1021/ja406601v.

[43] Z. Gholami, Z. Tišler, V. Rubáš, Recent advances in Fischer-Tropsch synthesis using cobalt-based catalysts: a review on supports, promoters, and reactors, Catalysis Reviews. 63 (2021) 512–595. https://doi.org/10.1080/01614940.2020.1762367.

[44] C.G. Okoye-Chine, M. Moyo, X. Liu, D. Hildebrandt, A critical review of the impact of water on cobalt-based catalysts in Fischer-Tropsch synthesis, Fuel Processing Technology. 192 (2019) 105–129. https://doi.org/10.1016/j.fuproc.2019.04.006.

[45] O. Gutfleisch, High-Temperature Samarium Cobalt Permanent Magnets, in: Nanoscale Magnetic Materials and Applications, Springer US, Boston, MA, 2009: pp. 337–372. https://doi.org/10.1007/978-0-387-85600-1_12.

[46] X. Zhou, A. Huang, B. Cui, J.W. Sutherland, Techno-economic Assessment of a Novel SmCo Permanent Magnet Manufacturing Method, Procedia CIRP. 98 (2021) 127–132. https://doi.org/10.1016/j.procir.2021.01.017.

[47] J.-H. Yi, Development of samarium–cobalt rare earth permanent magnetic materials, Rare Metals. 33 (2014) 633–640. https://doi.org/10.1007/s12598-014-0405-1.

[48] M. Li, J. Lu, Cobalt in lithium-ion batteries, Science (1979). 367 (2020) 979–980. https://doi.org/10.1126/science.aba9168.

[49] X. Liu, Y. Tan, W. Wang, C. Li, Z.W. Seh, L. Wang, Y. Sun, Conformal Prelithiation Nanoshell on $LiCoO_2$ Enabling High-Energy Lithium-Ion Batteries, Nano Lett. 20 (2020) 4558–4565. https://doi.org/10.1021/acs.nanolett.0c01413.

[50] A.M. Kannan, L. Rabenberg, A. Manthiram, High Capacity Surface-Modified $LiCoO_2$ Cathodes for Lithium-Ion Batteries, Electrochemical and Solid-State Letters. 6 (2003) A16–A18. https://doi.org/10.1149/1.1526782.

[51] S. Luo, K. Wang, J. Wang, K. Jiang, Q. Li, S. Fan, Binder-Free $LiCoO_2$ /Carbon Nanotube Cathodes for High-Performance Lithium Ion Batteries, Advanced Materials. 24 (2012) 2294–2298. https://doi.org/10.1002/adma.201104720.

[52] H.U. Sverdrup, A.H. Olafsdottir, Assessing the Long-Term Global Sustainability of the Production and Supply for Stainless Steel, BioPhysical Economics and Resource Quality. 4 (2019) 8. https://doi.org/10.1007/s41247-019-0056-9.

[53] J.H. Potgieter, P.A. Olubambi, L. Cornish, C.N. Machio, E.-S.M. Sherif, Influence of nickel additions on the corrosion behaviour of low nitrogen 22% Cr series duplex stainless steels, Corros Sci. 50 (2008) 2572–2579. https://doi.org/10.1016/j.corsci.2008.05.023.

[54] J. Pilhagen, R. Sandström, Influence of nickel on the toughness of lean duplex stainless steel welds, Materials Science and Engineering: A. 602 (2014) 49–57. https://doi.org/10.1016/j.msea.2014.01.093.

[55] V.S. Saji, H.-C. Choe, Electrochemical behavior of Co-Cr and Ni-Cr dental cast alloys, Transactions of Nonferrous Metals Society of China. 19 (2009) 785–790. https://doi.org/10.1016/S1003-6326(08)60350-7.

[56] M. Manjaiah, S. Narendranath, S. Basavarajappa, V.N. Gaitonde, Wire electric discharge machining characteristics of titanium nickel shape memory alloy, Transactions of Nonferrous Metals Society of China. 24 (2014) 3201–3209. https://doi.org/10.1016/S1003-6326(14)63461-0.

[57] J.A. Mary, A. Manikandan, L.J. Kennedy, M. Bououdina, R. Sundaram, J.J. Vijaya, Structure and magnetic properties of Cu-Ni alloy nanoparticles prepared by rapid microwave combustion method, Transactions of Nonferrous Metals Society of China. 24 (2014) 1467–1473. https://doi.org/10.1016/S1003-6326(14)63214-3.

[58] G.R. Thellaputta, P.S. Chandra, C.S.P. Rao, Machinability of Nickel Based Superalloys: A Review, Mater Today Proc. 4 (2017) 3712–3721. https://doi.org/10.1016/j.matpr.2017.02.266.

[59] T.M. Pollock, S. Tin, Nickel-Based Superalloys for Advanced Turbine Engines: Chemistry, Microstructure and Properties, J Propuls Power. 22 (2006) 361–374. https://doi.org/10.2514/1.18239.

[60] Z. Hua, Y. Liu, G. Yao, L. Wang, J. Ma, L. Liang, Preparation and Characterization of Nickel-Coated Carbon Fibers by Electroplating, J Mater Eng Perform. 21 (2012) 324–330. https://doi.org/10.1007/s11665-011-9958-4.

[61] C.A. Loto, Electroless Nickel Plating – A Review, Silicon. 8 (2016) 177–186. https://doi.org/10.1007/s12633-015-9367-7.

[62] T. Benvenuti, R.S. Krapf, M.A.S. Rodrigues, A.M. Bernardes, J. Zoppas-Ferreira, Recovery of nickel and water from nickel electroplating wastewater by electrodialysis, Sep Purif Technol. 129 (2014) 106–112. https://doi.org/10.1016/j.seppur.2014.04.002.

[63] C. Jeyaseelan, A. Jain, P. Khurana, D. Kumar, S. Thatai, Ni-Cd Batteries, in: Rechargeable Batteries, Wiley, 2020: pp. 177–194. https://doi.org/10.1002/9781119714774.ch9.

[64] Y. Liu, H. Pan, M. Gao, Q. Wang, Advanced hydrogen storage alloys for Ni/MH rechargeable batteries, J. Mater. Chem. 21 (2011) 4743–4755. https://doi.org/10.1039/C0JM01921F.

[65] W.H. Zhu, Y. Zhu, Z. Davis, B.J. Tatarchuk, Energy efficiency and capacity retention of Ni–MH batteries for storage applications, Appl Energy. 106 (2013) 307–313. https://doi.org/10.1016/j.apenergy.2012.12.025.

[66] J.L. Rhinehart, L.A. Brown, B.K. Long, A Robust Ni(II) α-Diimine Catalyst for High Temperature Ethylene Polymerization, J Am Chem Soc. 135 (2013) 16316–16319. https://doi.org/10.1021/ja408905t.

[67] E.F. Connor, T.R. Younkin, J.I. Henderson, A.W. Waltman, R.H. Grubbs, Synthesis of neutral nickel catalysts for ethylene polymerization. The influence of ligand size on catalyst stability Electronic supplementary information (ESI) available: experimental protocol for (tmeda)Ni(Me)2 and compounds 3,4,7,8,9 and 10 and 1H-NMR magnetization transfer data for compound 7. See http://www.rsc.org/suppdata/cc/b3/b306701g/, Chemical Communications. (2003) 2272. https://doi.org/10.1039/b306701g.

[68] B.Y. Lee, G.C. Bazan, J. Vela, Z.J.A. Komon, X. Bu, α-Iminocarboxamidato−Nickel(II) Ethylene Polymerization Catalysts, J Am Chem Soc. 123 (2001) 5352–5353. https://doi.org/10.1021/ja004191h.

[69] J. Fang, X. Sui, Y. Li, C. Chen, Synthesis of polyolefin elastomers from unsymmetrical α-diimine nickel catalyzed olefin polymerization, Polym Chem. 9 (2018) 4143–4149. https://doi.org/10.1039/C8PY00725J.

[70] J. Liu, D. Chen, H. Wu, Z. Xiao, H. Gao, F. Zhu, Q. Wu, Polymerization of α-Olefins Using a Camphyl α-Diimine Nickel Catalyst at Elevated Temperature, Macromolecules. 47 (2014) 3325–3331. https://doi.org/10.1021/ma5004634.

[71] A. Dechal, M. Khoshsefat, S. Ahmadjo, S.M.M. Mortazavi, G.H. Zohuri, H. Abedini, Mono- and binuclear nickel catalysts for 1-hexene polymerization, Appl Organomet Chem. 32 (2018). https://doi.org/10.1002/aoc.4355.

[72] H. Hu, H. Gao, D. Chen, G. Li, Y. Tan, G. Liang, F. Zhu, Q. Wu, Ligand-Directed Regioselectivity in Amine–Imine Nickel-Catalyzed 1-Hexene Polymerization, ACS Catal. 5 (2015) 122–128. https://doi.org/10.1021/cs501081a.

[73] S. Avar, S.M.M. Mortazavi, S. Ahmadjo, G.H. Zohuri, α-Diimine nickel catalyst for copolymerization of hexene and acrylate monomers activated by different cocatalysts, Appl Organomet Chem. 32 (2018) e4238. https://doi.org/10.1002/aoc.4238.

[74] D.J. Paustenbach, B.E. Tvermoes, K.M. Unice, B.L. Finley, B.D. Kerger, A review of the health hazards posed by cobalt, Crit Rev Toxicol. 43 (2013) 316–362. https://doi.org/10.3109/10408444.2013.779633.

[75] L. Leyssens, B. Vinck, C. Van Der Straeten, F. Wuyts, L. Maes, Cobalt toxicity in humans—A review of the potential sources and systemic health effects, Toxicology. 387 (2017) 43–56. https://doi.org/10.1016/j.tox.2017.05.015.

[76] L.O. Simonsen, H. Harbak, P. Bennekou, Cobalt metabolism and toxicology—A brief update, Science of The Total Environment. 432 (2012) 210–215. https://doi.org/10.1016/j.scitotenv.2012.06.009.

[77] G.M. Keegan, I.D. Learmonth, C. Case, A Systematic Comparison of the Actual, Potential, and Theoretical Health Effects of Cobalt and Chromium Exposures from Industry and Surgical Implants, Crit Rev Toxicol. 38 (2008) 645–674. https://doi.org/10.1080/10408440701845534.

[78] M.S. Caicedo, P.H. Pennekamp, K. McAllister, J.J. Jacobs, N.J. Hallab, Soluble ions more than particulate cobalt-alloy implant debris induce monocyte costimulatory molecule expression and release of proinflammatory cytokines critical to metal-induced lymphocyte reactivity, J Biomed Mater Res A. 9999A (2009) NA-NA. https://doi.org/10.1002/jbm.a.32627.

[79] B.L. Finley, A.D. Monnot, S.H. Gaffney, D.J. Paustenbach, Dose-Response Relationships For Blood Cobalt Concentrations and Health Effects: A Review of the Literature and Application of a Biokinetic Model, Journal of Toxicology and Environmental Health, Part B. 15 (2012) 493–523. https://doi.org/10.1080/10937404.2012.744287.

[80] M.J. Maroney, S. Ciurli, Nonredox Nickel Enzymes, Chem Rev. 114 (2014) 4206–4228. https://doi.org/10.1021/cr4004488.

[81] W. Lubitz, H. Ogata, O. Rüdiger, E. Reijerse, Hydrogenases, Chem Rev. 114 (2014) 4081–4148. https://doi.org/10.1021/cr4005814.

[82] M. Can, F.A. Armstrong, S.W. Ragsdale, Structure, Function, and Mechanism of the Nickel Metalloenzymes, CO Dehydrogenase, and Acetyl-CoA Synthase, Chem Rev. 114 (2014) 4149–4174. https://doi.org/10.1021/cr400461p.

[83] B. Jaun, R.K. Thauer, Methyl-Coenzyme M Reductase and its Nickel Corphin Coenzyme F_{430} in Methanogenic Archaea, in: Nickel and Its Surprising Impact in Nature, John Wiley & Sons, Ltd, Chichester, UK, 2007: pp. 323–356. https://doi.org/10.1002/9780470028131.ch8.

[84] Y. Sheng, I.A. Abreu, D.E. Cabelli, M.J. Maroney, A.-F. Miller, M. Teixeira, J.S. Valentine, Superoxide Dismutases and Superoxide Reductases, Chem Rev. 114 (2014) 3854–3918. https://doi.org/10.1021/cr4005296.

[85] B. Desguin, T. Zhang, P. Soumillion, P. Hols, J. Hu, R.P. Hausinger, A tethered niacin-derived pincer complex with a nickel-carbon bond in lactate racemase, Science (1979). 349 (2015) 66–69. https://doi.org/10.1126/science.aab2272.

[86] B. Zambelli, V.N. Uversky, S. Ciurli, Nickel impact on human health: An intrinsic disorder perspective, Biochimica et Biophysica Acta (BBA) - Proteins and Proteomics. 1864 (2016) 1714–1731. https://doi.org/10.1016/j.bbapap.2016.09.008.

[87] M. Monachese, J.P. Burton, G. Reid, Bioremediation and Tolerance of Humans to Heavy Metals through Microbial Processes: a Potential Role for Probiotics, Appl Environ Microbiol. 78 (2012) 6397–6404. https://doi.org/10.1128/AEM.01665-12.

[88] Q.Y. Chen, J. Brocato, F. Laulicht, M. Costa, Mechanisms of Nickel Carcinogenesis, in: 2017: pp. 181–197. https://doi.org/10.1007/978-3-319-55448-8_8.

[89] G. Genchi, A. Carocci, G. Lauria, M.S. Sinicropi, A. Catalano, Nickel: Human Health and Environmental Toxicology, Int J Environ Res Public Health. 17 (2020) 679. https://doi.org/10.3390/ijerph17030679.

[90] M.T. Lin, M.F. Beal, Mitochondrial dysfunction and oxidative stress in neurodegenerative diseases, Nature. 443 (2006) 787–795. https://doi.org/10.1038/nature05292.

[91] S. Xu, M. He, M. Zhong, L. Li, Y. Lu, Y. Zhang, L. Zhang, Z. Yu, Z. Zhou, The neuroprotective effects of taurine against nickel by reducing oxidative stress and maintaining mitochondrial function in cortical neurons, Neurosci Lett. 590 (2015) 52–57. https://doi.org/10.1016/j.neulet.2015.01.065.

[92] C.M. Diaz, C.A. Landolt, A. Vahed, A.E.M. Warner, J.C. Taylor, A Review of Nickel Pyrometallurgical Operations, JOM. 40 (1988) 28–33. https://doi.org/10.1007/BF03258548.

[93] E. Ma, Recovery of Waste Printed Circuit Boards Through Pyrometallurgy, in: Electronic Waste Management and Treatment Technology, Elsevier, 2019: pp. 247–267. https://doi.org/10.1016/B978-0-12-816190-6.00011-X.

[94] B. Makuza, Q. Tian, X. Guo, K. Chattopadhyay, D. Yu, Pyrometallurgical options for recycling spent lithium-ion batteries: A comprehensive review, J Power Sources. 491 (2021) 229622. https://doi.org/10.1016/j.jpowsour.2021.229622.

[95] M.S. Safarzadeh, J.D. Miller, The pyrometallurgy of enargite: A literature update, Int J Miner Process. 157 (2016) 103–110. https://doi.org/10.1016/j.minpro.2016.09.008.

[96] E. Keskinkilic, Nickel Laterite Smelting Processes and Some Examples of Recent Possible Modifications to the Conventional Route, Metals (Basel). 9 (2019) 974. https://doi.org/10.3390/met9090974.

[97] D.C. Liu, B. Yang, F. Wang, Q.C. Yu, L. Wang, Y.N. Dai, Research on the Removal of Impurities from Crude Nickel by Vacuum Distillation, Phys Procedia. 32 (2012) 363–371. https://doi.org/10.1016/j.phpro.2012.03.570.

[98] F. Vegliò, R. Quaresima, P. Fornari, S. Ubaldini, Recovery of valuable metals from electronic and galvanic industrial wastes by leaching and electrowinning, Waste Management. 23 (2003) 245–252. https://doi.org/10.1016/S0956-053X(02)00157-5.

[99] S.K. Sahu, B. Chmielowiec, A. Allanore, Electrolytic Extraction of Copper, Molybdenum and Rhenium from Molten Sulfide Electrolyte, Electrochim Acta. 243 (2017) 382–389. https://doi.org/10.1016/j.electacta.2017.04.071.

[100] X. Ge, X. Wang, S. Seetharaman, Copper extraction from copper ore by electro-reduction in molten CaCl2–NaCl, Electrochim Acta. 54 (2009) 4397–4402. https://doi.org/10.1016/j.electacta.2009.03.015.

[101] K. Daehn, A. Allanore, Electrolytic production of copper from chalcopyrite, Curr Opin Electrochem. 22 (2020) 110–119. https://doi.org/10.1016/j.coelec.2020.04.011.

[102] A. Allanore, Features and Challenges of Molten Oxide Electrolytes for Metal Extraction, J Electrochem Soc. 162 (2015) E13–E22. https://doi.org/10.1149/2.0451501jes.

[103] H.Y. Lee, S.G. Kim, J.K. Oh, Electrochemical leaching of nickel from low-grade laterites, Hydrometallurgy. 77 (2005) 263–268. https://doi.org/10.1016/j.hydromet.2004.11.011.

[104] T. Hennebel, N. Boon, S. Maes, M. Lenz, Biotechnologies for critical raw material recovery from primary and secondary sources: R&D priorities and future perspectives, N Biotechnol. 32 (2015) 121–127. https://doi.org/10.1016/j.nbt.2013.08.004.

[105] W.-Q. Zhuang, J.P. Fitts, C.M. Ajo-Franklin, S. Maes, L. Alvarez-Cohen, T. Hennebel, Recovery of critical metals using biometallurgy, Curr Opin Biotechnol. 33 (2015) 327–335. https://doi.org/10.1016/j.copbio.2015.03.019.

[106] D.B. Johnson, Biomining—biotechnologies for extracting and recovering metals from ores and waste materials, Curr Opin Biotechnol. 30 (2014) 24–31. https://doi.org/10.1016/j.copbio.2014.04.008.

[107] G.M. Gadd, Bioremedial potential of microbial mechanisms of metal mobilization and immobilization, Curr Opin Biotechnol. 11 (2000) 271–279. https://doi.org/10.1016/S0958-1669(00)00095-1.

[108] M. Ijadi Bajestani, S.M. Mousavi, S.A. Shojaosadati, Bioleaching of heavy metals from spent household batteries using Acidithiobacillus ferrooxidans: Statistical evaluation and optimization, Sep Purif Technol. 132 (2014) 309–316. https://doi.org/10.1016/j.seppur.2014.05.023.

[109] R. Zhang, S. Hedrich, F. Römer, D. Goldmann, A. Schippers, Bioleaching of cobalt from Cu/Co-rich sulfidic mine tailings from the polymetallic Rammelsberg mine, Germany, Hydrometallurgy. 197 (2020) 105443. https://doi.org/10.1016/j.hydromet.2020.105443.

[110] S. Akbari, A. Ahmadi, Recovery of copper from a mixture of printed circuit boards (PCBs) and sulphidic tailings using bioleaching and solvent extraction processes, Chemical Engineering and Processing - Process Intensification. 142 (2019) 107584. https://doi.org/10.1016/j.cep.2019.107584.

[111] G. Chen, H. Yang, H. Li, L. Tong, Recovery of Cobalt as Cobalt Oxalate from Cobalt Tailings Using Moderately Thermophilic Bioleaching Technology and Selective Sequential Extraction, Minerals. 6 (2016) 67. https://doi.org/10.3390/min6030067.

[112] J.-W. Choi, M.-H. Song, J.K. Bediako, Y.-S. Yun, Sequential recovery of gold and copper from bioleached wastewater using ion exchange resins, Environmental Pollution. 266 (2020) 115167. https://doi.org/10.1016/j.envpol.2020.115167.

[113] A. Deepatana, M. Valix, Recovery of nickel and cobalt from organic acid complexes: Adsorption mechanisms of metal-organic complexes onto aminophosphonate chelating resin, J Hazard Mater. 137 (2006) 925–933. https://doi.org/10.1016/j.jhazmat.2006.03.015.

[114] H.R. Watling, The bioleaching of sulphide minerals with emphasis on copper sulphides — A review, Hydrometallurgy. 84 (2006) 81–108. https://doi.org/10.1016/j.hydromet.2006.05.001.

[115] D.B. Johnson, Development and application of biotechnologies in the metal mining industry, Environmental Science and Pollution Research. 20 (2013) 7768–7776. https://doi.org/10.1007/s11356-013-1482-7.

[116] D.E. Cameron, C.J. Bashor, J.J. Collins, A brief history of synthetic biology, Nat Rev Microbiol. 12 (2014) 381–390. https://doi.org/10.1038/nrmicro3239.

[117] A.H. Kaksonen, X. Deng, T. Bohu, L. Zea, H.N. Khaleque, Y. Gumulya, N.J. Boxall, C. Morris, K.Y. Cheng, Prospective directions for biohydrometallurgy,

Hydrometallurgy. 195 (2020) 105376. https://doi.org/10.1016/j.hydromet.2020.105376.

[118] A.B. Botelho Junior, D.B. Dreisinger, D.C.R. Espinosa, A Review of Nickel, Copper, and Cobalt Recovery by Chelating Ion Exchange Resins from Mining Processes and Mining Tailings, Min Metall Explor. 36 (2019) 199–213. https://doi.org/10.1007/s42461-018-0016-8.

[119] P. Wu, L. Zhang, C. Lin, X. Xie, X. Yong, X. Wu, J. Zhou, H. Jia, P. Wei, Extracting heavy metals from electroplating sludge by acid and bioelectrical leaching using Acidithiobacillus ferrooxidans, Hydrometallurgy. 191 (2020) 105225. https://doi.org/10.1016/j.hydromet.2019.105225.

[120] Z. Suiyi, W. Jian, H. Yuhong, W. Ying, Z. Yuxin, Q. Jiabao, L. Jiancong, Y. Jinlu, J. Meichun, Perspective on pH adjustment in hydrometallurgical recycling of valuable metals from waste, Front Chem. 11 (2023). https://doi.org/10.3389/fchem.2023.1177173.

[121] R.G. McDonald, B.I. Whittington, Atmospheric acid leaching of nickel laterites review, Hydrometallurgy. 91 (2008) 35–55. https://doi.org/10.1016/j.hydromet.2007.11.009.

[122] N.M. Rice, A hydrochloric acid process for nickeliferous laterites, Miner Eng. 88 (2016) 28–52. https://doi.org/10.1016/j.mineng.2015.09.017.

[123] T. Agacayak, V. Zedef, Leaching of a Turkish Lateritic Nickel Ore in Nitric Acid Solution, in: Mine Planning and Equipment Selection, Springer International Publishing, Cham, 2014: pp. 1039–1045. https://doi.org/10.1007/978-3-319-02678-7_100.

[124] G. Li, Q. Zhou, Z. Zhu, J. Luo, M. Rao, Z. Peng, T. Jiang, Selective leaching of nickel and cobalt from limonitic laterite using phosphoric acid: An alternative for value-added processing of laterite, J Clean Prod. 189 (2018) 620–626. https://doi.org/10.1016/j.jclepro.2018.04.083.

[125] W. Astuti, T. Hirajima, K. Sasaki, N. Okibe, Comparison of atmospheric citric acid leaching kinetics of nickel from different Indonesian saprolitic ores, Hydrometallurgy. 161 (2016) 138–151. https://doi.org/10.1016/j.hydromet.2015.12.015.

[126] A. Deepatana, J.A. Tang, M. Valix, Comparative study of chelating ion exchange resins for metal recovery from bioleaching of nickel laterite ores, Miner Eng. 19 (2006) 1280–1289. https://doi.org/10.1016/j.mineng.2006.04.015.

[127] L. Li, W. Qu, X. Zhang, J. Lu, R. Chen, F. Wu, K. Amine, Succinic acid-based leaching system: A sustainable process for recovery of valuable metals from spent

Li-ion batteries, J Power Sources. 282 (2015) 544–551. https://doi.org/10.1016/j.jpowsour.2015.02.073.

[128] S. Sahu, N.C. Kavuri, M. Kundu, Dissolution kinetics of nickel laterite ore using different secondary metabolic acids, Brazilian Journal of Chemical Engineering. 28 (2011) 251–258. https://doi.org/10.1590/S0104-66322011000200009.

[129] D. Song, T. Wang, Z. Liu, S. Zhao, J. Quan, G. Li, H. Zhu, J. Huang, W. He, Characteristic comparison of leaching valuable metals from spent power Li-ion batteries for vehicles using the inorganic and organic acid system, J Environ Chem Eng. 10 (2022) 107102. https://doi.org/10.1016/j.jece.2021.107102.

[130] J. Schuster, B. Ebin, Investigation of indium and other valuable metals leaching from unground waste LCD screens by organic and inorganic acid leaching, Sep Purif Technol. 279 (2021) 119659. https://doi.org/10.1016/j.seppur.2021.119659.

[131] L.A. Al-Makhadmeh, M.A. Batiha, M.S. Al-Harahsheh, I.S. Altarawneh, S.E. Rawadieh, The Effectiveness of Zn Leaching from EAFD Using Caustic Soda, Water Air Soil Pollut. 229 (2018) 33. https://doi.org/10.1007/s11270-018-3694-4.

[132] S.M. Seyed Ghasemi, A. Azizi, Alkaline leaching of lead and zinc by sodium hydroxide: kinetics modeling, Journal of Materials Research and Technology. 7 (2018) 118–125. https://doi.org/10.1016/j.jmrt.2017.03.005.

[133] K. Gargul, P. Jarosz, S. Małecki, Alkaline Leaching of Low Zinc Content Iron-Bearing Sludges, Archives of Metallurgy and Materials. 61 (2016) 43–50. https://doi.org/10.1515/amm-2016-0013.

[134] A. Aracena, F. Pérez, D. Carvajal, Leaching of cuprite through NH4OH in basic systems, Transactions of Nonferrous Metals Society of China. 28 (2018) 2545–2552. https://doi.org/10.1016/S1003-6326(18)64901-5.

[135] D. Bingöl, M. Canbazoğlu, S. Aydoğan, Dissolution kinetics of malachite in ammonia/ammonium carbonate leaching, Hydrometallurgy. 76 (2005) 55–62. https://doi.org/10.1016/j.hydromet.2004.09.006.

[136] R. Francis, S. Clarke, Corrosion in Caustic Soda in Mineral Processing Operations, Corrosion. 76 (2020) 707–715. https://doi.org/10.5006/3520.

[137] J. Frenay, Leaching of oxidized zinc ores in various media, Hydrometallurgy. 15 (1985) 243–253. https://doi.org/10.1016/0304-386X(85)90057-X.

[138] C.A. Johnson, The fate of cyanide in leach wastes at gold mines: An environmental perspective, Applied Geochemistry. 57 (2015) 194–205. https://doi.org/10.1016/j.apgeochem.2014.05.023.

[139] G. Hilson, A.J. Monhemius, Alternatives to cyanide in the gold mining industry: what prospects for the future, J Clean Prod. 14 (2006) 1158–1167. https://doi.org/10.1016/j.jclepro.2004.09.005.

[140] D.M. Muir, M.G. Aylmore, Thiosulphate as an alternative to cyanide for gold processing – issues and impediments, Mineral Processing and Extractive Metallurgy. 113 (2004) 2–12. https://doi.org/10.1179/037195504225004661.

[141] D. Feng, J.S.J. van Deventer, Thiosulphate leaching of gold in the presence of ethylenediaminetetraacetic acid (EDTA), Miner Eng. 23 (2010) 143–150. https://doi.org/10.1016/j.mineng.2009.11.009.

[142] D. Feng, J.S.J. Van Deventer, Leaching behaviour of sulphides in ammoniacal thiosulphate systems, Hydrometallurgy. 63 (2002) 189–200. https://doi.org/10.1016/S0304-386X(01)00225-0.

[143] I.R. Boboev, S.K. Kurbonov, R.S. Sel'nitsyn, Use of Thiourea Leaching During Gold-Containing Dump Treatment, Metallurgist. 63 (2019) 633–641. https://doi.org/10.1007/s11015-019-00869-w.

[144] S. Syed, Recovery of gold from secondary sources—A review, Hydrometallurgy. 115–116 (2012) 30–51. https://doi.org/10.1016/j.hydromet.2011.12.012.

[145] J.A. Whitehead, J. Zhang, A. McCluskey, G.A. Lawrance, Comparative leaching of a sulfidic gold ore in ionic liquid and aqueous acid with thiourea and halides using Fe(III) or $HSO5^-$ oxidant, Hydrometallurgy. 98 (2009) 276–280. https://doi.org/10.1016/j.hydromet.2009.05.012.

[146] M. Sahin, A. Akcil, C. Erust, S. Altynbek, C.S. Gahan, A. Tuncuk, A Potential Alternative for Precious Metal Recovery from E-waste: Iodine Leaching, Sep Sci Technol. (2015) 150629132750004. https://doi.org/10.1080/01496395.2015.1061005.

[147] A.M. Wilson, P.J. Bailey, P.A. Tasker, J.R. Turkington, R.A. Grant, J.B. Love, Solvent extraction: the coordination chemistry behind extractive metallurgy, Chem. Soc. Rev. 43 (2014) 123–134. https://doi.org/10.1039/C3CS60275C.

[148] A.S. Guimarães, M.B. Mansur, Solvent extraction of calcium and magnesium from concentrate nickel sulfate solutions using D2HEPA and Cyanex 272 extractants, Hydrometallurgy. 173 (2017) 91–97. https://doi.org/10.1016/j.hydromet.2017.08.005.

[149] G. Granata, F. Pagnanelli, E. Moscardini, Z. Takacova, T. Havlik, L. Toro, Simultaneous recycling of nickel metal hydride, lithium ion and primary lithium batteries: Accomplishment of European Guidelines by optimizing mechanical pre-

treatment and solvent extraction operations, J Power Sources. 212 (2012) 205–211. https://doi.org/10.1016/j.jpowsour.2012.04.016.

[150] B. Swain, S.-S. Cho, G.H. Lee, C.G. Lee, S. Uhm, Extraction/Separation of Cobalt by Solvent Extraction: A Review, Applied Chemistry for Engineering. 26 (2015) 631–639. https://doi.org/10.14478/ace.2015.1120.

[151] V. Sridhar, J.K. Verma, S.A. Kumar, Selective separation of copper and nickel by solvent extraction using LIX 984N, Hydrometallurgy. 99 (2009) 124–126. https://doi.org/10.1016/j.hydromet.2009.07.007.

[152] A. Mellah, D. Benachour, The solvent extraction of zinc and cadmium from phosphoric acid solution by di-2-ethyl hexyl phosphoric acid in kerosene diluent, Chemical Engineering and Processing: Process Intensification. 45 (2006) 684–690. https://doi.org/10.1016/j.cep.2006.02.004.

[153] M.F. Bari, M.N. Begum, S.B. Jamaludin, K. Hussin, Solvent extraction separation and recovery of copper, nickel and zinc from printed circuit board by Cyanex 272, Mineral Processing and Extractive Metallurgy. 118 (2009) 227–234. https://doi.org/10.1179/174328509X455331.

[154] T. Wang, Y. Nagaosa, Solvent extraction of some metal ions with di-2-methylnonylphosphoric acid into heptane, Journal of Chemical Technology & Biotechnology. 77 (2002) 1316–1322. https://doi.org/10.1002/jctb.714.

[155] E. Quijada-Maldonado, F. Olea, R. Sepúlveda, J. Castillo, R. Cabezas, G. Merlet, J. Romero, Possibilities and challenges for ionic liquids in hydrometallurgy, Sep Purif Technol. 251 (2020) 117289. https://doi.org/10.1016/j.seppur.2020.117289.

[156] F. Habashi, A short history of hydrometallurgy, Hydrometallurgy. 79 (2005) 15–22. https://doi.org/10.1016/j.hydromet.2004.01.008.

[157] W.-S. Chen, H.-J. Ho, Recovery of Valuable Metals from Lithium-Ion Batteries NMC Cathode Waste Materials by Hydrometallurgical Methods, Metals (Basel). 8 (2018) 321. https://doi.org/10.3390/met8050321.

[158] S. Agatzini-Leonardou, P.E. Tsakiridis, P. Oustadakis, T. Karidakis, A. Katsiapi, Hydrometallurgical process for the separation and recovery of nickel from sulphate heap leach liquor of nickeliferrous laterite ores, Miner Eng. 22 (2009) 1181–1192. https://doi.org/10.1016/j.mineng.2009.06.006.

[159] P.E. Tsakiridis, P. Oustadakis, A. Katsiapi, S. Agatzini-Leonardou, Hydrometallurgical process for zinc recovery from electric arc furnace dust (EAFD). Part II: Downstream processing and zinc recovery by electrowinning, J Hazard Mater. 179 (2010) 8–14. https://doi.org/10.1016/j.jhazmat.2010.04.004.

[160] W.-S. Chen, Y.-C. Chen, C.-H. Lee, Hydrometallurgical Recovery of Iron, Nickel, and Chromium from Stainless Steel Sludge with Emphasis on Solvent Extraction and Chemical Precipitation, Processes. 10 (2022) 748. https://doi.org/10.3390/pr10040748.

[161] P. Laokhen, N. Ma-Ud, T. Yingnakorn, T. Patcharawit, S. Khumkoa, Recovery of nickel from spent electroplating solution by hydrometallurgical and electrometallurgical process, Journal of Metals, Materials and Minerals. 32 (2022) 95–100. https://doi.org/10.55713/jmmm.v32i2.1253.

[162] M. Takano, S. Asano, M. Goto, Recovery of nickel, cobalt and rare-earth elements from spent nickel–metal-hydride battery: Laboratory tests and pilot trials, Hydrometallurgy. 209 (2022) 105826. https://doi.org/10.1016/j.hydromet.2022.105826.

[163] P. Meshram, B.D. Pandey, T.R. Mankhand, Hydrometallurgical processing of spent lithium ion batteries (LIBs) in the presence of a reducing agent with emphasis on kinetics of leaching, Chemical Engineering Journal. 281 (2015) 418–427. https://doi.org/10.1016/j.cej.2015.06.071.

[164] A. Dib, L. Makhloufi, Mass transfer correlation of simultaneous removal by cementation of nickel and cobalt from sulphate industrial solution containing copper, Chemical Engineering Journal. 123 (2006) 53–58. https://doi.org/10.1016/j.cej.2006.06.020.

[165] H.H. Abdel Rahman, E.M. Abdel Wahed, Removal of nickel ions by cementation on zinc from NiSO4 solution in presence of accelerator non-toxic organic compounds, Hydrometallurgy. 129–130 (2012) 111–117. https://doi.org/10.1016/j.hydromet.2012.08.007.

[166] I.B. Illés, T. Kékesi, Efficient deposition of indium by cementation from chloride solutions, Hydrometallurgy. 208 (2022) 105806. https://doi.org/10.1016/j.hydromet.2021.105806.

[167] L. Makhloufi, B. Saidani, C. Cachet, R. Wiart, Cementation of Ni2+ ions from acidic sulfate solutions onto a rotating zinc disc, Electrochim Acta. 43 (1998) 3159–3164. https://doi.org/10.1016/S0013-4686(98)00006-1.

[168] A. Nelson, G.P. Demopoulos, G. Houlachi, The Effect of Solution Constituents and Novel Activators on Cobalt Cementation, Canadian Metallurgical Quarterly. 39 (2000) 175–186. https://doi.org/10.1179/cmq.2000.39.2.175.

[169] S. Choi, S. Jeon, I. Park, C.B. Tabelin, M. Ito, N. Hiroyoshi, Enhanced cementation of Cd2+, Co2+, Ni2+, and Zn2+ on Al from sulfate solutions by activated carbon addition, Hydrometallurgy. 201 (2021) 105580. https://doi.org/10.1016/j.hydromet.2021.105580.

[170] V. Gold, ed., The IUPAC Compendium of Chemical Terminology, in: International Union of Pure and Applied Chemistry (IUPAC), Research Triangle Park, NC, 2019. https://doi.org/10.1351/goldbook.

[171] N.D. Lang, A.R. Williams, Chemical Trends in Atomic Adsorption on Simple Metals, Phys Rev Lett. 37 (1976) 212–215. https://doi.org/10.1103/PhysRevLett.37.212.

[172] G.G. Kleiman, U. Landman, Theory of Physisorption: He on Metals, Phys Rev B. 8 (1973) 5484–5495. https://doi.org/10.1103/PhysRevB.8.5484.

[173] G.Z. Kyzas, E.A. Deliyanni, K.A. Matis, Activated carbons produced by pyrolysis of waste potato peels: Cobalt ions removal by adsorption, Colloids Surf A Physicochem Eng Asp. 490 (2016) 74–83. https://doi.org/10.1016/j.colsurfa.2015.11.038.

[174] M. Teker, Ö. Saltabaş, M. İmamoğlu, Adsorption of cobalt by activated carbon from the rice hulls, Journal of Environmental Science and Health. Part A: Environmental Science and Engineering and Toxicology. 32 (1997) 2077–2086. https://doi.org/10.1080/10934529709376668.

[175] K. Kadirvelu, Adsorption of nickel(II) from aqueous solution onto activated carbon prepared from coirpith, Sep Purif Technol. 24 (2001) 497–505. https://doi.org/10.1016/S1383-5866(01)00149-6.

[176] A. Gafoor, Dhanasekar, S. Kumar, Sankaran, Sivaranjani, S. Begum, Z. Rahman, Elimination of nickel (II) ions using various natural/modified clay minerals: A review, Mater Today Proc. 37 (2021) 2033–2040. https://doi.org/10.1016/j.matpr.2020.07.500.

[177] S.A. Al-Jlil, Adsorption of cobalt ions from waste water on activated Saudi clays, Appl Water Sci. 7 (2017) 383–391. https://doi.org/10.1007/s13201-014-0253-z.

[178] A. Rodríguez, P. Sáez, E. Díez, J.M. Gómez, J. García, I. Bernabé, Highly efficient low-cost zeolite for cobalt removal from aqueous solutions: Characterization and performance, Environ Prog Sustain Energy. 38 (2019) S352–S365. https://doi.org/10.1002/ep.13057.

[179] O.I. Pomazkina, E.G. Filatova, Yu.N. Pozhidaev, Adsorption of nickel(II) cations by natural zeolites, Protection of Metals and Physical Chemistry of Surfaces. 50 (2014) 312–316. https://doi.org/10.1134/S2070205114030113.

[180] H. Parab, S. Joshi, M. Sudersanan, N. Shenoy, A. Lali, U. Sarma, Removal and recovery of cobalt from aqueous solutions by adsorption using low cost lignocellulosic biomass—coir pith, Journal of Environmental Science and Health, Part A. 45 (2010) 603–611. https://doi.org/10.1080/10934521003595662.

[181] S. Kalyani, P. Srinivasa Rao, A. Krishnaiah, Removal of nickel (II) from aqueous solutions using marine macroalgae as the sorbing biomass, Chemosphere. 57 (2004) 1225–1229. https://doi.org/10.1016/j.chemosphere.2004.08.057.

[182] U.K. Garg, M.P. Kaur, V.K. Garg, D. Sud, Removal of Nickel(II) from aqueous solution by adsorption on agricultural waste biomass using a response surface methodological approach, Bioresour Technol. 99 (2008) 1325–1331. https://doi.org/10.1016/j.biortech.2007.02.011.

[183] T.A. Aragaw, F.M. Bogale, Biomass-Based Adsorbents for Removal of Dyes From Wastewater: A Review, Front Environ Sci. 9 (2021). https://doi.org/10.3389/fenvs.2021.764958.

[184] F. Younas, A. Mustafa, Z.U.R. Farooqi, X. Wang, S. Younas, W. Mohy-Ud-Din, M. Ashir Hameed, M. Mohsin Abrar, A.A. Maitlo, S. Noreen, M.M. Hussain, Current and Emerging Adsorbent Technologies for Wastewater Treatment: Trends, Limitations, and Environmental Implications, Water (Basel). 13 (2021) 215. https://doi.org/10.3390/w13020215.

[185] B. Wang, J. Lan, C. Bo, B. Gong, J. Ou, Adsorption of heavy metal onto biomass-derived activated carbon: review, RSC Adv. 13 (2023) 4275–4302. https://doi.org/10.1039/D2RA07911A.

[186] M. Delkash, B. Ebrazi Bakhshayesh, H. Kazemian, Using zeolitic adsorbents to cleanup special wastewater streams: A review, Microporous and Mesoporous Materials. 214 (2015) 224–241. https://doi.org/10.1016/j.micromeso.2015.04.039.

[187] L.C. Klein, Sol-Gel Processing of Silicates, Annual Review of Materials Science. 15 (1985) 227–248. https://doi.org/10.1146/annurev.ms.15.080185.001303.

[188] A. Safavi, N. Iranpoor, N. Saghir, S. Momeni, Glycerol–silica gel: A new solid sorbent for preconcentration and determination of traces of cobalt(II) ion, Anal Chim Acta. 569 (2006) 139–144. https://doi.org/10.1016/j.aca.2006.03.079.

[189] N. Pourreza, J. Zolgharnein, A.R. Kiasat, T. Dastyar, Silica gel–polyethylene glycol as a new adsorbent for solid phase extraction of cobalt and nickel and determination by flame atomic absorption spectrometry, Talanta. 81 (2010) 773–777. https://doi.org/10.1016/j.talanta.2010.01.010.

[190] H. Faghihian, H. Nourmoradi, M. Shokouhi, Removal of copper (II) and nickel (II) from aqueous media using silica aerogel modified with amino propyl triethoxysilane as an adsorbent: equilibrium, kinetic, and isotherms study, Desalination Water Treat. 52 (2014) 305–313. https://doi.org/10.1080/19443994.2013.785367.

[191] A. Heidari, H. Younesi, Z. Mehraban, Removal of Ni(II), Cd(II), and Pb(II) from a ternary aqueous solution by amino functionalized mesoporous and nano mesoporous silica, Chemical Engineering Journal. 153 (2009) 70–79. https://doi.org/10.1016/j.cej.2009.06.016.

[192] M.H. Salmani, M.H. Ehrampoush, H. Eslami, B. Eftekhar, Synthesis, characterization and application of mesoporous silica in removal of cobalt ions from contaminated water, Groundw Sustain Dev. 11 (2020) 100425. https://doi.org/10.1016/j.gsd.2020.100425.

[193] Y. Wang, F. Lin, B. Shang, B. Peng, Z. Deng, Self-template synthesis of nickel silicate and nickel silicate/nickel composite nanotubes and their applications in wastewater treatment, J Colloid Interface Sci. 522 (2018) 191–199. https://doi.org/10.1016/j.jcis.2018.03.044.

[194] P.N.E. Diagboya, E.D. Dikio, Silica-based mesoporous materials; emerging designer adsorbents for aqueous pollutants removal and water treatment, Microporous and Mesoporous Materials. 266 (2018) 252–267. https://doi.org/10.1016/j.micromeso.2018.03.008.

[195] Z. Wu, D. Zhao, Ordered mesoporous materials as adsorbents, Chemical Communications. 47 (2011) 3332. https://doi.org/10.1039/c0cc04909c.

[196] A. Islam, M.A. Laskar, A. Ahmad, Characterization of a novel chelating resin of enhanced hydrophilicity and its analytical utility for preconcentration of trace metal ions, Talanta. 81 (2010) 1772–1780. https://doi.org/10.1016/j.talanta.2010.03.035.

[197] L. Elçi, M. Soylak, A. Uzun, E. Büyükpatır, M. Doğan, Determination of trace impurities in some nickel compounds by flame atomic absorption spectrometry after solid phase extraction using Amberlite XAD-16 resin, Fresenius J Anal Chem. 368 (2000) 358–361. https://doi.org/10.1007/s002160000448.

[198] A. Ahmad, J.A. Siddique, M.A. Laskar, R. Kumar, S.H. Mohd-Setapar, A. Khatoon, R.A. Shiekh, New generation Amberlite XAD resin for the removal of metal ions: A review, Journal of Environmental Sciences. 31 (2015) 104–123. https://doi.org/10.1016/j.jes.2014.12.008.

[199] M. Torre, M.L. Marina, The State of the Art of Ligand-Loaded Complexing Resins. Characteristics and Applications, Crit Rev Anal Chem. 24 (1994) 327–361. https://doi.org/10.1080/10408349408048823.

[200] Md.I. ul Hoque, D.A. Chowdhury, R. Holze, A.-N. Chowdhury, Md.S. Azam, Modification of Amberlite XAD-4 resin with 1,8-diaminonaphthalene for solid phase extraction of copper, cadmium and lead, and its application to determination

of these metals in dairy cow's milk, J Environ Chem Eng. 3 (2015) 831–842. https://doi.org/10.1016/j.jece.2015.03.020.

[201] R.K. Sharma, P. Pant, Preconcentration and determination of trace metal ions from aqueous samples by newly developed gallic acid modified Amberlite XAD-16 chelating resin, J Hazard Mater. 163 (2009) 295–301. https://doi.org/10.1016/j.jhazmat.2008.06.120.

[202] B. Jally, M. François, M. Kessler, B. Laubie, M.-O. Simonnot, Recovery of nickel from strongly acidic bio-ore leachate using a bispicolylamine-based chelating resin, Sep Purif Technol. 293 (2022) 121126. https://doi.org/10.1016/j.seppur.2022.121126.

[203] B. Li, F. Liu, J. Wang, C. Ling, L. Li, P. Hou, A. Li, Z. Bai, Efficient separation and high selectivity for nickel from cobalt-solution by a novel chelating resin: Batch, column and competition investigation, Chemical Engineering Journal. 195–196 (2012) 31–39. https://doi.org/10.1016/j.cej.2012.04.089.

[204] X. Zhao, L. Song, Z. Zhang, R. Wang, J. Fu, Adsorption investigation of MA-DTPA chelating resin for Ni(II) and Cu(II) using experimental and DFT methods, J Mol Struct. 986 (2011) 68–74. https://doi.org/10.1016/j.molstruc.2010.11.049.

[205] R. Shah, Chelating resin containing s-bonded dithizone for the separation of copper(II), nickel(II) and zinc(II), Talanta. 45 (1998) 1089–1096. https://doi.org/10.1016/S0039-9140(97)00215-4.

[206] G. Ndayambaje, K. Laatikainen, M. Laatikainen, E. Beukes, O. Fatoba, N. van der Walt, L. Petrik, T. Sainio, Adsorption of nickel(II) on polyacrylonitrile nanofiber modified with 2-(2′-pyridyl)imidazole, Chemical Engineering Journal. 284 (2016) 1106–1116. https://doi.org/10.1016/j.cej.2015.09.065.

[207] Y. Chen, W. Zhao, X. Yang, Y. Li, Efficient removal of heavy metal ions from aqueous solution by a novel poly (1-vinylimidazole) chelate resin, Polymer Bulletin. 76 (2019) 1081–1097. https://doi.org/10.1007/s00289-018-2426-7.

[208] M. Kumar, Amberlite XAD-2 functionalized with o-aminophenol: synthesis and applications as extractant for copper(II), cobalt(II), cadmium(II), nickel(II), zinc(II) and lead(II), Talanta. 51 (2000) 1187–1196. https://doi.org/10.1016/S0039-9140(00)00295-2.

[209] W.S. Chai, J.Y. Cheun, P.S. Kumar, M. Mubashir, Z. Majeed, F. Banat, S.-H. Ho, P.L. Show, A review on conventional and novel materials towards heavy metal adsorption in wastewater treatment application, J Clean Prod. 296 (2021) 126589. https://doi.org/10.1016/j.jclepro.2021.126589.

[210] S. Tamjidi, H. Esmaeili, B. Kamyab Moghadas, Application of magnetic adsorbents for removal of heavy metals from wastewater: a review study, Mater Res Express. 6 (2019) 102004. https://doi.org/10.1088/2053-1591/ab3ffb.

[211] R. Chakraborty, A. Asthana, A.K. Singh, B. Jain, A.B.H. Susan, Adsorption of heavy metal ions by various low-cost adsorbents: a review, Int J Environ Anal Chem. 102 (2022) 342–379. https://doi.org/10.1080/03067319.2020.1722811.

[212] M. Schönbächler, M.A. Fehr, Basics of Ion Exchange Chromatography for Selected Geological Applications, in: Treatise on Geochemistry, Elsevier, 2014: pp. 123–146. https://doi.org/10.1016/B978-0-08-095975-7.01408-X.

[213] T. Jumadilov, K. Khimersen, Z. Malimbayeva, R. Kondaurov, Effective Sorption of Europium Ions by Interpolymer System Based on Industrial Ion-Exchanger Resins Amberlite IR120 and AB-17-8, Materials. 14 (2021) 3837. https://doi.org/10.3390/ma14143837.

[214] A.B. Botelho Junior, D.C.R. Espinosa, D. Dreisinger, J.A.S. Tenório, Recovery of nickel and cobalt from nickel laterite leach solution using chelating resins and pre-reducing process, Can J Chem Eng. 97 (2019) 1181–1190. https://doi.org/10.1002/cjce.23359.

[215] S. Virolainen, I. Suppula, T. Sainio, Controlled partial neutralization of amphoteric ion exchange resin for improved metals separation, React Funct Polym. 73 (2013) 647–652. https://doi.org/10.1016/j.reactfunctpolym.2013.01.013.

[216] Y. Jurrius, K.C. Sole, E. Hardwick, Removal of copper and zinc from a cobalt electrolyte by ion exchange at Kamoto copper company's Luilu plant, in: Hydrometallurgy, Canadian Institute of Mining, Metallurgy and Petroleum, 2014: pp. 281–293.

[217] J.J. Taute, K.C. Sole, E. Hardwick, Removal of zinc from a base-metal solution using ion exchange at Rustenburg Base Metal Refiners, Journal of Chemical Technology & Biotechnology. 89 (2014) 919–926. https://doi.org/10.1002/jctb.4332.

[218] R. Shrestha, S. Ban, S. Devkota, S. Sharma, R. Joshi, A.P. Tiwari, H.Y. Kim, M.K. Joshi, Technological trends in heavy metals removal from industrial wastewater: A review, J Environ Chem Eng. 9 (2021) 105688. https://doi.org/10.1016/j.jece.2021.105688.

[219] D.W. O'Connell, C. Birkinshaw, T.F. O'Dwyer, Heavy metal adsorbents prepared from the modification of cellulose: A review, Bioresour Technol. 99 (2008) 6709–6724. https://doi.org/10.1016/j.biortech.2008.01.036.

[220] H. Vasylyeva, I. Mironyuk, M. Strilchuk, I. Maliuk, K. Savka, O. Vasyliev, Adsorption and possibility of separation of heavy metal cations by strong cation exchange resin, Chemical Physics Impact. 3 (2021) 100056. https://doi.org/10.1016/j.chphi.2021.100056.

[221] A. Baysal, N. Ozbek, S. Akm, Determination of Trace Metals in Waste Water and Their Removal Processes, in: Waste Water - Treatment Technologies and Recent Analytical Developments, InTech, 2013. https://doi.org/10.5772/52025.

[222] C.Y. Cheng, Purification of synthetic laterite leach solution by solvent extraction using D2EHPA, Hydrometallurgy. 56 (2000) 369–386. https://doi.org/10.1016/S0304-386X(00)00095-5.

[223] J.S. Preston, Recent developments in the separation of nickel and cobalt from sulphate solutions by solvent extraction, J South Afr Inst Min Metall. 83 (1983) 126–132. https://hdl.handle.net/10520/AJA0038223X_1387 (accessed October 18, 2023).

[224] P.R. Danesi, L. Reichley-Yinger, G. Mason, L. Kaplan, E.P. Horwltz, H. Diamond, Selectivity-structure trends in the extraction of Co(II) and Ni(II) by dialkyl phosphoric, alkyl alkylphosphonic, and dialkylphosphinic acids, Solvent Extraction and Ion Exchange. 3 (1985) 435–452. https://doi.org/10.1080/07366298508918522.

[225] K.-H. Park, D. Mohapatra, Process for cobalt separation and recovery in the presence of nickel from sulphate solutions by Cyanex 272, Metals and Materials International. 12 (2006) 441–446. https://doi.org/10.1007/BF03027712.

[226] J. Kang, G. Senanayake, J. Sohn, S.M. Shin, Recovery of cobalt sulfate from spent lithium ion batteries by reductive leaching and solvent extraction with Cyanex 272, Hydrometallurgy. 100 (2010) 168–171. https://doi.org/10.1016/j.hydromet.2009.10.010.

[227] M.Z. Mubarok, L.I. Hanif, Cobalt and Nickel Separation in Nitric Acid Solution by Solvent Extraction Using Cyanex 272 and Versatic 10, Procedia Chem. 19 (2016) 743–750. https://doi.org/10.1016/j.proche.2016.03.079.

[228] P.E. Tsakiridis, S.L. Agatzini, Process for the recovery of cobalt and nickel in the presence of magnesium and calcium from sulphate solutions by Versatic 10 and Cyanex 272, Miner Eng. 17 (2004) 535–543. https://doi.org/10.1016/j.mineng.2003.12.003.

[229] L.E.O.C. Rodrigues, M.B. Mansur, Hydrometallurgical separation of rare earth elements, cobalt and nickel from spent nickel–metal–hydride batteries, J Power Sources. 195 (2010) 3735–3741. https://doi.org/10.1016/j.jpowsour.2009.12.071.

[230] D.P. Mantuano, G. Dorella, R.C.A. Elias, M.B. Mansur, Analysis of a hydrometallurgical route to recover base metals from spent rechargeable batteries by liquid–liquid extraction with Cyanex 272, J Power Sources. 159 (2006) 1510–1518. https://doi.org/10.1016/j.jpowsour.2005.12.056.

[231] S.A. Olushola, A.A. Folahan, A.B. Alafara, J.X. Bhekumusa, S.F. Olalekan, Application of Cyanex extractant in Cobalt/Nickel separation process by solvent extraction, International Journal of Physical Sciences. 8 (2013) 89–97. https://doi.org/10.5897/IJPS12.135.

[232] K.C. Sole, The Evolution of Cobalt–Nickel Separation and Purification Technologies: Fifty Years of Solvent Extraction and Ion Exchange, in: 2018: pp. 1167–1191. https://doi.org/10.1007/978-3-319-95022-8_95.

[233] P. Oustadakis, S. Agatzini-Leonardou, P.E. Tsakiridis, Nickel and cobalt precipitation from sulphate leach liquor using MgO pulp as neutralizing agent, Miner Eng. 19 (2006) 1204–1211. https://doi.org/10.1016/j.mineng.2005.11.006.

[234] Y. Xie, Y. Xu, L. Yan, R. Yang, Recovery of nickel, copper and cobalt from low-grade Ni–Cu sulfide tailings, Hydrometallurgy. 80 (2005) 54–58. https://doi.org/10.1016/j.hydromet.2005.07.005.

[235] K.C. Sole, M.B. Mooiman, E. Hardwick, Ion Exchange in Hydrometallurgical Processing: An Overview and Selected Applications, Separation & Purification Reviews. 47 (2018) 159–178. https://doi.org/10.1080/15422119.2017.1354304.

[236] M. Seggiani, S. Vitolo, S. D'Antone, Recovery of nickel from Orimulsion fly ash by iminodiacetic acid chelating resin, Hydrometallurgy. 81 (2006) 9–14. https://doi.org/10.1016/j.hydromet.2005.09.005.

[237] A.A. Atia, A.M. Donia, A.M. Yousif, Synthesis of amine and thio chelating resins and study of their interaction with zinc(II), cadmium(II) and mercury(II) ions in their aqueous solutions, React Funct Polym. 56 (2003) 75–82. https://doi.org/10.1016/S1381-5148(03)00046-4.

[238] J.T.M. Amphlett, S. Choi, S.A. Parry, E.M. Moon, C.A. Sharrad, M.D. Ogden, Insights on uranium uptake mechanisms by ion exchange resins with chelating functionalities: Chelation vs. anion exchange, Chemical Engineering Journal. 392 (2020) 123712. https://doi.org/10.1016/j.cej.2019.123712.

[239] H. Nishide, J. Deguchi, E. Tsuchida, Selective adsorption of metal ions on crosslinked poly(vinylpyridine) resin prepared with a metal ion as a template, Chem Lett. 5 (1976) 169–174. https://doi.org/10.1246/cl.1976.169.

[240] M.M. Yusoff, N.R.N. Mostapa, M.S. Sarkar, T.K. Biswas, M.L. Rahman, S.E. Arshad, M.S. Sarjadi, A.D. Kulkarni, Synthesis of ion imprinted polymers for

selective recognition and separation of rare earth metals, Journal of Rare Earths. 35 (2017) 177–186. https://doi.org/10.1016/S1002-0721(17)60897-4.

[241] V.V. Kusumkar, M. Galamboš, E. Viglašov, M. Da, Ion-Imprinted Polymers: Synthesis, Characterization, and Adsorption of Radionuclides, Materials. 14 (2021) 1083.

[242] Y. El Ouardi, A. Giove, M. Laatikainen, C. Branger, K. Laatikainen, Benefit of ion imprinting technique in solid-phase extraction of heavy metals, special focus on the last decade, J Environ Chem Eng. 9 (2021) 106548. https://doi.org/https://doi.org/10.1016/j.jece.2021.106548.

[243] T. Prasada Rao, S. Daniel, J. Mary Gladis, Tailored materials for preconcentration or separation of metals by ion-imprinted polymers for solid-phase extraction (IIP-SPE), TrAC Trends in Analytical Chemistry. 23 (2004) 28–35. https://doi.org/10.1016/S0165-9936(04)00106-2.

[244] G. Zhu, H. Tang, H. Zhang, L. Pei, P. Zhou, Y. Shi, Z. Cai, H. Xu, Y. Zhang, A novel ion-imprinted polymer for selective removal of trace Fe(III) from Cr(III)-containing solutions, Hydrometallurgy. 186 (2019) 105–114. https://doi.org/10.1016/j.hydromet.2019.04.002.

[245] D.K. Singh, S. Mishra, Synthesis and characterization of Hg(II)-ion-imprinted polymer: Kinetic and isotherm studies, Desalination. 257 (2010) 177–183. https://doi.org/10.1016/j.desal.2010.02.026.

[246] GZ. Kyzas, DN. Bikiaris, Characterization of binding properties of silver ion-imprinted polymers with equilibrium and kinetic models, J Mol Liq. 212 (2015) 133–141. https://doi.org/10.1016/j.molliq.2015.09.018.

[247] R. Kang, L. Qiu, L. Fang, R. Yu, Y. Chen, X. Lu, X. Luo, A novel magnetic and hydrophilic ion-imprinted polymer as a selective sorbent for the removal of cobalt ions from industrial wastewater, J Environ Chem Eng. 4 (2016) 2268–2277. https://doi.org/10.1016/j.jece.2016.04.010.

[248] J.E. Francisco, F.N. Feiteira, W.A. da Silva, W.F. Pacheco, Synthesis and application of ion-imprinted polymer for the determination of mercury II in water samples, Environmental Science and Pollution Research. 26 (2019) 19588–19597. https://doi.org/10.1007/s11356-019-05178-y.

[249] T.O. Germiniano, M.Z. Corazza, M.G. Segatelli, E.S. Ribeiro, M.J.S. Yabe, E. Galunin, C.R.T. Tarley, Synthesis of novel copper ion-selective material based on hierarchically imprinted cross-linked poly(acrylamide-co-ethylene glycol dimethacrylate), React Funct Polym. 82 (2014) 72–80. https://doi.org/10.1016/j.reactfunctpolym.2014.05.012.

[250] V.M. Biju, J.M. Gladis, T.P. Rao, Ion imprinted polymer particles: synthesis, characterization and dysprosium ion uptake properties suitable for analytical applications, Anal Chim Acta. 478 (2003) 43–51. https://doi.org/https://doi.org/10.1016/S0003-2670(02)01416-2.

[251] N. Ashouri, A. Mohammadi, R. Hajiaghaee, M. Shekarchi, M.R. Khoshayand, Preparation of a new nanoparticle Cd(II)-imprinted polymer and its application for selective separation of cadmium(II) ions from aqueous solutions and determination via inductively coupled plasma optical emission spectrometry, Desalination Water Treat. 57 (2016) 14280–14289. https://doi.org/10.1080/19443994.2015.1072742.

[252] O.B. Nchoe, M.J. Klink, F.M. Mtunzi, V.E. Pakade, Synthesis, characterization, and application of β-cyclodextrin-based ion-imprinted polymer for selective sequestration of Cr(VI) ions from aqueous media: Kinetics and isotherm studies, J Mol Liq. 298 (2020) 111991. https://doi.org/10.1016/j.molliq.2019.111991.

[253] M. Roushani, S. Abbasi, H. Khani, Synthesis and application of ion-imprinted polymer nanoparticles for the extraction and preconcentration of mercury in water and food samples employing cold vapor atomic absorption spectrometry, Environ Monit Assess. 187 (2015). https://doi.org/10.1007/s10661-015-4820-z.

[254] Z. Zhou, D. Kong, H. Zhu, N. Wang, Z. Wang, Q. Wang, W. Liu, Q. Li, W. Zhang, Z. Ren, Preparation and adsorption characteristics of an ion-imprinted polymer for fast removal of Ni(II) ions from aqueous solution, J Hazard Mater. 341 (2018) 355–364. https://doi.org/10.1016/j.jhazmat.2017.06.010.

[255] M. Moussa, V. Pichon, C. Mariet, T. Vercouter, N. Delaunay, Potential of ion imprinted polymers synthesized by trapping approach for selective solid phase extraction of lanthanides, Talanta. 161 (2016) 459–468. https://doi.org/10.1016/j.talanta.2016.08.069.

[256] P. Metilda, K. Prasad, R. Kala, J.M. Gladis, T.P. Rao, G.R.K. Naidu, Ion imprinted polymer based sensor for monitoring toxic uranium in environmental samples, Anal Chim Acta. 582 (2007) 147–153. https://doi.org/10.1016/j.aca.2006.08.052.

[257] M.P. Rodríguez-Reino, R. Rodríguez-Fernández, E. Peña-Vázquez, R. Domínguez-González, P. Bermejo-Barrera, A. Moreda-Piñeiro, Mercury speciation in seawater by liquid chromatography-inductively coupled plasma-mass spectrometry following solid phase extraction pre-concentration by using an ionic imprinted polymer based on methyl-mercury–phenobarbital interaction, J Chromatogr A. 1391 (2015) 9–17. https://doi.org/10.1016/j.chroma.2015.02.068.

[258] F. Luo, S. Huang, X. Xiong, X. Lai, Synthesis and characterization of Hg(ii)-ion-imprinted polymer and its application for the determination of mercury in water samples, RSC Adv. 5 (2015) 67365–67371. https://doi.org/10.1039/c5ra10861f.

[259] S. Daniel, J.M. Gladis, T.P. Rao, Synthesis of imprinted polymer material with palladium ion nanopores and its analytical application, Anal Chim Acta. 488 (2003) 173–182. https://doi.org/10.1016/S0003-2670(03)00661-5.

[260] S.S. Lins, C.F. Virgens, W.N.L. dos Santos, I.H.S. Estevam, G.C. Brandão, C.S.A. Felix, S.L.C. Ferreira, On-line solid phase extraction system using an ion imprinted polymer based on dithizone chelating for selective preconcentration and determination of mercury(II) in natural waters by CV AFS, Microchemical Journal. 150 (2019) 104075. https://doi.org/10.1016/j.microc.2019.104075.

[261] S. Zarco-Fernández, M.J. Mancheño, R. Muñoz-Olivas, C. Cámara, A new specific polymeric material for mercury speciation: Application to environmental and food samples, Anal Chim Acta. 897 (2015) 109–115. https://doi.org/10.1016/j.aca.2015.09.016.

[262] W. Meouche, C. Branger, I. Beurroies, R. Denoyel, A. Margaillan, Inverse Suspension Polymerization as a New Tool for the Synthesis of Ion-Imprinted Polymers, Macromol Rapid Commun. 33 (2012) 928–932. https://doi.org/10.1002/marc.201200039.

[263] H.-G. Wu, X.-J. Ju, R. Xie, Y.-M. Liu, J.-G. Deng, C.H. Niu, L.-Y. Chu, A novel ion-imprinted hydrogel for recognition of potassium ions with rapid response, Polym Adv Technol. 22 (2011) 1389–1394. https://doi.org/10.1002/pat.1843.

[264] X. Luo, L. Liu, F. Deng, S. Luo, Novel ion-imprinted polymer using crown ether as a functional monomer for selective removal of Pb(II) ions in real environmental water samples, J Mater Chem A Mater. 1 (2013) 8280. https://doi.org/10.1039/c3ta11098b.

[265] Y. Huang, X. Li, L. Chen, G. Luo, D. Tao, J. Sun, Z. Qiu, Y. Chao, W. Zhu, Synthesis of a magnetic crown ether ion imprinted polymer material for the selective adsorption of lithium, New Journal of Chemistry. 47 (2023) 3134–3139. https://doi.org/10.1039/D2NJ05377B.

[266] H. Faghihian, F.G. Adivi, Separation and pre-concentration of Cu(II) ions by a synthesized ion-imprinted polymer, Adsorption Science and Technology. 30 (2012) 205–215. https://doi.org/10.1260/0263-6174.30.3.205.

[267] M. Jalilzadeh, S. Şenel, Removal of Cu(II) ions from water by ion-imprinted magnetic and non-magnetic cryogels: A comparison of their selective Cu(II) removal performances, Journal of Water Process Engineering. 13 (2016) 143–152. https://doi.org/10.1016/j.jwpe.2016.08.010.

[268] E. Tamahkar, M. Bakhshpour, M. Andaç, A. Denizli, Ion imprinted cryogels for selective removal of Ni(II) ions from aqueous solutions, Sep Purif Technol. 179 (2017) 36–44. https://doi.org/10.1016/j.seppur.2016.12.048.

[269] O. Okay, Macroporous copolymer networks, Prog Polym Sci. 25 (2000) 711–779. https://doi.org/10.1016/S0079-6700(00)00015-0.

[270] H. Faghihian, Z. Adibmehr, Comparative performance of novel magnetic ion-imprinted adsorbents employed for Cd2+, Cu2+ and Ni2+ removal from aqueous solutions, Environmental Science and Pollution Research. 25 (2018) 15068–15079. https://doi.org/10.1007/s11356-018-1732-9.

[271] A. Giove, Y. El Ouardi, A. Sala, F. Ibrahim, S. Hietala, E. Sievänen, C. Branger, K. Laatikainen, Highly selective recovery of Ni(II) in neutral and acidic media using a novel Ni(II)-ion imprinted polymer, J Hazard Mater. 444 (2023) 130453. https://doi.org/https://doi.org/10.1016/j.jhazmat.2022.130453.

[272] F.A. Mustafai, A. Balouch, Abdullah, N. Jalbani, M.I. Bhanger, M.S. Jagirani, A. Kumar, A. Tunio, Microwave-assisted synthesis of imprinted polymer for selective removal of arsenic from drinking water by applying Taguchi statistical method, Eur Polym J. 109 (2018) 133–142. https://doi.org/10.1016/j.eurpolymj.2018.09.041.

[273] M.S. Jagirani, A. Balouch, S.A. Mahesar, A. Kumar, Abdullah, F.A. Mustafai, M.I. Bhanger, Preparation of novel arsenic-imprinted polymer for the selective extraction and enhanced adsorption of toxic As3+ ions from the aqueous environment, Polymer Bulletin. (2019). https://doi.org/10.1007/s00289-019-03008-2.

[274] S. Mishra, A. Tripathi, Selective solid phase extraction and pre-concentration of Cu(II) ions from aqueous solution using Cu(II)-ion imprinted polymeric beads, J Environ Chem Eng. 8 (2020) 103656. https://doi.org/10.1016/j.jece.2020.103656.

[275] M. Hassanzadeh, M. Ghaemy, S.M. Amininasab, Z. Shami, An effective approach for fast selective separation of Cr(VI) from water by ion-imprinted polymer grafted on the electro-spun nanofibrous mat of functionalized polyacrylonitrile, React Funct Polym. 130 (2018) 70–80. https://doi.org/10.1016/j.reactfunctpolym.2018.05.013.

[276] M. Rammika, G. Darko, N. Torto, Optimal synthesis of a Ni(II)-dimethylglyoxime ion-imprinted polymer for the enrichment of Ni(II) ions in water, soil and mine tailing samples, Water SA. 38 (2012). https://doi.org/10.4314/wsa.v38i2.12.

[277] A. Kumar, A. Balouch, Abdullah, A.A. Pathan, Synthesis, adsorption and analytical applicability of Ni-imprinted polymer for selective adsorption of Ni2+ ions from the aqueous environment, Polym Test. 77 (2019) 105871. https://doi.org/10.1016/j.polymertesting.2019.04.018.

[278] B. Godlewska-Yłkiewicz, B. Leśniewska, I. Wawreniuk, Assessment of ion imprinted polymers based on Pd(II) chelate complexes for preconcentration and

FAAS determination of palladium, Talanta. 83 (2010) 596–604. https://doi.org/10.1016/j.talanta.2010.10.005.

[279] T. Zhang, X. Yue, K. Zhang, F. Zhao, Y. Wang, K. Zhang, Synthesis of Cu(II) ion-imprinted polymers as solid phase adsorbents for deep removal of copper from concentrated zinc sulfate solution, Hydrometallurgy. 169 (2017) 599–606. https://doi.org/10.1016/j.hydromet.2017.04.005.

[280] L. Zhu, Z. Zhu, R. Zhang, J. Hong, Y. Qiu, Synthesis and adsorption performance of lead ion-imprinted micro-beads with combination of two functional monomers, Journal of Environmental Sciences. 23 (2011) 1955–1961. https://doi.org/10.1016/S1001-0742(10)60611-0.

[281] S.C. Lopes Pinheiro, A.B. Descalzo, I.M. Raimundo, G. Orellana, M.C. Moreno-Bondi, Fluorescent ion-imprinted polymers for selective Cu(II) optosensing, Anal Bioanal Chem. 402 (2012) 3253–3260. https://doi.org/10.1007/s00216-011-5620-0.

[282] Y. Zhai, D. Yang, X. Chang, Y. Liu, Q. He, Selective enrichment of trace copper(II) from biological and natural water samples by SPE using ion-imprinted polymer, J Sep Sci. 31 (2008) 1195–1200. https://doi.org/10.1002/jssc.200700392.

[283] R. Liang, R. Zhang, W. Song, X. Hu, W. Qin, Potentiometric Sensor Based on an Ion-Imprinted Polymer for Determination of Copper, Sens Lett. 9 (2011) 557–562. https://doi.org/10.1166/sl.2011.1512.

[284] C. Xie, X. Huang, S. Wei, C. Xiao, J. Cao, Z. Wang, Novel dual-template magnetic ion imprinted polymer for separation and analysis of Cd2+ and Pb2+ in soil and food, J Clean Prod. 262 (2020). https://doi.org/10.1016/j.jclepro.2020.121387.

[285] N. Khoddami, F. Shemirani, A new magnetic ion-imprinted polymer as a highly selective sorbent for determination of cobalt in biological and environmental samples, Talanta. 146 (2016) 244–252. https://doi.org/10.1016/j.talanta.2015.08.046.

[286] R. Huang, X. Ma, X. Li, L. Guo, X. Xie, M. Zhang, J. Li, A novel ion-imprinted polymer based on graphene oxide-mesoporous silica nanosheet for fast and efficient removal of chromium (VI) from aqueous solution, J Colloid Interface Sci. 514 (2018) 544–553. https://doi.org/10.1016/j.jcis.2017.12.065.

[287] C.R.T. Tarley, F.N. Andrade, H. De Santana, D.A.M. Zaia, L.A. Beijo, M.G. Segatelli, Ion-imprinted polyvinylimidazole-silica hybrid copolymer for selective extraction of Pb(II): Characterization and metal adsorption kinetic and thermodynamic studies, React Funct Polym. 72 (2012) 83–91. https://doi.org/10.1016/j.reactfunctpolym.2011.10.008.

[288] F. Zhu, L. Li, J. Xing, Selective adsorption behavior of Cd(II) ion imprinted polymers synthesized by microwave-assisted inverse emulsion polymerization: Adsorption performance and mechanism, J Hazard Mater. 321 (2017) 103–110. https://doi.org/10.1016/j.jhazmat.2016.09.012.

[289] H.T. Fan, X. Fan, J. Li, M. Guo, D. Zhang, F. Yan, T. Sun, Selective removal of arsenic(V) from aqueous solution using a surface-ion-imprinted amine-functionalized silica gel sorbent, Ind Eng Chem Res. 51 (2012) 5216–5223. https://doi.org/10.1021/ie202655x.

[290] Z. Fan, J. Shen, R. Li, S. Li, Synthesis and Adsorption Behavior of Surface Cu(II) Ion-Imprinted Poly(allylamine)-Silica Gel Material, Polymer - Plastics Technology and Engineering. 51 (2012) 1289–1295. https://doi.org/10.1080/03602559.2012.700543.

[291] W. Liu, M. Zhang, X. Liu, H. Zhang, J. Jiao, H. Zhu, Z. Zhou, Z. Ren, Preparation of surface ion-imprinted material based on modified chitosan for highly selective recognition and adsorption of nickel ions in aqueous solution, Ind Eng Chem Res. (2020). https://doi.org/10.1021/acs.iecr.9b04755.

[292] W. Meouche, K. Laatikainen, A. Margaillan, T. Silvonen, H. Siren, T. Sainio, I. Beurroies, R. Denoyel, C. Branger, Effect of porogen solvent on the properties of nickel ion imprinted polymer materials prepared by inverse suspension polymerization, Eur Polym J. 87 (2017) 124–135. https://doi.org/10.1016/j.eurpolymj.2016.12.022.

[293] W. Peng, Z. Xie, G. Cheng, L. Shi, Y. Zhang, Amino-functionalized adsorbent prepared by means of Cu(II) imprinted method and its selective removal of copper from aqueous solutions, J Hazard Mater. 294 (2015) 9–16. https://doi.org/10.1016/j.jhazmat.2015.03.046.

[294] B. Özkahraman, Z. Özbaş, A. Bal Öztürk, Synthesis of Ion-Imprinted Alginate Based Beads: Selective Adsorption Behavior of Nickel (II) Ions, J Polym Environ. 26 (2018) 4303–4310. https://doi.org/10.1007/s10924-018-1292-6.

[295] M. Zhang, R. Helleur, Y. Zhang, Ion-imprinted chitosan gel beads for selective adsorption of Ag+ from aqueous solutions, Carbohydr Polym. 130 (2015) 206–212. https://doi.org/10.1016/j.carbpol.2015.05.038.

[296] Z. Adibmehr, H. Faghihian, Novel ion-imprinted adsorbent for lead removal from aqueous solutions, selectivity and adsorption capacity improvement, and evaluation of adsorption isotherms and kinetic, Separation Science and Technology (Philadelphia). 53 (2018) 2388–2400. https://doi.org/10.1080/01496395.2018.1459703.

[297] D. Kong, F. Zhang, K. Wang, Z. Ren, W. Zhang, Fast removal of Cr(VI) from aqueous solution using Cr(VI)-imprinted polymer particles, Ind Eng Chem Res. 53 (2014) 4434–4441. https://doi.org/10.1021/ie403484p.

[298] R. Jalilian, M. Shahmari, A. Taheri, K. Gholami, Ultrasonic-assisted micro solid phase extraction of arsenic on a new ion-imprinted polymer synthesized from chitosan-stabilized pickering emulsion in water, rice and vegetable samples, Ultrason Sonochem. 61 (2020) 104802. https://doi.org/https://doi.org/10.1016/j.ultsonch.2019.104802.

[299] L. Mergola, T. Stomeo, R. Del Sole, Synthesis of photoswitchable submicroparticles and their evaluation as ion-imprinted polymers for Pd(II) uptake, Polym J. (2020). https://doi.org/10.1038/s41428-020-0319-8.

[300] J.X. Duan, X. Li, C.C. Zhang, The synthesis and adsorption performance of polyamine Cu2+ imprinted polymer for selective removal of Cu2+, Polymer Bulletin. 74 (2017) 3487–3504. https://doi.org/10.1007/s00289-017-1905-6.

[301] R. Msaadi, S. Ammar, M.M. Chehimi, Y. Yagci, Diazonium-based ion-imprinted polymer/clay nanocomposite for the selective extraction of lead (II) ions in aqueous media, Eur Polym J. 89 (2017) 367–380. https://doi.org/10.1016/j.eurpolymj.2017.02.029.

[302] X. Luo, H. Yu, Y. Xi, L. Fang, L. Liu, J. Luo, Selective removal Pb(II) ions form wastewater using Pb(II) ion-imprinted polymers with bi-component polymer brushes, RSC Adv. 7 (2017) 25811–25820. https://doi.org/10.1039/c7ra03536e.

[303] J. Gatabi, Y. Sarrafi, M.M. Lakouraj, M. Taghavi, Facile and efficient removal of Pb(II) from aqueous solution by chitosan-lead ion imprinted polymer network, Chemosphere. 240 (2020). https://doi.org/10.1016/j.chemosphere.2019.124772.

[304] Q.O. Dos Santos, M.A. Bezerra, G. De Fátima Lima, K.M. Diniz, M.G. Segatelli, T.O. Germiniano, V. Da Silva Santos, C.R.T. Tarley, Synthesis, characterization and application of ion imprinted poly(vinylimidazole) for zinc ion extraction/preconcentration with faas determination, Quim Nova. 37 (2014) 63–68. https://doi.org/10.1590/S0100-40422014000100012.

[305] P.E. Hande, S. Kamble, A.B. Samui, P.S. Kulkarni, Chitosan-Based Lead Ion-Imprinted Interpenetrating Polymer Network by Simultaneous Polymerization for Selective Extraction of Lead(II), Ind Eng Chem Res. 55 (2016) 3668–3678. https://doi.org/10.1021/acs.iecr.5b04889.

[306] M. Behbahani, F. Omidi, M.G. Kakavandi, G. Hesam, Selective and sensitive determination of silver ions at trace levels based on ultrasonic-assisted dispersive solid-phase extraction using ion-imprinted polymer nanoparticles, Appl Organomet Chem. 31 (2017) 1–9. https://doi.org/10.1002/aoc.3758.

[307] M. Laatikainen, K. Laatikainen, S.-P. Reinikainen, H. Hyvönen, C. Branger, H. Siren, T. Sainio, Complexation of Nickel with 2-(Aminomethyl)pyridine at High Zinc Concentrations or in a Nonaqueous Solvent Mixture, J Chem Eng Data. 59 (2014) 2207–2214. https://doi.org/10.1021/je500164h.

[308] M. Saraji, H. Yousefi, Selective solid-phase extraction of Ni(II) by an ion-imprinted polymer from water samples, J Hazard Mater. 167 (2009) 1152–1157. https://doi.org/10.1016/j.jhazmat.2009.01.111.

[309] M. Shamsipur, A. Besharati-Seidani, J. Fasihi, H. Sharghi, Synthesis and characterization of novel ion-imprinted polymeric nanoparticles for very fast and highly selective recognition of copper(II) ions, Talanta. 83 (2010) 674–681. https://doi.org/10.1016/j.talanta.2010.10.021.

[310] B. Gao, F. An, Y. Zhu, Novel surface ionic imprinting materials prepared via couple grafting of polymer and ionic imprinting on surfaces of silica gel particles, Polymer (Guildf). 48 (2007) 2288–2297. https://doi.org/10.1016/j.polymer.2006.12.041.

[311] J. Fasihi, S. Ammari Alahyari, M. Shamsipur, H. Sharghi, A. Charkhi, Adsorption of uranyl ion onto an anthraquinone based ion-imprinted copolymer, React Funct Polym. 71 (2011) 803–808. https://doi.org/10.1016/j.reactfunctpolym.2011.03.014.

[312] M. Shamsipur, J. Fasihi, A. Khanchi, R. Hassani, K. Alizadeh, H. Shamsipur, A stoichiometric imprinted chelating resin for selective recognition of copper(II) ions in aqueous media, Anal Chim Acta. 599 (2007) 294–301. https://doi.org/10.1016/j.aca.2007.08.013.

[313] A. Bahrami, A. Besharati-Seidani, A. Abbaspour, M. Shamsipur, A highly selective voltammetric sensor for sub-nanomolar detection of lead ions using a carbon paste electrode impregnated with novel ion imprinted polymeric nanobeads, Electrochim Acta. 118 (2014) 92–99. https://doi.org/10.1016/j.electacta.2013.11.180.

[314] S. Daniel, P. Prabhakara Rao, T. Prasada Rao, Investigation of different polymerization methods on the analytical performance of palladium(II) ion imprinted polymer materials, Anal Chim Acta. 536 (2005) 197–206. https://doi.org/10.1016/j.aca.2004.12.052.

[315] D. James, G. Venkateswaran, T. Prasada Rao, Removal of uranium from mining industry feed simulant solutions using trapped amidoxime functionality within a mesoporous imprinted polymer material, Microporous and Mesoporous Materials. 119 (2009) 165–170. https://doi.org/10.1016/j.micromeso.2008.10.011.

[316] R. Kala, V.M. Biju, T.P. Rao, Synthesis, characterization, and analytical applications of erbium(III) ion imprinted polymer particles prepared via γ-irradiation with different functional and crosslinking monomers, Anal Chim Acta. 549 (2005) 51–58. https://doi.org/10.1016/j.aca.2005.06.024.

[317] P. Gans, A. Sabatini, A. Vacca, SUPERQUAD: an improved general program for computation of formation constants from potentiometric data, J. Chem. Soc.{,} Dalton Trans. (1985) 1195–1200. https://doi.org/10.1039/DT9850001195.

[318] Y. Lee, S. Ahn, H. Cho, V. Ogunro, S. Bae, Solventless solid-phase extraction using Zn ion-imprinted polymer detected by colorimetric method, Bull Korean Chem Soc. 43 (2022) 429–437. https://doi.org/10.1002/bkcs.12460.

[319] L. Trzonkowska, B. Leśniewska, B. Godlewska-Żyłkiewicz, Development of Solid Phase Extraction Method Based on Ion Imprinted Polymer for Determination of Cr(III) Ions by ETAAS in Waters, Water (Basel). 14 (2022) 529. https://doi.org/10.3390/w14040529.

[320] N. Abu Samah, N.A. Mat Rosli, A.H. Abdul Manap, Y.F. Abdul Aziz, M. Mohd Yusoff, Synthesis & characterization of ion imprinted polymer for arsenic removal from water: A value addition to the groundwater resources, Chemical Engineering Journal. 394 (2020). https://doi.org/10.1016/j.cej.2020.124900.

[321] M. Behbahani, M. Salarian, A. Bagheri, H. Tabani, F. Omidi, A. Fakhari, Synthesis, characterization and analytical application of Zn(II)-imprinted polymer as an efficient solid-phase extraction technique for trace determination of zinc ions in food samples, Journal of Food Composition and Analysis. 34 (2014) 81–89. https://doi.org/10.1016/j.jfca.2013.10.003.

[322] M.G. Segatelli, V.S. Santos, A.B.T. Presotto, I.V.P. Yoshida, C.R.T. Tarley, Cadmium ion-selective sorbent preconcentration method using ion imprinted poly(ethylene glycol dimethacrylate-co-vinylimidazole), React Funct Polym. 70 (2010) 325–333. https://doi.org/10.1016/j.reactfunctpolym.2010.02.006.

[323] L.D. Mafu, T.A.M. Msagati, B.B. Mamba, Ion-imprinted polymers for environmental monitoring of inorganic pollutants: synthesis, characterization, and applications, Environmental Science and Pollution Research. 20 (2013) 790–802. https://doi.org/10.1007/s11356-012-1215-3.

[324] F.G. Tamayo, J.L. Casillas, A. Martin-Esteban, Highly selective fenuron-imprinted polymer with a homogeneous binding site distribution prepared by precipitation polymerisation and its application to the clean-up of fenuron in plant samples, Anal Chim Acta. 482 (2003) 165–173. https://doi.org/10.1016/S0003-2670(03)00213-7.

[325] F. Shakerian, K.H. Kim, E. Kwon, J.E. Szulejko, P. Kumar, S. Dadfarnia, A.M. Haji Shabani, Advanced polymeric materials: Synthesis and analytical application of ion imprinted polymers as selective sorbents for solid phase extraction of metal ions, TrAC - Trends in Analytical Chemistry. 83 (2016) 55–69. https://doi.org/10.1016/j.trac.2016.08.001.

[326] M. Taghizadeh, S. Hassanpour, Selective adsorption of Cr(VI) ions from aqueous solutions using a Cr(VI)-imprinted polymer supported by magnetic multiwall carbon nanotubes, Polymer (Guildf). 132 (2017) 1–11. https://doi.org/10.1016/j.polymer.2017.10.045.

[327] E. Kazemi, S. Dadfarnia, A.M. Haji Shabani, M. Ranjbar, Synthesis, characterization, and application of a Zn (II)-imprinted polymer grafted on graphene oxide/magnetic chitosan nanocomposite for selective extraction of zinc ions from different food samples, Food Chem. 237 (2017) 921–928. https://doi.org/10.1016/j.foodchem.2017.06.053.

[328] V. Lenoble, W. Meouche, K. Laatikainen, C. Garnier, H. Brisset, A. Margaillan, C. Branger, Assessment and modelling of Ni(II) retention by an ion-imprinted polymer: Application in natural samples, J Colloid Interface Sci. 448 (2015) 473–481. https://doi.org/10.1016/j.jcis.2015.02.055.

[329] M. Hossein Beyki, F. Shemirani, M. Shirkhodaie, Aqueous Co(II) adsorption using 8-hydroxyquinoline anchored γ-Fe2O3@chitosan with Co(II) as imprinted ions, Int J Biol Macromol. 87 (2016) 375–384. https://doi.org/10.1016/j.ijbiomac.2016.02.077.

[330] M. Roushani, Z. Saedi, F. Hamdi, H.R. Rajabi, Application of ion-imprinted polymer synthesized by precipitation polymerization as an efficient and selective sorbent for separation and pre-concentration of chromium ions from some real samples, Journal of the Iranian Chemical Society. 15 (2018) 2241–2249. https://doi.org/10.1007/s13738-018-1413-0.

[331] J.S. Downey, R.S. Frank, W.-H. Li, H.D.H. Stöver, Growth Mechanism of Poly(divinylbenzene) Microspheres in Precipitation Polymerization, Macromolecules. 32 (1999) 2838–2844. https://doi.org/10.1021/ma9812027.

[332] Y. Jiang, B. Tang, P. Zhao, M. Xi, Y. Li, Synthesis of Copper and Lead Ion Imprinted Polymer Submicron Spheres to Remove Cu2+ and Pb2+, J Inorg Organomet Polym Mater. 31 (2021) 4628–4636. https://doi.org/10.1007/s10904-021-02065-3.

[333] S. Pardeshi, S.K. Singh, Precipitation polymerization: a versatile tool for preparing molecularly imprinted polymer beads for chromatography applications, RSC Adv. 6 (2016) 23525–23536. https://doi.org/10.1039/C6RA02784A.

[334] H.G. Yuan, G. Kalfas, W.H. Ray, Suspension polymerization, Journal of Macromolecular Science, Part C: Polymer Reviews. 31 (1991) 215–299. https://doi.org/10.1080/15321799108021924.

[335] X. Cai, J. Li, Z. Zhang, F. Yang, R. Dong, L. Chen, Novel Pb2+ ion imprinted polymers based on ionic interaction via synergy of dual functional monomers for selective solid-phase extraction of Pb2+ in water samples, ACS Appl Mater Interfaces. 6 (2014) 305–313. https://doi.org/10.1021/am4042405.

[336] M. Kim, Y. Jiang, D. Kim, Zn2+-imprinted porous polymer beads: Synthesis, structure, and selective adsorption behavior for template ion, React Funct Polym. 73 (2013) 821–827. https://doi.org/10.1016/j.reactfunctpolym.2013.03.012.

[337] B. Brooks, Suspension Polymerization Processes, Chem Eng Technol. 33 (2010) 1737–1744. https://doi.org/10.1002/ceat.201000210.

[338] J. Livage, Basic Principles of Sol-Gel Chemistry, in: Sol-Gel Technologies for Glass Producers and Users, Springer US, Boston, MA, 2004: pp. 3–14. https://doi.org/10.1007/978-0-387-88953-5_1.

[339] Jun.P. Huan. He, Deli. Xiao, Jia. He, Hui. Li, Hua. He, Hao. Dai, Preparation of core–shell magnetic ion-imprinted polymer by sol-gel process for selective extraction of Cu(II) from herbal medicines, Analyst. 139 (2014) 2459–2466.

[340] Z. Zhang, J. Li, X. Song, J. Ma, L. Chen, Hg2+ ion-imprinted polymers sorbents based on dithizone-Hg2+ chelation for mercury speciation analysis in environmental and biological samples, RSC Adv. 4 (2014) 46444–46453. https://doi.org/10.1039/c4ra08163c.

[341] M.V. Dinu, I.A. Dinu, M.M. Lazar, E.S. Dragan, Chitosan-based ion-imprinted cryo-composites with excellent selectivity for copper ions, Carbohydr Polym. 186 (2018) 140–149. https://doi.org/10.1016/j.carbpol.2018.01.033.

[342] A. Mujahid, P.A. Lieberzeit, F.L. Dickert, Chemical Sensors Based on Molecularly Imprinted Sol-Gel Materials, Materials. 3 (2010) 2196–2217. https://doi.org/10.3390/ma3042196.

[343] A.-M. Siouffi, Silica gel-based monoliths prepared by the sol–gel method: facts and figures, J Chromatogr A. 1000 (2003) 801–818. https://doi.org/10.1016/S0021-9673(03)00510-7.

[344] H.-F. Wang, Y.-Z. Zhu, X.-P. Yan, R.-Y. Gao, J.-Y. Zheng, A Room Temperature Ionic Liquid (RTIL)-Mediated, Non-Hydrolytic Sol–Gel Methodology to Prepare Molecularly Imprinted, Silica-Based Hybrid Monoliths for Chiral Separation, Advanced Materials. 18 (2006) 3266–3270. https://doi.org/10.1002/adma.200601024.

[345] I. Langmuir, The adsorption of gases on plane surfaces of glass, mica and platinum, J Am Chem Soc. 345 (1918) 1361–1403.

[346] H. Freundlich, Über die Adsorption in Lösungen, Zeitschrift Für Physikalische Chemie. 57 (1906) 385–470.

[347] R. Sips, On the structure of a catalyst surface, J Chem Phys. 16 (1948) 490–495. https://doi.org/10.1063/1.1746922.

[348] M. Temkin, Kinetics of ammonia synthesis on promoted iron catalysts, Acta Physiochim. URSS. 12 (1940) 327–356.

[349] G. Scatchard, the Attractions of Protelns for Small, Annals New York Academy of Sciences. 51 (1949) 660–672. https://doi.org/10.1111/j.1749-6632.1949.tb27297.x.

[350] N.F. Yusof, F.S. Mehamod, F.B. Mohd Suah, Fabrication and binding characterization of ion imprinted polymers for highly selective Co2+ ions in an aqueous medium, J Environ Chem Eng. 7 (2019) 103007. https://doi.org/10.1016/j.jece.2019.103007.

[351] M.S. Jagirani, A. Balouch, E. Alveroğlu, S.A. Mahesar, B. Zeytuncu, Abdullah, A.R. Khaskhali, Fabrication of Cobalt tagged smart ion-imprinted polymeric material applied for the elimination of Co2+ ions from real environmental samples, Polymer Bulletin. 79 (2022) 10135–10153. https://doi.org/10.1007/s00289-021-04025-w.

[352] W. Guo, R. Chen, Y. Liu, M. Meng, X. Meng, Z. Hu, Z. Song, Preparation of ion-imprinted mesoporous silica SBA-15 functionalized with triglycine for selective adsorption of Co(II), Colloids Surf A Physicochem Eng Asp. 436 (2013) 693–703. https://doi.org/10.1016/j.colsurfa.2013.08.011.

[353] G. Yuan, H. Tu, J. Liu, C. Zhao, J. Liao, Y. Yang, J. Yang, N. Liu, A novel ion-imprinted polymer induced by the glycylglycine modified metal-organic framework for the selective removal of Co(II) from aqueous solutions, Chemical Engineering Journal. 333 (2018) 280–288. https://doi.org/10.1016/j.cej.2017.09.123.

[354] J. Li, Y. Li, K. Cui, H. Li, J. Feng, X. Pu, W. Xiong, N. Liu, G. Yuan, Novel MOFs-based ion-imprinted polymer for selective separation of cobalt ions from waste battery leaching solution, Inorganica Chim Acta. 536 (2022) 120922. https://doi.org/10.1016/j.ica.2022.120922.

[355] Z. Zhao, H. Jiang, L. Wu, N. Yu, Z. Luo, W. Geng, Preparation of Magnetic Surface Ion-Imprinted Polymer Based on Functionalized Fe3O4 for Fast and

Selective Adsorption of Cobalt Ions from Water, Water (Basel). 14 (2022) 261. https://doi.org/10.3390/w14020261.

[356] N. Ashouri, A. Mohammadi, M. Shekarchi, R. Hajiaghaee, H. Rastegar, Synthesis of a new ion-imprinted polymer and its characterization for the selective extraction and determination of nickel ions in aqueous solutions, Desalination Water Treat. 56 (2015) 2135–2144. https://doi.org/10.1080/19443994.2014.960469.

[357] J. Otero-Romaní, A. Moreda-Piñeiro, P. Bermejo-Barrera, A. Martin-Esteban, Synthesis, characterization and evaluation of ionic-imprinted polymers for solid-phase extraction of nickel from seawater, Anal Chim Acta. 630 (2008) 1–9. https://doi.org/https://doi.org/10.1016/j.aca.2008.09.049.

[358] J. Otero-Romaní, A. Moreda-Piñeiro, P. Bermejo-Barrera, A. Martin-Esteban, Ionic imprinted polymer for nickel recognition by using the bi-functionalized 5-vinyl-8-hydroxyquinoline as a monomer: Application as a new solid phase extraction support, Microchemical Journal. 93 (2009) 225–231. https://doi.org/10.1016/j.microc.2009.07.011.

[359] D.K. Singh, S. Mishra, Synthesis, characterization and analytical applications of Ni(II)-ion imprinted polymer, Appl Surf Sci. 256 (2010) 7632–7637. https://doi.org/10.1016/j.apsusc.2010.06.018.

[360] S. Abbasi, M. Roushani, H. Khani, R. Sahraei, G. Mansouri, Synthesis and application of ion-imprinted polymer nanoparticles for the determination of nickel ions, Spectrochim Acta A Mol Biomol Spectrosc. 140 (2015) 534–543. https://doi.org/10.1016/j.saa.2014.11.107.

[361] J. Long, X. Luo, X. Yin, X. Wu, An ion-imprinted polymer based on the novel functional monomer for selective removal of Ni(II) from aqueous solution, J Environ Chem Eng. 4 (2016) 4776–4785. https://doi.org/10.1016/j.jece.2016.11.004.

[362] H. He, Q. Gan, C. Feng, Preparation and application of Ni(II) ion-imprinted silica gel polymer for selective separation of Ni(II) from aqueous solution, RSC Adv. 7 (2017) 15102–15111. https://doi.org/10.1039/c7ra00101k.

[363] N. Jiang, X. Chang, H. Zheng, Q. He, Z. Hu, Selective solid-phase extraction of nickel(II) using a surface-imprinted silica gel sorbent, Anal Chim Acta. 577 (2006) 225–231. https://doi.org/10.1016/j.aca.2006.06.049.

[364] A.I. Okewole, N.P. Magwa, Z.R. Tshentu, The separation of nickel(II) from base metal ions using 1-octyl-2-(2′-pyridyl)imidazole as extractant in a highly acidic sulfate medium, Hydrometallurgy. 121–124 (2012) 81–89. https://doi.org/10.1016/j.hydromet.2012.04.002.

[365] A.I. Okewole, E. Antunes, T. Nyokong, Z.R. Tshentu, The development of novel nickel selective amine extractants: 2,2′-Pyridylimidazole functionalised chelating resin, Miner Eng. 54 (2013) 88–93. https://doi.org/10.1016/j.mineng.2013.04.019.

[366] J.K. Romary, J.D. Barger, J.E. Bunds, New multidentate .alpha.-pyridyl ligand. Coordination of bis(2-pyridylmethyl)amine with transition metal ions, Inorg Chem. 7 (1968) 1142–1145. https://doi.org/10.1021/ic50064a018.

[367] Z. Liu, L. Wang, Y. Lv, X. Xu, C. Zhu, F. Liu, A. Li, Impactful modulation of micro-structures of acid-resistant picolylamine-based chelate resins for efficient separation of heavy metal cations from strongly acidic media, Chemical Engineering Journal. 420 (2021) 129684. https://doi.org/10.1016/j.cej.2021.129684.

[368] S. Bruda, M.M. Turnbull, C.P. Landee, Q. Xu, Synthesis, structures and magnetic properties of 2-aminomethylpyridine–Ni(II) complexes, Inorganica Chim Acta. 359 (2006) 298–308. https://doi.org/10.1016/j.ica.2005.07.039.

[369] K. Sirola, M. Laatikainen, M. Lahtinen, E. Paatero, Removal of copper and nickel from concentrated ZnSO4 solutions with silica-supported chelating adsorbents, Sep Purif Technol. 64 (2008) 88–100. https://doi.org/https://doi.org/10.1016/j.seppur.2008.08.001.

[370] E. Rosenberg, D.C. Pang, System for extracting soluble heavy metals from liquid solutions, US5997748A, 1997.

[371] J. Spencer, J. Stevens, C. Perry, D.M. Murphy, An EPR Investigation of Binding Environments by N-Donor Chelating Exchange Resins for Cu Extraction from Aqueous Media, Inorg Chem. 57 (2018) 10857–10866. https://doi.org/10.1021/acs.inorgchem.8b01519.

[372] D.M. García, J.L. Escobar, N. Bada, J. Casquero, E. Hernáez, I. Katime, Synthesis and characterization of poly(methacrylic acid) hydrogels for metoclopramide delivery, Eur Polym J. 40 (2004) 1637–1643. https://doi.org/10.1016/j.eurpolymj.2004.03.011.

[373] P. Cao, V. Pichon, C. Dreanno, K. Boukerma, N. Delaunay, Development of ion-imprinted polymers for the selective extraction of Cu(II) ions in environmental waters, Talanta. 256 (2023) 124295. https://doi.org/10.1016/j.talanta.2023.124295.

[374] W. René, V. Lenoble, K. Laatikainen, B. Viguier, C. Branger, Influence of the synthesis parameters on the efficiency of fluorescent ion-imprinted polymers for lead detection, React Funct Polym. 170 (2022) 105134. https://doi.org/10.1016/j.reactfunctpolym.2021.105134.

[375] J. Chen, C. Zhao, H. Huang, M. Wang, X. Ge, Highly crosslinked poly(ethyleneglycol dimethacrylate)-based microspheres via solvothermal precipitation polymerization in alcohol–water system, Polymer (Guildf). 83 (2016) 214–222. https://doi.org/10.1016/j.polymer.2015.12.028.

[376] E.P. Barrett, L.G. Joyner, P.P. Halenda, The Determination of Pore Volume and Area Distributions in Porous Substances. I. Computations from Nitrogen Isotherms, J Am Chem Soc. 73 (1951) 373–380. https://doi.org/10.1021/ja01145a126.

[377] S. Brunauer, P.H. Emmett, E. Teller, Adsorption of Gases in Multimolecular Layers, J Am Chem Soc. 60 (1938) 309–319. https://doi.org/10.1021/ja01269a023.

[378] L. Zhang, L. Zhong, S. Yang, D. Liu, Y. Wang, S. Wang, X. Han, X. Zhang, Adsorption of Ni(II) ion on Ni(II) ion-imprinted magnetic chitosan/poly(vinyl alcohol) composite, Colloid Polym Sci. 293 (2015) 2497–2506. https://doi.org/10.1007/s00396-015-3626-4.

[379] U.S. Ramelow, S. Pingili, Synthesis of Ethylene Glycol Dimethacrylate-Methyl Methacrylate Copolymers, Determination of their Reactivity Ratios, and a Study of Dopant and Temperature Effects on their Conductivities, Polymers (Basel). 2 (2010) 265–285. https://doi.org/10.3390/polym2030265.

[380] Y. Liu, X. Meng, Z. Liu, M. Meng, F. Jiang, M. Luo, L. Ni, J. Qiu, F. Liu, G. Zhong, Preparation of a Two-Dimensional Ion-Imprinted Polymer Based on a Graphene Oxide/SiO2 Composite for the Selective Adsorption of Nickel Ions, Langmuir. 31 (2015) 8841–8851. https://doi.org/10.1021/acs.langmuir.5b01201.

[381] Y. Marcus, Thermodynamics of solvation of ions. Part 5.—Gibbs free energy of hydration at 298.15 K, J. Chem. Soc. Faraday Trans. 87 (1991) 2995–2999. https://doi.org/10.1039/FT9918702995.

[382] K.S.W. Sing, Reporting physisorption data for gas/solid systems with special reference to the determination of surface area and porosity (Recommendations 1984), Pure and Applied Chemistry. 57 (1985) 603–619. https://doi.org/doi:10.1351/pac198557040603.

Annex

A.1 - Assignation of liquid-phase ^{1}H-NMR and ^{13}C-NMR spectra peaks

The peak assignation of PIM-MMA ^{1}H-NMR spectrum is reported in Table A.1.

Table A.1. Peak assignation of PIM-MMA ^{1}H NMR spectrum in $CDCl_3$.

Peak position (ppm)	**Assignation**
8.50	H_1 2-pyridine (doublet)
8.09	H_4 2-pyridine (doublet)
7.76	H_3 pyridine (multiplet)
7.35	$H_{5'}$ imidazole (triplet)
7.23	H_2 2-pyridine (triplet)
7.21	H_5 imidazole (multiplet)
5.43	H_7 ethylene (singlet)
5.12	H_6 ethylene (singlet)
2.13	H_8 methyl (singlet)

The peak assignation of bis-AMP-MMA ^{1}H-NMR and ^{13}C-NMR spectra is reported in Tables A.2. and A.3.

Table A.2. Peak assignation of bis-AMP-MMA ^{1}H NMR spectrum.

Peak position (ppm)	**Assignation**
8.52	$H_{1',1}$ 2-pyridine (doublet)
7.66	$H_{3',3}$ 2-pyridine (triplet)
7.30	$H_{4',4}$ 2-pyridine (doublet)
7.19	$H_{2',2}$ 2-pyridine (multiplet)
5.18	H_7 1-ethylene (multiplet)
4.80	$H_{5',5}$ methylene (doublet)
2.03	H_6 methyl (triplet)

Table A.3. Peaks assignation of bis-AMP-MMA ^{13}C NMR spectrum.

Peak position (ppm)	**Assignation**
173.3	C_7 carbonyl
156.7	$C_{5',5}$ 2-pyridine
149.6	$C_{1',1}$ 2-pyridine
140.4	C_9 1-ethylene
136.6	$C_{3',3}$ 2-pyridine
122.4	$C_{4',4}$ 2-pyridine
121.1	$C_{2',2}$ 2-pyridine
115.5	C_{10} 2-ethylene
54.3	$C_{6'}$ methylene
49.7	C_6 methylene
20.7	C_8 methyl

The peak assignation of AMP-MMA ^{1}H-NMR and ^{13}C-NMR spectra is reported in Tables A.4. and A.5.

Table A.4. Peak assignation of AMP-MMA ^{1}H NMR spectrum.

Peak position (ppm)	**Assignation**
8.55	H_1 pyridine (doublet)
7.68	H_3 pyridine (triplet)
7.29	H_4 pyridine (doublet)
7.21	H_2 pyridine (triplet)
5.83	H_6 ethylene (multiplet)
5.38	H_7 ethylene (multiplet)
4.61	H_5 methylene (doublet)

2.03	H_8 methyl (triplet)

Table A.5. Peak assignation of AMP-MMA ^{13}C NMR spectrum.

Peak position (ppm)	**Assignation**
168.3	C_g carbonyl
156.3	C_e pyridine
148.8	C_a pyridine
139.7	C_h ethylene
137.1	C_c pyridine
122.5	$C_{b,d}$ pyridine
120.0	C_i ethylene
44.4	C_f methylene
18.6	C_j methyl

A.2 - IUPAC classification of nitrogen adsorption-desorption isotherms and hysteresis loops

The study of polymer morphology was carried out with nitrogen adsorption-desorption experiments. These measurements allowed for drawing the adsorption-desorption isotherms, and to determine the specific surface area, the pore volume, and pore size of each material. The International Union of Pure and Applied Chemistry (IUPAC) published a classification system for characterizing the nature of a material's pores based on experimental nitrogen adsorption-desorption isotherm curves of six types (Figure A.1) [382].

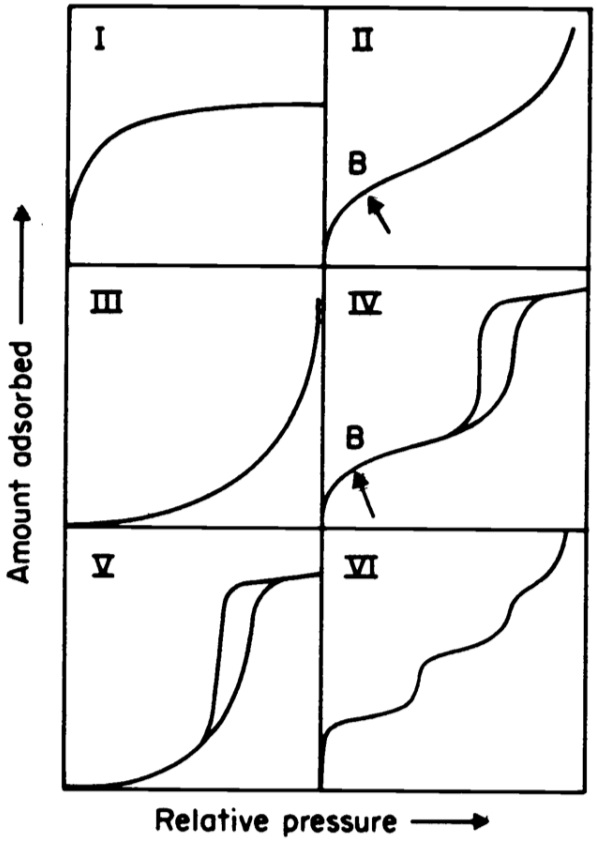

Figure A.1. Different types of nitrogen adsorption-desorption isotherms according to IUPAC classification. Point B indicates when the monolayer coverage is completed. Reprinted without modification from reference [382].

The type of isotherm provides indications regarding the porosity of the material. As an example, type I, II, and IV isotherms are indicative of microporous (pore diameter below 2 nm), non-porous or macroporous (pore diameter from 50 nm), and mesoporous (pore diameter from 2 to 50 nm) materials, respectively. Further information could be obtained from these measurements observing the shape of the hysteresis loop in the adsorption-desorption isotherms. The hysteresis loops are usually associated with capillary condensation in mesopore structures, and a classification based on their shape was proposed by IUPAC (Figure A.2) [382].

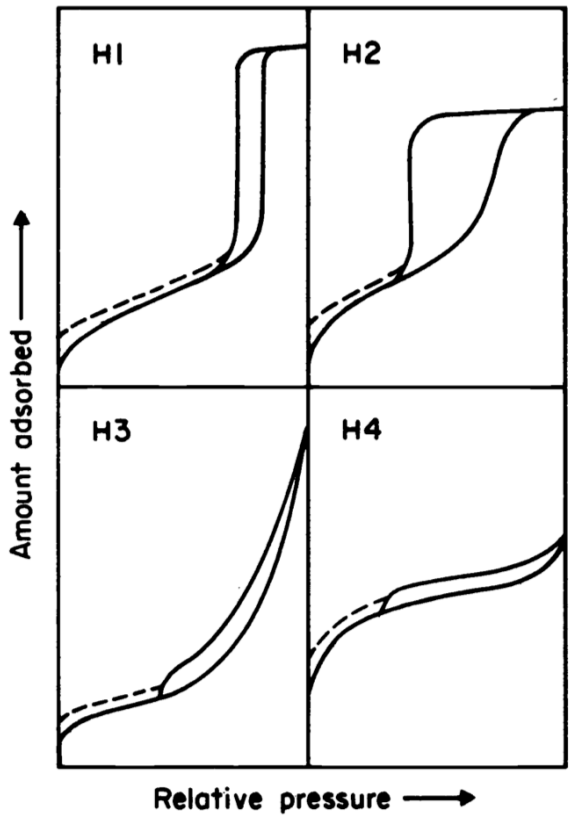

Figure A.2. Different types of hysteresis loop in nitrogen adsorption-desorption isotherms according to IUPAC classification. Reprinted without modification from reference [382].

According to IUPAC classification, the hysteresis loop H1 was associated with either agglomerates or compacts of uniform spheres with a narrow distribution of pores size, the hysteresis loop H2 with materials with not well-defined distribution of pores size and shape, the hysteresis loop H3 with aggregates of plate-like particles giving rise to slit-shaped pores, and the hysteresis loop H4 with the presence of narrow slit-like pores [382].

Finally, the specific surface and the pore volumes and sizes in material subjected to nitrogen adsorption-desorption experiments can be determined using the Brunauer, Emmett and Teller (BET) [377] and Barrett, Joyner and Halenda (BJH) [376] methods.

A.3 - Polymerization test of bis-AMP-MMA

The monomer bis-AMP-MMA was copolymerized with MMA and the composition of the reaction mixture was assessed after 6 h, 24 h, and 48 h of reaction time with ^{1}H NMR spectroscopy (Figure A.3). The conversion of each monomer into polymer was monitored by determining the integral values of the vinyl proton peaks at 5.15 ppm for the two vinyl

protons of bis-AMP-MMA and at 6.03 ppm for a single vinyl proton of MMA. Both integral values were compared to that of the pyridine proton peak of bis-AMP-MMA at 8.53 ppm, which served as a reference.

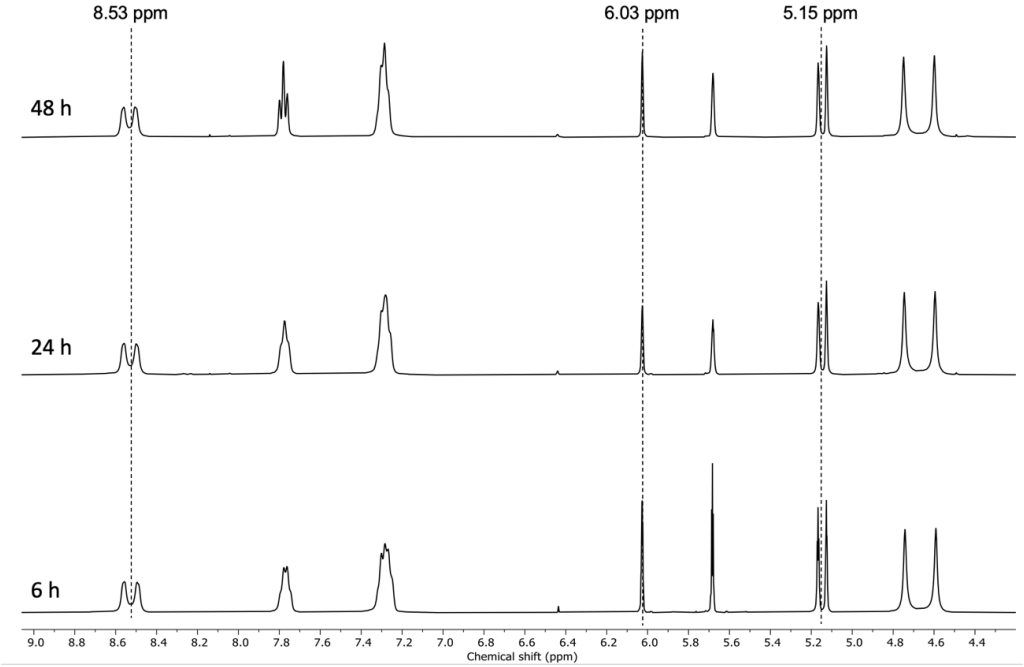

Figure A.3. ^{1}H NMR spectrum in DMSO-d_6 of the polymerization mixture after 6 h, 24 h, and 48 h of reaction conducted with a bis-AMP-MMA concentration equal to 0.99 M.

The conversion percentage of bis-AMP-MMA and MMA monomers into polymers were calculated with Eq. A.1 and Eq. A.2, respectively.

$$Conv.(bis-AMP-MMA)_t =$$

$$1 - \frac{\left(integral_{vinyl,bis-AMP-MMA} / integral_{pyridine}\right)_{t=n}}{\left(integral_{vinyl,bis-AMP-MMA} / integral_{pyridine}\right)_{t=0}} \times 100 \qquad \text{Eq. A.1}$$

$$Conv.(MMA)_t = 1 - \frac{\left(integral_{vinyl,MMA} / integral_{pyridine}\right)_{t=n}}{\left(integral_{vinyl,MMA} / integral_{pyridine}\right)_{t=0}} \times 100 \qquad \text{Eq. A.2}$$

Where $integral_{vinyl,bis-AMP-MMA}$ is the integral of the peak at δ = 5.15 ppm, $integral_{pyridine}$ is the integral of the peak at δ = 8.53 ppm (normalized to 2 and used as a reference), and $integral_{vinyl,MMA}$ is the integral of the peak at δ = 6.03 ppm (Figure A.3). The integral values are reported in Table A.6 The data with t = n is related to the

sampling times 6 h, 24 h, or 48 h, while that with t = 0 represents the initial conditions before the reaction was initiated.

Table A.6. Values of $integral_{pyridine}$, $integral_{vinyl,bis-AMP-MMA}$, and $integral_{vinyl,MMA}$ for bis-amp-MMA polymerization test.

Reaction time	$\boldsymbol{integral_{pyridine}}$	$\boldsymbol{integral_{vinyl,bis-AMP-MMA}}$	$\boldsymbol{integral_{vinyl,MMA}}$
0 h	2.00 (ref)	2.00	9.00
6 h	2.00 (ref)	1.72	0.86
24 h	2.00 (ref)	1.68	0.66
48 h	2.00 (ref)	1.68	0.64

The molar fraction of bis-AMP-MMA into the final product $F_{bis-AMP-MMA,t}$ was calculated with Eq. A.3.

$$F_{bis-AMP-MMA,t} = \frac{Conv.(bis-AMP-MMA)_t \times n_{bis-AMP-MMA,t=0}}{(Conv.(bis-AMP-MMA)_t \times n_{bis-AMP-MMA,t=0} + Conv.(MMA)_t \times n_{MMA,t=0})} \quad \text{Eq. A.3}$$

Where $n_{bis-AMP-MMA,t=0}$ and $n_{MMA,t=0}$ are the initial molar amount of bis-AMP-MMA and MMA in the polymerization mixture, respectively.

A.4 - Polymerization test of AMP-MMA

The ^{1}H NMR spectrum of AMP-MMA in DMSO-d_6, the solvent used for the polymerization test, is shown in Figure A.4.

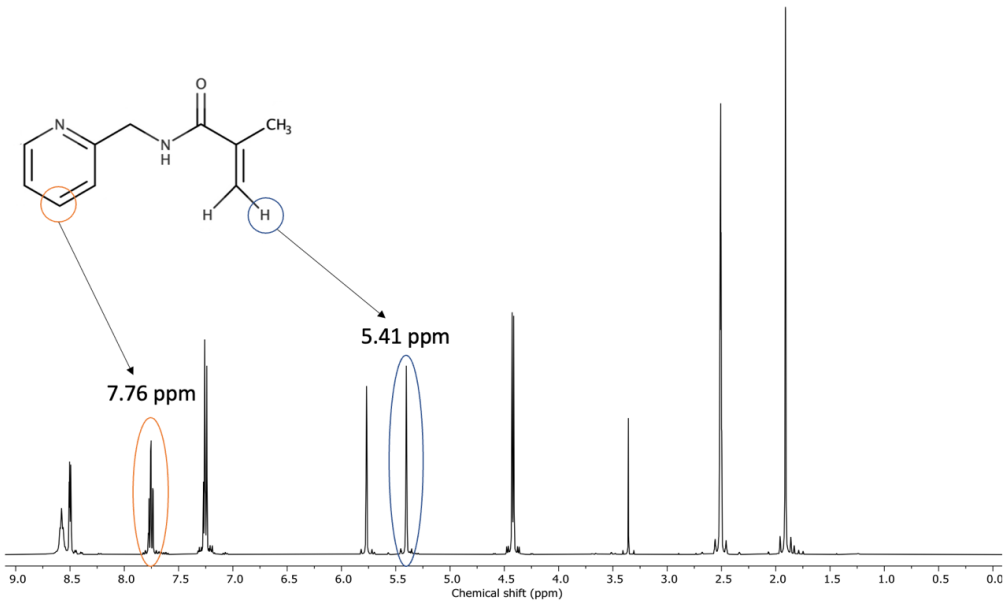

Figure A.4. ^{1}H NMR spectrum of AMP-MMA in DMSO-d_6.

The monomer AMP-MMA was copolymerized with MMA and the composition of the reaction mixture was assessed after 4, 6, and 24 hours of reaction by ^{1}H NMR spectroscopy (Figure A.5). The conversion of each monomer into polymer was determined by monitoring the integral values of a single vinyl proton peak at 5.41 ppm for AMP-MMA and at 6.03 ppm for MMA. Both integral values were compared to that of the pyridine proton peak of AMP-MMA at 7.76 ppm, which served as a reference.

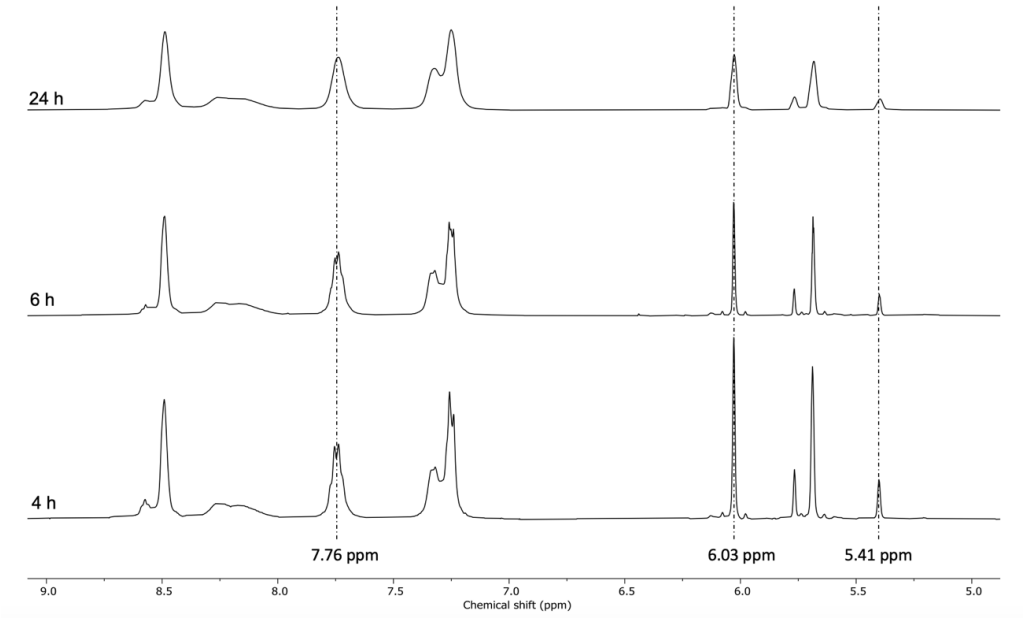

Figure A.5. ^{1}H NMR spectra in DMSO-d_6 of the polymerization mixture after 4 h, 6 h, and 24 h of reaction.

The conversion percentage of AMP-MMA and MMA monomers into polymers were calculated with the equations Eq. A.4 and Eq. A.5, respectively.

$$Conv.(AMP-MMA)_t = 1 - \frac{\left(integral_{vinyl,amp-MMA} / integral_{pyridine}\right)_{t=n}}{\left(integral_{vinyl,amp-MMA} / integral_{pyridine}\right)_{t=0}} \times 100 \quad \text{Eq. A.4}$$

$$Conv.(MMA)_t = 1 - \frac{\left(integral_{vinyl,MMA} / integral_{pyridine}\right)_{t=n}}{\left(integral_{vinyl,MMA} / integral_{pyridine}\right)_{t=0}} \times 100 \quad \text{Eq. A.5}$$

Where $integral_{vinyl,AMP-MMA}$ is the integral of the peak at δ = 5.41 ppm, $integral_{pyridine}$ is the integral of the peak at δ = 7.76 ppm (normalized to 1 and used as a reference), and $integral_{vinyl,MMA}$ is the integral of the peak at δ = 6.03 ppm. The integral values are reported in Table A.7. The data with t = n is related to the sampling times 4 h, 6 h, or 24 h, while that with t = 0 represents the initial conditions before the reaction was initiated.

Table A.7. Values of $integral_{pyridine}$, $integral_{vinyl,AMP-MMA}$, and $integral_{vinyl,MMA}$ for AMP-MMA polymerization test.

Reaction time	$integral_{pyridine}$	$integral_{vinyl,AMP-MMA}$	$integral_{vinyl,MMA}$
0 h	1.00 (ref)	1.00	9.00
4 h	1.00 (ref)	0.61	0.16
6 h	1.00 (ref)	0.46	0.10
24 h	1.00 (ref)	0.39	0.08

The molar fraction of AMP-MMA in the final product $x_{AMP-MMA,t}$ was calculated with Eq. A.6.

$$x_{AMP-MMA,t} = \frac{Conv.(AMP-MMA)_t \times n_{AMP-MMA,t=0}}{(Conv.(AMP-MMA)_t \times n_{AMP-MMA,t=0} + Conv.(MMA)_t \times n_{MMA,t=0})} \quad \text{Eq. A.6}$$

Where $n_{AMP-MMA,t=0}$ and $n_{MMA,t=0}$ are the initial molar amount of AMP-MMA and MMA in the polymerization mixture, respectively.

ACTA UNIVERSITATIS LAPPEENRANTAENSIS

1091. HÄRKÖNEN, KALEVI. Smart buildings in the green energy transition. 2023. Diss.

1092. TSYTSYNA, EVGENIYA. Motives, uncertainties, and imbalances in the evolution of a sustainable business ecosystem. 2023. Diss.

1093. JÄÄSKELÄINEN, ATTE. Business model innovation opportunities when news has become a public good. 2023. Diss.

1094. ADEDIPE, TAIWO. Atmospheric boundary-layer characteristics and their significance in wind energy and urban air quality assessment. 2023. Diss.

1095. SOSUNOVA, INNA. Model and guidelines for designing Internet-of-Things-enabled smart waste management system in smart cities. 2023. Diss.

1096. VUORELA, JYRI. Operative business development through system model and changing business structures. 2023. Diss.

1097. TRIAPITCIN, ILIA. Knowledge injection method for real-time decision support. 2023. Diss.

1098. RÄISÄNEN, OTTO. Open data in distribution network asset management. 2023. Diss.

1099. MATELA, MIKA. Procurement improvement in the public agency. 2023. Diss.

1100. SHAH, DIPAL. Quantification of synchronization. 2023. Diss.

1101. GHAFOURI, MEHRAN. Thermomechanical finite element simulation of welding, and elevated-temperature mechanical behaviour of high and ultra-high strength steels. 2023. Diss.

1102. NEUVONEN, RIKU. Numerical ductile fracture assessment of weldments in direct-quenched, ultra-high-strength steel. 2023. Diss.

1103. HUPPONEN, MARI. Long-term evolution of greenhouse gas emissions from municipal solid waste management. 2023. Diss.

1104. WANG, QI. Dynamic analysis and parameter identification for robotic manipulators. 2023. Diss.

1105. KIMPIMÄKI, JAAN-PAULI. From observation to insight: Computational abduction and its applications in sustainable strategy research. 2023. Diss.

1106. YIN, RUOCHEN. Research on key technologies for lightweight maintenance operations of the remote handling system for a fusion reactor. 2023. Diss.

1107. MUNIR, QAISAR. Designing printing parameters for geopolymer concrete prepared from construction and demolition waste and industrial side streams. 2023. Diss.

1108. ROHANI RAFTAR, HAMIDREZA. Assessment of weld root fatigue strength of load-carrying fillet welded joints using notch stress approaches and finite element analysis. 2023. Diss.

1109. SADIQA, AYESHA. Sustainable energy transition for Pakistan: Assessing the role of energy, water supply, social and gender equity dimensions. 2023. Diss.

1110. GHOREISHI, MALAHAT. The role of artificial intelligence in circular value creation: A conceptual framework and evidence from case studies. 2023. Diss.

1111. SUURONEN, JARKKO. On numerical implementation of α-stable priors in Bayesian inversion. 2023. Diss.

1112. PIILI, HEIDI. A conceptual, holistic framework to overcome limitations and constraints of design in laser based powder bed fusion of metals: Case novel separation and purification units. 2023. Diss.

1113. LOPATINA, ANASTASIIA. From alternative sources of cellulose to ultrafiltration membranes. 2023. Diss.

1114. MARTTINEN, KATI. Toward more sustainable supply management: Practices, determinants, and enablers for ensuring sustainability across multiple supply chain tiers. 2023. Diss.

1115. HU, HAO. Development of hybrid microdevices composed of Ni-Mn-Ga and silicon layers: fabrication and metrology. 2023. Diss.

1116. MARAIA, RAMONA. Bayesian likelihood for intractable data. 2023. Diss.

1117. ULLAH, MEHAR. Framework for digitalizing different industrial sectors via the internet of things. 2023. Diss.

1118. SIHVONEN, TUOMAS. Adaptive binning and spatial profile partial least squares methods in scanning electron microscopy energy-dispersive X-ray spectroscopy and satellite hyperspectral pansharpening. 2023. Diss.

1119. VOIPIO, VILLE. The role of radio-frequency identification in the sustainable digital transformation of the supply chain. 2023. Diss.

1120. WICKER, REBECCA. Bioprospecting for Nordic photosynthetic consortia for wastewater treatment, carbon capture, and value creation. 2023. Diss.

1121. SAUD, ALI. Sustainable recovery of nitrogen from sewage sludge. 2023. Diss.

1122. SHABBOUEI HAGH, YASHAR. Sigma-point Kalman filtering in physics-based digital twin applications: Synchronization between simulation and real world. 2023. Diss.

1123. KALITEEVSKII, VASILII. Artificial Inventiveness: Towards AI supported model-driven systematic conceptual design. 2023. Diss.

1124. TIKKA, VILLE. On load modeling of electric vehicles - energy system viewpoints. 2024. Diss.

1125. NYKYRI, MIKKO. Promoting local renewable energy production with energy communities and serious games. 2024. Diss.

1126. LAMMERT, DOMINIC. Bridging academic software sustainability design with corporate business planning. 2024. Diss.

1127. KAVUN, VITALII. Post-synthetic modification of metal-oxo clusters of metal-organic frameworks (MOFs) for aqueous applications. 2024. Diss.

1128. MANNER, PEKKA. Opportunities of households to contribute to primary frequency regulation in power systems – Proof of concepts. 2024. Diss.

LUT University

ISBN 978-952-412-064-7
ISBN 978-952-412-065-4 (PDF)
ISSN 1456-4491 (Print)
ISSN 2814-5518 (Online)
Lappeenranta 2024